Evaluation of New Therapies in Niemann-Pick Type C Disease

Nada Al Eisa

Wolfson College

Hilary Term, 2014

Department of Pharmacology

A thesis submitted to the Medical Sciences Division, University of Oxford, in partial fulfilment of the requirements for the degree of Doctor of Philosophy

Evaluation of New Therapies in Niemann-Pick Type C Disease

Nada Al Eisa, Wolfson College, D.Phil. Thesis, Hilary Term 2014

ABSTRACT

Niemann Pick type C (NPC) disease is a rare autosomal recessive neurodegenerative lysosomal storage disease caused by a mutation in the *NPC1* or *NPC2* genes. The functions of the proteins these genes encode are not fully understood, but are thought to be involved in free cholesterol egress from the acidic compartment. The pathogenic cascade in proposed to begin with sphingosine accumulation followed by reduction of acidic store calcium levels. This results in impairing intracellular trafficking and storage of multiple lipid substrates in the late endosome/lysosomal compartment.

In this thesis, multiple potential therapies have been tested in a mouse model of NPC1 disease including neuroprotective compounds. Positive effects were observed with some compounds, as reflected by increased life span and/or improved neurological function. In the course of these studies, I discovered another factor that affects the outcome of treatment with liver metabolised drugs. In the NPC1 mouse the cytochrome P450 system is impaired as is the case in the NPC1 cats and in patients. This thesis therefore sheds light on the impairment of this system at the genetic and functional level and presents data on why this aspect of pathology must be considered when designing therapeutics for this fatal neurodegenerative disease. This defect was partially corrected with bile acid supplementation, resulting in an unexpected functional improvement suggesting benefit in the CNS. Another aspect of NPC disease investigated was Crohn's-like intestinal inflammation that occurs in some NPC patients. This has been investigated in the *Npc1*$^{-/-}$ mouse model using two colitis models showing a partial protection by the *Npc1* mutation with different infection kinetics and secretory cytokine profiles. Taken together, this thesis therefore provides insights into two novel aspects of pathogenesis (Crohn's-like intestinal inflammation and a drug metabolism defect) and provides new leads on treatments that target unique aspects of the pathogenic cascade.

PUBLICATIONS

Publications of material related to this thesis

1. te Vruchte D, Speak A O, Wallom KL, **Al Eisa N**, Smith DA, Hendriksz CJ, Simmons L, Lachmann RH, Cousins A, Hartung R, Mengel E, Runz H, Beck M, Amraoui Y, Imrie J, Jacklin E, Riddick K, Yanjanin NM, Wassif CA, Rolfs A, Rimmele F, Wright N, Taylor C, Ramaswami U, Cox TM, Hastings C, Jiang X, Sidhu R, Ory DS, Arias B, Jeyakumar M, Sillence DJ, Wraith JE, Porter FD, Cortina-Borja M, Platt FM. The Journal of Clinical Investigation. 2014;124(3):1320-8. Relative acidic compartment volume as a lysosomal storage disorder–associated biomarker.
2. Williams IM, Wallom KL, Smith DA, **Al Eisa N**, Smith C, Platt FM. Neurobiology of Disease. 2014;67C:9-17. Improved neuroprotection using miglustat, curcumin and ibuprofen as a triple combination therapy in Niemann-Pick disease type C1 mice.

See Appendix

ACKNOWLEDGEMENTS

Firstly, I would like to sincerely thank my supervisor; Professor Fran Platt, for her unlimited support and guidance with regards to all aspects of my studies.

A huge, massive thank you to current members of the lab for basically everything (it would be extremely difficult for me to specify as every single person has been of tremendous help and support and I am extremely grateful): Allie, Chris, Danielle, Dave, David, James, Jenny, Jo, Kerri, Lauren, Nick, Paul and Ralu as well as previous members; Annie, Claire, Emyr, Ian, Ksenia, Oscar and Wendy.

Thanks to the BMS and PSB staff for their help with the mouse work.

I would also like to thank and acknowledge collaborators: for the IBD work; Dr. Kevin Maloy and Dr. George Song-Zhao form Sir William Dunn School of Pathology, Dr. Holm Uhlig and Prof. Fiona Powrie from Translational Gastroenterology Unit and Dr. Elisabeth Jameson, Dr. Uma Ramaswami, Jackie Imrie and Prof. Ed Wraith from the Royal Manchester Children's Hospital. For the drug metabolism work; Dr. Forbes Porter, Dr. Celine Cluzeau, Christopher Wassif, Steve Pisle, Dr. Cody Peer, Dr. Tristan Sissung, Dr. Shawn Spencer, Dr. William Figg and Dr. William Pavan from the NIH and Dr. Charles Vite from the University of Pennsylvania and finally for the collaborative study with Phytopharm; Dr. Patrick Howson and Dr. Roger Hickling.

I would also like to thank Paula for her great help, assistance, support and guidance especially with the administrative side.

Acknowledgment and thanks also should go to King Saud bin Abdulaziz University for Health Sciences and the Ministry of Higher Education, Kingdom of Saudi Arabia for their generous support and funding over the years of my graduate studies.

Finally and most importantly, my deepest gratitude and greatest thanks must go to my parents, my sisters (and nephew!) and my brother, if it was not for them and with them, their endless and unconditional support, dedication, sacrifices and encouragement; I would not have achieved any success.

TABLE OF CONTENTS

ABBREVIATIONS

(P)	Pelleted diet
2AA	2-aminobenzoic acid (Anthranilic acid)
A/E	Attaching and effacing
A2AR	Adenosine 2A receptors
ABCA1	ATP binding cassette transporter A1
Akt-mTOR-p70 S6K	Akt and mammalian target of rapamycin (mTOR)/ P70S6 kinase
ALS	Amyotrophic lateral sclerosis
ALT	Alanine transaminase
ARE	AU-rich element
ASC	Apoptosis-associated speck-like protein containing a carboxy-terminal CARD
ASM	Acid sphingomyelinase
AST	Aspartate transaminase
ATP (ase)	Adenosine 5'-triphosphate (triphosphatase)
AUC	Area under the plasma concentration vs. time curves
BA	Bile acids
BCA	Bicnichoninic acid
BDNF	Brain-derived neurotrophic factor
BMP	Bis-(monoacylglycerol) phosphate
bp	Base pair
BROD	Bezyloxyresorufin-O-dealkylation
BRT	By-product replacement therapy
BSA	Bovine serum albumin
BW	Body weight
CA	Cholic acid
cAMP	Cyclic adenosine monophosphate
CAR	Constitutive androstane receptor

CARD15	caspase activation and recruitment domain
CCL18/	Chemokine (C-C motif) ligand 18/
PARC	pulmonary- and activation-regulated chemokine
CD	2-hydroxypropyl-β-cyclodextrin or Cyclodextrin
CDCA	Chenodeoxycholic acid
CDK5	Cyclin-dependent kinase 5
CFU	Colony forming units
CG	Ceramide glycanase
cGMP	Cyclic guanosine monophosphate
CHO	Chinese Hamster Ovary
CNPase	2',3'-cyclic nucleotide 3'-phosphodiesterase
CNS	Central nervous system
CSF	Cerebrospinal fluid
CYP450	Cytochrome P450
DMSO	Dimethylsulphoxide
DNA	Deoxyribonucleic acid
DSS	Dextran sodium sulphate
EDTA	Ethylenediaminetetraacetic acid
EHEC	Enterohemorrhagic *E. coli*
eNOS	Endothelial Nitric Oxide Synthase
ENU	Ethylnitrosourea
EPEC	Enteropathogenic *E. coli*
ER	Endoplasmic reticulum
EROD	Ethoxyresorufin-O-dealkylation
ERT	Enzyme replacement/reconstitution therapy
FACS	Fluorescence-activated cell sorting
FADD	Fas-associated death domain
FC	Fold-change
FDA	Food and drug administration

FXR	Farnesoid x receptor
GA1	Asialoganglioside GM1 (Galβ3GalNAcβ4Galβ4GlcCer)
GA2	Asialoganglioside GM2 (GalNAcβ4Galβ4GlcCer)
GalCer	GalactosylCeramide
Gb3	Globotriaosylceramide (Galα4Galβ4GlcCer)
Gb4	Globotetraosylceramide (globoside, GalNAcβ3Galα4Galβ4GlcCer)
GC	Glycocholic acid
GD1a	Disialoganglioside GM1a (Neu5Acα3Galβ3GalNAcβ4(Neu5Acα3)Galβ4GlcCer)
GD1b	Disialoganglioside GM1b (Galβ3GalNAcβ4(Neu5Acα8Neu5Acα3)Galβ4GlcCer)
GDNF	Glial cell line-derived neurotrophic factor
GI	Gastrointestinal
Glc	Glucose
GlcCer	GlucosylCeramide
GM1	Monosialoganglioside GM1 (Galβ3GalNAcβ4(Neu5Acα3)Galβ4GlcCer)
GM1a	Monosilaoganglioside GM1a (Galβ3GalNAcβ4(Neu5Acα3)Galβ4GlcCer)
GM1b	Monosilaoganglioside GM1b (Neu5Acα3Galβ3GalNAcβ4Galβ4GlcCer)
GM2	Monosialoganglioside GM2 (GalNAcβ4(Neu5Acα3)Galβ4GlcCer)
GM3	Monosialoganglioside GM3 (Neu5Acα3Galβ4GlcCer)
GSK3β	Glycogen synthase kinase 3β
GSL	Glycosphingolipid
GT1b	Trisialoganglioside GM1b (Neu5Acα3Galβ3GalNAcβ4(Neu5Acα8Neu5Acα3)Galβ4GlcCer)
GTPase	Guanosine 5'-triphosphatase
GU	Glucose unit
H&E	Haematoxylin and eosin
HDL	High-density lipoprotein

HMG-CoA	3-hydroxy-3-methyl-glutaryl-CoA
HPS	Hermansky-Pudlak Syndrome
HSP70	Heat Shock Protein 70
i.p.	Intra-peritoneal
IBD	Inflammatory bowel disease
ICE	IL-1β converting enzyme
IEC	Intestinal epithelial cells
IL	Interleukin
ILV	Inner lysosomal vesicles
INF-ɣ	Interferon gamma
iNOS	Inducible nitric oxide synthase
JNK2	c-Jun N-terminal protein kinase 2
LacCer	Lactosyl ceramide
LB	Luria Bertani
LC-MS/MS	Liquid chromatographic-tandem mass spectrometric
LE/Lys	Late endosome/lysosome
LPS	Lipopolysaccharide
LRO	Lysosome-related organelles
LRR	Leucine rich repeats
LSD	Lysosomal Storage Disease
LXR	Liver X receptor
LZP	Lorazepam
M6P	Mannose-6-phosphate
MDZ	Midazolam
MF	Milk-derived fat
MK2	MAPKAP kinase 2
ML	Molecular layer
MLN64	Metastatic lymph node 64 protein
MPP^+	1-methyl-4-phenylpyridinium

MPS	Mucopolysaccharidosis
MPTP	1-methyl-4-phenyl-1,2,3,6-tetrahydropyridine
MRI	Magnetic Resonance Imaging
MROD	Methoxyresorufin-O-dealkylation
MTBE	Methyl-t-butyl-ether
MW	Molecular weight
NAADP	Nicotinic acid adenine dinucleotide phosphate
NADPH	Nicotinaminde adenine dinucleotide phaosphate (reduced form)
*N*B-DGJ	*N*-butyldeoxygalactonojirimycin
*N*B-DNJ	*N*-butyldeoxynojirimycin
NeuAc	N-Acetylneuraminic acid
NF-κB	Nuclear factor kabba κ B
NFT	Neurofibrillary Tangles
NK	Natural killer
NLRP3	NOD-like receptor family, pyrin domain containing 3
NOD2	Nucleotide-binding oligomerization domain-containing protein 2
NP-HPLC	Normal phase high performance liquid chromatography
NPA	Niemann-Pick type A
NPB	Niemann-Pick type B
NPC	Niemann-Pick type C
NPC1L1	Niemann-Pick C1-Like 1
NSAIDs	Non-steroidal anti-inflammatory drugs
PBMCs	Peripheral blood mononuclear cells
PBS	Phosphate-buffered saline
PCR	Polymerase chain reaction
PDE-1	phosphodiesterase-1
PFA	Paraformaldehyde
PKC	Protein kinase C
PPARα	Peroxisome proliferator-activated receptor α

PROD	Pentoxyresorufin-O-dealkylation
PUFA	Polyunsaturated fat
PVDF	Polyvinylidene difluoride
PXR	Pregnane X receptor
RER	Rough endoplasmic reticulum
RIPK1	Receptor-interacting serine/threonine-protein kinase 1
RND	The resistance-nodulation-division
ROS	Reactive Oxygen Species
S1P	Sphingosine-1-phosphate
SCAP	Sterol regulatory element-binding protein cleavage-activating protein
SDS	Sodium dodecyl sulphate
SER	Smooth endoplasmic reticulum
SERCA	Sarco(endo)plasmic reticulum ATPase
SIM	Single ion monitoring
SK1	Sphingosine kinase 1
SM	Sphingomyelin
SMPD1	Sphingomyelin phosphodiesterase 1
SPF	Specific pathogen free
Sphk2	Sphingosine kinase 2
SRT	Substrate reduction therapy
TAE	Tris-acetate EDTA
TC	Taurocholic acid
Th1	T helper cells type 1
TIA	T-cell intracellular antigen
TMCH	Transmissible murine colonic hyperplasia
TNF	Tumor necrosis factor
TNFRp55	Tumor necrosis factor receptor-55
TPC	Two-pore channel
Tpl2	Tumor Progression Locus 2

TRADD	TNF receptor-associated death domain
Trk	Tropomyosin-receptor-kinase
TTP	Tristetraprolin
UDCA	Ursodeoxycholic acid
UGT	UDP-glucuronosyltransferase
UPDRS	Unified Parkinson's Disease Rating Scale
VDR	Vitamin D receptor
VSGP	Vertical supranuclear gaze palsy

Chapter 1. Introduction

1.1. Niemann-Pick diseases

Neimann-Pick (NP) diseases were first described in 1914 by the German paediatrician Albert Niemann, who published his findings on "An unknown disease" in a child with hepatosplenomegaly and CNS disease, leading to premature death around the age of 2 years (1). It was the German pathologist Ludwig Pick in 1927 who further characterised the disease by analysing tissues from patients.

Crocker first suggested in 1961 the classification of these diseases into 4 groups, based on clinical manifestations. He classified the diseases into: type A (the originally described case that presented as a fatal infantile form); type B (the visceral form with no other symptoms or systems involved); types C and D correspond to the later onset neurological forms. Types E and F were identified and described later (2).

Type A and B are caused by mutations in the sphingomyelin phosphodiesterase-1 (*SMPD1*) gene which encodes for lysosomal acid sphingomyelinase (ASM) leading to sphingomyelin accumulation (3).

Type D resembles type C but was initially considered a separate disease, as it appeared to have arisen from a common ancestry in the Nova Scotian Acadian population. However, it is now considered an allelic variant of type C and does not stand as a separate entity, since different population-specific mutations have been identified with regards to NPA, B and C which are the three recognised forms of NP diseases (2).

The various forms (A, B and C) are grouped under one disease as they all are associated with sphingomyelin storage. Type C also results in a secondary reduction in ASM activity (4).

As the focus of this thesis is on NPC disease I will discuss this disorder in more detail.

1.2. Niemann-Pick type C disease

Niemann-Pick disease type C (NPC) is an autosomal recessive lysosomal storage disease characterised by abnormal lipid storage resulting in progressive neurodegeneration. NPC1, which is caused by mutations in the *NPC1* gene, accounts for approximately 95% of cases while the remaining 5% are attributed to defects in the *NPC2* gene (5). Mapping of the *NPC1* gene to chromosome18 was achieved in 1993 (6), while the *NPC2* gene (previously known as HE1) was described in 2000 (7). The clinical presentation of this disease is indistinguishable irrespective of which gene is mutated suggesting they act cooperatively in a common cellular pathway (8).

According to the National Niemann-Pick Disease Foundation, there are about 500 live NPC1 patients worldwide at any time. However, this is probably an underestimate due to its fatal nature and the lack of accurate diagnosis and considerable diagnostic delay in many cases (http://www.nnpdf.org).

1.2.1. Clinical presentation

NPC has a variable clinical presentation with onset ranging from birth to as old as the 70 years (9, 10). Clinical manifestations vary accordingly, from mixed neurovisceral symptoms with multiple system involvement to isolated neurological symptoms that manifest as cognitive, motor and psychiatric symptoms. Based on the heterogeneity in the age of onset, the degree of disease severity and the extent of organ involvement; survival and life span can vary from the first days of life to the 6^{th} decade with the average survival ranging from 10 and 25 years (11).

Classically, NPC presents as a progressive neurodegenerative disease with neurological symptoms developing following visceral symptoms in the liver (typically cholestatic jaundice), if present, which in some cases can be fatal. Typical neurological manifestations include cerebellar ataxia, cataplexy, dysarthria, seizures, dysphagia, progressive dementia, dystonia and vertical supranuclear gaze palsy (VSGP). Psychiatric disorders usually features at late-onset patients (12, 13). Systemic disease, although potentially fatal when present at an early age (immediately post-natal period), is usually not a feature of late-onset disease and has been reported to tend to regress prior to neurological symptoms development even in early onset patients (5).

Systemic and neurological disorders are generally independent; however, age of onset of neuropathology is the main determinant of the subsequent course of the disease and therefore life expectancy **(Figure 1.1** and **Table 1.1)**.

The figure originally presented here cannot be made freely available via ORA because of ‘copyright’.

The table originally presented here cannot be made freely available via ORA because of ‘copyright’.

1.2.2. Genetics

The *NPC1* gene was mapped to chromosome 18 (18q11.2) and encodes a 1278 amino acid membrane protein which resides mostly in the late endosomal/lysosomal membrane (22, 23). It consists of a cytoplasmic C-terminus, 13 transmembrane domains, a sterol sensing domain (amino acids 615-797, transmembrane domains 3-7) which exhibit homology to 3-hydroxy-3-methyl-glutaryl-CoA (HMG-CoA) reducatse, sterol regulatory element-binding protein cleavage-activating protein (SCAP), Patched and Niemann-Pick C1-Like 1 (NPC1L), but its role is not clear. Of the three large luminal loops; the cysteine rich domain (amino acids 855-1098, loop I) which accounts for about one third of the identified mutations in patients, and the

N-terminus domain (amino acids 25-264, loop A, also called NPC1 domain) that is conserved among all NPC1 orthologs and contains a leucine-zipper motif that has a cholesterol binding site **(Figure 1.2)** (24, 25). The protein is proposed to be involved in the transport of low-density lipoprotein **(**LDL)-derived cholesterol from late endosomes/lysosomes (LE/Lys) and its dysfunction results in the accumulation of cholesterol, sphingomyelin, sphingosine and GSLs in the LE/Lys (25).

NPC1 protein has a sequence homology with the resistance-nodulation-division (RND) family of permeases, both have the following structure twice: six transmembrane domains with a large hydrophilic loop between domains 1 and 2 (27). Prokaryotic permeases of the RND family are membrane transporters of

detergent-like hydrophobic substrates (28). Supporting the role of the NPC1 protein as a transmembrane transporter (4, 25, 29).

NPC2/HE1 on the other hand is a relatively small (the mature protein is 151 amino acids in length) soluble lysosomal protein that is trafficked to the lysosomal lumen via mannose-6-phosphate (M6P) receptor and binds cholesterol. The *HE1* (*NPC2*) gene was mapped to chromosome 14q24.3 (7).

A mouse with *Npc2* underexpression (only expressing 0-4% protein in various tissues) was generated by Sleat *et al.* (2004) to study this protein's function with and without a functional NPC1 protein. Both the *Npc1* and *Npc2* single mutants and the double mutants presented similarly in terms of age of onset, disease progression, lipid storage and pathology. This further supported the link between the two proteins acting together to facilitate cholesterol/lipid efflux from the LE/Lys (5, 30).

About over 300 in the *NPC1* gene have been described in NPC1 patients (5, 29). The most common mutation is I1061T that is associated with the severe neurological infantile form (31). The second most common mutation in Europe is the P1007A mutation, seen in the neurological adult onset form (32). The following mutations have shown to be associated with the early onset form of the disease with typical biochemical presentation: nonsense or frameshift mutations, mutations in the sterol-sensing domain and A1054T in the cysteine-rich luminal loop (18). Variable disease presentation occurs with mutations in the cysteine-rich luminal loop, in which one third of all identified mutations occur (18).

In NPC2, about 15 mutations have been identified (32). The nonsense mutation E20X is the most common (18). Other missense mutations present with varied phenotypes, for instance, homozygosity for the C99R mutation in the *NPC2* gene

were associated with early-onset disease (neonatal or infantile) with premature death in early childhood, whereas homozygosity for the V39M and S67P mutations correlated with a milder disease where patients lived to adulthood (33).

1.2.3. Biochemistry of NPC disease

In contrast to peripheral tissues where cholesterol is the most abundant accumulating class of lipid, NPC brain has shown to most abundantly accumulate glycosphingolipids (GSLs), predominantly GM2 and GM3 gangliosides, glucosylceramide and lactosylceramide (34). This abnormal neuronal storage results in characteristic features including: neurofibrillary tangles (NFT) and meganeurite formation, extensive ectopic dendrite growth, neuroinflammation and neuroaxonal dystrophy (35).

1.2.4. Cell biology of NPC disease

The sequence of pathogenic events in NPC disease is controversial and the relevance of this sequence of biochemical events to the pathogenesis is still not clear. In the U188666A cellular model of NPC disease (a drug that inhibits egress of LDL-cholesterol from the lysosome mimicking NPC cellular phenotype (36)), sphingosine has been shown to accumulate first, followed by abnormal calcium depletion within the lysosome and subsequent build up of cholesterol, sphingomyelin and GSLs several hours later (34, 37). Accordingly, NPC1 is proposed to play a role in sphingosine efflux from the lysosome (37) and is possibly regulated by cholesterol, whereas NPC2 is proposed to transfer cholesterol to NPC1 (38). Defects in either gene cause abnormal acidic calcium store homeostasis and subsequent abnormal lipid storage with intracellular mistrafficking (4) **(Figure 1.3, Figure 1.4** and **Figure 1.5).**

The figure originally presented here cannot be made freely available via ORA because of ‘copyright’.

The figure originally presented here cannot be made freely available via ORA because of ‘copyright’.

1.2.5. Animal models of NPC1

Pentchev *et al.* (39) in 1984 first described the *Npc1nih* mouse (**BALB/cNctr-*Npc1*^{m1N}/J)** that has a frame-shift mutation due to a spontaneous retroposon insertion in exon 9 of the *Npc1* gene, resulting in a truncated protein (loss of 11 out of the 13 transmembrane domains). Presenting as an early onset, severe disease, this model is more useful in studying the early onset, infantile form of the disease. This mouse model starts to show symptoms at the age of 6-7 weeks with weight loss, tremor and ataxic gait, which continue to progress and become more severe until

premature death at the age of 12 to 14 weeks. The mouse presents with hepatosplenomegaly with sphingomyelin and unesterified cholesterol storage, cerebellar Purkinje cell loss.

The other null allele of *Npc1* is the *Npc1*^{spm} (*Npc1*^{spm} mouse, **C57BLKS/J-*Npc1*^{spm}/J)** identified in 1975 as spontaneous mutation which results in a frame shift and subsequent truncated protein with total loss of the functional NPC1 protein and homozygous mice for this mutation present with similar disease phenotypes as the Npc1nih mice (40, 41).

Clinical features of these mouse models are summarised in **Table 1.2.**

Age (weeks)	Disease stage	Clinical symptoms and signs	Biochemical and histological changes
6-7	Early symptomatic	Weight loss, ataxia and gait abnormalities, progressive deterioration in motor and neurological function, tremor, lack of responsiveness to external stimuli and infertility	
8-10	Late symptomatic	Hepatosplenomegaly, progressive worsening of all neurological problems, inability to walk, eat or drink.	Hepatosplenomegaly and enlargement of lymph nodes, foam cells in liver and spleen, loss of cerebellar Purkinje cells, elevated levels of sphingomyelin and free cholesterol in the liver and spleen, significant reduction in the activity of sphingomyelinase in liver (to 30%), spleen (to 50%) and brain (to 70-80%).
12-14	End-stage	Death	

Table 1.2. Summary of the of *Npc1nih* and *Npc1spm* mouse with the main signs associated disease stages (39, 40).

The other mouse model of NPC is the *Npc1*^{nmf164} mouse (**C57BL/6J-*Npc1*^{nmf164}/J)**, the result of a point mutation in the *Npc1* gene (amino acid change D1005G) affecting the cysteine rich luminal loop of the protein, the region which accounts for

about 30% of the identified mutation in NPC1 patients, the I1061T and P1007A alleles (5, 42). Unlike the two null *Npc1* mouse models, this point mutation results in a partial loss of the functional of the NPC1 protein and therefore this mouse model has a milder form of the disease with later onset and slow progressing with progressive ataxia and motor dysfunction, weight loss, sphinigomyelin, GSLs and cholesterol storage in the liver and spleen, depletion of cerebellar Purkinje cells, GM2 and GM3 gangliosides accumulation and microglial activation and cholesterol storage in neurons leading to premature death at about 16 weeks. This allele was identified from ethylnitrosourea (ENU) mutagenesis in C57BL mice while screening for induced recessive mutations with neurological manifestations at the Neuroscience Mutagenesis Facility at The Jackson Laboratory (26). The amino acid positions of the three murine mutations are shown in **(Figure 1.2).**

The feline form of NPC disease was described in a domestic short-hair kitten in 1990 (43) and a breeding colony was established. The feline model has a spontaneous missense mutation (44). Description of the biochemistry and clinical signs in the cat model followed in 1994 by Brown *et al* (45). Neurological signs include head and whole body intention tremor developing from 8 to 12 weeks of age, followed by rapid progression to dysmetria and ataxia, and premature death occurs at 8 to 10 months of age. Systemically, kittens present with low birth weight and hepatomegaly.

1.2.6. Clinical diagnosis

There is no gold standard diagnostic test for NPC disease and thus diagnosis is mainly aided by suspicion arising from unexplained psychiatric illness, dementia, cognitive impairment especially when accompanied by cerebellar ataxia and dystonia.

Electron microscopy showing heterogeneous intracellular storage particles can be diagnostic in expert hands. The classical testing for NPC disease has for many years been a cytological test using skin fibroblasts stained with filipin to visualise cholesterol storage (46). Diagnosis is confirmed by mutation analysis (47, 48). An algorithm of diagnostic laboratory tests is summarised in **Figure 1.6**.

1.2.7. Markers of NPC disease

Until recently, there have been no biomarkers of NPC disease that aid diagnosis, monitoring disease progression and response to therapy.

The involvement of oxidative stress in the pathogenesis of NPC disease causes non-enzymatic oxidation of cholesterol. The resulting oxysterols have been validated as a biomarker that found to be elevated in NPC1 patients before the onset of the symptoms and are reduced in response to cyclodextrin (CD) treatment in the feline model of NPC1 disease (50). A sensitive, non-invasive, robust assay has been developed that employs a liquid chromatographic-tandem mass spectrometric (LC-MS/MS) method which quantifies two oxysterol species: in human (patient plasma) following derivatisaton with N,N-dimethylglycine (51). Two oxysterol species in particular were found to be elevated and have been suggested to be used as markers: cholestane-3β,5α,6β-triol and 7-ketocholesterol (51). Whether these oxysterols are also elevated in NPA and NPB remains to be determined.

Lysotracker® is a fluorescent probe that accumulates in intracellular acidic organelles. Recently, the use of a FACS assay to measure relative lysosomal volume using Lysotracker® in peripheral blood B-lymphocytes has been described in a long-term, prospective multi-centre collaborative study with over 100 NPC patients. This marker was able to detect response to treatment and correlated with age adjusted severity scores (52, 53).

Chitotriosidase is a chitinase that is secreted by activated macrophages and is thought to be important for host defence against chitin-containing pathogens. Plasma chitotriosidase is elevated in multiple lysosomal storage diseases (LSDs) and is used as a marker for Gaucher disease (54, 55). It has also been shown to be also elevated in NPC patients (56) but as an NPC disease marker, it has a relatively low sensitivity and specificity (57).

Chemokine (C-C motif) ligand 18 (CCL18), previously known as pulmonary-and activation-regulated chemokine (PARC), is a small cytokine from the CC chemokine family. Its function is to mediate chemotaxis of leukocytes (58). It has shown to be elevated in young NPC patients and been tested as a potential marker for NPC and also Gaucher disease, but its sensitivity and specificity have not been established. It is particularly useful for patients with normal chitotriosidase levels (59).

1.2.8. Inflammatory components of NPC disease

Inflammation is a complex physiological process involving multiple cellular and molecular elements that are tightly regulated to maintain homeostasis. Loss of such tight control and regulation of inflammation could transform this healthy physiological response into chronic inflammation (60). Insults that trigger an inflammatory response in neurodegenerative diseases are typically misfolded proteins that build up/aggregate due to their abnormal conformation or an affected/damaged neuron which signals to the immune system (60).

Although the CNS has long been described as immune privileged, it is known now that it has its own immune elements such as microglia which play a key role in clearing damaged neurons and release inflammatory cytokines tumor necrosis factor (TNF) and interleukin-1β (IL-1β) to initiate a local immune response in the CNS (61).

Over a century ago, the description of activated microglia (potentially caused by signals resulting from neuronal cell death and release of proinflammatory cytokines) predicted a role for the immune systems in the pathogenesis of neurodegenerative diseases. This link between chronic CNS inflammation and pathology is indeed a

common feature of many neurodegenerative disease including LSDs, Alzheimer's disease and Parkinson's disease (62). Another element of CNS inflammation in neurodegenerative diseases is the recruitment of other pro-inflammatory cells and the generation of reactive oxygen species which lead to oxidative stress which further feeds the local inflammatory process by stimulating the production of adhesion molecules and the secretion of inflammatory cytokines (63).

The involvement of multiple elements of the immune response in neurodegenerative disease such as Alzheimer's disease, Parkinson's disease, amyotrophic lateral sclerosis (ALS), multiple sclerosis has been reported (62). Inflammation in these disorders does not present as an early initiating event, however, results from animal studies support the role and contribution of inflammatory events in progression of neurodegenerative disease. A crucial point regarding this component of neurodegenerative diseases is the benefit of blocking such responses to slow further damage induced by inflammation may be a universal adjunct therapy if it can be achieved without immunocompromising the individual (64).

In NPC disease, the expression of multiple genes related to lipid metabolism and inflammation have been shown to be significantly elevated in *Npc1*$^{-/-}$ mice (such as TNF receptor 1α, 1β and complement C1q and C3) (65) while those associated with an anti-inflammatory response were markedly under-expressed (interleukins IL-4/10/13) (66, 67). Also, multiple apoptotic signalling molecules stimulated by TNF such as caspase-8, FADD, TNFRp55, TRADD, and RIP were also elevated contributing to both CNS and peripheral inflammation in NPC disease (68, 69). Programmed necrosis "necroptosis" is mediated by receptor-interacting serine/threonine-protein kinase 1 (RIPK1) and RIPK3 upon TNF receptor activation. The expression of both RIPK1 and RIPK3 was not changed in *Npc1*$^{-/-}$

mouse brain, as opposed to upregulation seen in brains from mouse models of Krabbe and Gaucher diseases indicative of a different inflammatory pathways activated in these LSD mouse models (70).

CNS inflammation in *Npc1*$^{-/-}$ mice starts prior to symptom onset at two weeks of age, showing microglial activation in some brain areas, which then extends to reach most regions by the age of 4 weeks and is then sustained through out the life span of the mice until they reach end-point and premature death at about 12 weeks (71). Therefore it appears that CNS inflammation (presenting as astrocyte and microglial activation) is a very early event in disease progression suggestive of a correlation or link between microglial activation and CNS disease and neurodegeneration in NPC disease (72) **(Figure 1.7)**.

1.2.9. Clinical management of NPC disease

Symptomatic management targeting individual manifestation of the disease using established drugs has been the basis for clinical management of NPC disease for many decades. Examples include antiepileptic drugs for seizures, clomipramine, protriptyline, or modafinil for cataplexy, which is a common feature seen in NPC patients (74), anticholinergic agents for dystonia and tremor all of which has been shown to be beneficial in NPC patients. Additionally, physiotherapy along with occupational and speech therapy should accompany such standard regimens for better outcome. Special education may prove useful for infantile cases where the disease is slowly progressing. However, when the disease further progresses, some special arrangements should be considered for further neurological impairments such as special feeding by modifying food formulations (softening or thickening) or feeding through gastrostomy tube in more advanced cases to insure sufficient caloric intake. More information and additional support can always be provided by national, continental and world specialised organisations, fully dedicated to NPC disease (5). Bronchodilators and antibiotics are commonly employed for the management of the associated respiratory tract infections. Sleep disturbances (narcolepsy) have been noticed in this group of patients, for which no intervention has been proposed (although melatonin has been suggested to treat insomnia), which necessitate continuous supervision. The finding of the biochemical basis of these sleep disorders could be a key finding toward developing an effective therapy for this aspect of the disease (75).

1.2.10. Overview of therapies for NPC disease

An ideal treatment for NPC disease should target an aspect of the underlying pathogenesis to achieve maximal clinical benefit and be used in conjunction with existing therapies for treating specific symptoms. In addition to symptomatic treatment, several therapeutic options have been developed and extensively examined; some are still undergoing clinical trials while others have been already approved for human treatment. To date the only specific approved therapy for NPC disease is miglustat, a substrate reduction therapy that targets GSL biosynthesis (see below). **Figure 1.8** and **Table 1.3** summarise the different therapeutics and their targets.

	Therapy	Target/(mechanism)	Models	Reference
Tested clinically	Bone marrow transplantation (BMT)	NPC dysfunction /(replace a defective protein) Benefit in NPC2 but not NPC1 patient	NPC1 patient NPC2 patient *Npc1*$^{-/-}$ mouse and *NPC1*$^{-/-}$ cat	(77) (78) (79)
	Cholesterol lowering therapy Lovastatin, cholestyramine, and nicotinic acid (statins). Probucol and Nifedipine.	Cholesterol storage /(reduce cholesterol biosynthesis) No clinical efficacy demonstrated in trials.	NPC patients *Npc1*$^{-/-}$ mouse	(80) (81)
	Substrate reduction therapy (SRT) Miglustat	Sphingosine and GSL storage/(reduce GSL storage) Clinical efficacy demonstrated and approved world-wide except by FDA	*Npc1*$^{-/-}$ mouse and *NPC1*$^{-/-}$ cat NPC patients	(82) (83, 84)
Tested in animal models	Curcumin	Altered calcium homeostasis /(calcium modulating, SERCA antagonist elevating cytosolic calcium)	*Npc1*$^{-/-}$ mouse	(37)
	Gleevec (imatinib mesylate)	Neurodegeneration (proapoptotic c-Abl/p73 system)/(anti-apoptotic effect)	*Npc1*$^{-/-}$ mouse	(85)
	By-product replacement therapy (BRT) Allopregnanolone	Defective steroidogenesis (allopregnanolone replacement)	*Npc1*$^{-/-}$ mouse	(86)
	Cyclodextrin (CD)	Cholesterol and GSL storage/(facilitate cholesterol efflux from the lysosome)	*Npc1*$^{-/-}$ and *Npc2*$^{-/-}$ mouse	(87, 88)
	Liver X receptor (LXR) agonist T0901317	Defective sterol metabolism/(increase sterol metabolism, facilitate cholesterol efflux)	*Npc1*$^{-/-}$ mouse	(89)
	Rab9 Overexpression	Intracellular mistrafficking/(alter trafficking/endocytic function)	*Npc1*$^{-/-}$ mouse	(90)
	Cyclin-dependent kinase 5 (CDK5) inhibitors	Cytoskeletal lesion formation (NFT) induced by hyperphosphorylation of tau proteins/(inhibit cytoskeletal lesion formation)	*Npc1*$^{-/-}$ mouse	(91)
	Anti-inflammatory agents	Neuroinflammation/(anti-		

	NSAIDs (ibuprofen) Anti-TNF biologics (CNTO5048)	inflammatory effect) Peripheral inflammation (liver)/(anti-inflammatory effect)	*Npc1*$^{-/-}$ mouse NPC1 liver specific knockdown mouse	(92) (93)
	Antioxidants: Tamoxifen (antioxidant properties) vitamin E and C	Oxidative stress/damage/(anti-oxidant effect)	*Npc1*$^{-/-}$ mouse	(92, 94)
	Molecular chaperones Heat shock protein 70 (HSP70) (95)	Impaired lysosomal membrane stability/(increase lysosomal membrane stability)	*Npc1*$^{-/-}$ mouse NPC patients	Unpublished Trial planned
Tested *in vitro*	Histone deacetylase inhibitors (HDACi)	underexpression of NPC1, impaired neuronal regeneration, morphology and differentiation, defective cholesterol homeostasis/(upregulating NPC1, reduce cholesterol)	*Npc1*$^{-/-}$ mouse neuronal stem cells NPC patients	(96) Trial planned
	Acid sphingomyelinase (ASM) enzyme replacement or gene transfection (*SMPD1*)	Secondary ASM deficiency/(increase ASM activity)	NPC1 patient fibroblasts	(97)

Table 1.3. Summary of therapeutic options for NPC disease discussed in this overview, with their pathological targets and tested models.

1.2.10.1. Bone marrow transplantation (BMT)/ gene therapy/protein replacement therapy

Monogenic enzyme deficiency LSDs, can be targeted using gene therapy replacing the mutant gene and thus restoring normal hydrolytic enzyme function. Multiple animal studies have provided proof of concept (98, 99). The aim is to deliver enough functional enzyme to prevent pathogenic storage, provided that the hydrolases from the normal cells can secreted and taken up by adjacent mutant cells (typically via cell surface M6P receptors) (100). There is also the need to be able to deliver the functional gene to the CNS and peripheral organs for the majority of LSDs which remains a technical challenge (101).

Based on the same principle of gene therapy utilising the advantage of cross correction, protein replacement therapy is another approach involving the administration of soluble protein in a form that could be recognised and bound to cellular receptors and taken up by lysosomes in various tissues. Modification usually includes the addition of M6P since it is ubiquitously expressed at the cell surface, thus insuring targeting to the lysosome. Although initiation of immune response (antibodies) against these proteins has been reported in some cases, this approach has proven efficient, safe and well-tolerated way of delivering therapeutic efficacy particularly in type 1 Gaucher disease (102). However, CNS delivery of the defective protein cannot be achieved by intravenous administration as lysosomal enzymes do not cross the blood-brain barrier, and therefore correction of central defects and neurodegeneration is not achieved. Targeting the cerebrospinal fluid (CSF) could be a useful therapeutic potential. Intrathecal administration of the recombinant enzyme in high concentration has proved successful in normalising lysosomal storage in the brain of animal models of some lysosomal diseases, for example mucopolysaccharidosis I (MPS I, Hurler syndrome) (103).

However, in the case of NPC1 disease, where the defective protein is not an enzyme and is a multi-membrane spanning protein, this approach has limited applicability (7). However, due to the nature of the NPC2 protein (a M6P targeted soluble intra-lysosomal protein), correction by haematopoietic stem cell transplantation (gene therapy or bone marrow transplantation) or by M6P targeted protein (protein therapy) is possible (5).

Bone marrow transplantation was first examined in murine and feline models of NPC1 disease, however, the outcome was not satisfactory and no improvement has been observed. A trial transplanting haematopoietic stem cells (BMT) producing the

soluble NPC2 protein in a child has produced encouraging results throughout the 18 month monitoring period, provided that sufficient immunosuppressive therapy is properly given (78). Whereas in NPC1 disease, BMT did not prevent further neurological deterioration observed in NPC1 patient (5, 77).

1.2.10.2. Lipid (cholesterol) lowering therapy

Since the establishment of NPC disease as a distinct disease entity, several therapeutic approaches has been proposed and examined based on the data accumulated on the underlying biochemical defect. The very first trials targeted cholesterol, as the offending molecule, through lipid lowering drugs, dietary manipulation or cytotoxic agents aiming to reduce free cholesterol levels. These trials were further encouraged by the availability of a wide range of cholesterol lowering agents and the evidence of involvement of both NPC1 and NPC2 protein in cholesterol transport. Moreover, the critical role of cholesterol homeostasis in the brain (104) could imply that such therapy would restore normal neuronal functioning and reverse the toxic effect of excessive cholesterol in these cells. In the first clinical trial in 1993 (80), three different classes of hypolipidaemic agents were used: cholestyramine (bile acid sequestrant), lovastatin (HMG-CoA reductase inhibitor) and nicotininc acid (hormone-sensitive lipase inhibitor) with an average follow up period of 4 months, cholesterol levels were successfully normalised in peripheral tissues (liver and serum) (80). However, there was no evidence of any beneficial effects of such treatments on neurological disease progression, although visceral tissues responded to some extent. Similar outcomes were seen with liver and bone marrow transplantation (5, 81, 100). When this approach was revisited in the mouse model of NPC1 disease, similar pattern of response was observed with

significant reduction in peripheral cholesterol levels but no effect on neuropathology (81).

1.2.10.3. Substrate reduction therapy (SRT)

The imino sugar *N*-butyldeoxynojirimycin (*N*B-DNJ, miglustat, Zavesca, OGT 918) was first considered for NPC disease treatment as a way of investigating the involvement of GSL storage in NPC disease pathogenesis through reversible inhibition of the first and rate limiting step of GSL synthesis (glucosylceramide synthesis). This small molecule offers the advantage of crossing the blood-brain-barrier thus exert its inhibitory effect in the CNS in addition to peripheral tissues, as shown in murine models of Tay-Sachs and Sandhoff disease (105, 106). Both *N*B-DNJ and its galactose analogue, *N*B-DGJ (being more selective than *N*B-DNJ and thus avoiding its undesirable side effects) (107) have been reported to delay onset of neurological symptoms and extend life expectancy in murine and feline models of NPC disease, concomitant with a significant reduction in GSL storage, further supporting their involvement in neuropathogenesis (82).

Miglustat, previously (2002) approved for mild to moderate type 1 Gaucher disease (108), have progressed into controlled clinical trials in NPC1 disease (83, 84, 109). Results have shown stabilisation of disease for one year or longer (in about 70% of cases). As a result, the use of miglustat was further extended by the European Union in 2009 for treating neurological symptoms in paediatric and adult NPC patients. That was then followed by other countries world-wide approving miglustat for the same use, with the notable exception of the FDA.

Another international, cohort study where assessment of patients on miglustat was made based on a disease disability scale. Treated patients had a significant delay in

disease progression assessed annually (110). Due to its adverse effects its not recommended for patients with only systemic disease as it has no effect on non-neurological manifestation (5).

1.2.10.4. Calcium-modulating agents

Many intracellular processes are dependent on cytosolic calcium, such processes include LE/Lys fusion and transport across acidic compartment membrane (111). Calcium is released from the acidic compartment in response to the second messenger NAADP, failure of sufficient calcium release and subsequent impairment of fusion/transport events has been shown to give rise to NPC phenotypes *in vitro* (111). NPC cellular phenotypes were readily corrected by calcium mobilisation from other cellular organelles following the administration of calcium-modulating agents (thapsigargin and curcumin) which are known to act as inhibitors of the sarco(endo)plasmic reticulum ATPase (SERCA) thereby elevating cytosolic calcium **(Figure 1.9)**.

It should be further emphasised that none of these calcium-mobilising agents correct the acidic compartment calcium levels (which are significantly lower in NPC cells), they rather act via elevating cytosolic calcium through inducing calcium release from other cellular compartments, thus compensating for the impaired release from the acidic compartment (37).

The figure originally presented here cannot be made freely available via ORA because of 'copyright'.

1.2.10.5. Curcumin

Since lipid accumulation in the LE/Lys compartment in NPC1 cells is thought to be the result of calcium depletion in this compartment, a logical approach to treating NPC disease cells would be to evaluate compounds, which are known to elevate calcium levels in the cell to compensate for this deficiency in the acidic store. One of these molecule is curcumin, the active component of turmeric, it has shown to be both effective and is known to be nontoxic and safe to administer.

In vivo experiments in murine model of NPC using curcumin as the therapeutic agent (a weaker SERCA antagonist than thapsigargin (112)) significantly improved life span and function of the *Npc1*$^{-/-}$ mouse. Sphingosine was the only metabolite which was not significantly reduced in NPC brain following curcumin treatment, compared to untreated *Npc1*$^{-/-}$ mice, suggesting that sphingosine mistrafficking precedes, and possibly precipitates the calcium defect in the sequence of events leading to NPC disease (37). The results from the original *in vivo* study with oral dose of 150 mg/kg were in agreement with the *in vitro* data, which raised the question of whether this is a dose-dependent response and that a higher dose could

be desirable in this case. Borbon *et al* (113) has tested this theory where *Npc1*$^{-/-}$ mice where fed a diet supplemented with 2% curcumin in two formulations. However, no additional benefit resulted from the higher dose, in contrast and due to the proposed "toxicity" of the high dose, this dose failed to increase survival rate even to the levels associated with the 150 mg/kg dose. Various curcumin formulations were tested in this trial, although they were associated with higher blood and brain levels, they did not achieve the maximal efficacy seen when the standard high purity curcumin was used. This may suggest an associated toxicity from higher plasma curcumin levels. This "hypothesis" has been further supported by experiments in animal models of neurodegenerative disease where curcumin has been shown to having neuroprotective effect, and when tested *in vitro* lower concentration was "proliferative" while increasing the concentration was cytotoxic. *In vivo* studies have shown that low levels were also neuroprotective, stimulating neurogenesis in the mouse hippocampus.

Curcumin has an established safety profile and efficacy as an anti-inflammatory, antioxidant, and anti-protein-aggregate agent at sub-micromolar concentration. It exerts its neuroprotective effect via many pleiotropic actions including anti-inflammatory, antioxidant, and anti-protein-aggregation activities, induction of heat shock protein synthesis, reducing total cholesterol and increasing high density lipoprotein cholesterol levels and also protects against neurotoxicity and excitotoxicity (114).

1.2.10.6. Gleevec (imatinib mesylate)

The p73 member of the p53 family of transcription factors regulates neuronal cell death by inducing the expression of proapoptotic genes (115) upon activation by c-Abl kinase (116). Alvarez *et al* (85) have shown the expression of the proapoptotic

c-Abl/p73 system in cerebellar neurons in *Npc1*$^{-/-}$ mice plays a role in cerebellar neurodegeneration. The study also demonstrated a positive clinical effect of inhibiting c-Abl in *Npc1*$^{-/-}$ mice using imatinib, an FDA approved drug for treating chronic myelogenous leukaemia (117). Treated mice had a significant increase in cerebellar Purkinje cell survival and a marked reduction in apoptosis in the cerebellum, accompanied by functional benefit and increased survival of treated mice.

1.2.10.7. By-product replacement therapy (BRT, allopregnanolone)

Due to the findings that *Npc1*$^{-/-}$ mice are infertile and have abnormal reproductive system, it was suggested that cholesterol sequestering has lead to defective steroidogenesis and steroid hormone deficiency. Such biosynthetic pathway is also crucial for neurosteroids, which are essential for neuronal integrity and function (86). Neurosteroidogenesis has been shown to be defective in *Npc1*$^{-/-}$ mice with significant reduction in the levels of allopregnanolone associated with diminished neuronal development (118). This represents a potential target for therapeutic intervention in NPC disease, which could be responsive to this end-product replacement therapy. Treatment of *Npc1*$^{-/-}$ mice with a single dose of allopregnanolone in the neonatal period has shown encouraging outcome with increased survival time with delayed onset of neurological symptoms, improved neurological function, increased Purkinje cell survival and reduced brain ganglioside storage (86, 118, 119). This was the first study to test the administration of potentially therapeutic compound early in the life span (day 7 postnatal) and show significant improvement associated with early intervention, due to higher penetration of the compound into the brain (86). Also, this trial has tested different formulations and routes of delivering the test compound: in drinking water,

subcutaneous pellets and subcutaneous injections, while better outcome was observed with skin pellets, suspicion has arisen regarding subcutaneous injections due to the nature of the vehicle (cyclodextrin) as it has shown to produce intrinsic effect on its own as opposed to the delivered substance (87). The findings from the first trial on allopregnanolone were further confirmed by subsequent studies where single injection of allopregnanolone at P7 resulted in a marked increase in the survival of treated mice with significant improvement of the weight loss profile, reduction of neuroinflammation, cerebellar degeneration and increase in brain myelination with greater efficacy seen with repetitive injection every two weeks following P7 dose (120, 121). However, it remains controversial as to whether all the positive effects of allopregnanolone were actually from the cyclodextrin vehicle used in these studies (87, 88).

1.2.10.8. Cyclodextrin (sterol/cholesterol binding/chelating therapy)

A trial in *Npc1*$^{-/-}$ mice combining SRT (miglustat) and BRT (allopregnanolone) have accidently revealed a beneficial therapeutic effect of the vehicle; 2-hydroxypropyl-β-cyclodextrin (CD). Although the combination therapy had an additive positive effect, the vehicle alone was associated with marked improvement (87). Simultaneously, others have shown a significant increase in the life span with delay of neurodegeneration of *Npc1*$^{-/-}$ mice receiving a single dose of CD (122).

Npc1$^{-/-}$ mice receiving chronic CD treatment alone has shown a marked improvement reflected in their increased survival with delayed onset of the disease manifestation (tremor, ataxia and gait abnormalities) in addition to reduction of neuronal cholesterol and GSL storage levels. A similar improvement was also seen in *Npc2*$^{-/-}$ mice (87).

A single injection of CD at P7 acutely increased cholesterol efflux from the lysosome in multiple organs, with enhanced synthesis of cholesterol esters and suppression of cholesterol synthesis. In addition downregulatoin of proinflammatory proteins was observed in brain and liver. Also, at early symptomatic stage of disease (~7 weeks) liver function tests were improved with marked reduction in neurodegeneration (88).

CD has also shown efficacy in the feline model (123) and is in clinical trials at the NIH. A dose-dependent negative effect of CD treatment on hearing has been reported in the feline model as well as normal cats, which may arise as a limitation for the use of high doses in the patients potentially necessitating the implementation of auditory monitoring (124).

1.2.10.9. Liver X receptor and pregnane X receptor activation

Many transcription factors are involved in sterol metabolism in the CNS and periphery, including those regulated by liver X receptor (LXR) and pregnane X receptor (PXR) (125). These receptors therefore have been the target of both genetic and pharmalogical manipulation in order to correct the defective sterol metabolismin NPC1 cells. Nuclear hormone receptors LXR in particular (including the two subclasses LXRα and LXRβ) are expressed in the brain amongst other tissues and are responsive to the pool of cytosolic cholesterol. Upon activation, for example by their native endogenous agonists oxysterols, they induce the transcription of genes involved in sterol metabolism to facilitate the flux of cholesterol (126). Oral administration of T0901317, which was developed as a selective agonist of these receptors, has been tested in *Npc1*$^{-/-}$ mice and shown to increase life span and stimulate cholesterol utilisation via these receptor responsive genes, improve neurological function and reduce CNS inflammation (89).

Activation of PXR has been also reported to be beneficiary in the NPC1 mouse (120), however, it is not as highly expressed in the cerebellum (89, 127) but the benefit could be attributed to activation in other cell populations present in the cerebellum.

1.2.10.10. Rab9 over-expression

Rab9, a small GTPase protein, plays a role in membrane trafficking (128) and represents a target to correct the mistrafficking in the endocytic system observed in NPC cells. Upregulation of Rab9 expression had a positive effect in correcting the trafficking defects in both NPC1 and NPC2 cells (129). Moreover, NPC phenotype was induced in wild-type cells by the expression of the negative mutant of Rab9 (129). Such observations suggest the involvement of the Rab9 protein in the pathology of the NPC disease. *In vivo* results form murine model of NPC disease has shown that overexpression or upregulation of the Rab9 protein is associated with correction of GSL storage and increase in life span (90). According to the current proposed model of NPC disease pathologenesis, inhibition of protein kinase C results in hypophosphorylation of vimentin (an intermediate filament) causing the entrapment of Rab9 and subsequent LE/Lys dysfunction (130) **(Figure 1.10).**

1.2.10.11. Glycogen synthase kinase 3β and cyclin-dependent kinase 5 inhibition

Glycogen synthase kinase 3β (GSK3β) and cyclin-dependent kinase 5 (Cdk5) are two proline-directed serine/threonine kinases that are involved in regulating neuronal growth, development and function (131-133). They have been implicated in the pathogenesis of Alzheimer's disease and the focus of active research in this field (134, 135). Their dysregulation and hyperactivation is associated with hyperphosphorylation of cytoskeletal proteins such as tau resulting in pathological lesions such as neurofibrillary tangles characteristic of multiple neurodegenertative diseases such as Alzheimer's, ALS and NPC disease (136, 137). The use of lithium and other GSK3β inhibitors achieved a marked reduction in tau phosphorylation (138). In addition, R-Roscovitine, a CDK5 inhibitor resulted in improvement of neurological symptoms in *Npc1*$^{-/-}$ mice (91).

1.2.10.12. Anti-inflammatory agents

Since inflammation has been implicated in the pathogenesis of neurodegenerative disease including NPC, the use of anti-inflammatory drugs (such as non-steroidal anti-inflammatory drugs (NSAIDs)) has been an attractive target for therapeutic intervention using existing drugs.

Ibuprofen was successful in alleviating CNS inflammation and improving neurological function in the *Npc1*$^{-/-}$ mice and extended their life span, with a more pronounced effect when administered in combination with miglustat (92).

The anti-TNF monoclonal antibody, CNTO5048 (mouse-rat chimeric) has been trialled in NPC1 knockdown mice (wild-type C57BL/6 mice treated with NPC1-specific antisense oligonucleotides to knockdown NPC1 protein expression in the liver) and shown an alleviation of liver disease (hepatic apoptosis and stellate cell activation were both slightly but not significantly reduced). However, the impact on neurological manifestation could not be evaluated in this model and this approach has not been tested in the authentic NPC1 mouse model (93).

1.2.10.13. Anti-oxidants

Oxidative stress in NPC1 cells generated from increased levels of reactive oxygen species (139, 140) along with marked reduction in the endogenous levels of some antioxidants such as ubiquinone (Co-enzyme Q10) (141) have been the target for multiple therapeutic interventions using antioxidants.

Female *Npc1*$^{-/-}$ mice treated with vitamin E have shown benefit in slowing disease progression and improving motor function (94).

CoQ10 supplementation was not of great efficacy due to its inability to cross the blood-brain barrier (76). Also, the use of ascorbic acid (vitamin C) in the *Npc1*$^{-/-}$ mice was associated with no significant improvement (92).

1.2.10.14. Molecular chaperones (heat shock protein 70)

Heat shock protein 70 (HSP70) is a molecular chaperone involved in reducing cell stress through decreasing lysosomal membrane permeability (142). An *in vitro* study has shown a benefit in multiple LSDs and its effects have been suggested to be mediated through stress-induced translocation of segments of the protein to the lysosome. HSP70 has shown to induce lysosomal membrane stability via its binding *in vitro* to bis(monoacylglycero)phosphate (BMP, a LE/Lys phospholipid), which is an important cofactor for the activity of ASM. NPA and NPB cells have also shown to have a significant reduction in lysosomal stability, which was successfully reversed upon treatment with recombinant Hsp70 (95). Preclinical studies in *Npc1* null mice have been conducted (Kirkegaard *et al.*, submitted) and a clinical trial in NPC patients is planned.

1.2.10.15. Histone deacetylase inhibitors

Histone deacetylases (HDAC) are important regulatory enzymes of gene transcription mediating acetylation and deacetylation of key proteins such as histones, transcription factors and chaperones. The link between this regulatory element and NPC1 disease arose from studies showing a correlation between histone hyperacetylation and cAMP induced expression of NPC1 (143). Additionally, the use of the weak HDAC inhibitor (HDACi), valporic acid, improved cholesterol mistrafficking in neuronal stem cells from *Npc1*$^{-/-}$ mice (96).

The use of small molecule HDACi in human NPC1 fibroblasts has been reported to be associated with improved phenotype reflected in significant reduction in cholesterol levels almost back to normal levels within 72 hours as well as an increase in the expression of the NPC1 protein. HDAC1 and HDAC2 have been suggested as the most implicated isofroms and therefore represent the most

promising targets for therapy. An example of an orally available HDACi capable of crossing the blood-brain barrier and have shown efficacy in cultured fibroblasts is LBH589 (panobinostat) which has been tested in a Phase III clinical trial for cancer (144).

This pathway was also identified as a potential disease modifier in a genome-wide screen in the NPC1 yeast model and subsequently multiple HDACs were shown to be upregulated in NPC1 patients' fibroblasts, the expression levels of most of them were successfully restored by the approved HDACi suberoylanilide hydroxamic acid (145). A clinical trial of HDACi is planned.

1.2.10.16. Acid sphingomyelinase (ASM) enzyme replacement or *SMPD1* gene transfection

ASM is a lysosomal enzyme that is responsible for sphingomyelin hydrolysis to ceramide and phosphocholine and therefore is important in regulating cholesterol and sphingomyelin metabolism. Its deficiency is the hallmark of Niemann-Pick type A and B diseases. Although the acid sphingomyelinase gene is not defective in NPC disease, the enzyme activity seems to be reduced to some extent as a secondary consequence of storage *in vitro* and *in vivo* (mice and patients) (146-148). Correction by transfection with the normal functioning *SMPD1* gene or acid sphingomyelinase enzyme replacement has been shown to be effective in reducing the lysosomal cholesterol storage *in vitro* (NPC1-deficient CHO cells and patient-derived fibroblasts**)** (97).

1.3. Aims of this thesis

This thesis aimed to test potential therapeutic agents in NPC disease based on targeting novel steps in the pathogenic cascade. Efficacy was determined on the basis of improving neurological function. Based on a novel discovery I have also focused on our understanding of drug metabolism in this disease and how this could help in optimising drug dosing and delivery to achieve optimal efficacy. The major elements of the thesis are organised as follows:

Chapter 2 – Characterisation of the Cytochrome P450 system and drug metabolism in NPC disease.

Chapter 3 – Evaluation of therapeutic approaches in an authentic mouse model of NPC1 disease.

Chapter 4 – Evaluation of the neuroprotective effects of Cogane and Myogane two structurally related, orally available, neurotrophic compounds in NPC1 disease.

Chapter 5 - Investigation of Crohn's disease-like intestinal inflammation in the mouse model of NPC1 disease and in NPC patients.

Chapter 6 - Conclusions drawn from Chapters 2-5.

Chapter 2. Drug Metabolism Defects in Niemann-Pick Type C Disease

2.1. Introduction

We recently suggested that *Npc1*$^{-/-}$ mice might have defective drug metabolism, as they show signs of toxicity and reduced tolerability to some liver metabolised compounds when administered at doses well tolerated in other mouse models (92). In contrast, miglustat, which is not metabolised in the liver and excreted unchanged in the urine (149), can be safely introduced even at very high dose in *Npc1*$^{-/-}$ mice (82). In this chapter I have therefore explored dug metabolism in *Npc1*$^{-/-}$ mice.

Most drugs are primarily metabolised via the cytochrome P450 system. This superfamily of enzymes was investigated to identify any underlying defect in this disease model.

In NPC1 disease, liver phenotypes include significant lipid storage and pathology that can present in the neonatal period as cholestatic jaundice, which in most cases resolves spontaneously whereas in about 10% of cases it progresses to fatal liver disease and premature death (5, 150, 151). Lipid sequestration (e.g. cholesterol) in the LE/Ly leads to paradoxical deficiency in other compartments (e.g. ER) has the potential to lead to defects in the biosynthesis of downstream metabolites (such as steroid hormones, bile acids and vitamin D) (86, 152).

Marked increase in liver enzymes (aspartate transaminase AST and alanine transaminase ALT) and apoptosis was seen in the *Npc1*$^{-/-}$ mouse (153). Furthermore isolated liver disease was successfully induced in BALB/c mice by specifically knocking down the expression of *Npc1* only in the liver, the liver autonomous phenotype was rescued by partial expression of NPC1 protein (154).

In the course of assessing potential small molecule therapies in the *Npc1*$^{-/-}$ mouse, we have made a consistent observation of drug toxicity at doses tolerated in normal

mice. This only applied to drugs metabolised in the liver (examples include; curcumin, ibuprofen, and vinpocetine). This observation suggested a potential deficit in the cytochrome P450 system.

The cytochrome P450 system plays a role in both lipid homeostasis (via regulating cholesterol, vitamin D, oxysterol and bile acid metabolism) and detoxification of xenobiotics and endogenous compounds (e.g. toxic bile acids) (155).

We therefore in this chapter, have investigated drug metabolism in detail where both cytochrome P450 enzyme activity and gene expression were assessed in the mouse and cat models of NPC1 disease and in NPC patients. We have also investigated a potential mechanism underlying this defect and implicated bile acid deficiency as playing a role. In addition, we have investigated bile acid supplementation and its effect on both drug metabolism (discussed in this chapter) and neurological function (**Chapter 3)** in *Npc1*$^{-/-}$ mice.

2.2. Methods

2.2.1. Mice

The spontaneous mutant mouse model of NPC on a BALB/C background (BALBc/NPCnih, BALB/cNctr-*Npc1*^{m1N}/J, *Npc1*$^{-/-}$) with wild-type (*Npc1*$^{+/+}$) and heterozygotes littermates (*Npc1*$^{+/-}$) was maintained by breeding heterozygotes obtained from The Jackson Laboratory (The Jackson Laboratory, Charles River, UK) (39).

All mice were bred and housed under non-sterile conditions, under specific pathogen-free conditions in the animal facilities at the University of Oxford (Oxford, UK), with food and water available ad libitum and a 12-h light–dark cycle (light on from 6.00 a.m. until 6.00 p.m.) with a temperature of 22-24°C and a relative humidity of 50-60%.

All animal studies were conducted using protocols approved by the UK Home Office for the conduct of regulated procedures under a project licence (Animal Scientific Procedures Act, 1986).

2.2.2. Genotyping

Genotypes of the mice were determined by polymerase chain reaction (PCR) analysis of ear DNA, as described previously (156, 157). At 10 days, ear biopsies were collected for DNA extraction. The tissue pieces were digested in alkaline lysis buffer (25 mM NaOH /0.2 mM EDTA) for 15 minutes at 95°C and neutralised with 40 mM Tris HCl (pH 5.5). PCR was used to determine genotypes at the *Npc1* locus using Dream Taq Green PCR Master mix 2X (K1081, Fermentas, Fisher, UK) and the following primers: 8F-GGTGCTGGACAGCCAAGTA and INTR3-GATGGTCTGTTCTCCCATG, expected fragment size, WT allele: 1048bp and NPC^{nih} allele: 1209 bp; annealing temperature was 58°C. Cycle Conditions: 94°C (3

min), (94°C, 30 seconds; 58°C, 30 seconds; 72°C, 30 seconds) 35 Cycles, 72°C (7 minutes) and separated on 1.5% agarose gel with TAE buffer (0.04 M tris-acetate, 0.001 M EDTA) with 0.5 µg/mL ethidium bromide. DNA ladder (Q-step 2, Yorkshire Bioscience Ltd, York, UK), positive (heterozygous sample) and negative controls (milliQ water) were run alongside the samples. Bands were visualised using ethidium bromide corresponding to 1048 bp (for wild-types) or 1209 bp (for homozygotes) and both bands seen in heterozygotes.

Alternatively, DNA was extracted from mouse ear biopsies by digesting overnight at 55 °C in lysis buffer (0.5 mL containing: 0.5 mg/mL proteinase-K (Calbiochem, Nottingham, UK), 1% SDS, 10 mM Tris pH 7.5, 10 mM EDTA and 150 mM NaCl). Samples were heated at 95°C for 10 minutes to deactivate the proteinase-K and centrifuged at 13,000 rpm for 10 minutes at room temperature to remove debris. PCR was performed to determine the genotype at the *Npc1* locus using Dream Taq Green PCR Master mix 2X (K1081, Fermentas, Fisher, UK), the following primer pairs and 35 cycles of amplification: IMR928 5' CTG TAG CTC ATC TGC CAT CG 3', IMR929 5' TCT CAC AGC CAC AAG CTT CC 3', Annealing temperature 55 or 57°C, Expected fragment size 173 bp and IMR927 5' TGA GCC CAA GCA TAA CTT CC 3', IMP258F 5' GGT GCT GGA CAG CCA AGT A 3', Annealing temperature 53°C, Expected fragment size 475 bp. The PCR cycle conditions: pre-heating at 94°C for 4 minutes, annealing at 57°C for 30 seconds and extension at 72°C for 5 minutes. Amplified product was separated using 2% agarose gel with TAE buffer with ethidium bromide. DNA ladder, positive and negative controls were run alongside the samples. Bands were visualised using ethidium bromide corresponding to 173 bp (for wild-types, with primers IMR928 and IMR929) or 475

bp (for homozygotes with primers IMR927 and MP258F) and both bands seen in heterozygotes.

2.2.3. Samples

2.2.3.1. Murine Model of NPC disease: Tissue Samples

The text originally presented here cannot be made freely available via ORA.

Liver samples were collected from *Npc1*$^{-/-}$ and *Npc1*$^{+/+}$ mice at 3, 6 and 9 weeks of age (n=4-7 per group). Aged *Npc1*$^{+/-}$ heterozygotes (9 weeks, n=7) were also analysed in some studies.

2.2.3.2. Feline Model of NPC disease: Tissue Samples

Liver samples from the feline model of NPC1 disease were kindly provided by Dr. Charles Vite (University of Pennsylvania, USA) (45). Samples were collected from 24 week-old *NPC1*$^{-/-}$ cats and age-matched *NPC1*$^{+/+}$ and *NPC1*$^{+/-}$. Also, liver samples from cats treated with subcutaneous cycbrownblbodextrin (8000 mg/kg, every 7 days starting at 3 weeks of age) were collected at 21, 38 and 59 weeks of age. Cats were maintained in the animal colony of the School of Veterinary Medicine, University of Pennsylvania, under the guidelines of the National Institutes of Health and US Department of Agriculture for care and use of animals in research. The study was approved by the University of Pennsylvania Institutional Animal Care and Use Committee.

2.2.3.3. Human Samples

Human post mortem liver biopsies from three NPC (not confirmed whether NPC1 or NPC2) and three age- and gender-matched controls were obtained from the

NICHD Brain and Tissue Bank for Developmental Disorders at the University of Maryland, Baltimore, MD, contract HHSN275200900011C, Ref. No. N01-HD-9_0011. The NICHD Institutional Review Board approved human studies.

NPC patient IDs: UMB# M4002M, UMB# M4003M and UMB# M4004M), and the control IDs: UMB#1500 6 years old had a perforated bowel, haemopericardium, hypoxic ischaemic encephalopathy, secondary to a motor vehicle accident. UMB#662 12 years old died of a traumatic accident with multiple injuries. UMB#1672 died of asphyxia.

2.2.4. Phenobarbital induction study

Age-matched (7 weeks) *Npc1*$^{+/+}$ and *Npc1*$^{-/-}$ mice were injected with either phenobarbital (to induce liver microsomal CYP450 enzymes, 80 mg/kg body weight/ day, sodium phenobarbital Sigma-Aldrich) or a vehicle (equivalent amount of 0.9 % sodium chloride) intra-peritoneally for 4 consecutive days (n=3 per group). Twenty four hours after the final injection mice were sacrificed (following overnight starvation for 16 hours) and livers were collected following PBS perfusion (for CYP450 enzyme activity measurements) and fixed perfused livers were collected following perfusion via the left ventricle with a fixative (2% paraformaldehyde and 2% gluteraldehyde in 0.1 M phosphate buffer, pH 7.4) and livers were removed and analysed for electron microscopy and enzyme activity.

2.2.5. Electron microscopy

Liver samples were preserved in the fixative solution and post-fixed with a 1% osmium tetroxide, washed in several changes of 0.1 M phosphate buffer and divided further into two bottles per mouse, and given two changes of 70% ethanol. One group of four were stained en-bloc with para-phenylene diamine in 70% ethanol for

30 minutes on ice, the other with 1% magnesium uranyl acetate in 70% ethanol for 45 minutes at room temperature. Dehydration was continued through an ascending ethanol series; two changes each of 80%, 90%, 95% and three of 100% ethanol (dried over copper sulphate), followed by 2 changes of propylene oxide, before infiltration with resin and finally embedding into capsules. The resin was polymerised for 24 hours at 60°C. Both Araldite and an Araldite/Epon mixture were used.

All mice were perfused first with a normal saline solution, 5-10minutes and then in a perfusate containing 4% paraformaldehyde, 15% picric acid and 0.5% glutaraldehyde in 0.1 M cacodylate buffer for 20 minutes. After removal, the liver was immediately cut into slices using a single-edged razor blade and placed in large vials containing the perfusate fixative for immunocytochemistry. Some of these sections were selected from each mouse, cut further into smaller pieces, and transferred into small vials containing a higher percentage of glutaraldehyde (2.5%) for preservation of morphology together with 2% paraformaldehyde, 2mM calcium chloride and 0.1% picric acid in 0.1 M cacodylate buffer. All tissues were fixed on a rolling or tilting platform overnight at 4°C. The liver samples after fixation and embedding were cut into 1-2 mm cubes in 0.1 M cacodylate buffer containing 2 mM calcium chloride, washed with three changes of the cacodylate buffer, and post fixed for 90 minutes in buffered 1% osmium tetroxide solution. Post-fixation, the samples were washed in 0.1 M cacodylate buffer containing calcium (2 mM), and then with three changes of maleate buffer (sodium hydrogen maleate and sodium hydroxide) at pH 5.15, prior to further fixation and staining in 1.5% uranyl acetate in maleate buffer, pH 6.00 in the dark for one hour at room temperature.

After washing the samples were dehydrated rapidly through an ascending ethanol

series, with the final dehydration comprising three changes of dry ethanol performed at room temperature over one hour. Samples were put through three changes of propylene oxide and then infiltrated with a 1:1 mixture of propylene oxide and araldite for 1.5 hours, the tops of the vials were then removed and the propylene oxide allowed to evaporate from the resin for an hour in the hood, this more concentrated mixture was then removed and replaced with araldite for 2 hours. Pieces of the liver from each vial were then dropped onto the top of filled and labelled embedding moulds and left to sink to the bottom overnight. Embedding moulds were then put into a 60°C oven for polymerisation for 2-3 days. From each block of the polymerised samples, thick sections were cut to examine at the light microscope level for selection of areas for further sectioning for the microscope. Electron microscopy was performed in collaboration with Wendy Tynan, Department of Pharmacology, University of Oxford

2.2.6. Cytochrome P450 Activity Assay

2.2.6.1. Hepatic Microsomal Preparation

Livers were freshly harvested, weighed and minced in ice-cold KCl (1.15 %, w/v). Livers were homogenised using a Polytron in ice-cold SET buffer (0.25 M sucrose, 5 mM EDTA and 20 mM Tris-HCl, pH 7.4), 1:3 (w/v). Liver homogenates were then subjected to differential centrifugation at 4°C as follows: homogenates were first centrifuged at 1,000 g for 20 minutes, the post-nuclear supernatants were then centrifuged at 12,000 g for 30 minutes and the resultant post-mitochondrial fractions (supernatants) were centrifuged at 100,000 g for 60 minutes. Microsomal pellets were re-suspended in ice-cold homogenisation (SET) buffer (1:3 w/v) and either further analysed immediately or stored at –80°C. Microsomal protein concentrations were measured using the BCA assay with bovine serum albumin as a standard.

2.2.6.2. Enzyme Activity

P450 reductase activity was measured spectrophotometrically using a Jenway 6305 Spectrophotometer following the NADPH-dependent reduction of cytochrome C using a commercial cytochrome P450 reductase assay kit (Cytochrome C Reductase (NADPH) Assay Kit, CY0100, Sigma-Aldrich). Microsomal preparations (about 50 μg) were incubated with 950 μL of 36 μM cytochrome C in potassium phosphate buffer (300 mM, pH 7.8) containing 0.1 mM EDTA. The mixture was incubated at 25° C and the reaction was initiated by the addition of 100 μL of 0.85 mg/mL NADPH. The rate of the reduction of cytochrome C reaction was followed at 550 nm. Activity was expressed as nmol cytochrome C reduced per min per mg of microsomal protein, using an extinction coefficient of 21.1 $mM^{-1}.cm^{-1}$ for reduced cytochrome c, to convert change in absorbance to amount of product formed.

To investigate the individual subfamilies of enzymes or even some isoenzymes, the following reactions were assayed: ethoxyresorufin O-deethylation (EROD) for CYP1A1, 1A2, methoxyresorufin O-demethylation (MROD) for CYP1A2, pentoxyresorufin O-dealkylation (PROD) for CYP2B10 or 2B only and BROD for 3A, but it is also catalysed by other isoforms including 1A, 2A and 2B to a lesser extent (158-161). All samples were assayed in duplicate on a minimum of two separate occasions.

Microsomal preparations were incubated with 50 mM Tris–HCl (pH 7.6), $MgCl_2$ (25 mM), liver microsomes (0.5 mg protein/mL) and 5μM probe substrate (7-methoxyresorufin, 7-ethoxyresorufin, 7-pentoxyresorufin and 7-benzyloxyresorufin, obtained from Sigma-Aldrich, UK). Reactions were started by adding NADPH (0.25 mM, final concentration) and after 10 min of incubation at 37°C, the amount of resorufin formed was spectrofluorimetrically measured using a microplate reader

(FLUOstar OPTIMA), using wavelengths of (Ex. 570-10, Em. 600-10) 522 nm and 586 nm for excitation and emission, respectively. The amount of product formed and thus activity was determined by comparison to a standard curve made with pure resorufin (Sigma-Aldrich) (0-250 pmol) dissolved in DMSO and made up to the final volume with Tris–HCl/$MgCl_2$ buffer. Microsomal protein content was determined by bicinchoninic acid protein method (Sigma-Aldrich, Poole, Dorset, UK) and bovine serum albumin as standard.

The O-dealkylation of these compounds by the cytochrome P450 mixed function monooxygenase system has been shown to have selectivity towards the catalysing isoform, in mice: MROD is selectively being catalysed mainly by the 1A2 subfamily (1A1 and to lesser extent 1A2), EROD by 1A1, PROD by 2B and BROD by the 3A.

2.2.6.3. Western blotting

To detect the expression levels of cytochrome P450 reductase in microsomal preparations from liver homogenates:

15 μg of microsomal protein was electrophoretically separated on 12% SDS-PAGE at 100 V for 120 min using an XCell SureLock Mini-Cell (Invitrogen).

Proteins were transferred onto Hybond-P polyvinylidene difluoride (PVDF) membranes (GE healthcare, Chalfont St. Giles, UK) using the Xcell II Blot Module (Invitrogen), and the membranes were blocked with Tris-buffered saline containing 0.1% Tween 20 and 5% BSA at room temperature for 3 h.

After washing with Tris-buffered saline containing 0.1% Tween 20, the membranes were incubated overnight at 4°C with a primary antibody, rabbit anti-mouse cytochrome P450 reductase (Abcam Ltd., Cambridge, UK, ab13513) diluted 1:1,000 in blocking solution.

Membranes were washed with TBST and incubated at room temperature for 1 hour with a peroxidase-conjugated goat anti-rabbit IgG (1:5,000, Vector Laboratories) in blocking solution.

Immunoreactive bands were visualised by an enhanced chemiluminescence detection kit (SuperSignal West Pico Chemiluminescent Substrate ECL kit#34077, Thermo Scientific) and high performance chemiluminescence film (GE healthcare).

2.2.8. Bile Acid Supplementation

Npc1$^{-/-}$ mice (n=3 per group) were fed either normal chow (RM1 maintenance diet; SDS, London, UK) or normal chow supplemented with ursodeoxycholic acid (UDCA, 0.5%, w/w, Sigma-Aldrich) mixed with the powdered diet, while *Npc1*$^{+/+}$ littermates were maintained on normal chow. Treatment started at weaning and mice were sacrificed at 9 weeks of age and dealkylation reaction rates in the liver were determine as described above.

2.2.10. Statistics

Data presented as mean ± SEM, unless otherwise stated in the figure legend.

The text originally presented here cannot be made freely available via ORA.

A two-tailed, unpaired t test, with Welch's correction when necessary, was performed to determine the significance of the difference in cytochrome P450 gene expression levels/residual enzyme activities/AUC values between *Npc1*$^{+/+}$ and *Npc1*$^{-/-}$ mice at each age. One-way ANOVA with Tukey's post-hoc test was used to compare all sets of data where applicable. Statistical analysis was performed with GraphPad Prism v5.

2.3. Results

Many small molecule therapies have been evaluated as possible therapeutics in *Npc1*$^{-/-}$ mice. We have recently suggested that *Npc1*$^{-/-}$ mice might have defective drug metabolism, as they show signs of toxicity and reduced tolerability (reduced rate of growth, hunched posture, poor coat condition) to compounds, which are primarily subject to first-pass metabolism in the liver. This includes compounds administered at dose rate reported to be well tolerated in other mouse models/inbred mouse strains. However, when lower doses were used in *Npc1*$^{-/-}$ mice positive therapeutic benefits were observed (92). The reduced doses required in *Npc1*$^{-/-}$ mice are summarised along with the normal dose used in studies in other mouse strains **(Table 2.1)**. In contrast, miglustat, which is not metabolised in the liver and excreted unchanged in the urine (149), can be safely administered even at very high doses in *Npc1*$^{-/-}$ mice (82).

Drug	Normally Effective Dose (mg/kg/day)	Adjusted Reduced Dose (mg/kg/day) in *Npc1*$^{-/-}$ mice	Notes	References
Curcumin	300-1250	150	-Liver metabolised. -Inhibits some CYP450 isoforms.	(162-164)
Ibuprofen	300-800	100	-Cytochrome P450 metabolised.	(165)
Vinpocetine	10	2	-Cytochrome P450 metabolised.	(166)

Table 2.1. Examples of therapeutic agents in *Npc1*$^{-/-}$ mice, with their optimal doses reported in other mouse models and the reduced doses required in *Npc1*$^{-/-}$ mice to avoid toxicity.

Together, these observations prompted us to investigate whether there was reduced drug detoxification capability in the *Npc1*$^{-/-}$ mouse. Since the vast majority of drugs are primarily metabolised via the cytochrome P450 system, this superfamily of enzymes was investigated to identify any underlying defect in this mouse disease model.

We first studied dealkylation reactions at 3, 6 and 9 weeks of age in *Npc1*$^{-/-}$ mice and found significantly reduced rates at 9 weeks (late symptomatic stage) **(Figure 2.3 A, B and C)**. All dealkylation reactions were significantly lower at 9 weeks in the *Npc1*$^{-/-}$ (down to 47, 45, 71 and 51% of age-matched controls, p=0.0002, <0.0001, 0.0377 and 0.0013 for MROD, EROD, PROD and BROD respectively) **(Figure 2.3 C)**. *Npc1*$^{-/-}$ mice also had significantly reduced cytochrome P450 reductase activity, which was about 42% of age-matched controls (p=0.037) **(Figure 2.3 D)**. The reductase activity was significantly reduced by six weeks of age in the *Npc1*$^{-/-}$ versus *Npc1*$^{+/+}$ mice (p=0.022) **(Figure 2.3 D)**. The rates of these four reactions were slightly reduced at 3 weeks of age **(Figure 2.3 A)** with the diminishing activity persisting at the early symptomatic stage (6 weeks, **Figure 2.3 B)** and becoming more prominent at the late symptomatic stage nearing end stage at 9 weeks at which stage heterozygous mice seems to develop the phenotype as well (cytochrome P450 reductase activity was down to 34%, p=0.019 at 9 weeks) **(Figure 2.3 D).**

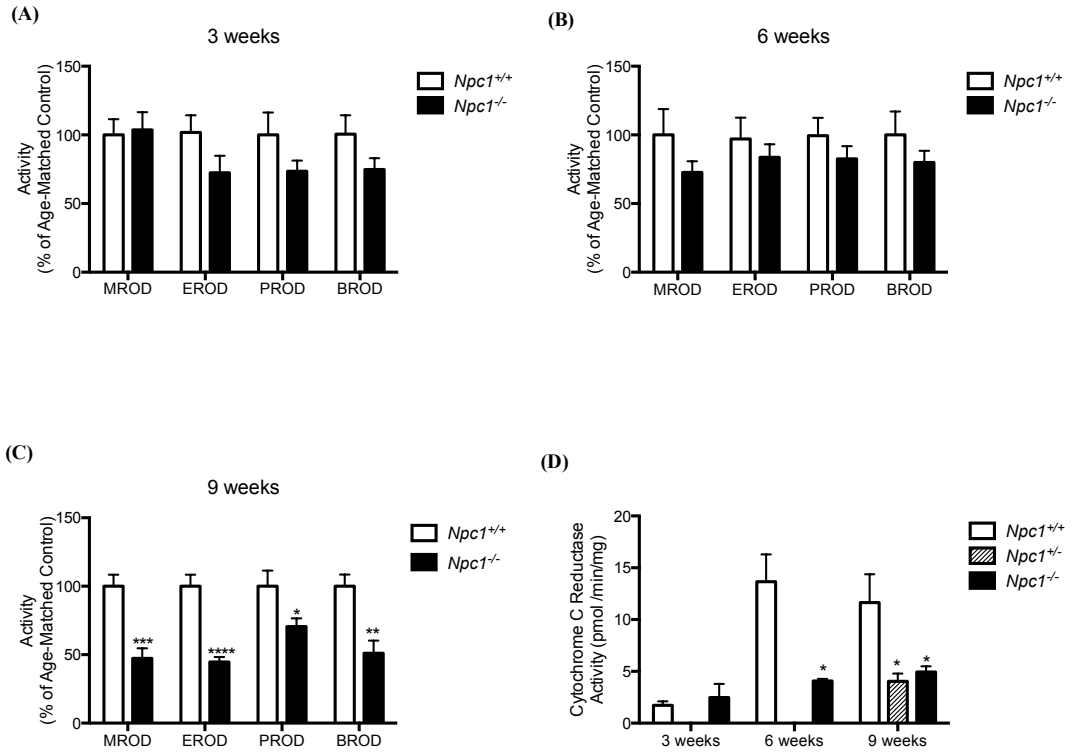

Figure 2.3. (A), (B) and (C) Activity of CYP450 catalysed reactions in mouse model of NPC1, shown as percent of age-matched controls at 3, 6 and 9 weeks of age. (D) Activity of Cytochrome c reductase in mouse model of NPC1 at 3, 6 and 9 weeks of age. Data are expressed as pmoles cytochrome c reduced per minutes normalised for microsomal protein content (mg). Data are presented as mean ± SEM, n=3-9, *p<0.05, **p<0.01, ***p<0.001 ****p<0.0001, calculated using two-tailed unpaired t test with Welch's correction as necessary and one-way ANOVA test with Tukey's post-hoc test. MROD, methoxyresorufin-O-dealkylation; EROD, ethoxyresorufin-O-dealkylation; PROD, pentoxyresorufin-O-dealkylation; and BROD, benzoxyresorufin-O-dealkylation.

In both human and mouse hepatocytes, cytochrome P450 isoforms show selectivity for specific substrates (158, 161). EROD and MROD are mainly catalysed by CYP1A, BROD catalysed predominantly by CYP3A (CYP1A and CYP2A to lesser extent) and PROD is catalysed by CYP2B (161).

This defect was also further delineated in the feline model of NPC1 disease. Although the NADPH: cytochrome P450 reductase activity was not conclusive, the rates of the cytochrome P450-catalysed O-dealkylatoin reactions were significantly lower in affected and in the heterozygous cats compared to the wild-types **(Figure 2.6 A to D)**. In liver tissue from *NPC1*$^{-/-}$ cats, MROD and EROD activity levels were down to 19% (p=0.006 and 0.001, respectively) of wild-type and PROD

activity was down to 41% (p=0.003) of age-matched controls. In *NPC1*$^{+/-}$ cats MROD, EROD, and PROD activity levels were down to 39, 57 and 42% of age-matched controls, respectively (p=0.026, 0.035 and 0.003, respectively). There was however no significant reduction in the BROD activity in the *NPC1*$^{-/-}$ cats (p=0.380) **(Figure 2.6 D)**, although the activity was reduced to 36.5% of the control mean but not significant due to high variability in the controls.

Expression levels of the CYP3A (the major subfamily of the P450 system, responsible for about 50 % of drug metabolism (168)), was also significantly reduced in the livers of *NPC1*$^{-/-}$ cats compared to control cats (85% reduction, p=0.009) **(Figure 2.6 E and F).**

In both the mouse and cat models of NPC1, cyclodextrin (2-hydroxypropyl-β-cyclodextrin (CD)) is an effective therapy that reduces pathology and significantly extends life span (123, 169). Although, CD treatment did not correct enzyme activity in *NPC1*$^{-/-}$ cat liver **(Figure 2.6 A-D)** (p=0.994, 0.961, 0.225 and 0.988 for MROD, EROD, PROD and BROD, respectively), Cyp3A expression showed significant improvement in response to cyclodextrin treatment (p=0.040), however this increase in protein did not translate into increased activity **(Figure 2.6 E and F)**, possibly due to known inhibition of this pathway by cyclodextrin (170). Although there was a slight increase in the activities of the O-dealkylation catalyzing enzymes in response to CD treatment, this increase was progressive with age **(Figure 2.7)**; which could imply that this trend reflects a developmental effect.

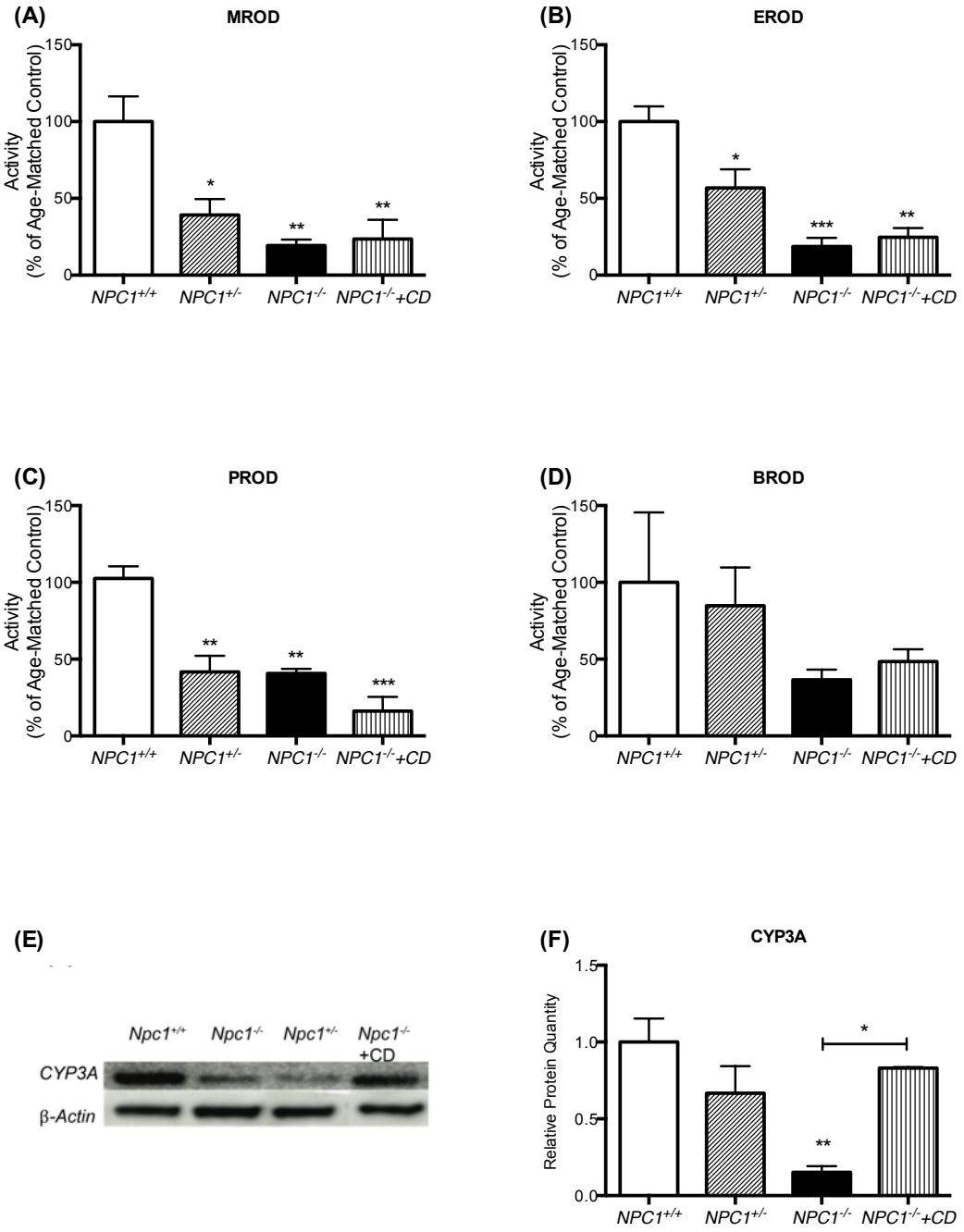

Figure 2.6. Activity of cytochrome P450 catalysed reactions in age-matched *NPC1*$^{+/+}$, *NPC1*$^{+/-}$ and *NPC1*$^{-/-}$ cats, presented as percentage of age-matched controls, 2-hydroxypropyl-β-cyclodextrin (CD) treated *NPC1*$^{-/-}$ cats were also included (A-D). (E) Representative western blot analysis of CYP3A and (F) Relative CYP3A protein quantitation in *NPC1*$^{+/-}$, and *NPC1*$^{-/-}$ compared to age-matched *NPC1*$^{+/+}$ cats, CD treated *NPC1*$^{-/-}$ cats were also included. Note due to small sample numbers all 3 ages (21, 38, and 59 weeks) CD treated animals were combined for this figure. Data are presented as mean ± SEM, n=3. *p<0.05, **p<0.01, ***p<0.001, calculated using one-way ANOVA test with Tukey's post-hoc test. MROD, methoxyresorufin-O-dealkylation; EROD, ethoxyresorufin-O-dealkylation; PROD, pentoxyresorufin-O-dealkylation; and BROD, benzoxyresorufin-O-dealkylation.

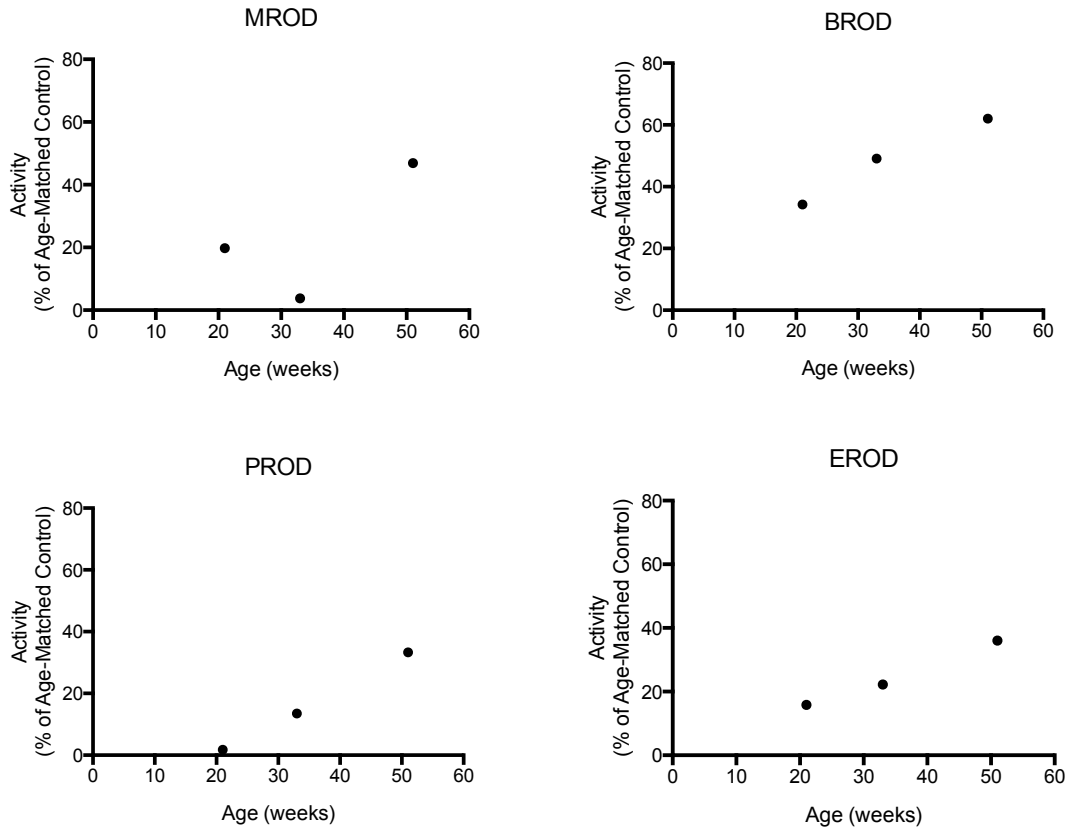

Figure 2.7. Effect of cyclodextrin treatment (CD, at a dose of 8,000 mg/kg/day) on the activity of CYP450 catalysed reactions in feline model of NPC1, shown at different disease stages and expressed as % of controls (n=1 per time point). MROD, methoxyresorufin-O-dealkylation; EROD, ethoxyresorufin-O-dealkylation; PROD, pentoxyresorufin-O-dealkylation; and BROD, benzoxyresorufin-O-dealkylation.

Autopsy liver samples from NPC1 patients and age-matched controls were also assessed to evaluate the findings in the murine and feline models translated to patients. An approximately 75% reduction (p=0.005) in cytochrome P450 reductase activity in liver microsomes was observed in post-mortem tissue biopsies taken from NPC patients compared to controls **(Figure 2.8 A and B)**. MROD and EROD activities were also lower in the patients; however, the differences were not statistically significant (p=0.269 and 0.378 for MROD and EROD, respectively) **(Figure 2.8 C)**, possibly due to too much individual variability (patients different ages). A significantly lower CYP3A expression was also seen in these patients (p=0.008) **(Figure 2.8 D)**.

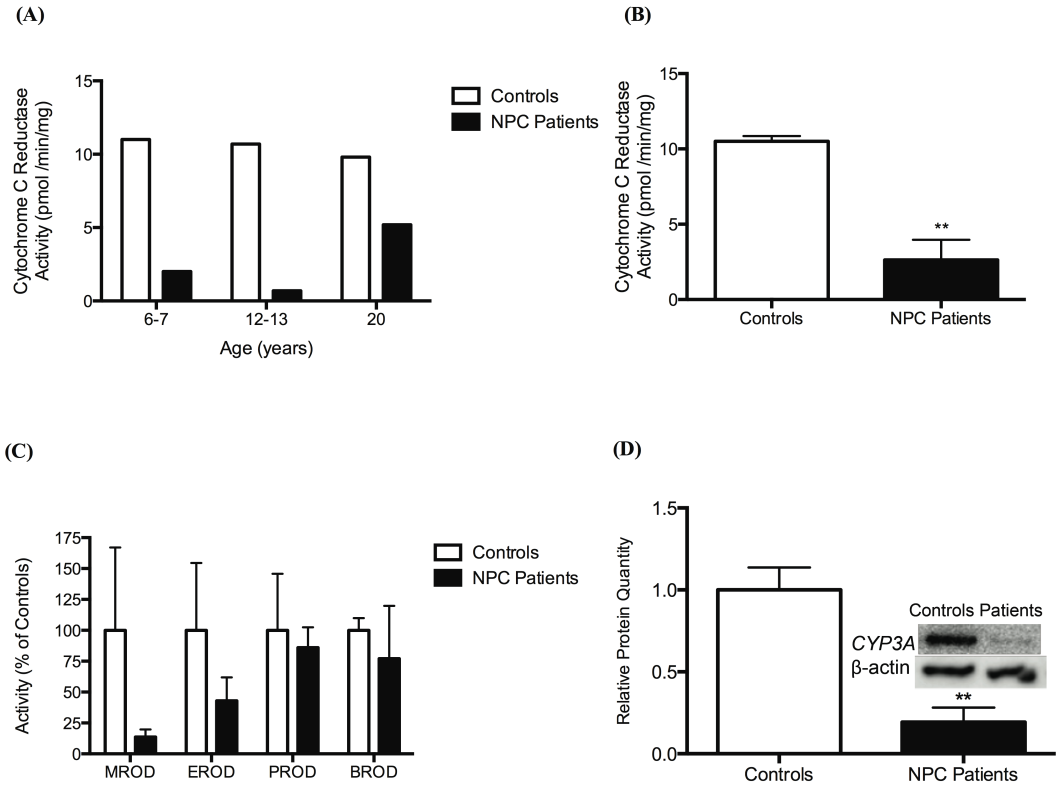

Figure 2.8. (A) Activity of Cytochrome c reductase in NPC patients at various disease stages and age-matched controls. Data are expressed as pmoles cytochrome c reduced per minute, normalised for microsomal protein content (mg). (B) Combined results from panel A. (C) Activity of CYP450 catalysed reactions in NPC patients and age-matched controls. Data are expressed as percentage of controls. (D) Representative western blot analysis of CYP3A in livers of NPC patients and their controls with relative CYP3A protein quantitation. Data are presented as mean ± SEM, n=3. $^{**}p<0.01$, calculated using two-tailed, unpaired t test. MROD, methoxyresorufin-O-dealkylation; EROD, ethoxyresorufin-O-dealkylation; PROD, pentoxyresorufin-O-dealkylation; and BROD, benzoxyresorufin-O-dealkylation.

phenobarbital, a CYPP450 2B inducer (enhancing the rate of both BROD and PROD reactions (175) in addition to CYP3A activity (176)), was administered to *Npc1*$^{-/-}$ and *Npc1*$^{+/+}$ animals to see the effect of NPC1 defect in inducible drug metabolism. Interestingly, although baseline activities were reduced in the *Npc1*$^{-/-}$ mice, pretreatment with phenobarbital resulted in an enhanced response compared to wild-type control animals **(Figure 2.11)**.

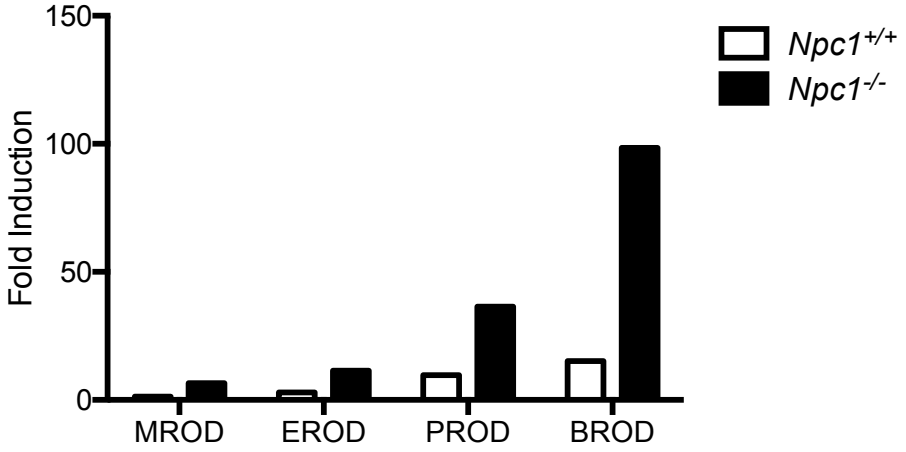

Figure 2.11. Effect of phenobarbital induction on the activity of CYP450 catalysed reactions in *Npc1*$^{-/-}$ and *Npc1*$^{+/+}$ mice. Data presented as fold induction (n=1).

Furthermore, electron micrographs of hepatocytes in liver samples from treated and untreated *Npc1*$^{-/-}$ and *Npc1*$^{+/+}$ mice, show differential proliferation of smooth ER (SER) **(Figure 2.12)**. Hepatocytes from wild-type mice treated with phenobarbital showed a typical proliferation of SER (177), whereas phenobarbital challenged *Npc1*$^{-/-}$ hepatocytes although had similar proliferation of SER, presented with marked elaboration of rough ER (RER).

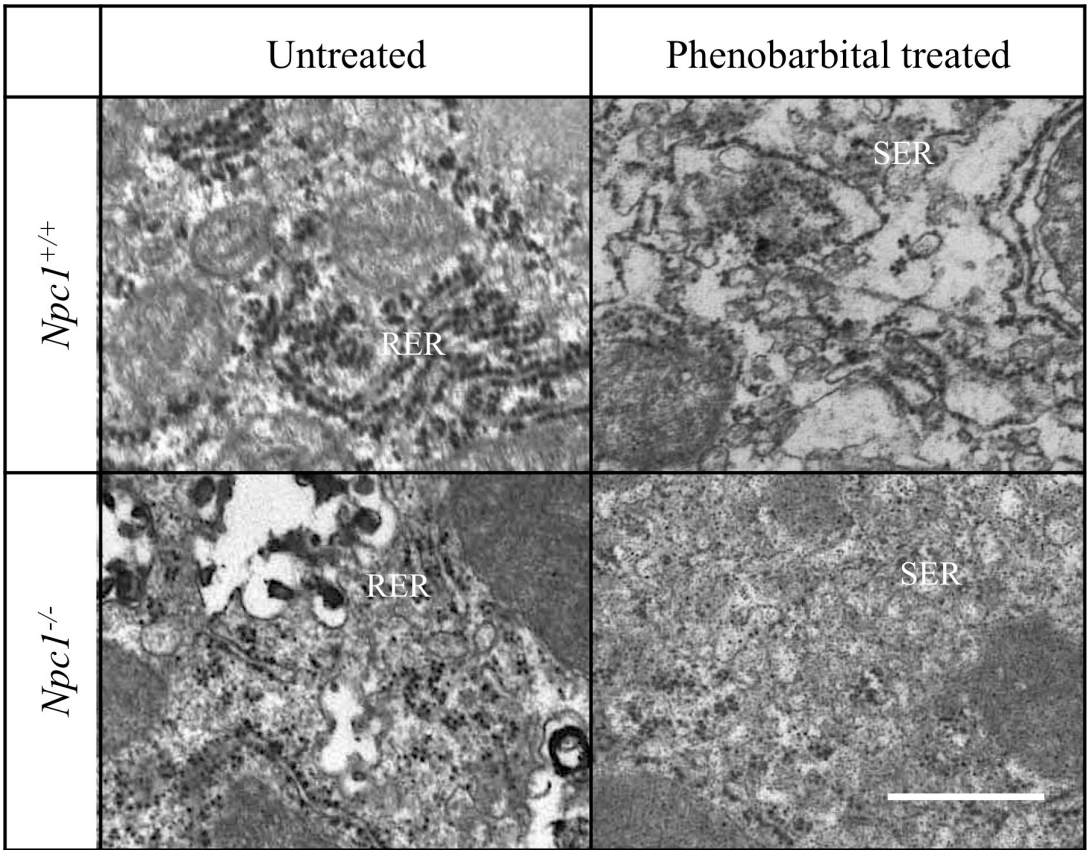

Figure 2.12. Representative electron micrographs of hepatocytes of phenobarbital treated and untreated *Npc1*$^{+/+}$ and *Npc1*$^{-/-}$ and mice. Scale bar represents 500 nm.

As bile acids regulate CYP gene expression and require cholesterol trafficking from lysosomes for their biosynthesis, which is impaired in NPC disease, we treated *Npc1* mutant mice with UDCA from weaning and measured P450 enzyme activity at 9 weeks of age. There was either partial or complete normalisation of the studied P450 enzyme activities with significant 3.8 (p=0.004) and 2.4-fold (p=0.006) increase in EROD and PROD activities, respectively, whereas BROD activities increased by 3.6 fold (p=0.067) and MROD by 1.4 fold (p=0.322) **(Figure 2.13)**. This would potentially implicate reduced/altered bile acid levels in NPC1 as an important mechanism underlying this defect.

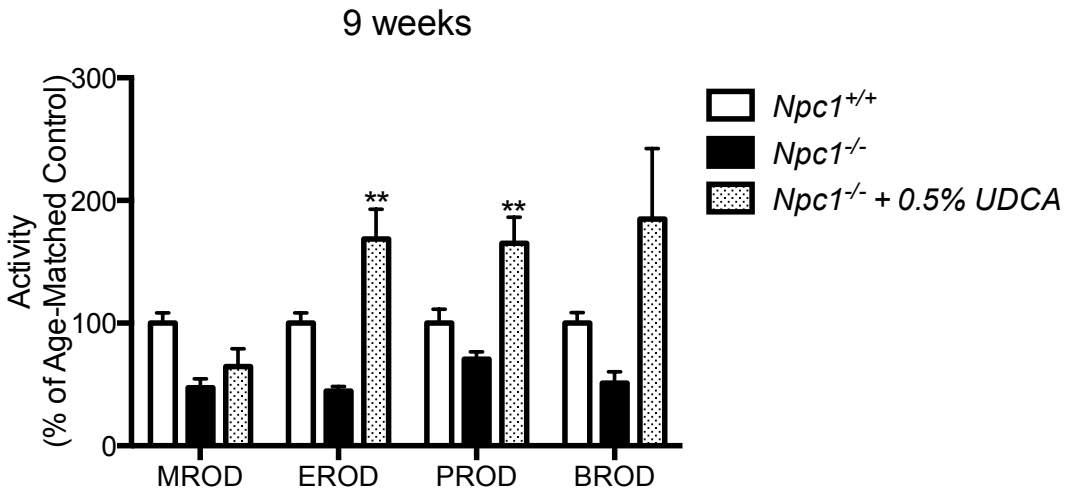

Figure 2.13. Effect of bile acid supplementation (0.5% UDCA, w/w) on the activity of CYP450 catalysed reactions in *Npc1*$^{-/-}$ mice measured at 9 weeks of age, shown as percent of age-matched controls. Data are presented as mean ± SEM for each genotype, n=3. *p<0.05, calculated using two-tailed, unpaired t test with Welch's correction.

2.4. Discussion

Since most of the drugs tested in the *Npc1*$^{-/-}$ mouse caused toxicity, are primarily metabolised via the cytochrome P450 system in the liver, this superfamily of enzymes was investigated to identify any underlying defect in the *Npc1*$^{-/-}$ mouse model. In agreement with our empirical observation (92), we have shown that *Npc1*$^{-/-}$ mice have a reduced cytochrome P450 reductase activity at 6 and 9 weeks of age (mid-late stage disease) compared to age-matched control mice. Cytochrome P450 reductase is the electron donor for multiple enzymes including among others heme oxygenase (178), cytochrome *b5* (179), squalene monooxygenase (180) and fatty acid elongase (181). Its deletion in mouse liver has been shown to be associated with a negative impact on drug clearance, due to the absence of an alternative electron donor to this enzyme system (182).

We have shown a reduction in the reductase activity and gene expression of the cytochrome P450 system resulting in an overall reduction of CYP activity in *Npc1*$^{-/-}$ mice.

This defect although first observed in the *Npc1*$^{-/-}$ mouse, is also present in the cat model of NPC1 disease and was detected in post-mortem liver samples from NPC1 patients.

In addition to reduced liver function in NPC mice (183), other mechanism linked to NPC pathogenesis could contribute to the down-regulation of the cytochrome P450 system genes, possibly resulting from cholesterol sequestration in LE/Lys. Endogenous sterols (e.g. cholesterol, oxysterols, vitamin D3 and bile acids) are

potent ligands for nuclear receptors involved in regulating cholesterol and drug metabolism "xenosensors" (184, 185). LXR regulates the expression of bile acid synthesising enzymes, while PXR, farnesoid X receptor (FXR), constitutive androstane receptor (CAR) and vitamin D receptor (VDR) are xenosensors regulating the expression of drug metabolising enzymes. The cross-talk between these two groups of receptors therefore links sterol homeostasis and drug metabolism. Oxysterols (cholesterol metabolites) are important mediators of this interplay between these nuclear receptors leading to a simultaneous regulation of genes involved in both cholesterol metabolism and drug metabolism, in addition to other pathways (155, 185, 186) **(Figure 2.14).**

We hypothesised that the defect in the cytochrome P450 system in NPC1 disease might be triggered by the cholesterol efflux defect from late endosomes/lysosomes in NPC1 disease and a failure to engage nuclear receptors. This is potentially

mediated by the following mechanisms **(Figure 2.15)**: lack of LXR activation by oxysterols, and reduced bile acid synthesis.

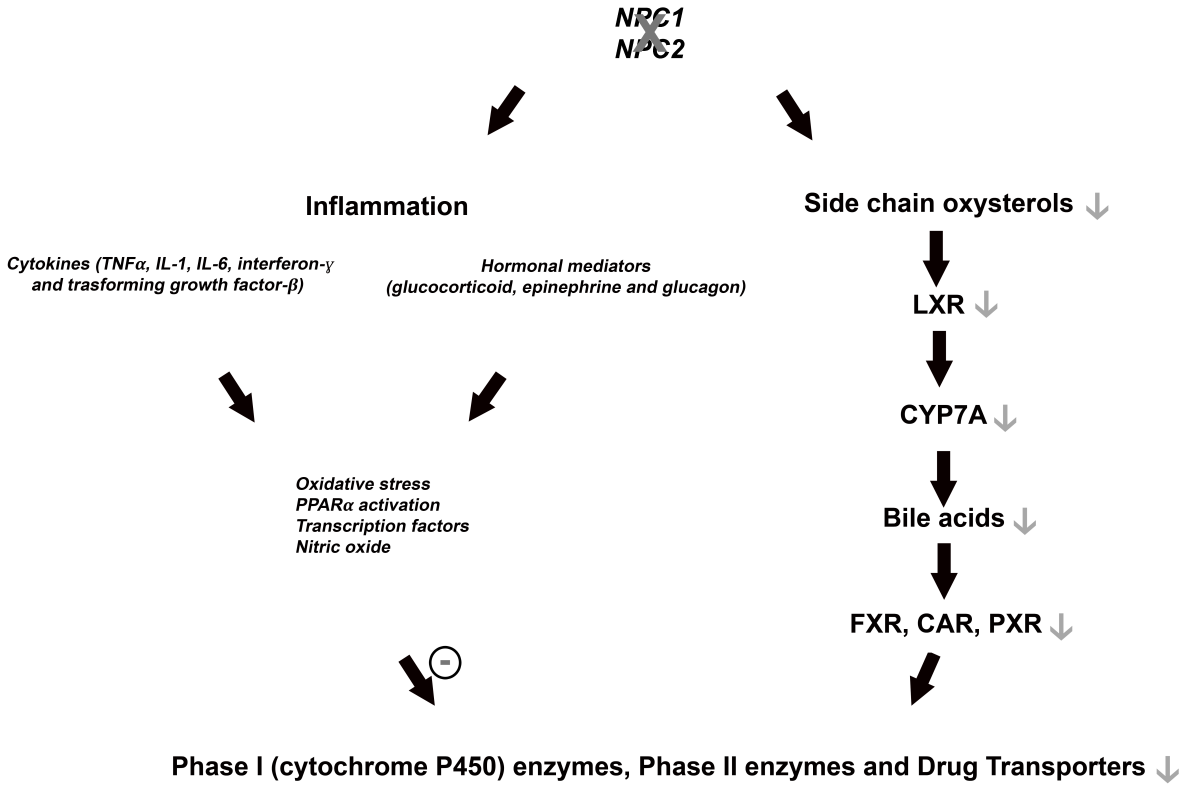

Figure 2.15. Proposed model of the effect of NPC mutation on liver drug metabolising enzymes. In the presence of a functional NPC1 and NPC2 protein, LDL-derived cholesterol is trafficked out of the lysosome where it can be converted to side chain oxysterols. Side chain oxysterols activate LXR target genes, including bile acid synthesis enzymes. Bile acids in turn activate other nuclear receptors FXR, CAR and PXR. These nuclear receptors stimulate the transcription of cytochrome P450 enzymes, Phase II enzymes and other xenobiotic transporters. However, NPC1/NPC2 dysfunction (changes in grey) reduces side chain oxysterols and subsequently down regulates the expression levels of downstream enzymes and nuclear receptors, finally resulting in low expression levels of the xenobiotic metabolising enzymes and transporter proteins. Other contributors to the reduction in cytochrome P450 enzyme activity include mechanisms relevant to inflammation including cytokines and other hormonal mediators released in response to inflammation.

NPC1 cells have less side chain enzymatically produced oxysterols due to decreased transport of unesterified cholesterol from the lysosome to the ER, where the enzymes catalysing the formation of 24(S)-, 25- and 27 hydroxycholesterol reside (152). Although NPC1 cells have elevated levels of the non-enzymatically produced oxysterols, 7-ketocholesterol and 3β,5α,6β-clolestanetriol (50), these products of

oxidative stress are weak LXR agonist (188), unlike enzymatically produced oxysterols, which are potent agonists (188-190). LXR activation by oxysterols induces the expression of its target genes, including CYP7A1, which catalyses the first step in bile acid biosynthesis (191). Bile acid biosynthesis is significantly lower in *Npc1*$^{-/-}$ mice challenged with a high cholesterol diet compared to normal mice, as these mice failed to upregulate bile acid synthesis in response cholesterol overload (192, 193). Bile acids in turn, are endogenous ligands for the xenosensor PXR, regulating the expression of multiple Phase I and Phase II drug metabolising enzymes (194). A neuroprotective effect was reported in the *Npc1*$^{-/-}$ mouse upon administration of PXR and LXR agonists (89, 120). Activation of their target genes mediated the beneficial effect by facilitating cholesterol efflux (195). One mechanism that triggered this cytochrome P450 defect was the diminished production of enzymatically generated oxysterols, which in turn triggers bile acid deficiency.

The outcome of the phenobarbital induction study further supports this mechanism. phenobarbital is known to induce cytochrome P450 enzyme activity, including CYP2B10, CYP3A11, and cytochrome P450 reductase and its effect is mediated through activation of xenobiotic nuclear receptor CAR, which regulates the expression of drug and steroid metabolising enzymes (176).

Inflammation is another component of NPC1 disease that could contribute to this P450 system defect. Cytokines as well as hormonal responses to inflammation are known to regulate the cytochrome P450 system at the transcriptional, post-transcriptional and post-translational levels (196). The pro-inflammatory cytokine TNF also has a regulatory effect on cytochrome P450 enzyme activities (196, 197).

PPARα (peroxisome proliferator-activated receptors α) activation (e.g. by endogenous ligands produced in response to inflammation), reactive oxygen species and nitric oxide generation are all inflammation-associated processes known to suppress the cytochrome P450 system (198).

To test whether bile acid deficiency was a significant factor in reduced P450 system gene expression we evaluated bile acid supplementation in *Npc1*$^{-/-}$ mice. Bile acid supplementation (UDCA) from weaning had a positive effect in the *Npc1*$^{-/-}$ mice functionally (reduced tremor and improved motor function) as well as partially correcting the cytochrome P450 defect. This finding suggests that xenobiotic neurotoxicity may play a role in the pathogenesis of NPC disease. These data also suggest that bile acid replacement therapy may be a useful adjunctive therapy in NPC1 patients. UDCA is a cheap FDA approved drug for the treatment of primary biliary cirrhosis (199). More studies will be needed to fully evaluate their therapeutic potential in NPC disease beyond the neonatal liver disease phase of the disease when they are transiently prescribed.

These findings could impact preclinical studies where drug efficacy could be masked by drug-induced toxicity. Dose adjustment might be therefore needed in NPC patients. Interestingly, curcumin, which has shown to be beneficial in the *Npc1*$^{-/-}$ mouse, also inhibits the cytochrome P450 system (200). It is therefore possible that its positive effect (weak SERCA antagonism) outweighs this negative effect, as different studies have reported varying outcomes using the same compound (37, 113).

These findings might potentially need to be considered when developing new therapies for NPC disease and when using established symptomatic management

(drugs to manage seizures for example) and using dietary supplements in NPC1 patients. Adjusting the dose may need to be considered for drugs which undergo Phase I metabolism and/or Phase II glucoronidation. Also, when developing prodrugs, failure to metabolise the prodrug to the active metabolite in NPC1 patients may result in the administration of suboptimal doses.

Hepatic involvement in NPC1 patients presents with heaptosplenomegaly, jaundice and neonatal cholestasis, which can be fatal in early life (150). Cellular and molecular mechanisms of liver disease in NPC disease are linked to apoptosis, inflammation and fibrosis (183). NPC1 patients in the neonatal period often present with cholestatic jaundice and hepatic dysfunction which usually resolves, although could be lethal in few cases. This could be explained by our findings. The normal maturation of both phase I and II metabolism post birth is established (201) and we would hypothesise that the defect in the this system in addition to its immaturity in the neonate, could contribute to this neonatal hepatic phenotypes in NPC1 disease.

The heterozygote phenotype described might have potential implications to the general population with the predicted carrier frequency of NPC mutation of 1/173 or 0.6% of the population, but this will need to be further evaluated and carefully studied.

Chapter 3. Behavioural Evaluation of Therapeutic Agents in Niemann-Pick Type C1 Disease

3.1. Introduction

Therapeutic options for NPC1 disease are currently limited to small molecule therapeutics. Small molecules are the main option due to the trans-membrane nature of the NPC1 protein, making gene/protein replacement therapy difficult, unlike NPC2, which is a soluble mannose-6-phosphate targeted protein amenable to cross-correction and therefore bone marrow transplantation (202). The potential targets of approved and experimental therapies are summarised in **Figure 3.1.**

Currently, the only approved therapy (approved world-wide except in the USA) is a small molecule therapy using the imino sugar *N*B-DNJ (miglustat) (83) which acts via reversible inhibition of the first and rate limiting step of GSL biosynthesis (glucosylceramide synthase), thus preventing pathological GSL accumulation (203) and reduces sphingosine levels in the lysosome. This small molecule is capable of crossing the blood-brain barrier exerting a protective effect in the CNS in addition to peripheral tissues (106). Miglustat has proven successful in delaying onset of neurological symptoms and extending life expectancy in animal models (cat and mouse) along with significant reduction in GSL storage (82). Cyclodextrin is in clinical trials at the NIH based on efficacy in murine (87, 88) and feline models (123) and HDAC inhibitor (144, 145) trials are planned.

Another class of therapeutics are calcium-modulating agents, which act by elevating cytosolic calcium (from intracellular organelles other than the acidic compartment) to compensate for defective calcium release from the acidic compartment, allowing cellular events (fusion and transport) to occur and thus prevent subsequent mistrafficking and storage of intracellular lipids (37).

This chapter aims to evaluate potential therapeutic agents for NPC disease in the authentic mouse model, including small molecules, biologics (recombinant proteins including monoclonal antibodies, fusion proteins and endotoxins that modulate immune response) and metabolite supplementation therapy.

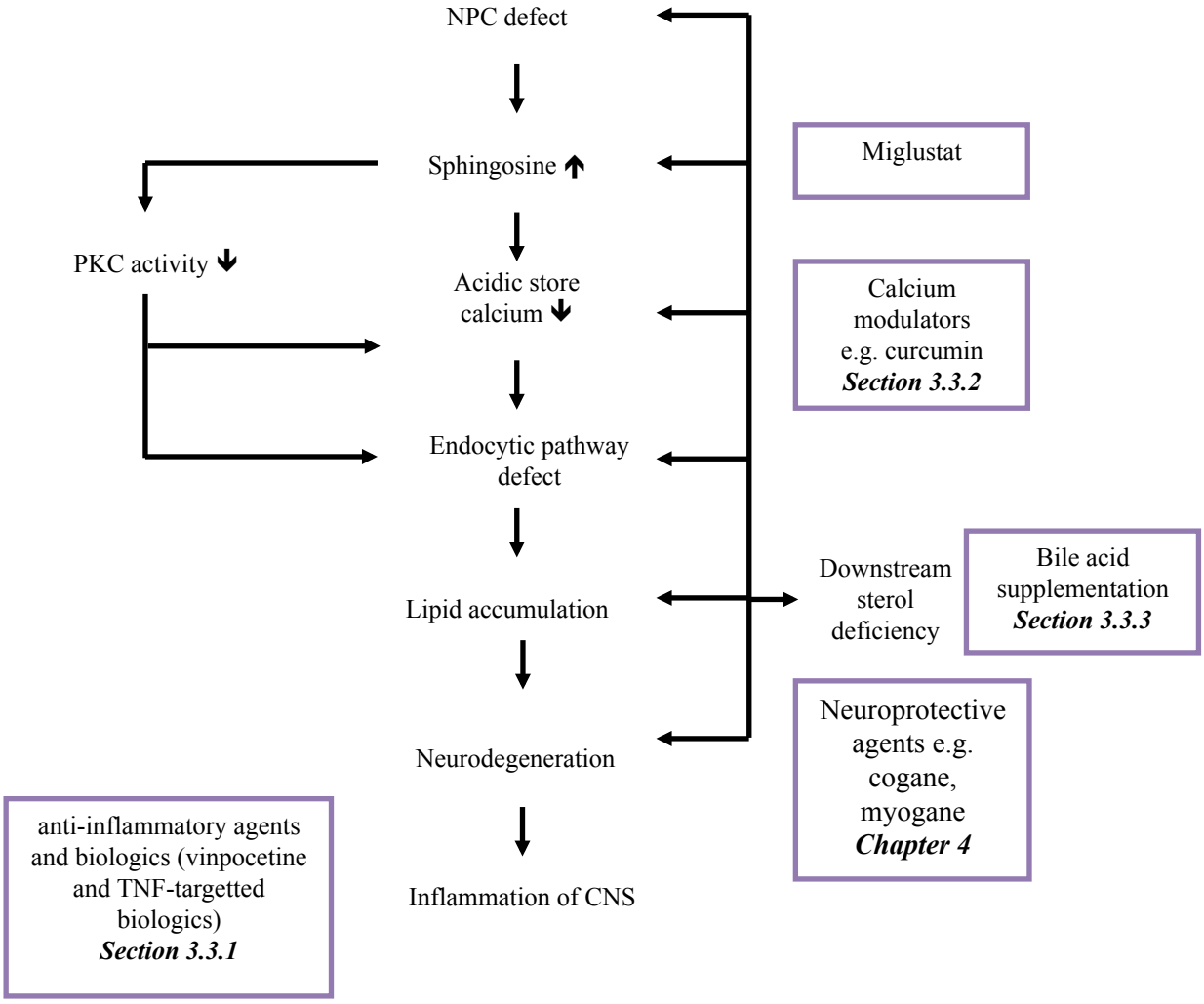

Figure 3.1. Outline of targets for potential therapies for NPC disease.

3.2. Methods

3.2.1. Mice

Npc1$^{-/-}$ mice were generated, maintained and genotyped as described in **Chapter 2**.

3.2.2. Treatment

Compounds were either mixed with the powdered standard mouse chow (RM1 (E) FG SQC Expanded Ground 811004, SDS UK, Witham, Essex, UK, expanded ground, Rat and Mouse No.1 Maintenance, SDS) and directly fed to the mice or reformulated into pellets when indicated. To avoid wasting the test compound when supplied with the powdered chow; the prepared powdered diet was given in glass "inkwells" placed on a glass petridish plate to prevent spillage mixing with bedding. Pre-weaning and for mice on treatments administered parenterally, mice were fed a Harlan Teklad 2016 diet.

3.2.3. Therapies

3.2.3.1. Anti-inflammatory agents

Vinpocetine (Sigma-Aldrich, Dorset, UK) was added to powdered mouse chow in a dose of 10 mg/kg body weight/day and 5 mg/kg body weight/day. Treatment was started at 6 weeks of age as recommended for anti-inflammatory drugs (92).

The anti-TNF biologic Enbrel (Etanercept; Amgen/Pfizer, Amgen, USA) was administered subcutaneously (200 μg/animal; (204)) twice a week (n=5). Humira (Adalimumab; Abbott) was administered intraperitoneally at 20 mg/kg three times a week (doses converted from human doses based on differential binding coefficients against murine and human TNF) (n=5) and Remicade (Infliximab; Centocor Orth Biotech) was administered intraperitoneally at 6.25 mg/kg once a week (205) (n=5). Control animals (n=7) were administered equal volumes of PBS subcutaneously and intraperitoneally as well as untreated controls. All treatments were started at 6

weeks of age. Anti-TNF biologics were kindly provided by Prof. Raashid Luqmani (Nuffield Orthopaedic Centre, Oxford). Some of the Enbrel and control groups were studied by Marcus Hui as part of his M.Sc. project.

3.2.3.2. Calcium modulators (curcumin)

Npc1$^{-/-}$ mice were fed a standard mouse diet supplemented with curucmin (Curcumin (65-70%) C1386, Sigma-Aldrich, Dorset, UK) at a dose 150 and 250 mg/kg BW/day, either mixed with normal diet in a powder form (curcumin 150) or reformatted into pellets (Curcumin (P)). A curcuminoids mixture (purum, mixture of curcumin, desmethoxycurcumin and bisdesmethoxycurcumin, ≥95.0% (TLC) Curcumin, Fluka 28260) at the same dose (150 mg/kg/day) was also tested, mixed with the mouse chow which was then reformulated into pellets (Curcuminoids (P)), as food pellets are consumed more efficiently and so allow more optimal dosing (206). These treatments were initiated at weaning (3 weeks).

3.2.3.3. Bile acid supplementation

Npc1$^{-/-}$ mice were fed a standard mouse diet supplemented with 0.5% UDCA (w/w, Sigma-Aldrich) starting from weaning (day 21). Combination therapies of UDCA (0.5%) with high dose curcumin (300 mg/kg), UDCA with high dose curcumin and *N*B-DGJ (*N*-butyldeoxygalactonojirimycin 1,200 mg/kg), UDCA with *N*B-DGJ, *N*B-DGJ with high dose curcumin, *N*B-DGJ alone as well as high dose curcumin alone were also investigated.

For a quick assessment of the acute effect of bile acid supplementation in this disease model, mice were fed a high dose ibuprofen (800 mg/kg, a dose that has shown to be toxic in this mouse model, starting at 6 weeks), these mice have been given a diet supplemented with 0.5% UDCA starting at 3 weeks. Two control

groups on normal diet and high dose ibuprofen alone groups. All groups had n=5 and were monitored for acute toxic effect reflected in body weight changes over 7 days.

Summary of all investigated compounds/biologics **(Table 3.1).**

Compound	Mechanism of Action	Dose	Form	Route of Administration	Start of treatment
*N*B-DGJ	Substrate reduction therapy	1,200 mg/kg BW/day	Solid admix with/ powdered chow	p.o.	Weaning (3 weeks)
Curcumin	Calcium modulator	150 mg/kg BW/day	/powdered chow /pelleted chow	p.o.	Weaning (3 weeks)
Vinpocetine	NSAID		/powdered chow	p.o.	6 weeks
UDCA	Bile acid supplementation	0.5% (w/w)	/powdered chow	p.o.	Weaning (3 weeks)
*N*B-DGJ high dose curcumin	Combination therapy	1,200 mg/kg BW/day 300 mg/kg BW/day	/powdered chow	p.o.	Weaning (3 weeks)
UDCA+ high dose curcumin	Combination therapy	0.5% (w/w) 300 mg/kg BW/day	/powdered chow	p.o.	Weaning (3 weeks)
*N*B-DGJ UDCA high dose curcumin	Combination therapy	1,200 mg/kg BW/day 0.5% (w/w) 300 mg/kg BW/day	/powdered chow	p.o.	Weaning (3 weeks, 21 days)
high dose curcumin	Calcium modulator for combination therapy	300 mg/kg BW/day	/powdered chow	p.o.	Weaning (3 weeks)
*N*B-DGJ UDCA	Combination therapy	1,200 mg/kg BW/day 0.5% (w/w)	/powdered chow	p.o.	Weaning (3 weeks)
Etanercept (Enbrel)	Anti-TNF antibody Human TNFR2-Fc fusion protein	200 µg	Solution in PBS	s.c. twice a week	6 weeks
Infliximab (Remicade)	Anti-TNF antibody Mouse/human chimeric monoclonal IgG1 TNF-specific antibody	6.25 mg/kg BW/day	Solution in PBS	i.p. once a week	6 weeks
Adalimumab (Humira)	Anti-TNF antibody Fully human monoclonal TNF-specific antibody	20 mg/kg BW/day	Solution in PBS	i.p., three times a week	6 weeks
Myogane	Neurotrophic factor inducing diosgenins	0.1, 1 and 10 mg/kg BW/ day	/powdered chow	p.o.	Weaning (3 weeks)

Table 3.1. Summary of the investigated therapies in NPC1 mouse model studied in this thesis. The table shows the compounds, their mechanism of action (by which they exert their proposed beneficial effects), the dose, form and route of administration (p.o.; orally, s.c.; subcutaneously, i.p.; intraperitoneally, BW; body weight).

3.2.4. Survival

For all therapeutic trials, a predetermined late humane end point was applied when a mouse has lost ~1 gram or more body weight within 24 hours (mice have stopped feeding due to severe ataxia).

3.2.5. Neurological function

Behavioural tests were performed weekly starting a week after the initiation of the treatment and until end-point. For all behavioural tests, mice were allowed to acclimatise in the room where the tests were conducted, in their home cages for at least 15 minutes. Also, testing was carried out with a background noise (radio) to reduce any disturbances (and therefore distress), which might interfere with the mouse behaviour under assessment. Tests were conducted at the same time of day.

3.2.5.1. Tremor monitoring

Tremor was measured weekly using a commercial tremor monitor (San Diego Instruments) following the manufacturer's instructions. It was placed on an anti-vibration table to minimise any interferences. Measurement time was 256 seconds and mice were allowed 60 seconds acclimatisation within the chamber before acquisition. A National Instruments PCI card was used to connect the tremor monitor to a computer. The LabView analysis software was used to analyse and transform (fast Fourier transform) the results (amplitude/time) to a measurement of power representing tremor amplitude at each frequency (0–64 Hz).

3.2.5.2. Open-field Test/ Rearing activity

Following acclimatisation, each mouse was placed in a plastic box (45 x 25 x 12 cm), the floor of which was covered with a layer of their home cage bedding, as a way of acclimatising and reducing any stress caused by moving away from the home cage to a new environment.

Each mouse was placed in the middle of the box, allowed to acclimatise for 5 minutes. The spontaneous activity measured as rearing activity of individual mice was recorded manually for 5 min. The count of mouse rears on its hind legs (either

unsupported or against the cage wall) were recorded as “centre rears” and “rears”, respectively.

3.2.6. Statistics

Data are expressed as means ± SEM. Prism GraphPad 6.0 was used to calculate survival curves (Kaplan-Meier) The survival data were analysed by the Kaplan-Meier test. The behavioural studies were assessed using one-way ANOVA with Tukey’s post hoc test for multiple comparisons. For the acute toxicity growth curve, two-way ANOVA with Tukey’s post hoc test was performed for multiple comparisons.

3.3. Results

3.3.1. Anti-inflammatory agents

Inflammation in the CNS has been reported in chronic neurodegenerative disorders (207), and the administration of the non-steroidal anti-inflammatory agent ibuprofen in *Npc1*$^{-/-}$ mice has been shown to be beneficial, extending the life span of treated mice and slowing disease progression (92).

In the current research, vinpocetine **(Figure 3.2)**, an alkaloid compound of plant origin that is known for its cognitive enhancement properties, was evaluated in *Npc1*$^{-/-}$ mice since it has been recently reported to have anti-inflammatory properties (208).

Vinpocetine at a dose of 10 mg/kg/day and a further adjusted lower dose of 2 mg/kg/day was administered orally starting at 6 weeks of age (early symptomatic stage). Adjusting the dose to avoid toxicity was successful in significantly extending life span (p=0.025) **(Figure 3.3).**

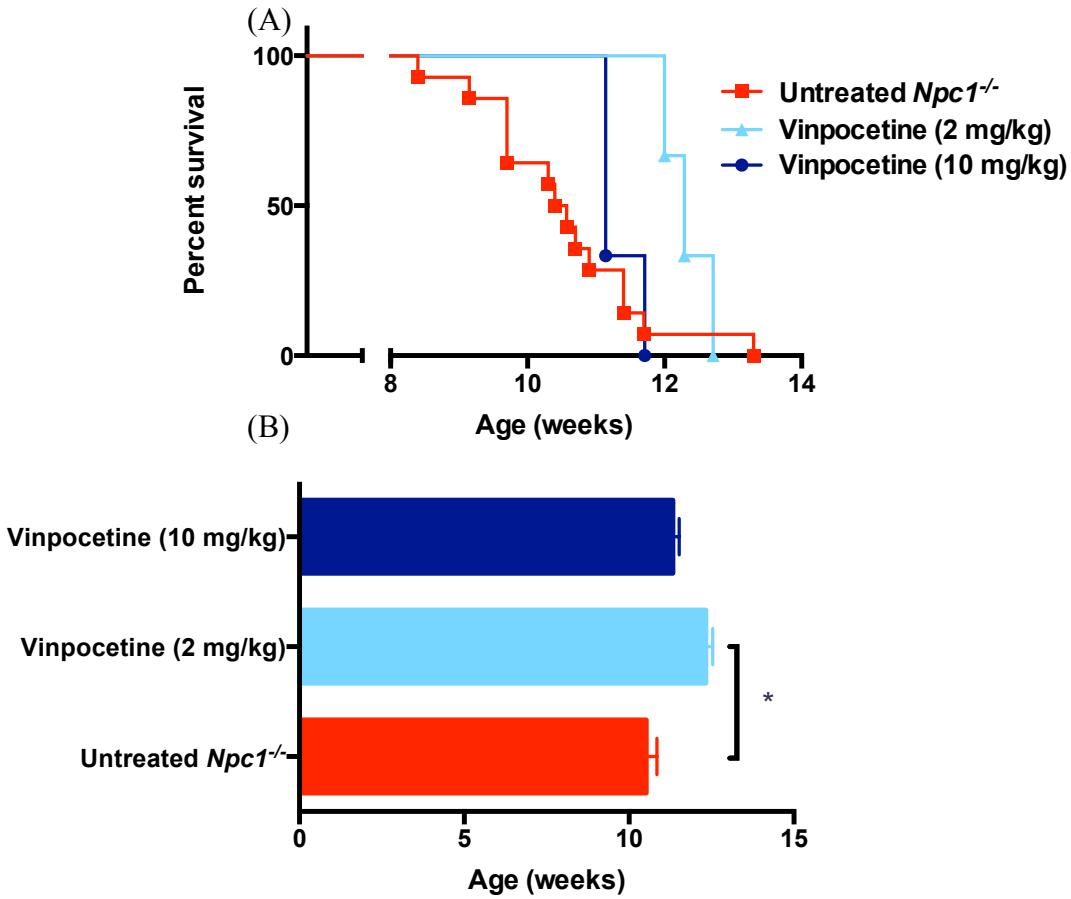

Figure 3.3. Effect of the anti-inflammatory compound vinpocetine on survival of *Npc1*$^{-/-}$ mice. (A) Kaplan–Meier survival curve (percent survival) and (B) Average survival ages. Data presented as mean ± SEM *p<0.05, calculated using one-way ANOVA with Tukey's post hoc test (n=3-14).

Both doses resulted in a worsening of the weight loss profile of treated mice, although not significant **(Figure 3.4).**

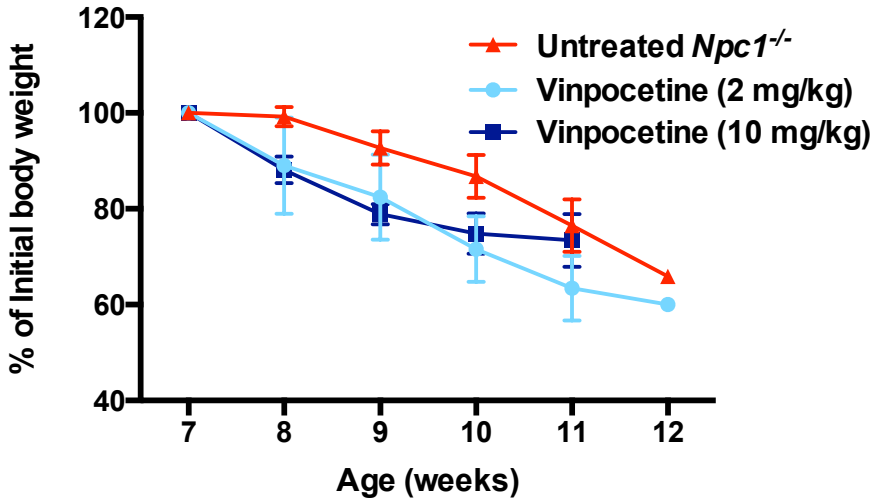

Figure 3.4. Effect of the anti-inflammatory compound vinpocetine on weight loss of *Npc1*$^{-/-}$ mice. Data presented as mean (percent of initial body weight) ± SEM. One-way ANOVA with Tukey's post hoc test was performed (n=3-14).

Motor function in response to treatment was evaluated by measuring rearing activity in a five-minute open field test. Vinpocetine was only beneficial at the higher dose at the late symptomatic phase **(Figure 3.5 A and B)** increasing rearing activity compared to both untreated and low dose groups at 10 weeks (p=0.018 and 0.022, respectively) and centre rearing count markedly compared to untreated controls at 9 weeks (p=0.042).

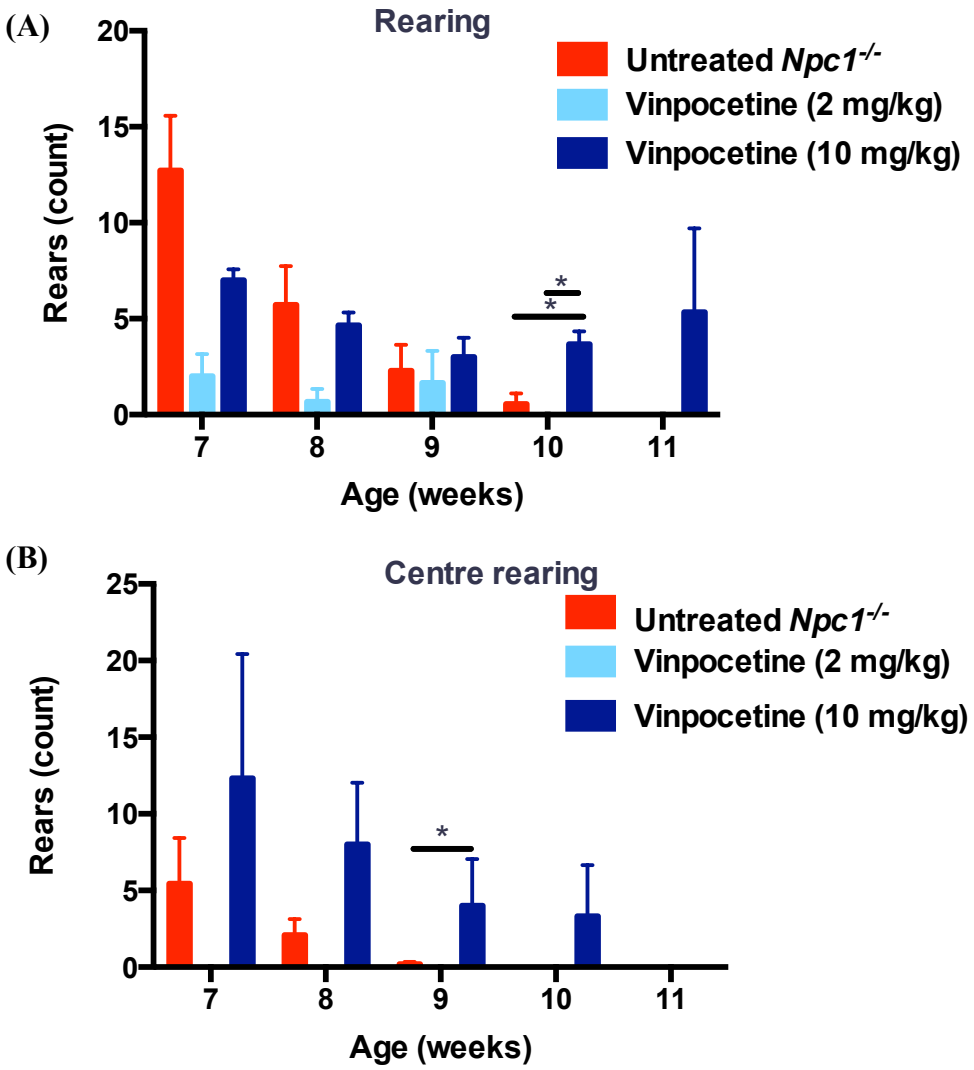

Figure 3.5. Effect of the anti-inflammatory compound vinpocetine on (A) rearing and (B) centre rearing of *Npc1*$^{-/-}$ mice. Data presented as mean (rearing count) ± SEM. **p*<0.05, calculated using one-way ANOVA with Tukey's post hoc test (n=3-14).

No significant reduction in tremor amplitude was observed with either dose at all disease stages **(Figure 3.6 and Figure 3.7)**, in fact the high dose was associated with worsening of the tremor at the late symptomatic stage possibly due to toxicity while the low dose may have been too low to produce any beneficial effect on the tremor amplitude.

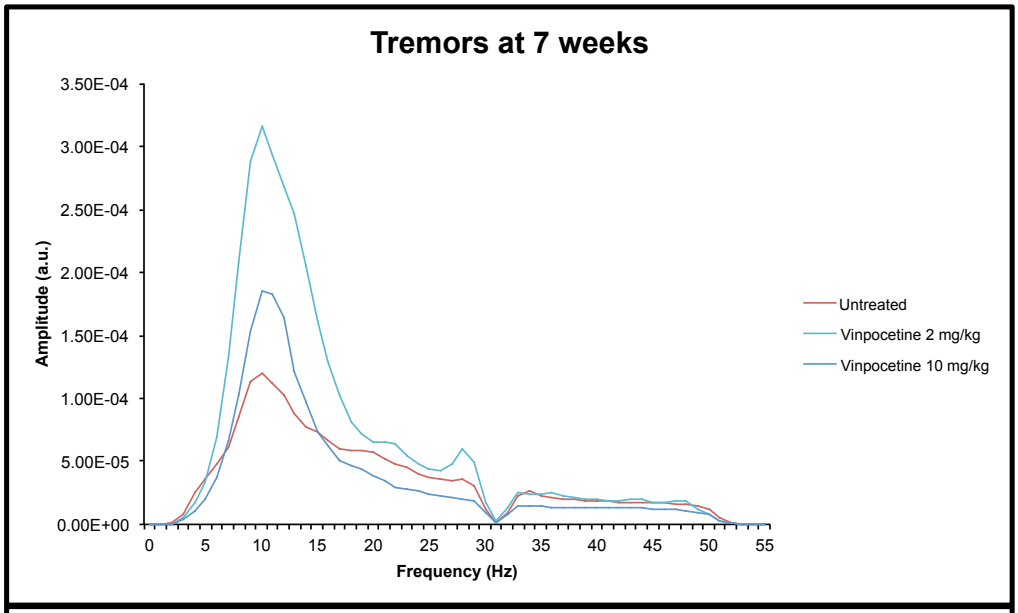
Tremors at 7 weeks
Amplitude (a.u.)
3.50E-04
3.00E-04
2.50E-04
2.00E-04
1.50E-04
1.00E-04
5.00E-05
0.00E+00
0 5 10 15 20 25 30 35 40 45 50 55
Frequency (Hz)
Untreated
Vinpocetine 2 mg/kg
Vinpocetine 10 mg/kg

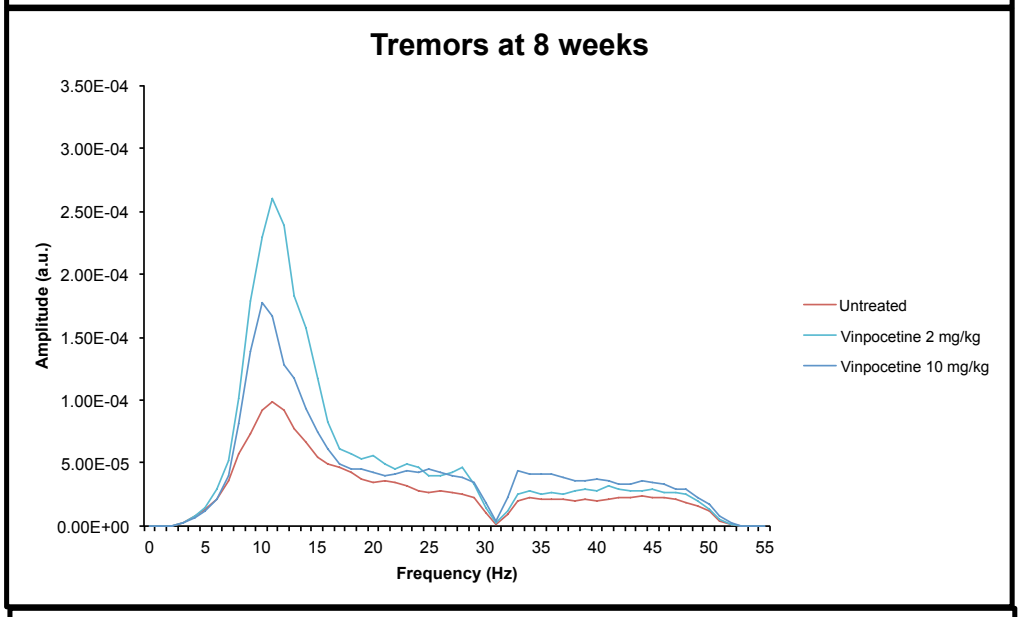
Tremors at 8 weeks
Amplitude (a.u.)
3.50E-04
3.00E-04
2.50E-04
2.00E-04
1.50E-04
1.00E-04
5.00E-05
0.00E+00
0 5 10 15 20 25 30 35 40 45 50 55
Frequency (Hz)
Untreated
Vinpocetine 2 mg/kg
Vinpocetine 10 mg/kg

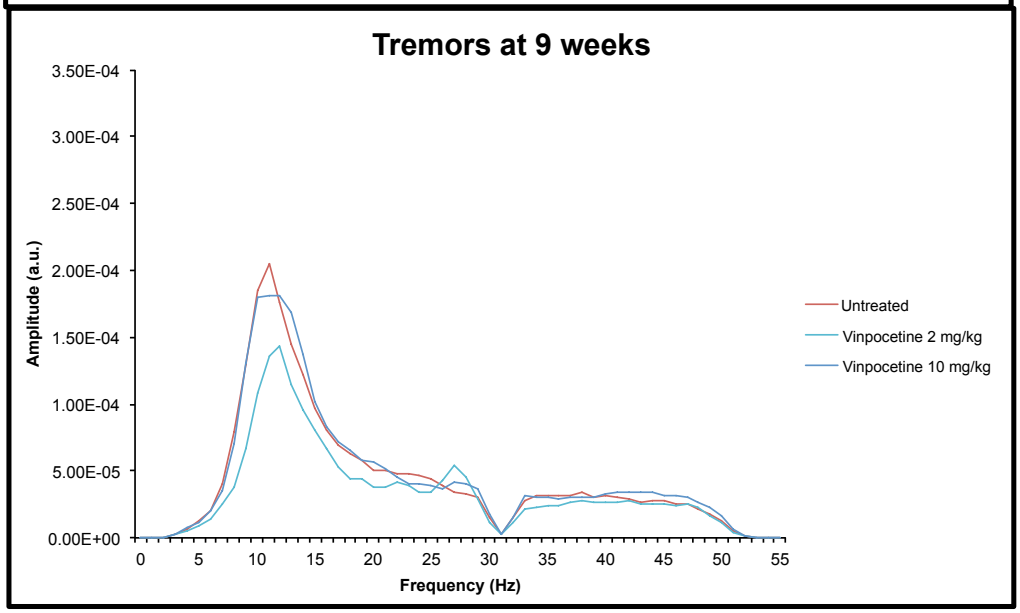
Tremors at 9 weeks
Amplitude (a.u.)
3.50E-04
3.00E-04
2.50E-04
2.00E-04
1.50E-04
1.00E-04
5.00E-05
0.00E+00
0 5 10 15 20 25 30 35 40 45 50 55
Frequency (Hz)
Untreated
Vinpocetine 2 mg/kg
Vinpocetine 10 mg/kg

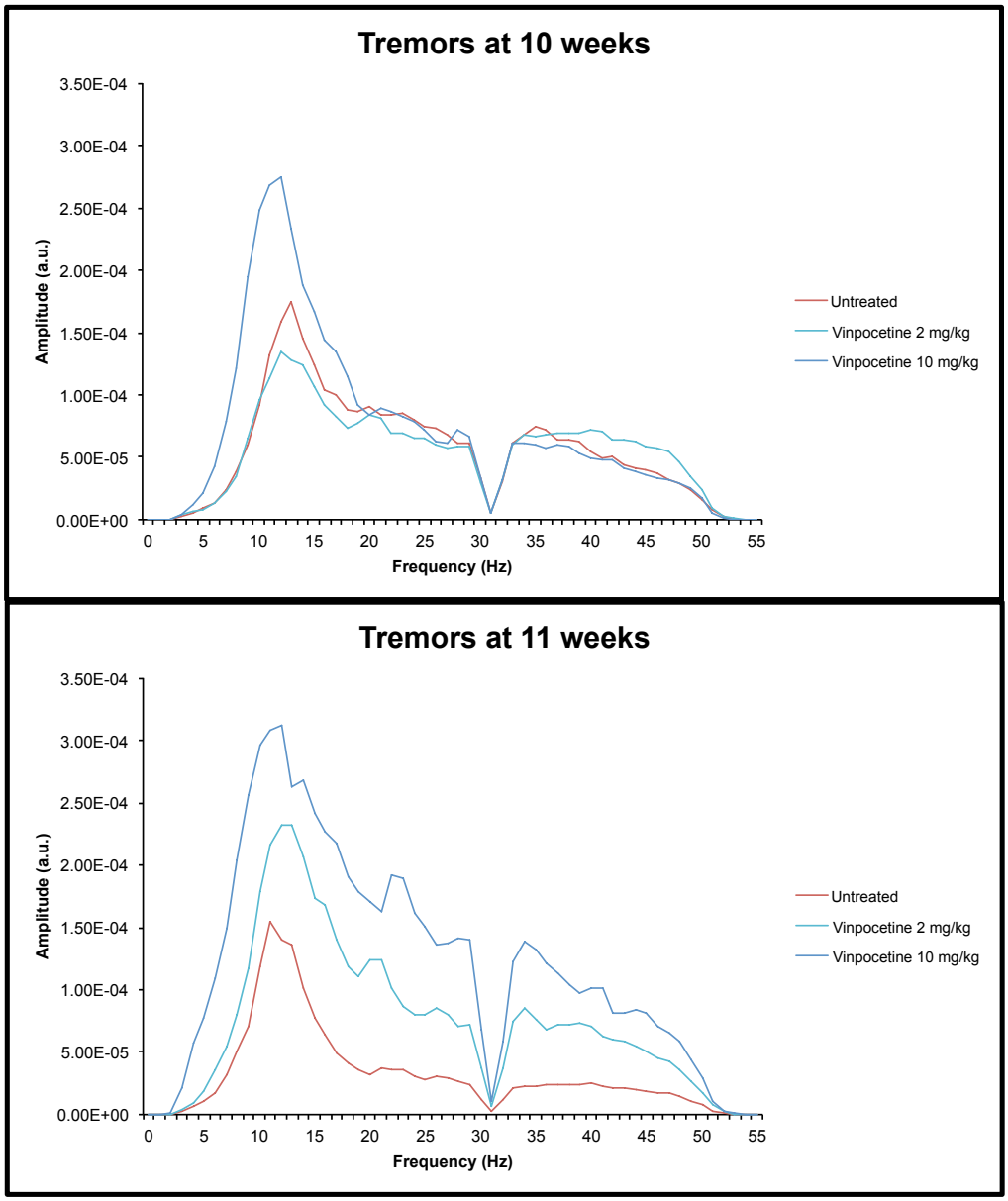

Figure 3.6. Effect of the anti-inflammatory compound vinpocetine on tremor of *Npc1*$^{-/-}$ mice. Data presented as mean tremor amplitude between 0 and 55 Hz (n=3-14), untreated controls are untreated *Npc1*$^{-/-}$ controls.

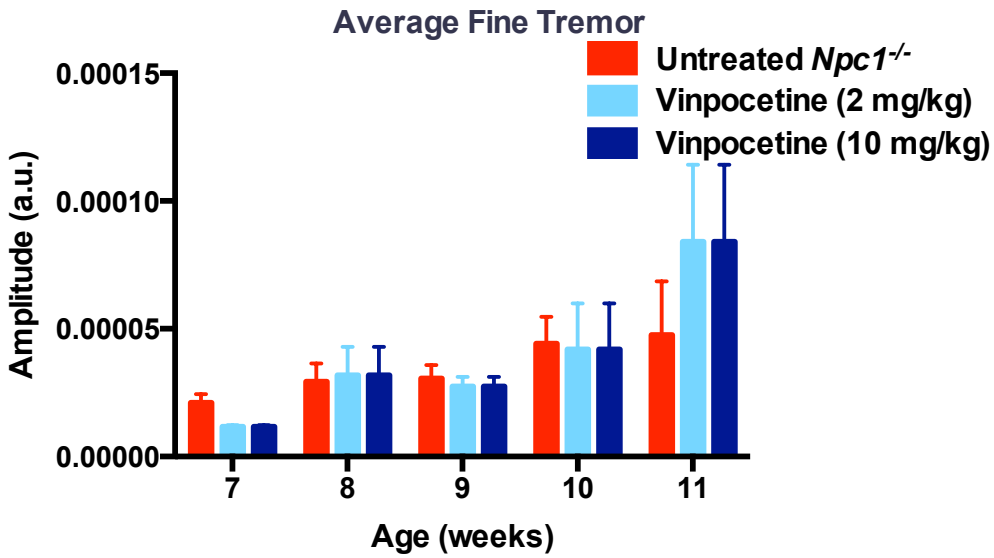

Figure 3.7. Effect of the anti-inflammatory compound vinpocetine on fine tremor of *Npc1*$^{-/-}$ mice. Tremor amplitudes quantified as averaged fine tremor amplitude (over the range 31-51 Hz). Data presented as mean ± SEM. One-way ANOVA with Tukey's post hoc test was performed (n=3-14).

Since inflammation in NPC1 disease is TNF dominated, targeting TNF using anti-TNF or TNF-targeting biologics could potentially be a promising therapeutic intervention targeting the inflammatory component of the disease and potentially, provided these biologics can cross the blood-brain barrier, effective in alleviating neuroinflammation.

This approach has been used in other inflammatory conditions such as Crohn's disease and rheumatoid arthritis **(Table 3.2)** (209). These biologics have established safety profiles and have been subjected to clinical trials in other inflammatory conditions (Crohn's disease and rheumatoid arthritis) with good efficacy and tolerability and are in routine clinical use for the indicated diseases **(Table 3.2)** (210-212).

The table originally presented here cannot be made freely available via ORA because of 'copyright'.

Indeed, a mouse-rat chimeric anti-TNF monoclonal antibody, CNTO5048, has been tested in the mouse model of liver specific knockdown of NPC1 and shown a marked improvement in multiple markers of peripheral (liver) inflammation. Since the model used was a liver specific knockdown, the neurological functional or neuroinflammation side of NPC disease could not be addressed (93).

Enbrel, Humira and Remicade **(Figure 3.8)** were administered to *Npc1*$^{-/-}$ mice starting from 7 weeks of age.

The figure originally presented here cannot be made freely available via ORA because of 'copyright'.

None of these biologics had an effect on the life span of the treated mice compared to their vehicle controls (Enbrel, p=0.991, Humira, p=0.979 and Remicade, p>0.999) **(Figure 3.9)**. Only Humira treatment was associated with significant increase in life span when compared to untreated control (p=0.015) but not in respect to vehicle only controls (i.e. the rehydration properties of the saline vehicle extends life span not the anti-TNF biologic).

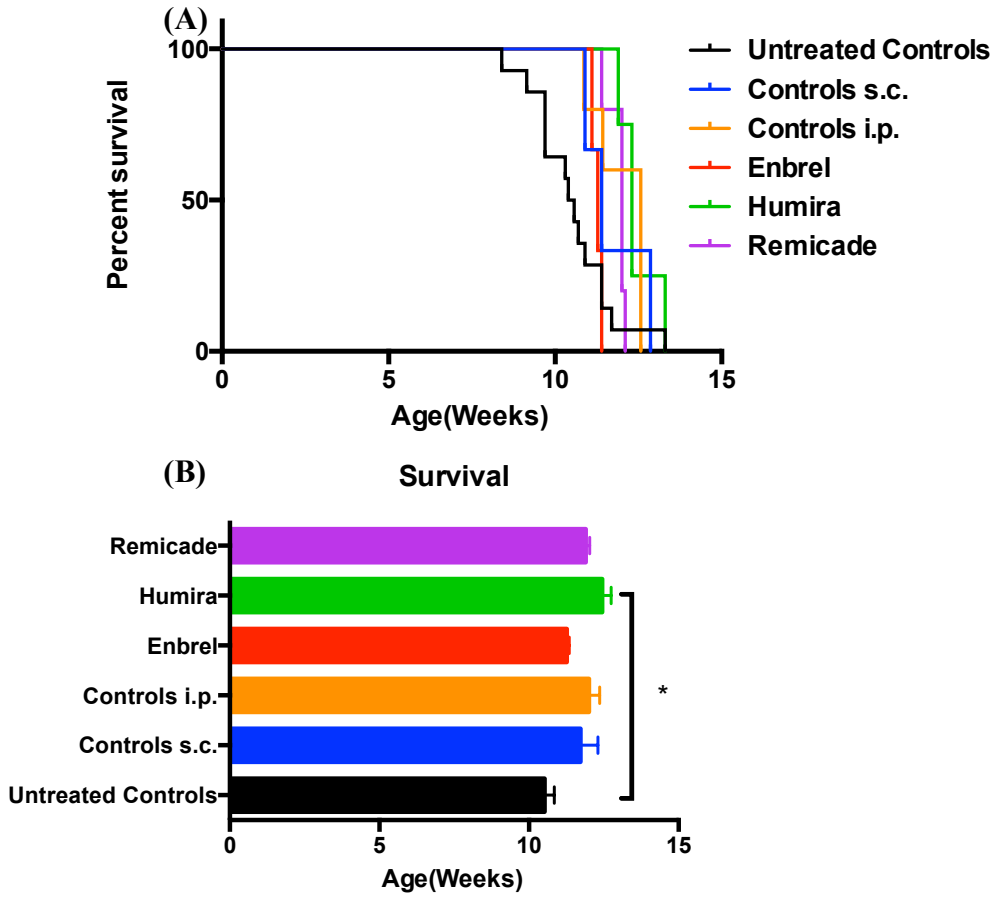

Figure 3.9. Effect of TNF-targeting biologics on survival of *Npc1*$^{-/-}$ mice. (A) Kaplan–Meier survival curve (percent survival) and (B) Average survival ages. Data presented as mean ± SEM, *p<0.05, calculated using one-way ANOVA with Tukey's post hoc test (n=5-14).

Similarly, body weight loss profile was not affected by any of the treatments (at 8 weeks; Enbrel, p>0.999, Humira, p=0.976 and Remicade, p>0.099 and at 9 weeks; Enbrel, p>0.999, Humira, p>0.999 and Remicade, p=0.194) **(Figure 3.10)**. Interestingly, Remicade caused a significant weight loss (at 8 weeks; p=0.007 vs.

untreated controls, p=0.002 vs. controls s.c. and Enbrel and p=0.018 vs. Humira, whereas at 9 weeks; p=0.036 vs. controls s.c.).

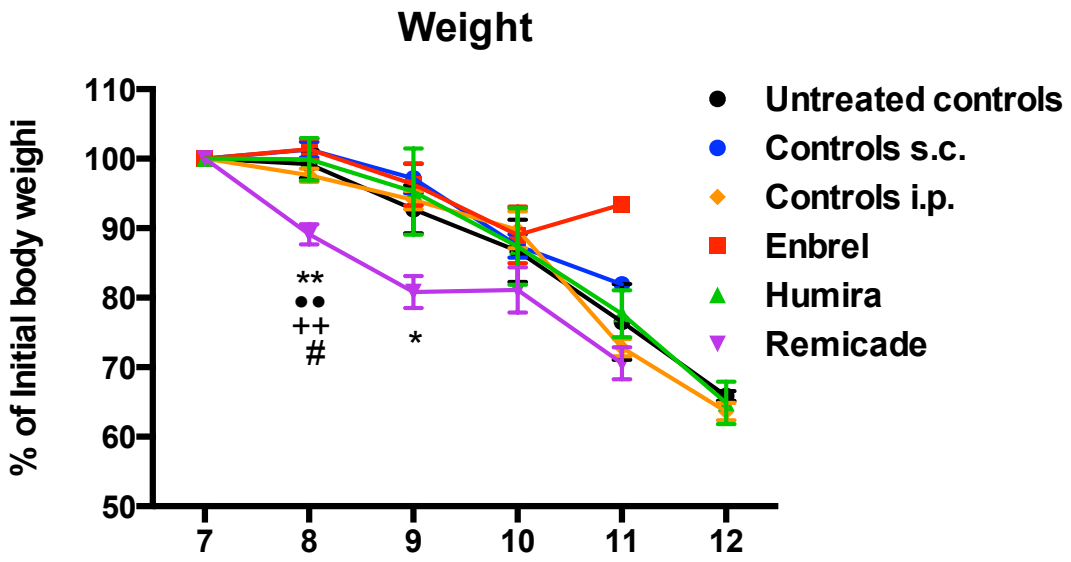

Figure 3.10. Effect of TNF-targeting biologics on body weight loss of *Npc1*$^{-/-}$ mice. Data presented as mean (percent of initial body weight) ± SEM. *p<0.05 and **p<0.01, calculated using one-way ANOVA with Tukey's post hoc test (n=5-14). * denotes comparison vs. controls s.c., • denotes comparison vs. untreated controls, + denotes comparison vs. Enbrel and # denotes comparison vs. Humira.

However, all treatments had a beneficial effect as they were associated with higher level of rearing activity (motor strength and coordination) than control mice, at later stages in particular **(Figure 3.11 A)**. Interestingly, when comparing rearing activity between treatment groups, i.p. saline produced a similar effect with significantly higher activity compared to untreated controls at 7 weeks (p=0.013), 9 weeks (p=0.049) and 11 weeks (p=0.006).

Humira was more effective amongst the other treatments starting from 8 weeks (p=0.037 vs. untreated controls), at 9 weeks (p=0.002 and 0.021 vs. untreated controls and importantly the s.c. PBS injected controls) and at 11 weeks (p=0.011 vs. untreated control).

Remicade group presented with a sustained level of rearing activity starting from 7

weeks, higher than the two control groups (untreated and s.c. injected), and maintained up to 12 weeks, however, did not reach statistical significance. Similarly, Enbrel treated mice rearing activity was higher compared to its s.c. control group throughout, however, the difference was not statistically significant (p=0.472 and 0.983, at 8 and 9 weeks, respectively).

In terms of centre rearing activity, centre rearing activity was sustained from 9 weeks until 12 weeks compared to both control group mice which have lost the ability to centre rear completely by 12 weeks, starting gradually from 10 weeks **(Figure 3.11 B)**.

In particular, Humira treated mice had significantly higher centre rearing counts at 8 weeks compared to controls that were PBS injected s.c. (p=0.023). By 9 weeks, both Humira and i.p. injected control mice had higher centre rearing counts compared to untreated controls (p=0.009 and 0.008, respectively), to controls injected s.c. (p=0.003 for both) and compared to Enbrel group (p=0.009 and 0.011, rescetively).

Although this could suggest a benefit of i.p. saline and general rehydration on the rearing activity of *Npc1*$^{-/-}$ mice, the ability of Humira treatment to sustain rearing activity beyond all control groups at later time points, suggest an additional benefit of delivering anti-TNF antibodies to *Npc1*$^{-/-}$ mice.

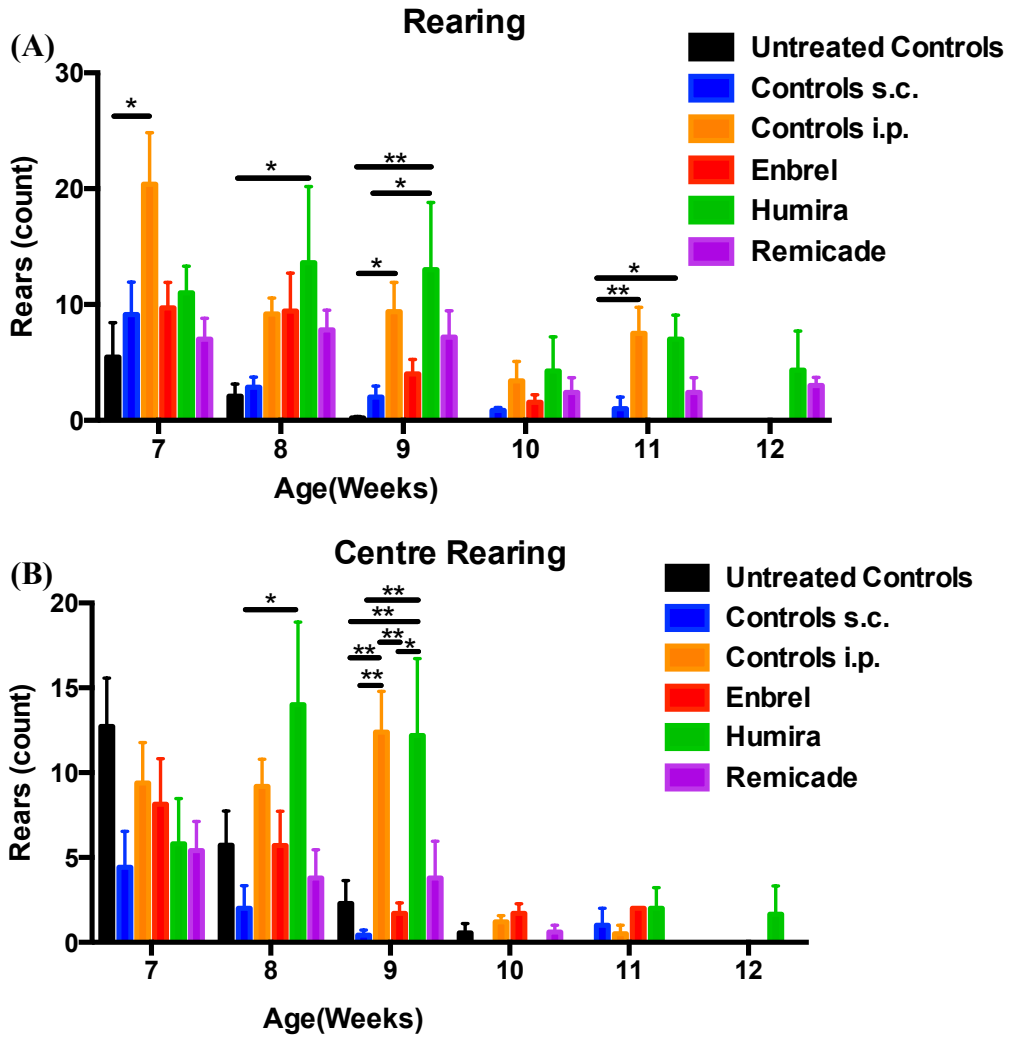

Figure 3.11. Effect of TNF-targeting biologics on (A) rearing and (B) centre rearing of *Npc1*$^{-/-}$ mice. Data presented as mean (rearing count) ± SEM. **p*<0.05 and ***p*<0.01, calculated using one-way ANOVA with Tukey's post hoc test (n=5-14).

Average tremor amplitude over the high frequency range (31-51 Hz) was not different between the groups until 11 weeks, where i.p. control group had a significantly higher tremor amplitude compared to both untreated controls and Humira treated group indicative of a potential positive effect of Humira on tremor at this time point compared to i.p. saline only **(Figure 3.12 and Figure 3.13).**

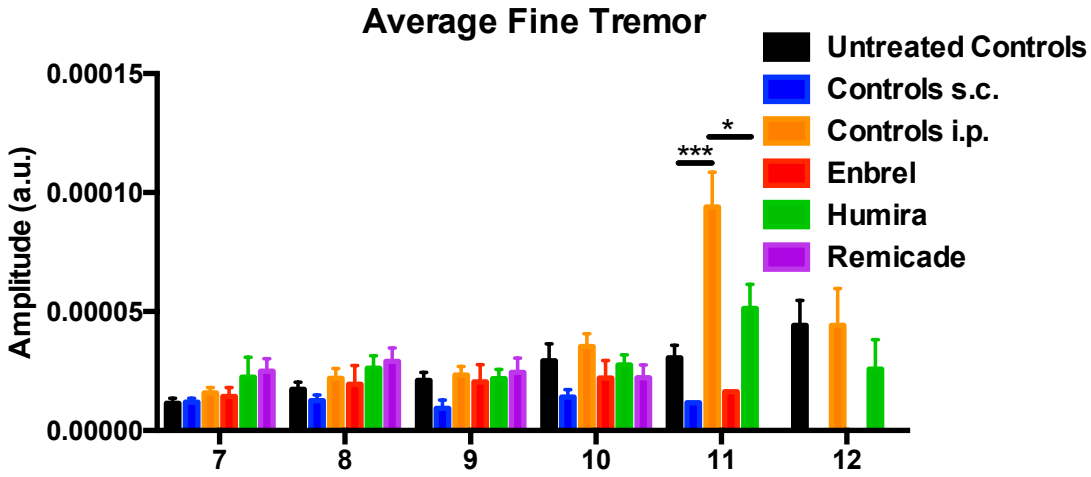

Figure 3.12. Effect of TNF-targeting biologics on fine tremor of *Npc1*$^{-/-}$ mice. Tremor amplitudes quantified as averaged fine tremor amplitude (over the range 31-51 Hz). Data presented as mean ± SEM. *p<0.05 and ***p<0.001, calculated using one-way ANOVA with Tukey's post hoc test (n=5-14), untreated controls are untreated *Npc1*$^{-/-}$ controls.

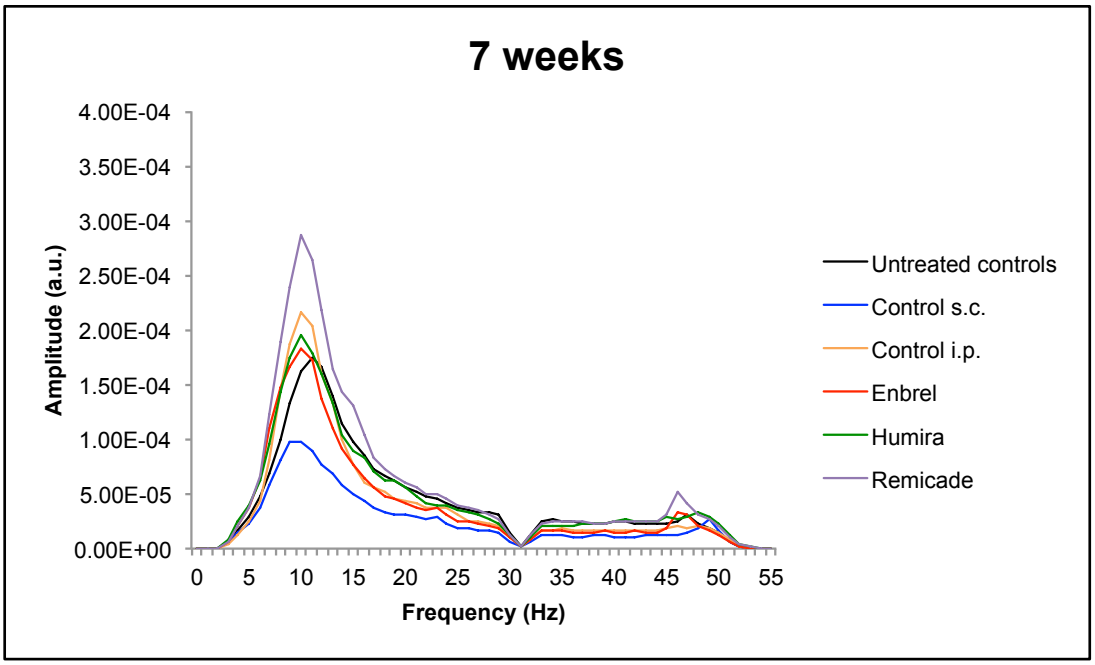

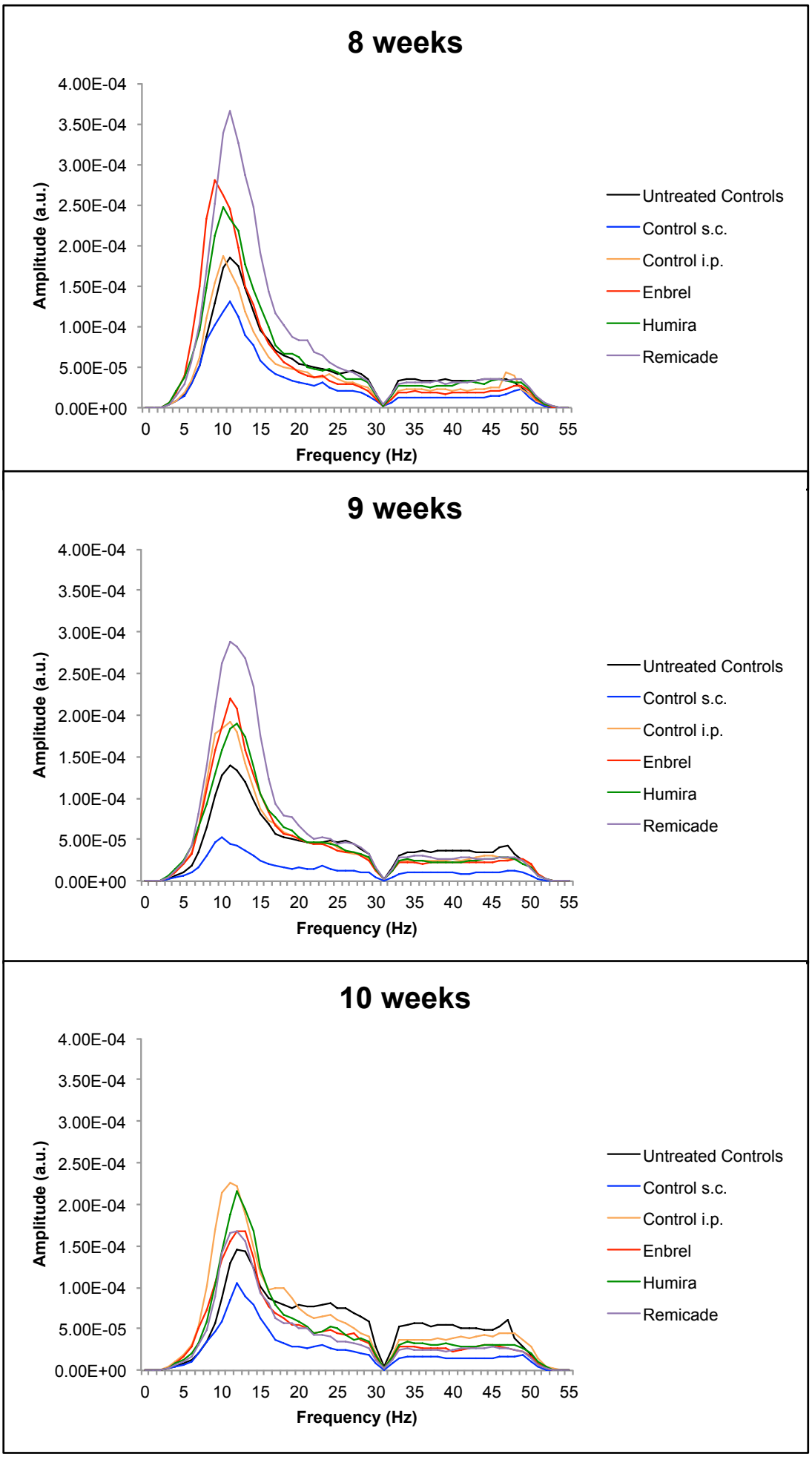
8 weeks
Amplitude (a.u.)
4.00E-04
3.50E-04
3.00E-04
2.50E-04
2.00E-04
1.50E-04
1.00E-04
5.00E-05
0.00E+00
0 5 10 15 20 25 30 35 40 45 50 55
Frequency (Hz)
Untreated Controls
Control s.c.
Control i.p.
Enbrel
Humira
Remicade
9 weeks
Amplitude (a.u.)
4.00E-04
3.50E-04
3.00E-04
2.50E-04
2.00E-04
1.50E-04
1.00E-04
5.00E-05
0.00E+00
0 5 10 15 20 25 30 35 40 45 50 55
Frequency (Hz)
Untreated Controls
Control s.c.
Control i.p.
Enbrel
Humira
Remicade
10 weeks
Amplitude (a.u.)
4.00E-04
3.50E-04
3.00E-04
2.50E-04
2.00E-04
1.50E-04
1.00E-04
5.00E-05
0.00E+00
0 5 10 15 20 25 30 35 40 45 50 55
Frequency (Hz)
Untreated Controls
Control s.c.
Control i.p.
Enbrel
Humira
Remicade

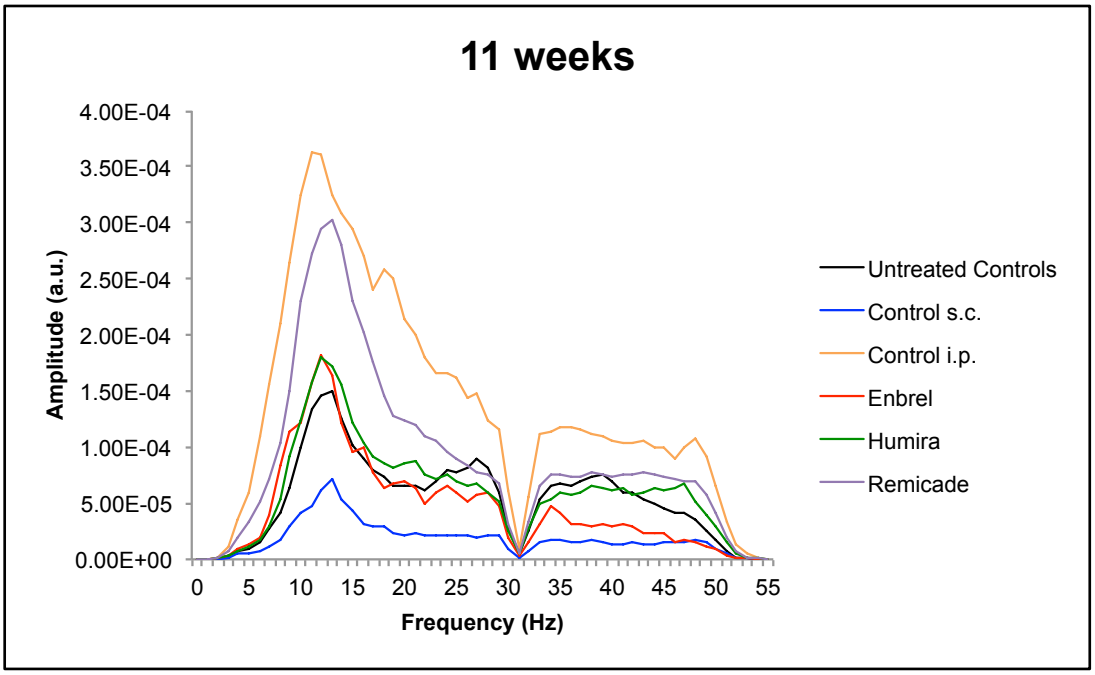

Figure 3.13. Effect of TNF-targeting biologics on tremor of *Npc1*$^{-/-}$ mice. Overall tremor range Data presented as mean tremor amplitude between 0 and 55 Hz (n=5-14), untreated controls are untreated *Npc1*$^{-/-}$ controls.

3.3.2. Calcium modulators (curcumin)

Curcumin, a calcium modulating agent (weak SERCA antagonist (112)), which has proven to be beneficial in NPC disease; increasing survival rates, slowing disease progression, improving motor function and reducing GSL storage in the brain (37), has also been investigated at two different doses: 150 and 250 mg/kg/day, mixed with normal diet in a powdered form. Curcumin at 150 mg/kg/day and a curcuminoids mixture (curcumin, demethoxycurcumin and bisdemethoxycurcumin, **Figure 3.14**) at the same dose were also tested in a different form, mixed with the mouse chow which was then reformulated into pellets (P), as food pellets are consumed more efficiently and so allow more optimal dosing (206). These treatments were initiated at weaning (3 weeks). Another set of animals generated from a new colony (as opposed to the old colony which has been maintained for long time and may have been exposed to environmental factors such as infections) was also included for comparison, with two higher doses 250 and 300 mg/kg curcumin in powdered form, with their untreated controls.

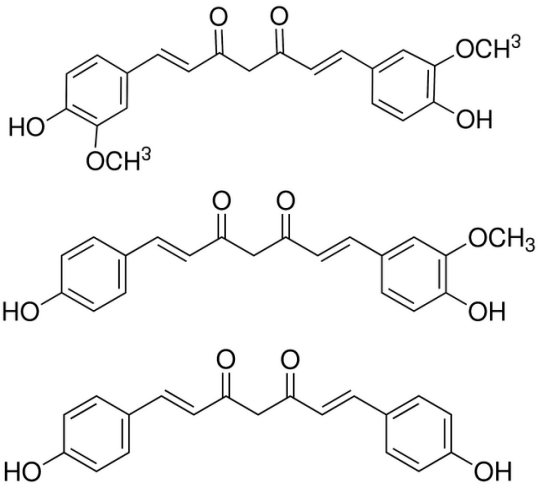

Figure 3.14. Structural formulae of (A) Curcumin, (B) Demethoxycurcumin and (C) Bisdemethoxycurcumin.

Life span increased significantly only with the low dose curucmin (curcumin/powdered chow: p=0.016) **(Figure 3.15)**.

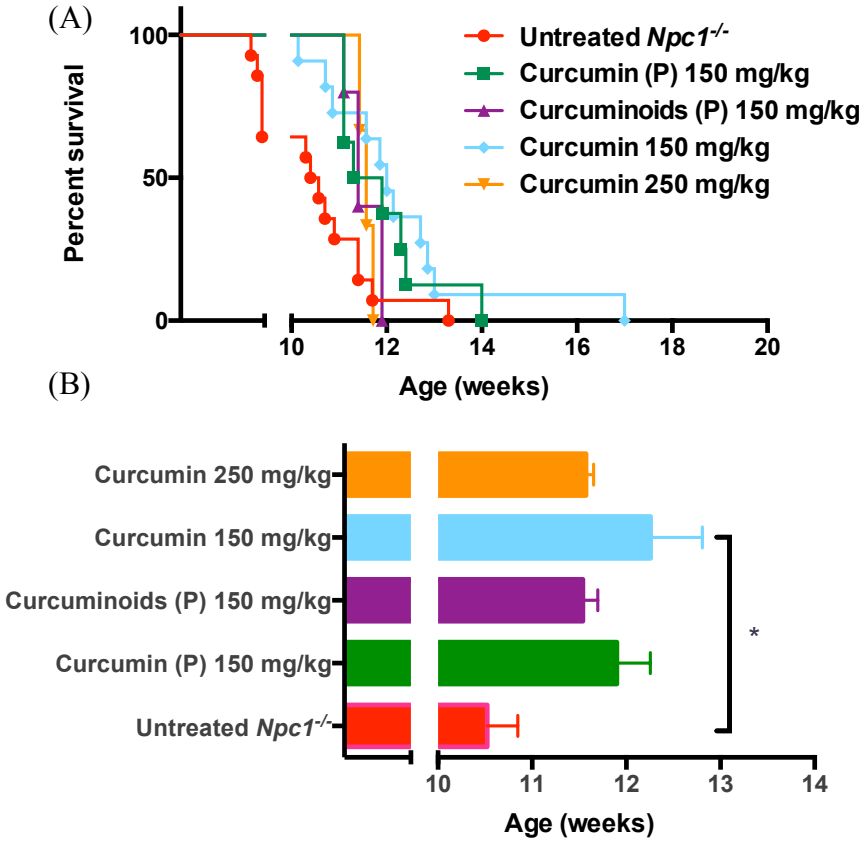

Figure 3.15. Effect of curcumin (at different doses and formulations) on survival of *Npc1*$^{-/-}$ mice. (A) Kaplan–Meier survival curve (percent survival) and (B) Average survival ages. Data presented as mean ± SEM. *p<0.05, calculated using one-way ANOVA with Tukey's post hoc test (n=3-14).

Growth curves **(Figure 3.16)** show similar pattern of weight gain throughout the life span except for the high dose curcumin where the mice dropped more weight at late symptomatic stage suggesting the toxicity associated with this dose.

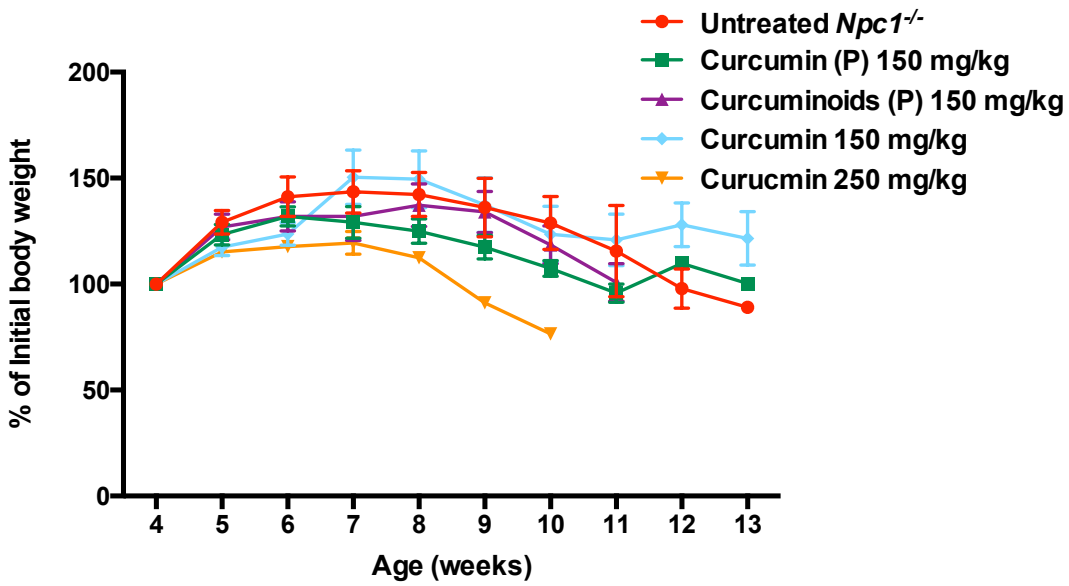

Figure 3.16. Effect of curcumin (at different doses and formulations) on weight loss of *Npc1*$^{-/-}$ mice. Data presented as mean (percent of initial body weight) ± SEM. One-way ANOVA with Tukey's post hoc test was performed (n=3-14).

Only curcuminids diet was associated with a significantly higher rearing count at 8 weeks (p=0.001, 0.010, 0.003 and <0.0001 compared to untreated controls, pelleted curcumin, high and low dose curcumin, respectively) **(Figure 3.17 A)**. By 9 weeks, pelleted curcumin diet resulted in increased rearing activity (p=0.006, 0.039 and 0.001 compared to untreated controls, high and low dose curcumin, respectively). Both groups on pelleted diets sustained their rearing activity up to 11 weeks where all other groups lost their rearing ability completely. Signs of toxicity associated with the higher dose of curcumin were seen with the motor function deterioration evident at all disease stages and reduced body weight. Mice on the high curcumin diet lost their centre rearing activity by 7 weeks and had lower centre rearing counts starting from 6 weeks.

Both curcumin and curcuminids administered with the pelleted diet were accompanied by a significantly higher centre rearing counts (p=0.040 and 0.028 vs. untreated controls and p=0.038 and 0.028 vs. curcumin administered with dry admix, respectively at 9 weeks), by 10 weeks only the pelleted curuminoids mix was associated with enhanced centre activity (p=0.034 and 0.030 vs. untreated controls and curcumin administered with dry admix, respectively) indicative of improved neurological/motor function **(Figure 3.17 B)**.

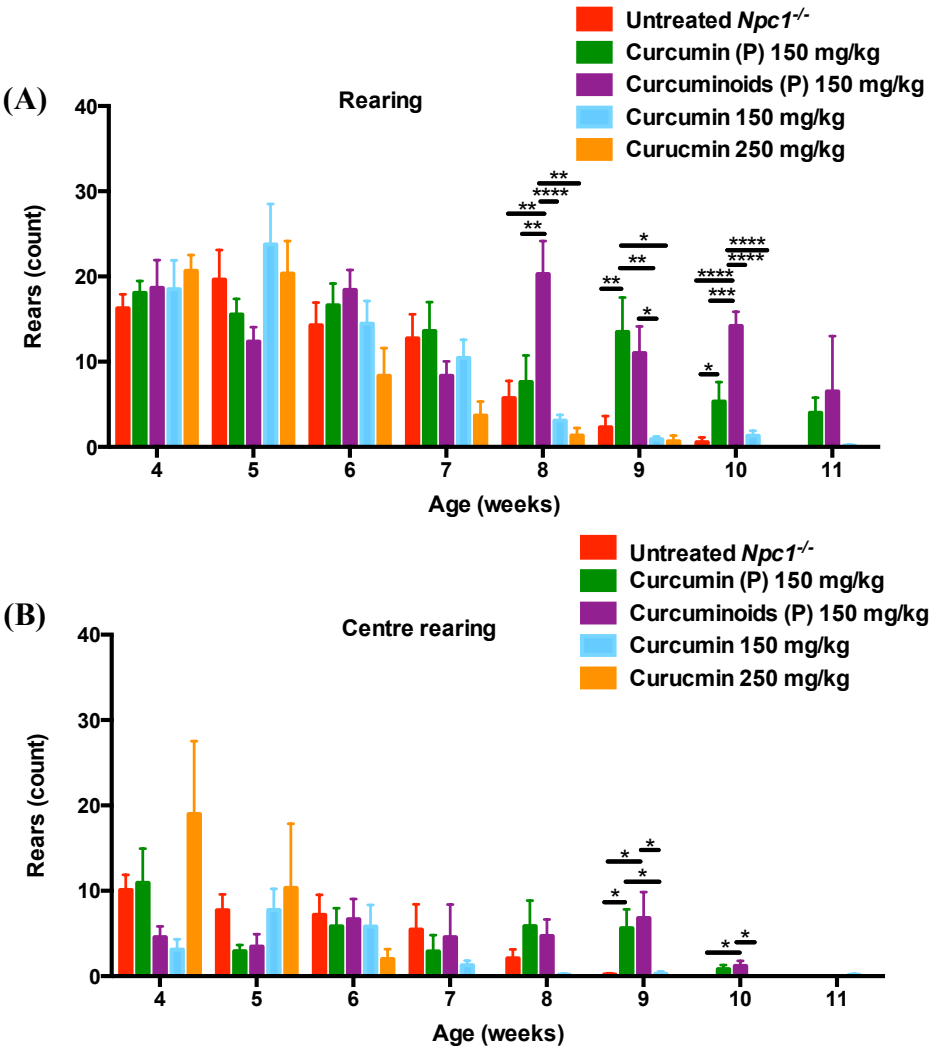

Figure 3.17. Effect of curcumin (at different doses and formulations) on (A) rearing and (B) centre rearing of *Npc1*$^{-/-}$ mice. Data presented as mean (rearing count) ± SEM. *p<0.05, **p<0.01, ***p<0.001 and p<0.0001, calculated using one-way ANOVA with Tukey's post hoc test (n=3-14).

On the other hand, weekly tremor monitoring **(Figure 3.18** and **Figure 3.19)** revealed that only the 150 mg/kg curucmin group had a significantly lower fine tremor amplitude throughout their life span compared to untreated controls (p=0.001, 0.005, <0.0001 and 0.023 at 5, 6, 7 and 9 weeks, respectively).

Interestingly, the 150 mg/kg curcumin was also more effective than the pelleted formulation (p=0.048, 0.038, 0.019 and 0.008 at 5, 6, 7 and 10 weeks, respectively) and than curcuminoid mix (p=0.022, 0.012 and 0.016 at 5, 7 and 10 weeks, respectively).

Both pelleted diets resulted in worsening of the tremor starting from 10 weeks, which was not statistically significant. The improved motor function upon pelleted curcumin diets suggested an additional advantage of reformulating the diet in a better-consumed form. Pure curcuimn (as opposed to curcuminoid mixture) offered the extra advantage of extending the life span of treated *Npc1*$^{-/-}$ mice and possibly not causing as much worsening of the tremor. This could be potentially due to all the effects being solely attributed to curcumin rather than the mixed actions of other components. The purest curcumin formulation (free of any curcuminoids) has shown to be associated with the best results in terms of correcting NPC1 cells (Lloyd-Evans, unpublished, personal communication).

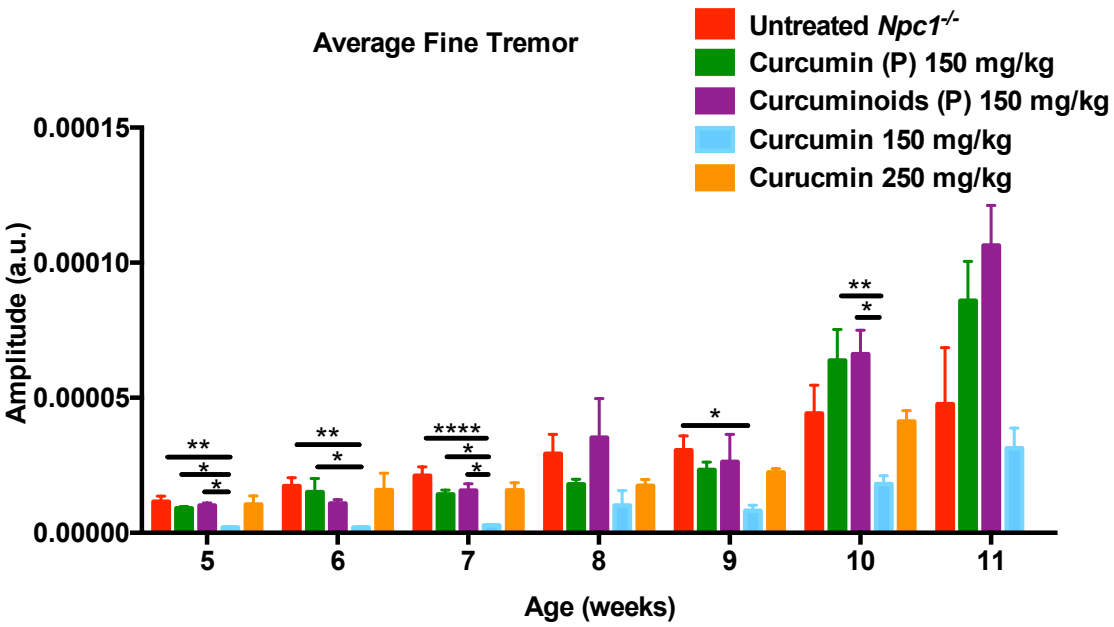

Figure 3.18. Effect of curcumin (at different doses and formulations) on fine tremor of *Npc1*$^{-/-}$ mice. Tremor amplitudes quantified as averaged fine tremor amplitude (over the range 31-51 Hz). Data presented as mean ± SEM. **p*<0.05, ***p*<0.01 and *****p*<0.0001, calculated using one-way ANOVA with Tukey's post hoc test (n=3-14).

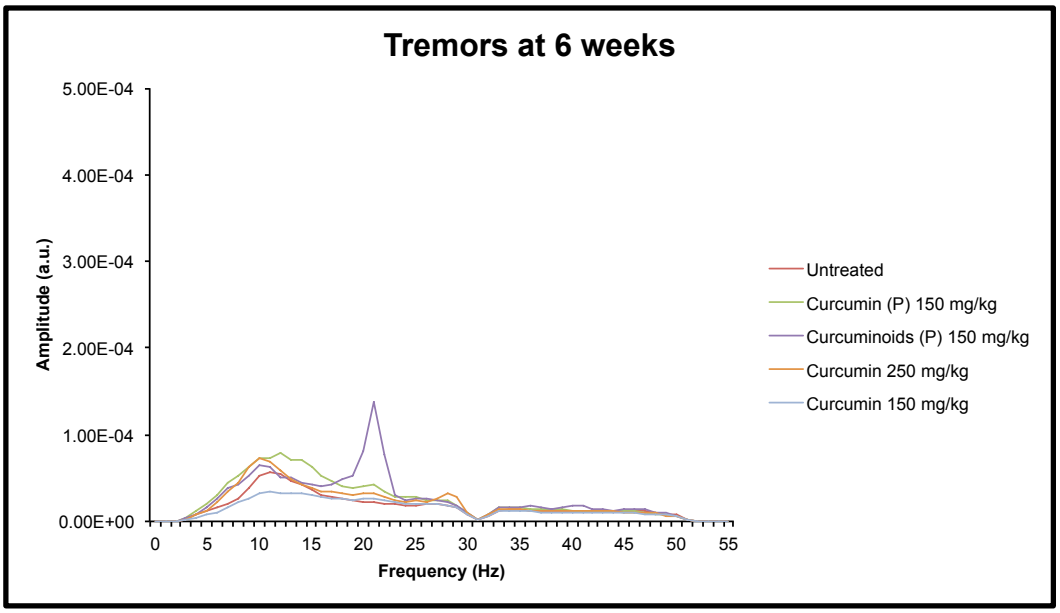

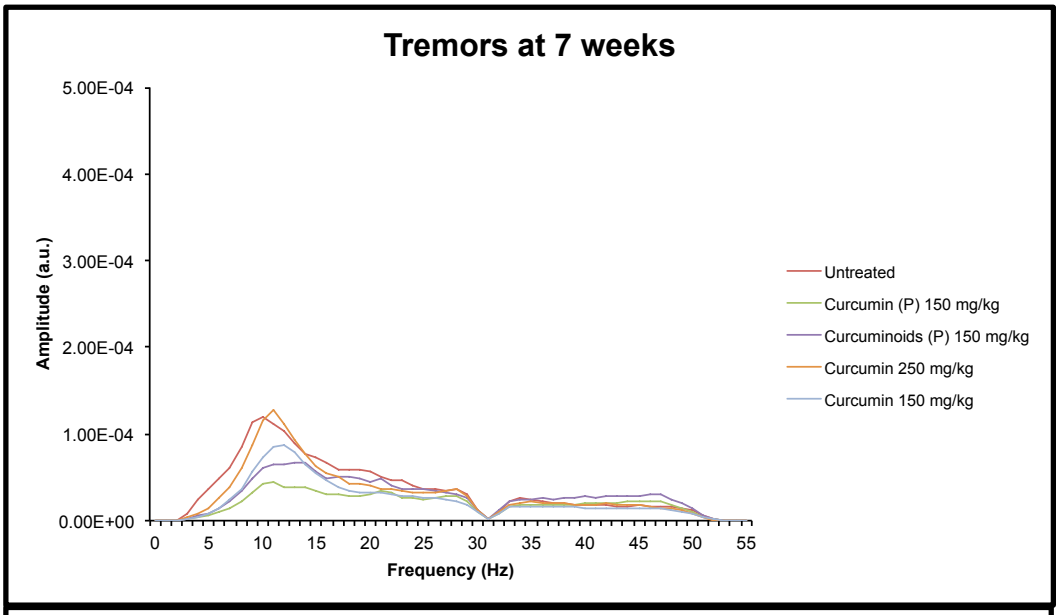
Tremors at 7 weeks
5.00E-04
4.00E-04
3.00E-04
2.00E-04
1.00E-04
0.00E+00
Amplitude (a.u.)
0
5
10
15
20
25
30
35
40
45
50
55
Frequency (Hz)
Untreated
Curcumin (P) 150 mg/kg
Curcuminoids (P) 150 mg/kg
Curcumin 250 mg/kg
Curcumin 150 mg/kg

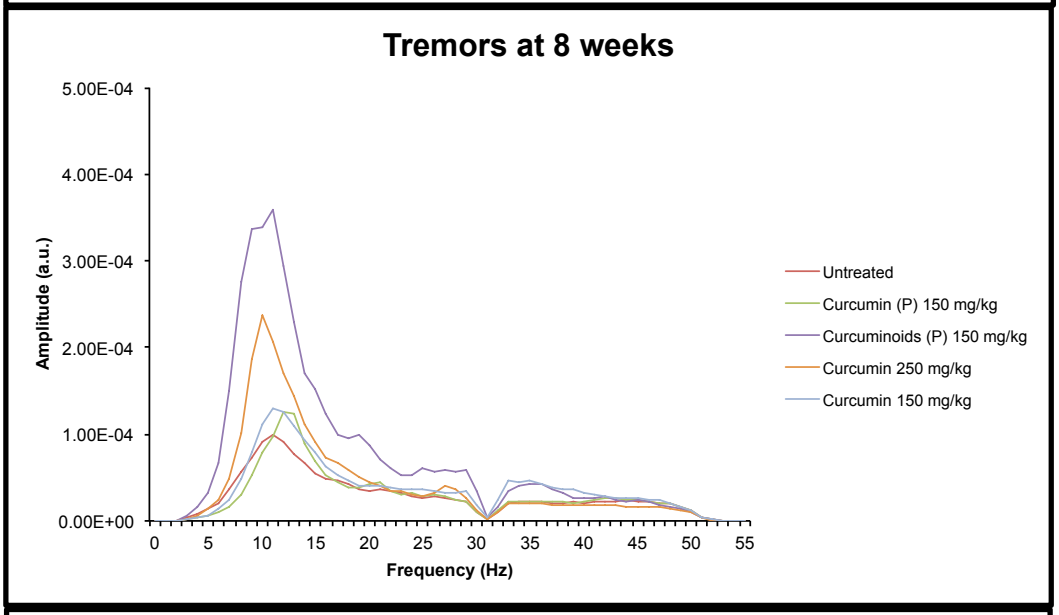
Tremors at 8 weeks
5.00E-04
4.00E-04
3.00E-04
2.00E-04
1.00E-04
0.00E+00
Amplitude (a.u.)
0
5
10
15
20
25
30
35
40
45
50
55
Frequency (Hz)
Untreated
Curcumin (P) 150 mg/kg
Curcuminoids (P) 150 mg/kg
Curcumin 250 mg/kg
Curcumin 150 mg/kg

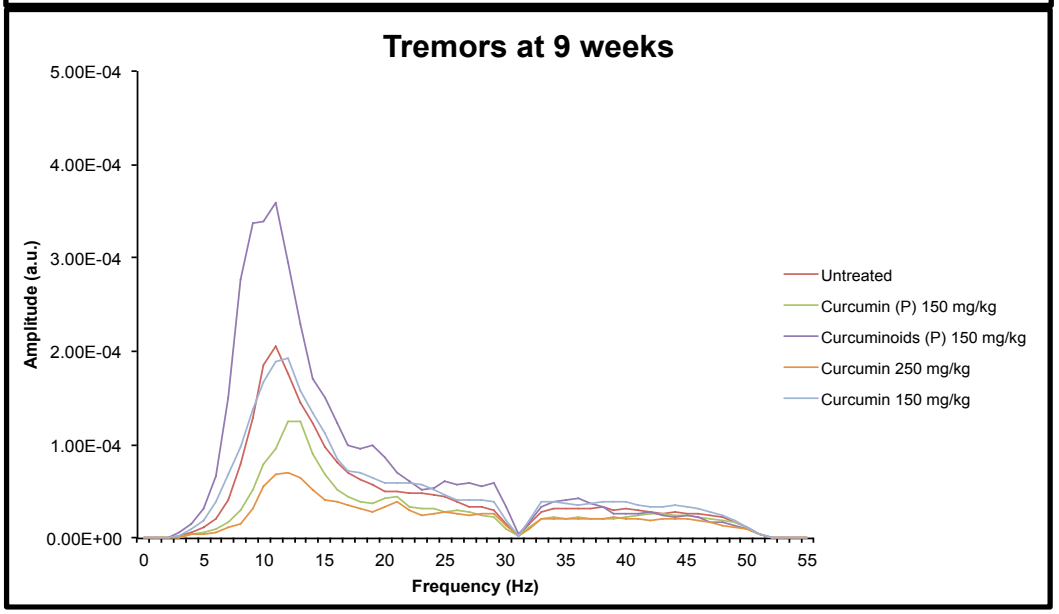
Tremors at 9 weeks
5.00E-04
4.00E-04
3.00E-04
2.00E-04
1.00E-04
0.00E+00
Amplitude (a.u.)
0
5
10
15
20
25
30
35
40
45
50
55
Frequency (Hz)
Untreated
Curcumin (P) 150 mg/kg
Curcuminoids (P) 150 mg/kg
Curcumin 250 mg/kg
Curcumin 150 mg/kg

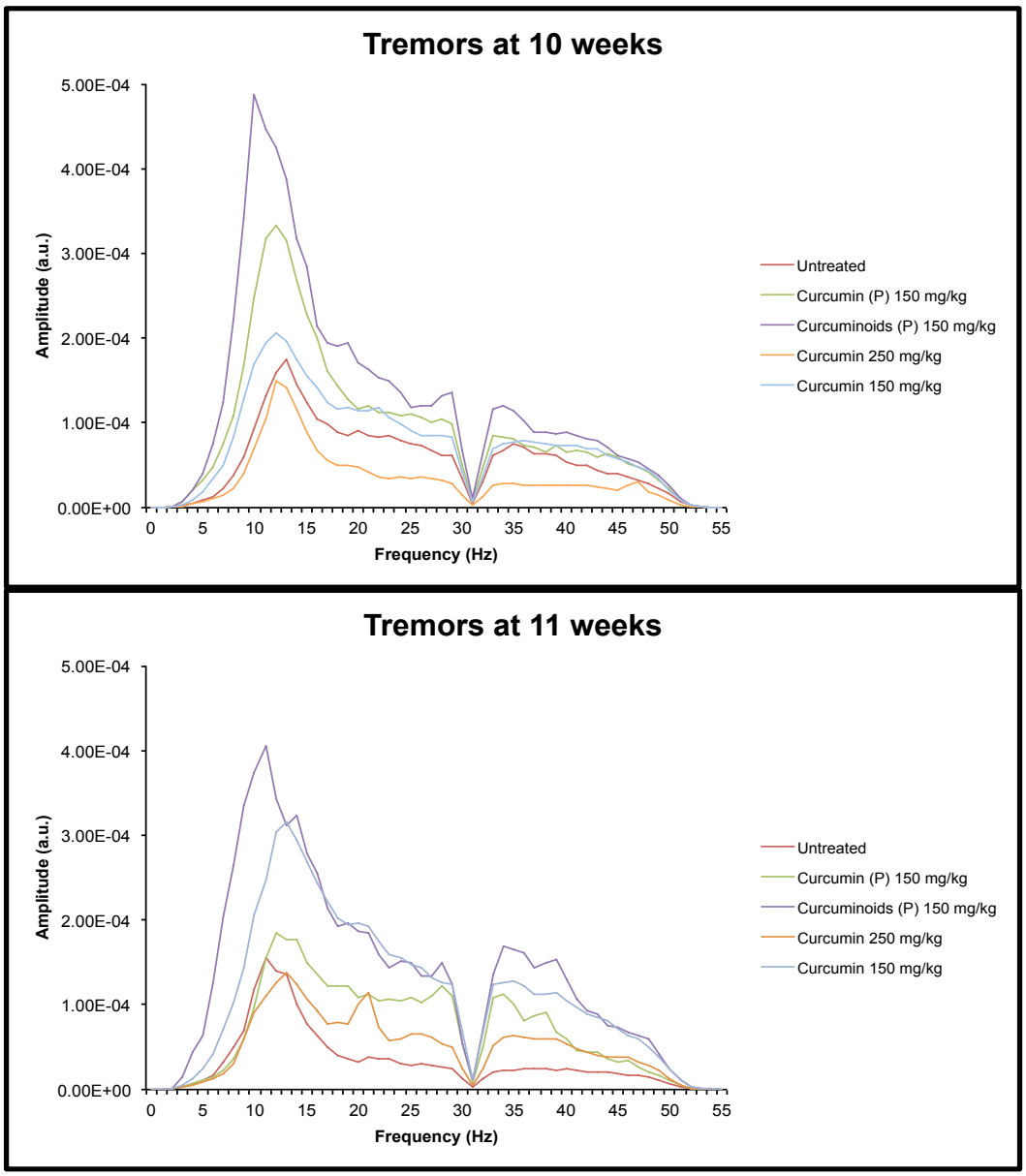

Figure 3.19. Effect of curcumin (at different doses and formulations) on tremor of *Npc1*$^{-/-}$ mice. Data presented as mean tremor amplitude between 0 and 55 Hz (n=3-14), untreated controls are untreated *Npc1*$^{-/-}$ controls.

We have then revisited the higher dose approach in a new colony to assess the effect of environmental factors and genetic drifts on the efficacy of the higher doses of curcumin in *Npc1*$^{-/-}$ mice. Although the life span of untreated controls has extended by 2 weeks, the high dose curcumin diets were not associated with an additional extension of the life span beyond that **(Figure 3.20)**.

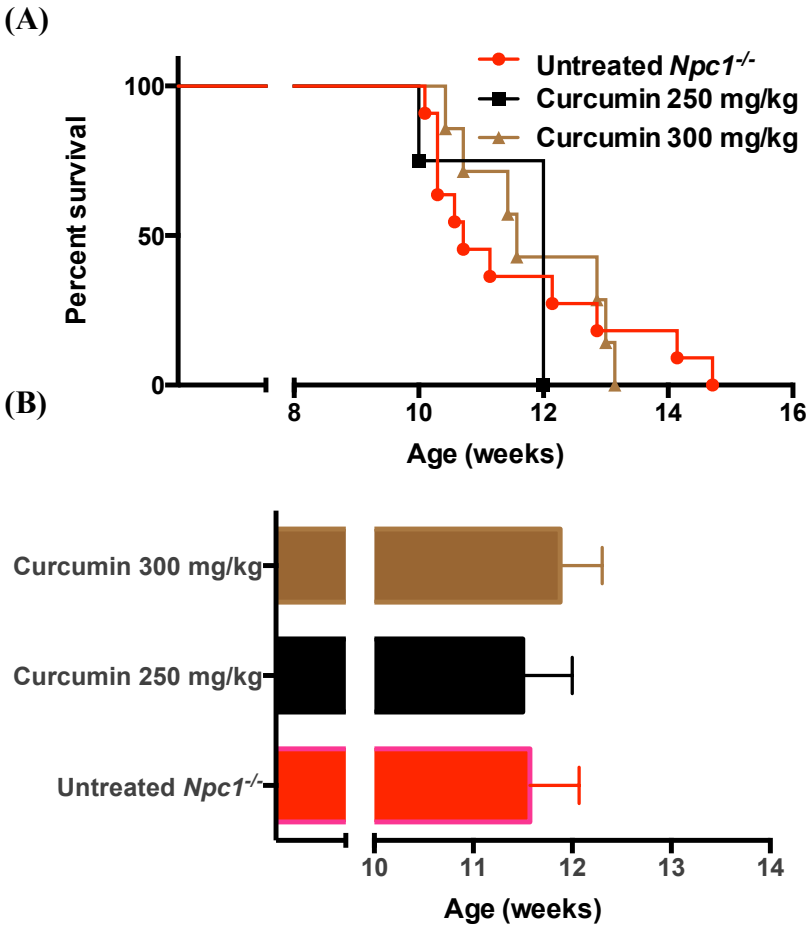

Figure 3.20. Effect of high dose curcumin on survival of *Npc1*$^{-/-}$ mice from the new colony. (A) Kaplan–Meier survival curve (percent survival) and (B) Average survival ages. Data presented as mean ± SEM. One-way ANOVA with Tukey's post hoc test (n=4-11).

However, the clean status of the colony has resulted in an improved weight loss profile of curcumin (high dose) treated *Npc1*$^{-/-}$ mice compared to untreated controls **(Figure 3.21)**. The rate of weight loss was slower in both treatment groups, the 250 mg/kg group gained more weight in early symptomatic stage while the 300 mg/kg group did not start losing weight until 9-10 weeks.

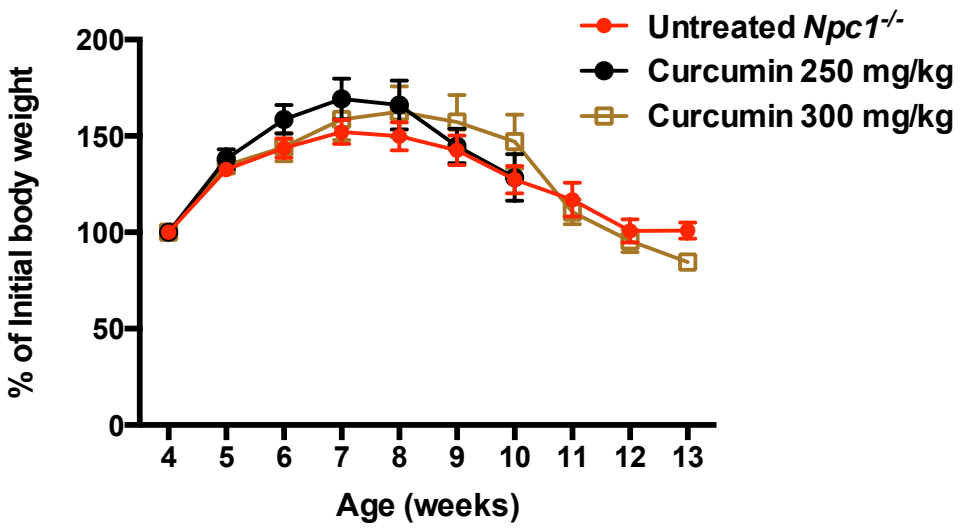

Figure 3.21. Effect of high dose curcumin on weight loss of *Npc1*$^{-/-}$ mice from the new colony. Data presented as mean (percent of initial body weight) ± SEM. One-way ANOVA with Tukey's post hoc test was performed (n=4-11).

The effect of the high dose curcumin in the new colony was also evident from improved rearing activity of the 250 mg/kg group (p=0.007 and 0.005 vs. untreated controls and the 300 mg/kg groups at 7 weeks and p=0.0007 and 0.002 vs. untreated controls and 300 mg group, respectively at 9 weeks). This was lower at 6 up to 9 weeks compared to all groups in the old colony **(Figure 3.22 A).**

Similarly, centre rearing activity of the 250 mg/kg group was significantly higher (p=0.013 vs. 300 mg group at 5 weeks, p=0.0004 and 0.0002 vs. untreated controls and 300 mg group, respectively at 6 weeks and p=0.037 vs. 300 mg group at 7 weeks). This was lower at 6 weeks than all groups and completely lost at 7 weeks, in the old colony **(Figure 3.22 B).**

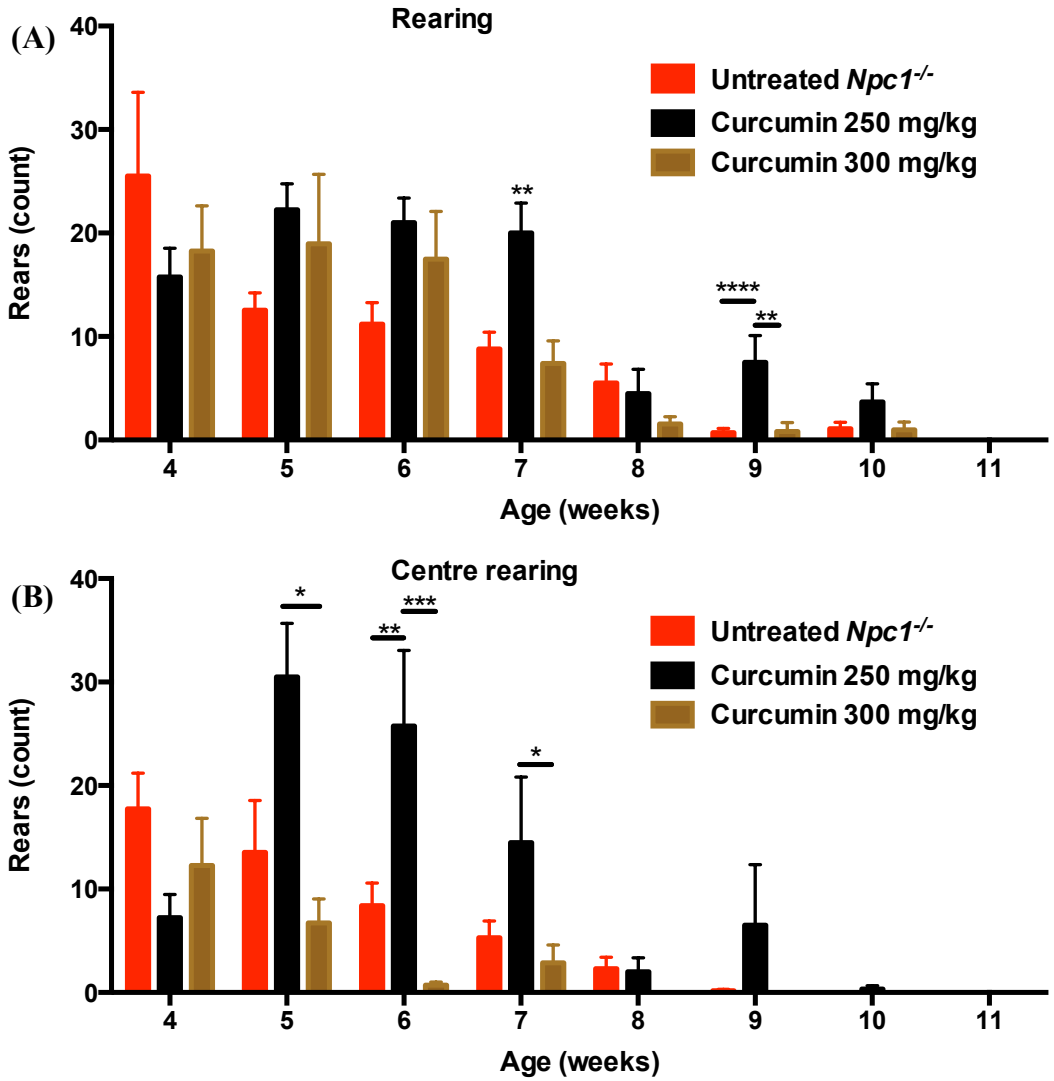

Figure 3.22. Effect of high dose curcumin on (A) rearing and (B) centre rearing of *Npc1*$^{-/-}$ mice from the new colony. Data presented as mean (rearing count) ± SEM. **p*<0.05, ***p*<0.01, ****p*<0.001 and *****p*<0.0001, calculated using one-way ANOVA with Tukey's post hoc test (n=4-11).

Although re-deriving the colony resulted also in a decrease in the fine tremor amplitude of untreated *Npc1*$^{-/-}$ mice, both high dose curcumin diets did not further reduce fine tremor in treated mice, however, they were not associated with a worsening of this phenotype **(Figure 3.23** and **Figure 3.24).**

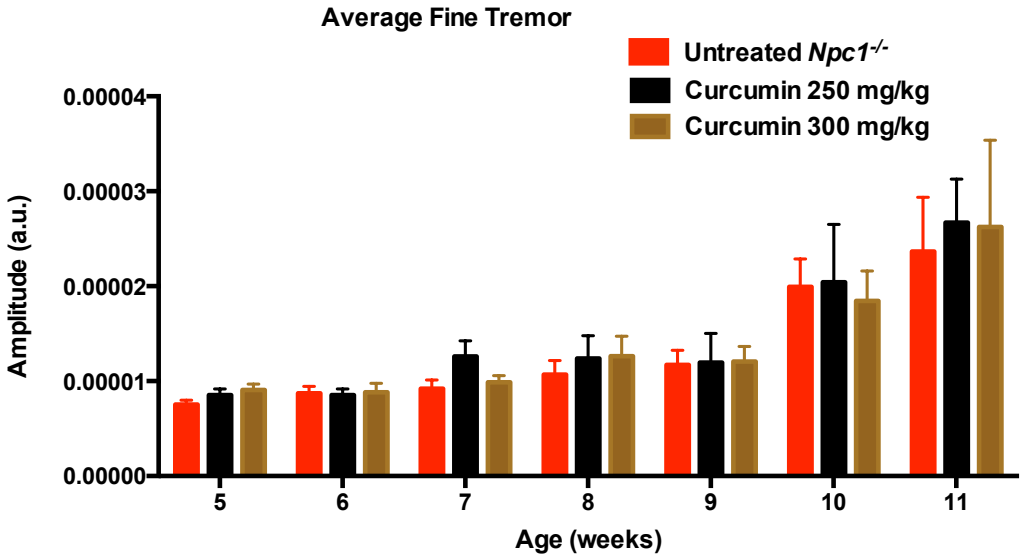

Figure 3.23. Effect of high dose curcumin on fine tremor of *Npc1*$^{-/-}$ mice from the new colony. Tremor amplitudes quantified as averaged fine tremor amplitude (over the range 31-51 Hz). Data presented as mean ± SEM. One-way ANOVA with Tukey's post hoc test (n=4-11).

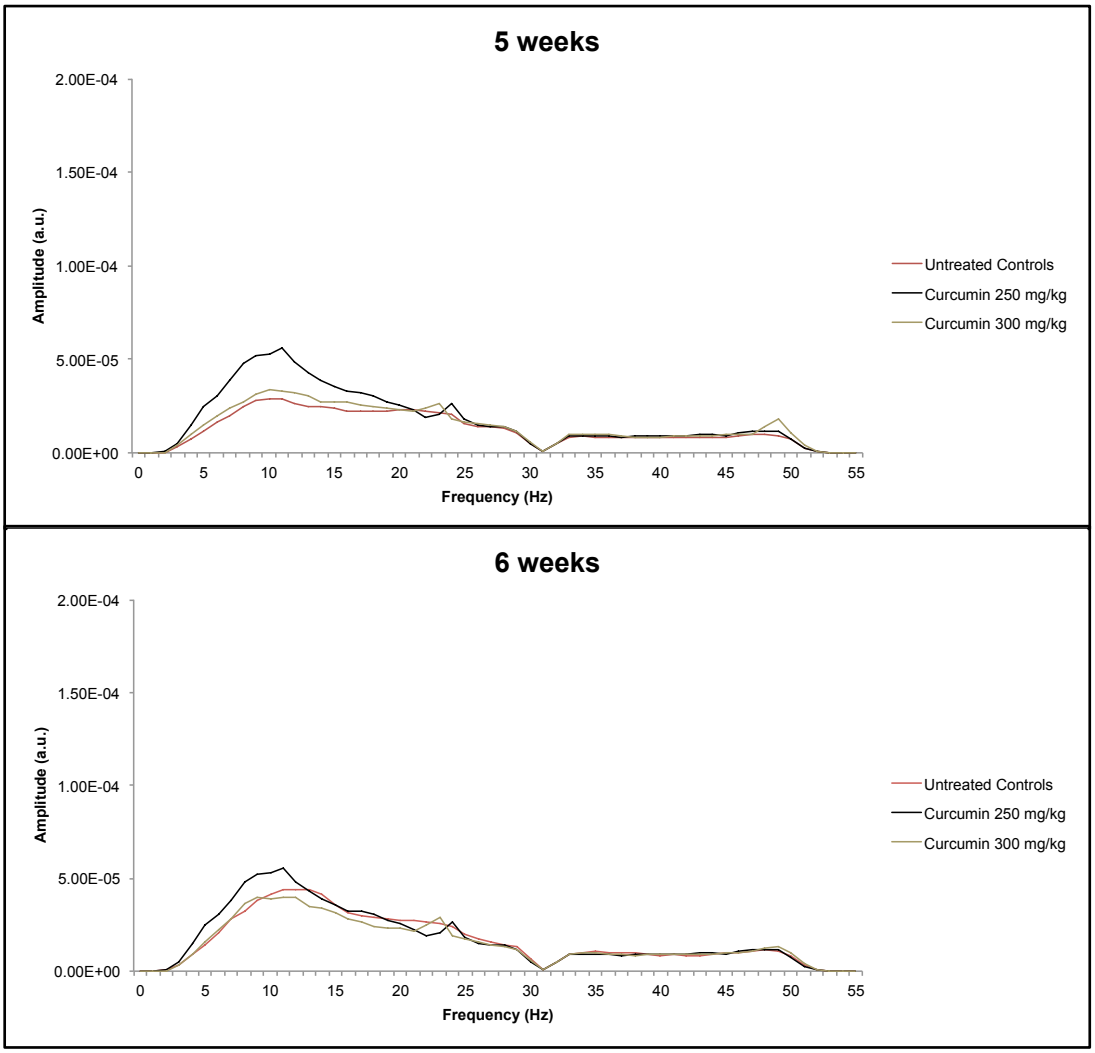

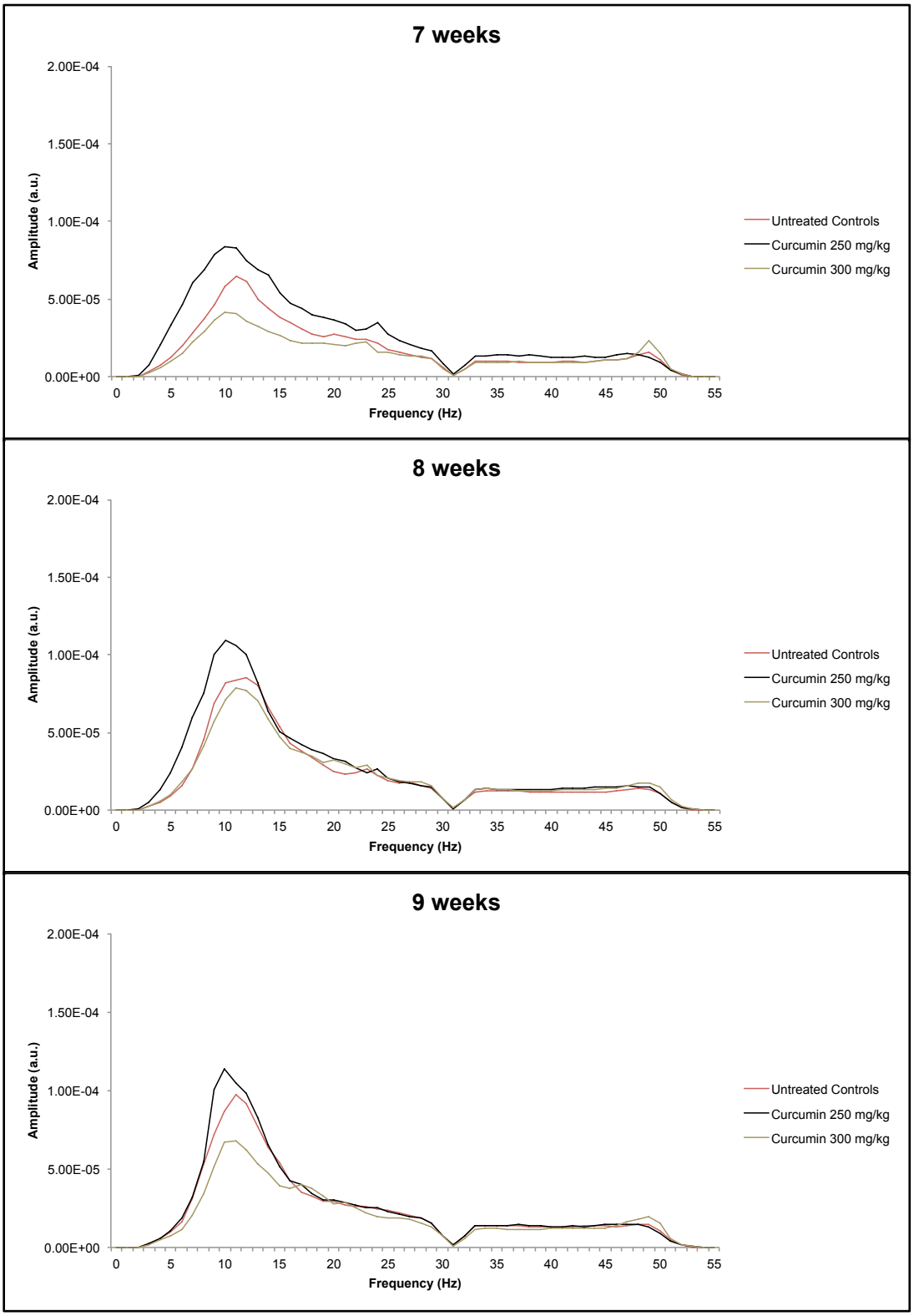
7 weeks
Amplitude (a.u.)
2.00E-04
1.50E-04
1.00E-04
5.00E-05
0.00E+00
0
5
10
15
20
25
30
35
40
45
50
55
Frequency (Hz)
Untreated Controls
Curcumin 250 mg/kg
Curcumin 300 mg/kg
8 weeks
Amplitude (a.u.)
2.00E-04
1.50E-04
1.00E-04
5.00E-05
0.00E+00
0
5
10
15
20
25
30
35
40
45
50
55
Frequency (Hz)
Untreated Controls
Curcumin 250 mg/kg
Curcumin 300 mg/kg
9 weeks
Amplitude (a.u.)
2.00E-04
1.50E-04
1.00E-04
5.00E-05
0.00E+00
0
5
10
15
20
25
30
35
40
45
50
55
Frequency (Hz)
Untreated Controls
Curcumin 250 mg/kg
Curcumin 300 mg/kg

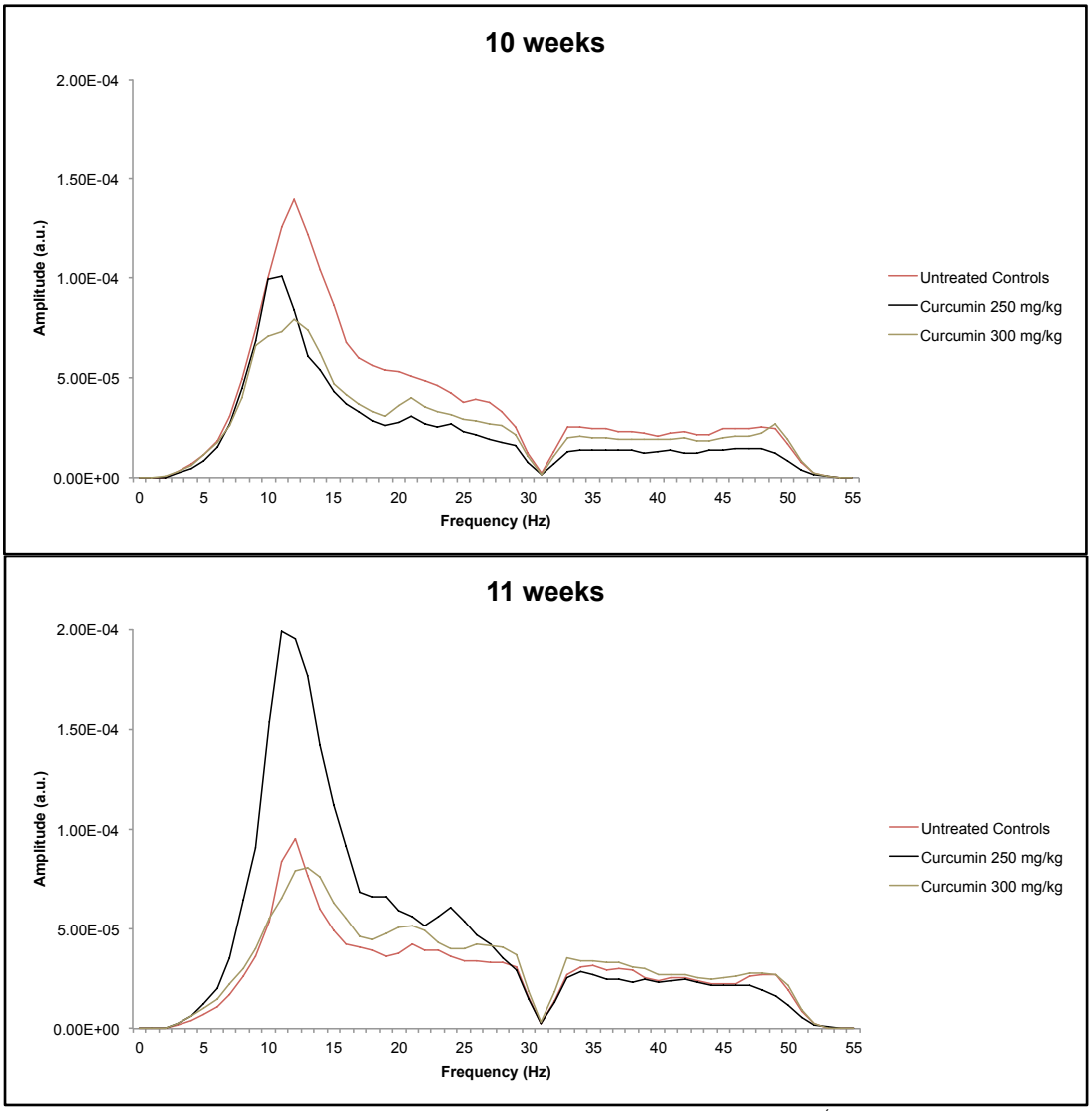

Figure 3.24. Effect of high dose curcumin on tremor of *Npc1*$^{-/-}$ mice from the new colony. Data presented as mean tremor amplitude between 0 and 55 Hz (n=3-14), untreated controls are untreated *Npc1*$^{-/-}$ controls.

3.3.3. Bile acid supplementation

While assessing the effect of bile acid supplementation on drug metabolising capacity of *Npc1*$^{-/-}$ mice (Chapter 2), we saw improvement in neurological function (enhanced rearing activity and reduced tremor amplitude) and therefore investigated this further and evaluated the combination of this therapy with high dose curcumin (to assess its effect on reducing accompanying toxicity) and with *N*B-DGJ. Only *N*B-DGJ (galactose analogue of miglustat, also a GSL biosynthesis inhibitor (214)) alone or in combination was associated with a marked increase in life span of treated mice **(Figure 3.25)**. No significant differences in survival were observed upon administration of UDCA (p=0.438), curcumin (p=0.949) or their combination (p=0.979). *N*B-DGJ treatment significantly extended the life span of treated mice compared to untreated, UDCA-treated, curcumin-treated and UDCA with curucmin treatment groups (p<0.0001). Both the triple combination and UDCA with *N*B-DGJ groups lived significantly longer than the untreated control group (p=0.002 and 0.0005), single treatment groups (p=0.0003 and <0.0001 vs. curcumin group and p=0.0002 and <0.0001 vs. UDCA) and UDCA with curcumin group (p=0.002 and 0.0005). Interestingly, the addition of UDCA to any diet was associated with a reduction in survival rates, although the differences were not significant (p=0.377 vs. *N*B-DGJ group and 0.949 vs. curcumin group). There was no difference in survival between the *N*B-DGJ double and triple combination groups (p=0.949).

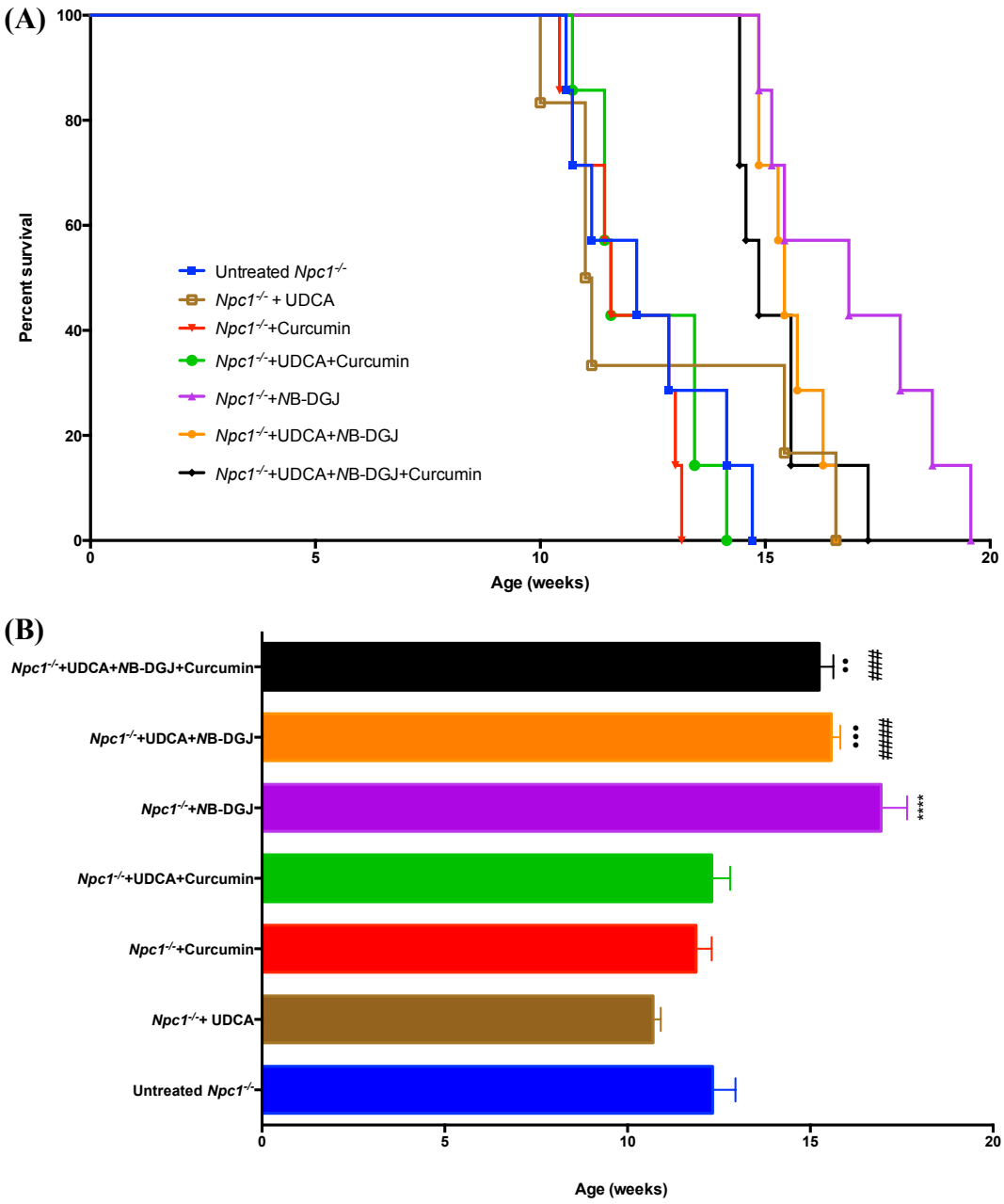

Figure 3.25. Effect of test compounds on survival of *Npc1*$^{-/-}$ mice. (A) Kaplan–Meier survival curve (percent survival) and (B) Average survival ages. Data presented as mean ± SEM. ***p*<0.01, ****p*<0.001 and *****p*<0.0001, calculated using one-way ANOVA with Tukey's post hoc test (n=7). * denotes comparison vs. untreated *Npc1*$^{-/-}$, *Npc1*$^{-/-}$+UDCA, *Npc1*$^{-/-}$+curcumin, and *Npc1*$^{-/-}$+UDCA+curcumin. • denote somparison vs. untreated *Npc1*$^{-/-}$, *Npc1*$^{-/-}$+UDCA+curcumin and # denotes comparison vs. *Npc1*$^{-/-}$+UDCA and *Npc1*$^{-/-}$ +curcumin.

UDCA treatment was associated with significant weight loss, which has been reported before and the mechanism of which is not clear (215). However, when

combined with *N*B-DGJ alone or with curcumin as well, UDCA was associated with a marked protection from weight loss at 9 and 10 weeks **(Figure 3.26)**.

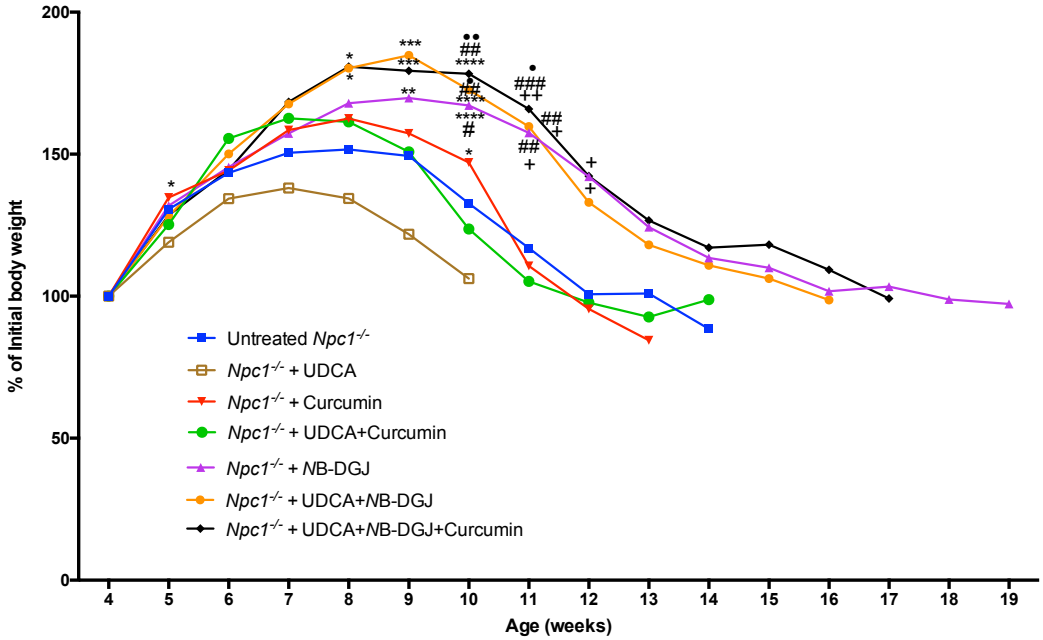

Figure 3.26. Effect of test compounds on weight loss of *Npc1*$^{-/-}$ mice. Data presented as mean (percent of initial body weight). *p<0.05, **p<0.01, ***p<0.001 and ****p<0.0001, calculated using one-way ANOVA with Tukey's post hoc test (n=7). * denotes comparison vs. *Npc1*$^{-/-}$+UDCA, # denotes comparison vs. *Npc1*$^{-/-}$+UDCA+curcumin, + denotes comparison vs. *Npc1*$^{-/-}$+curcumin and • denote somparison vs. untreated *Npc1*$^{-/-}$.

UDCA induced weight loss was evident from 5 weeks of age compared to curcumin treated mice (p=0.049). By 8 weeks the addition of either *N*B-DGJ on its own or with curcumin seems to have partially protected from this weight loss (p=0.014 and 0.013, respectively). This effect became even more significant at later disease stage at 9 weeks (p=0.0001 and 0.0006, respectively). Also *N*B-DGJ treatment on its own produced a better effect on weight loss profile of *Npc1*$^{-/-}$ mice at this point compared to UDCA treatment (p=0.006). By 10 weeks, UDCA treated group weight loss was more profound compared to the other treatment groups. The addition of curcumin resulted in a slight improvement, although neither compound significantly protected from the weight loss associated with the other (p=0.737 and 0.487 for the

combination vs. UDCA and curcumin, respectively), however, the greatest effects were seen with the addition of *N*B-DGJ (for UDCA; $p<0.00001$ vs. *N*B-DGJ alone, UDCA with *N*B-DGJ and triple combination, $p=0.016$ vs. curcumin and for UDCA with curcumin; $p=0.015$, 0.004, 0.001 vs. *N*B-DGJ alone, UDCA with *N*B-DGJ and triple combination).

The triple combination and UDCA with *N*B-DGJ treatments started to show significant difference compared to untreated control at this point ($p=0.009$ and 0.032, respectively). By 12 weeks, with the UDCA treatment being not associated with increased survival beyond around 10 weeks, the weight loss of the curcuimn group became more evident especially compared to the triple combination and *N*B-DGJ groups ($p=0.030$ and 0.031, respectively). For all the groups surviving past 12 weeks, the differences in weight loss were similar; notable they were all on *N*B-DGJ, which so far seems to have mediated the most profound effect on weight loss of *Npc1*$^{-/-}$ mice.

Similar effects on rearing activity were seen **(Figure 3.27)**, except that UDCA treatment on its own resulted in a significant increase in rearing activity starting from 7 weeks and sustained up until 14-15 weeks (for rearing) and 13-14 weeks (for centre rearing) for UDCA combination therapies.

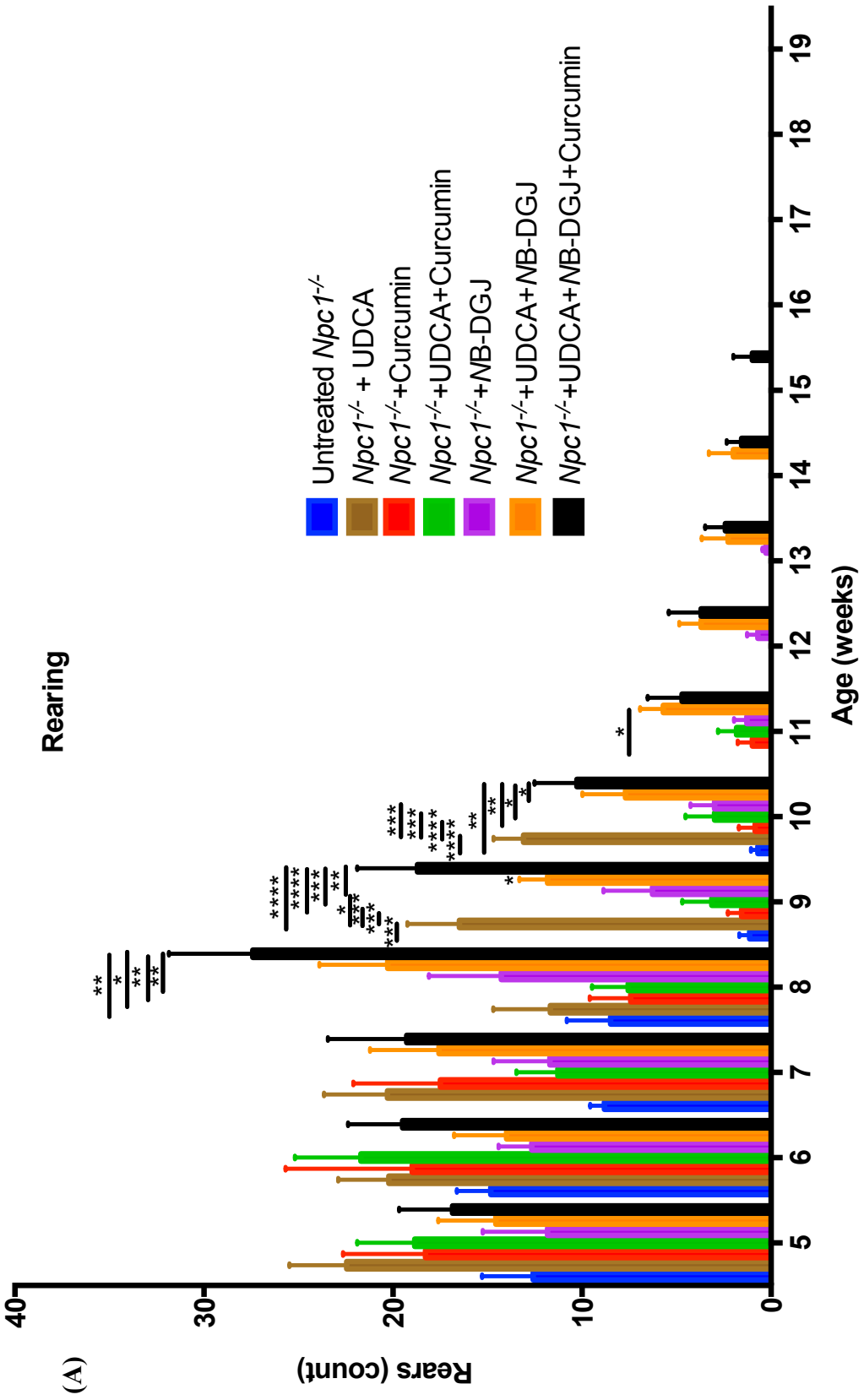
Rearing
Untreated Npc1-/-
Npc1-/- + UDCA
Npc1-/-+Curcumin
Npc1-/-+UDCA+Curcumin
Npc1-/-+NB-DGJ
Npc1-/-+UDCA+NB-DGJ
Npc1-/-+UDCA+NB-DGJ+Curcumin
Rears (count)
Age (weeks)
0
10
20
30
40
5
6
7
8
9
10
11
12
13
14
15
16
17
18
19
(A)

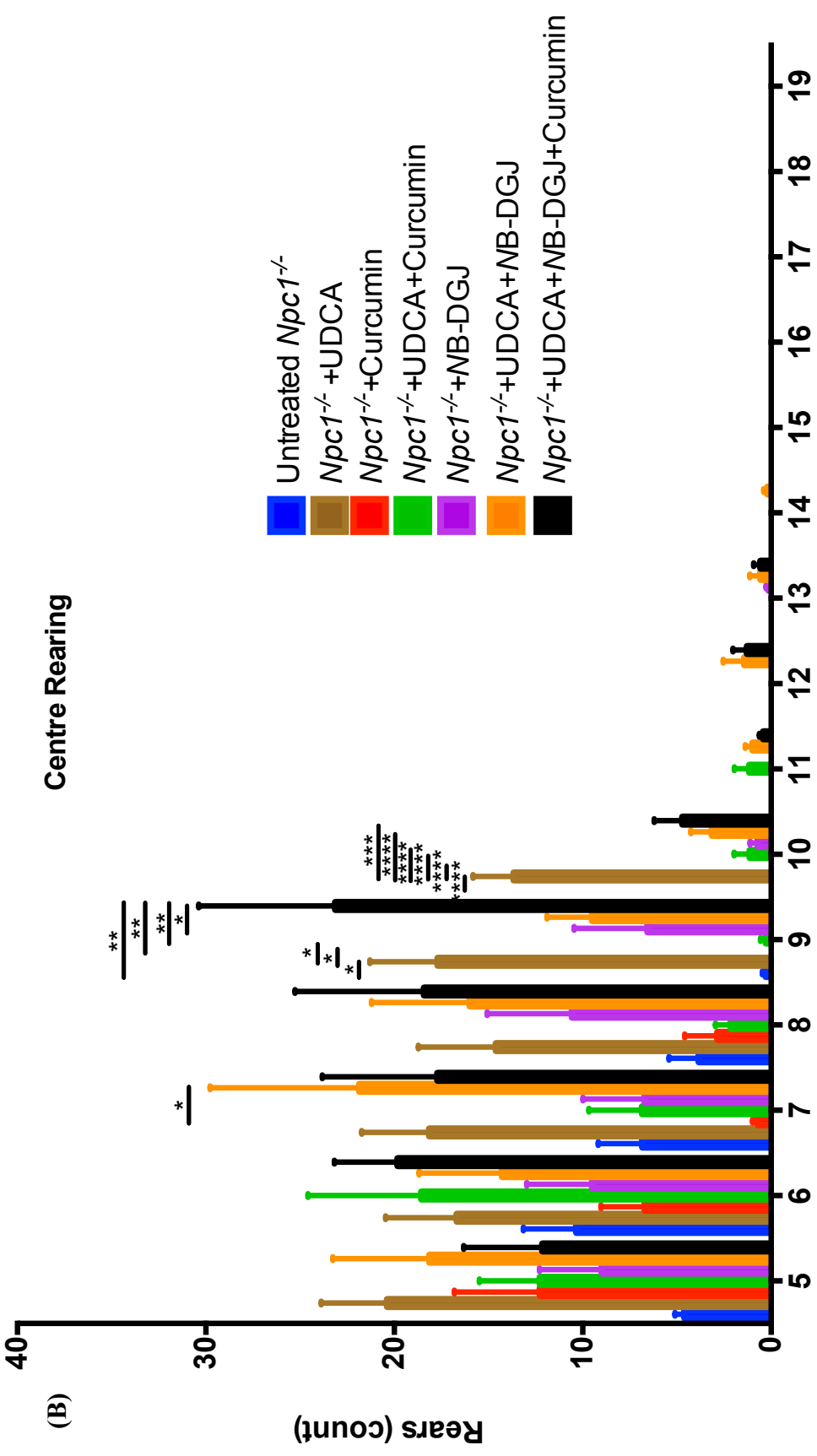

Figure 3.27. Effect of test compounds on (A) rearing and (B) centre rearing of *Npc1*$^{-/-}$ mice. Data presented as mean (rearing count) ± SEM. *p<0.05, **p<0.01 ***p<0.001 and ***p<0.001, calculated using one-way ANOVA with Tukey's post hoc test (n=7).

Rearing activity **(Figure 3.27 A)** of mice on the triple combination therapy starting from 8 weeks was significantly higher than the untreated controls (p=0.009), UDCA group (p=0.010), curcumin group (p=0.003) and UDCA with curcumin group (p=0.003) but similar levels were seen in the other *N*B-DGJ containing therapy groups.

By 9 weeks, the UDCA group became more active and the rearing activity was similar to that of the triple combination group (p=0.989) and the *N*B-DGJ group started to show a significant deterioration compared to the triple combination group (p=0.006). UDCA started to show an improvement starting from 9 weeks with marked increase in rearing activity compared to the untreated controls (p=0.0001), *N*B-DGJ (p=0.0199), curcumin treated group (p=0.0002) as well as the UDCA with curcumin group (p=0.0009). At this stage of the disease, the combination of UDCA and *N*B-DGJ had a positive effect with rearing activity significantly higher than the controls (p=0.038).

By 10 weeks only the triple combination group and the UDCA group sustained this functional improvement over the untreated and the other single treatment groups (p=0.003, 0.003 and 0.041 for the triple combination vs. control, curcumin and *N*B-DGJ groups and p<0.0001, for UDCA vs. control and curcumin groups and p=0.0005 for UDCA vs. *N*B-DGJ group). These two treatments were also superior to the curcumin and UDCA combination treatment (p=0.041 and 0.0005 for the triple combination and UDCA, respectively).

By 11 weeks, the combination of UDCA and *N*B-DGJ survived longer than the UDCA group and showed significantly higher rearing count only in comparison to the control untreated group (p=0.046). From 12 weeks, although the triple

combination and UDCA with *N*B-DGJ treated mice were still alive and sustained rearing activity, the differences were not statistically significant.

The differences in centre rearing capacity of treated mice started from 7 weeks with the UDCA and *N*B-DGJ combination treated mice having significantly higher count compared to the curcumin group (p=0.037) **(Figure 3.27 B)**.

At 9 weeks, similar effect consistent to the rearing activity was observed, the tripple combination and UDCA groups had a marked increase in the centre rearing activity over the untreated controls, (p=0.001 and 0.013, respectively), curcumin treated group (p=0.001 and 0.011, respectively) and UDCA with curucmin (0.001 and 0.012, respectively). The triple combination was also superior to *N*B-DGJ on its own at this stage (p=0.040).

At 10 weeks, only the UDCA treated mice had a significantly higher centre rearing count compared to all the other groups (p<0.0001) and p=0.0001 vs. the triple combination group. Although the triple combination and the UDCA with *N*B-DGJ groups sustained the ability to centre rear after 10 weeks, the differences were not significant and all treated mice completely lost their rearing capacity by 15 weeks.

Fine tremor amplitude of mice treated with either high dose curcumin or *N*B-DGJ in combination with UDCA and the triple combination was significantly lower than UDCA alone at 8 and 9 weeks of age (p=0.039, 0.025 and 0.021 and p=0.0002, 0.025 and 0.001, respectively) **(Figure 3.28** and **Figure 3.29)**.

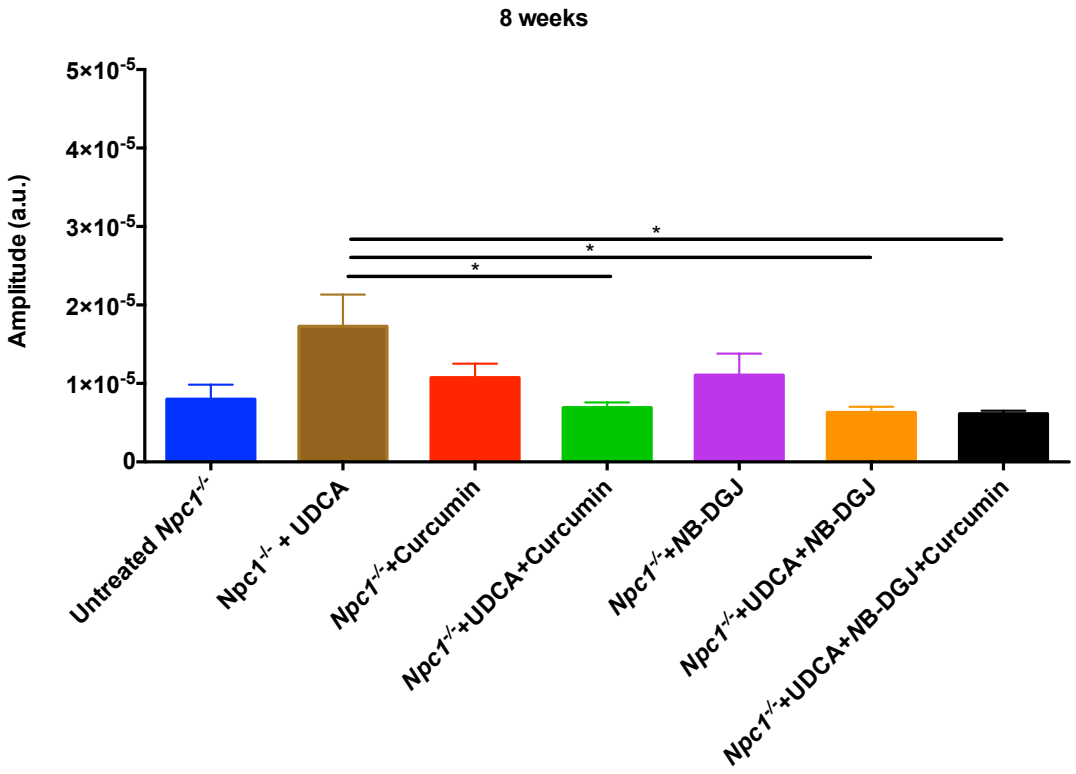
8 weeks
Amplitude (a.u.)
5×10-5
4×10-5
3×10-5
2×10-5
1×10-5
0
*
*
*
Untreated Npc1-/-
Npc1-/- + UDCA
Npc1-/-+Curcumin
Npc1-/-+UDCA+Curcumin
Npc1-/-+NB-DGJ
Npc1-/-+UDCA+NB-DGJ
Npc1-/-+UDCA+NB-DGJ+Curcumin

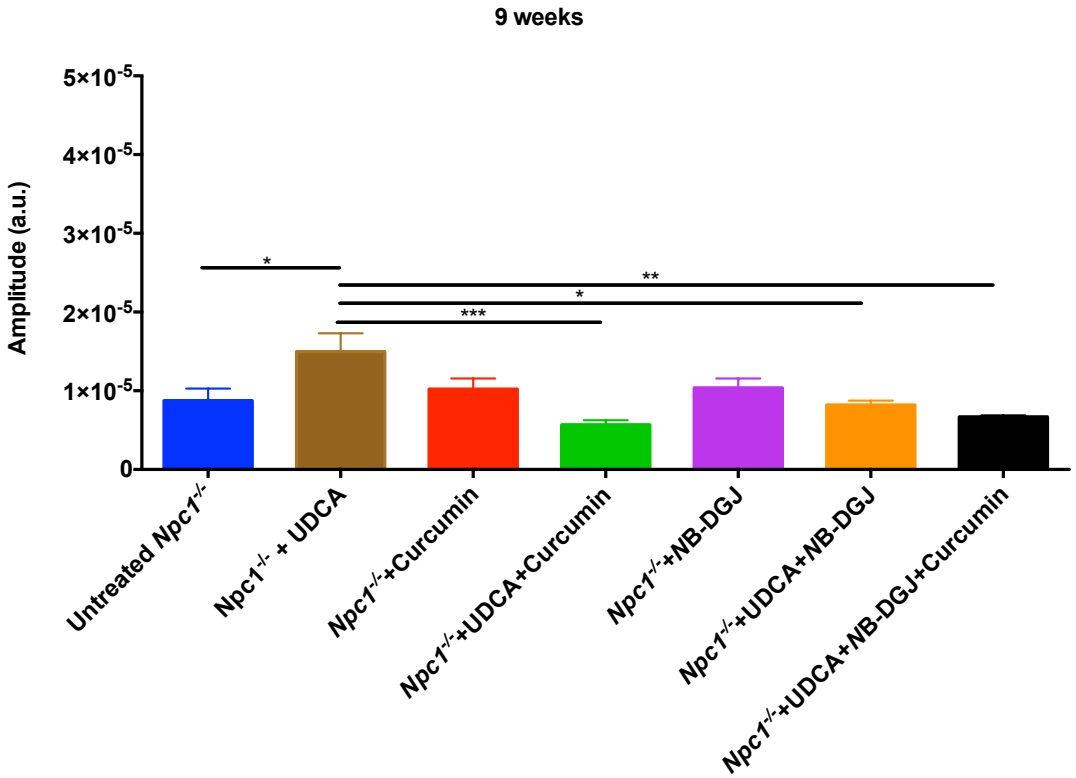
9 weeks
Amplitude (a.u.)
5×10-5
4×10-5
3×10-5
2×10-5
1×10-5
0
*
**
*
***
Untreated Npc1-/-
Npc1-/- + UDCA
Npc1-/-+Curcumin
Npc1-/-+UDCA+Curcumin
Npc1-/-+NB-DGJ
Npc1-/-+UDCA+NB-DGJ
Npc1-/-+UDCA+NB-DGJ+Curcumin

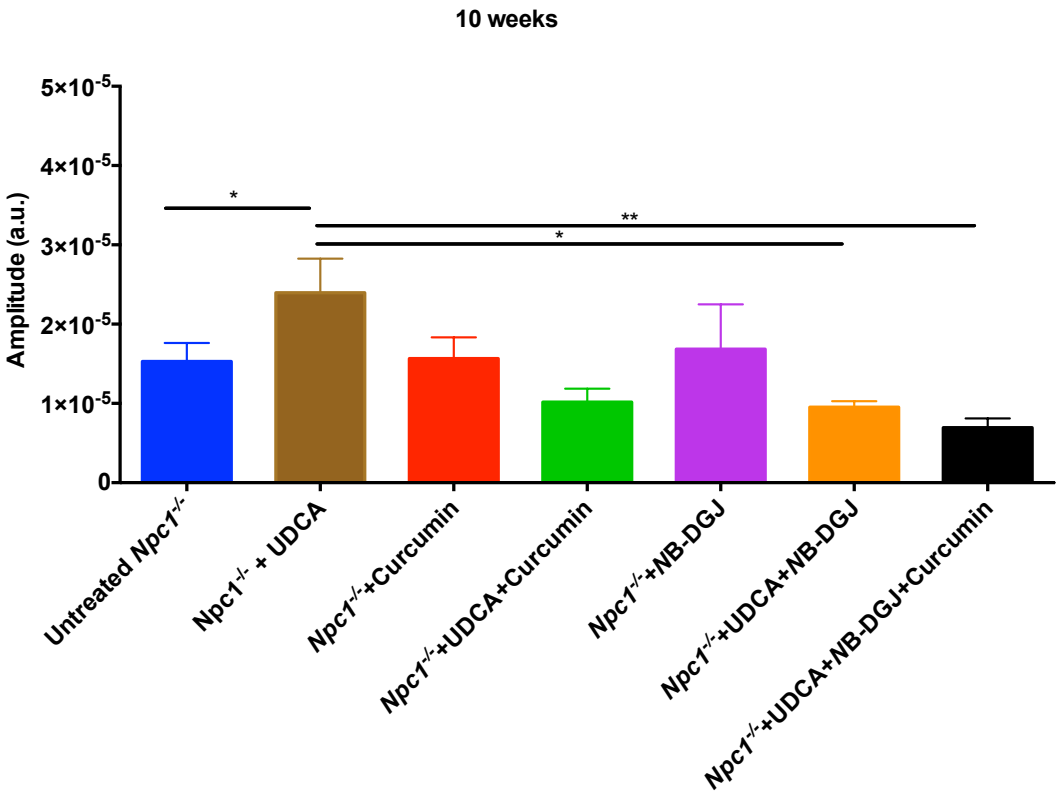
10 weeks
Amplitude (a.u.)
5×10-5
4×10-5
3×10-5
2×10-5
1×10-5
0
*
**
*
Untreated Npc1-/-
Npc1-/- + UDCA
Npc1-/-+Curcumin
Npc1-/-+UDCA+Curcumin
Npc1-/-+NB-DGJ
Npc1-/-+UDCA+NB-DGJ
Npc1-/-+UDCA+NB-DGJ+Curcumin

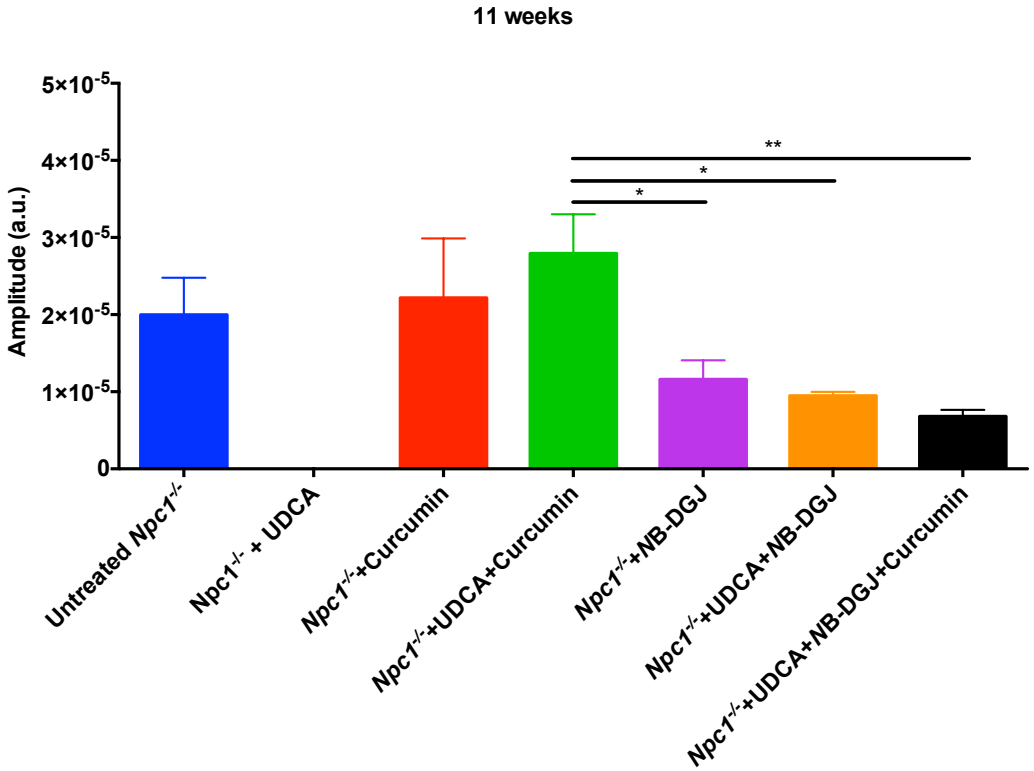
11 weeks
Amplitude (a.u.)
5×10-5
4×10-5
3×10-5
2×10-5
1×10-5
0
**
*
*
Untreated Npc1-/-
Npc1-/- + UDCA
Npc1-/-+Curcumin
Npc1-/-+UDCA+Curcumin
Npc1-/-+NB-DGJ
Npc1-/-+UDCA+NB-DGJ
Npc1-/-+UDCA+NB-DGJ+Curcumin

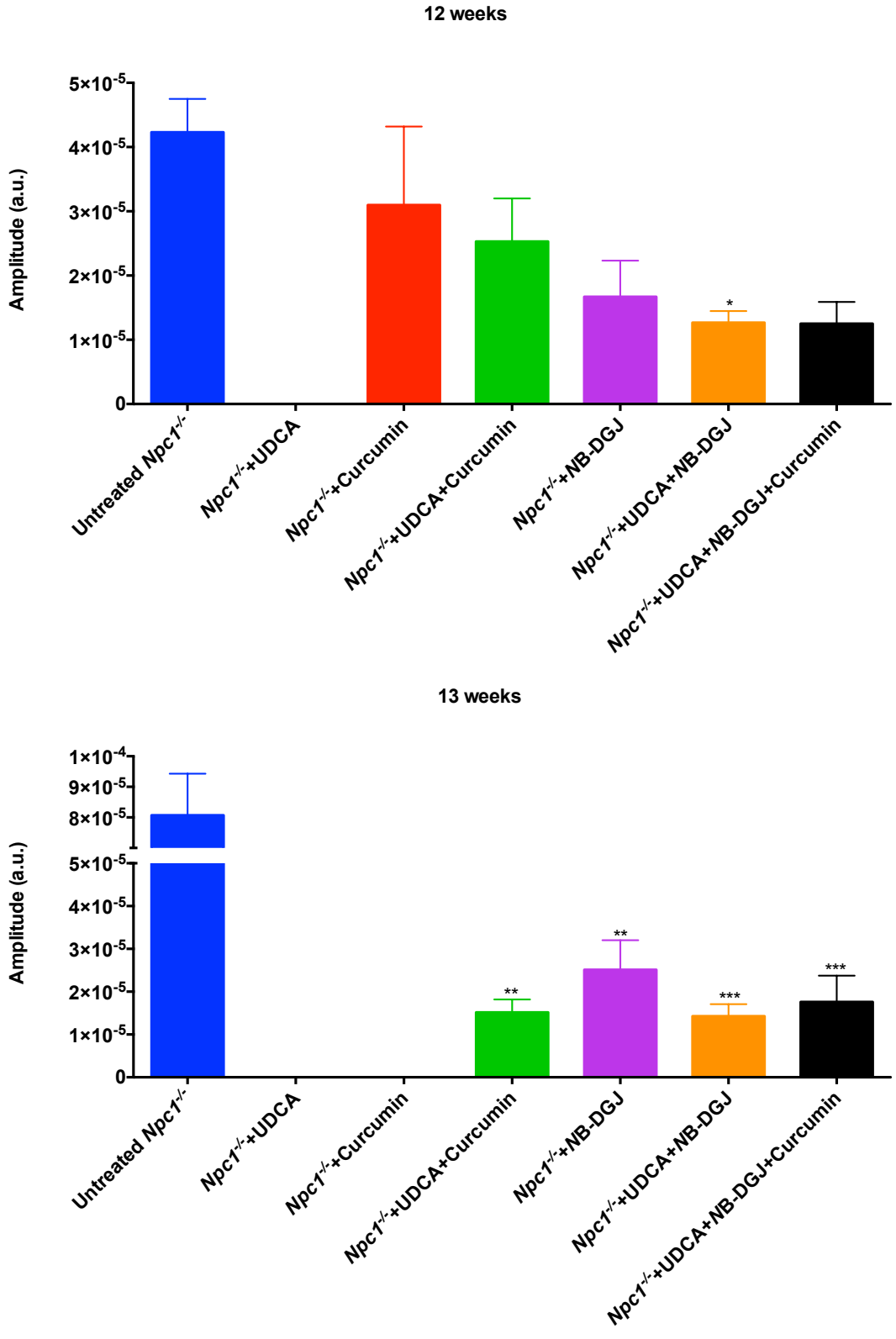

Figure 3.28. Effect of test compound on fine tremor of *Npc1*$^{-/-}$ mice. Tremor amplitudes quantified as averaged fine tremor amplitude (over the range 31-51 Hz). Data presented as mean ± SEM. *p<0.05, **p<0.01 and ***p<0.001, calculated using one-way ANOVA with Tukey's post hoc test (n=7).

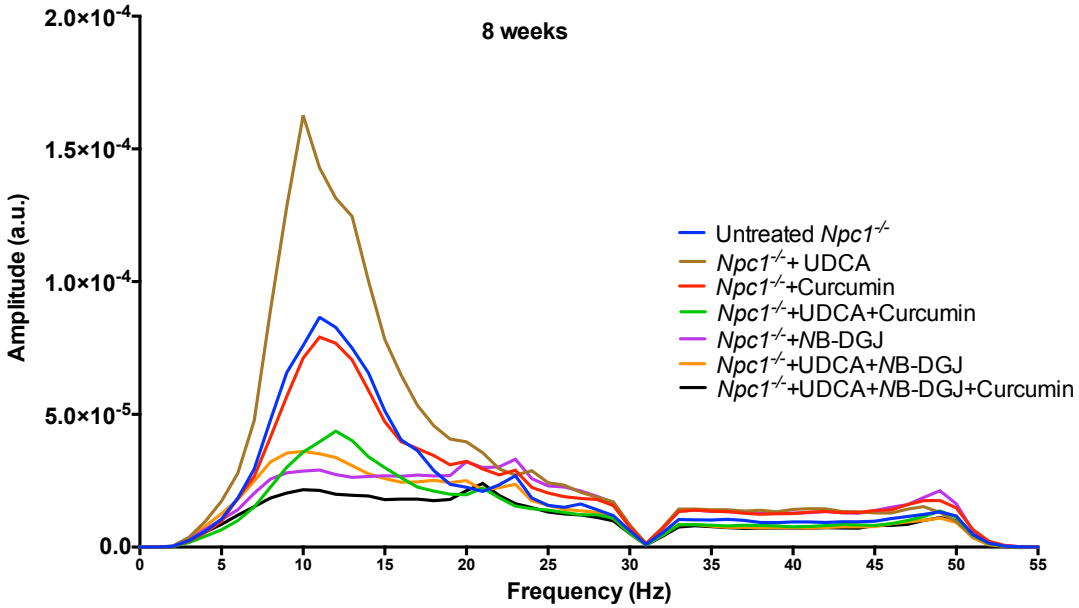
8 weeks
Amplitude (a.u.)
2.0×10-4
1.5×10-4
1.0×10-4
5.0×10-5
0.0
0
5
10
15
20
25
30
35
40
45
50
55
Frequency (Hz)
Untreated Npc1-/-
Npc1-/- + UDCA
Npc1-/-+Curcumin
Npc1-/-+UDCA+Curcumin
Npc1-/-+NB-DGJ
Npc1-/-+UDCA+NB-DGJ
Npc1-/-+UDCA+NB-DGJ+Curcumin

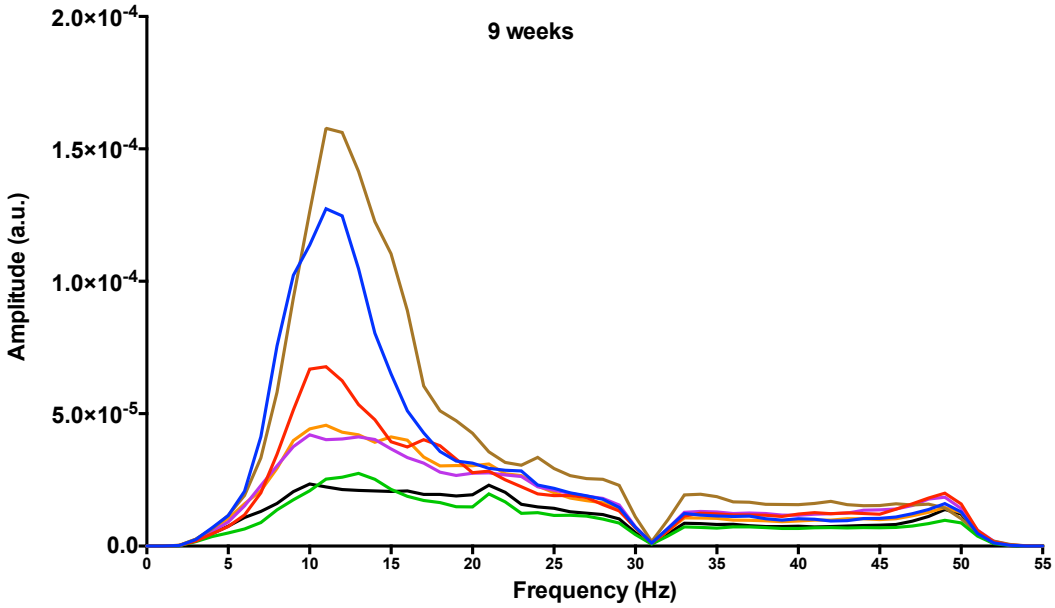
9 weeks
Amplitude (a.u.)
2.0×10-4
1.5×10-4
1.0×10-4
5.0×10-5
0.0
0
5
10
15
20
25
30
35
40
45
50
55
Frequency (Hz)

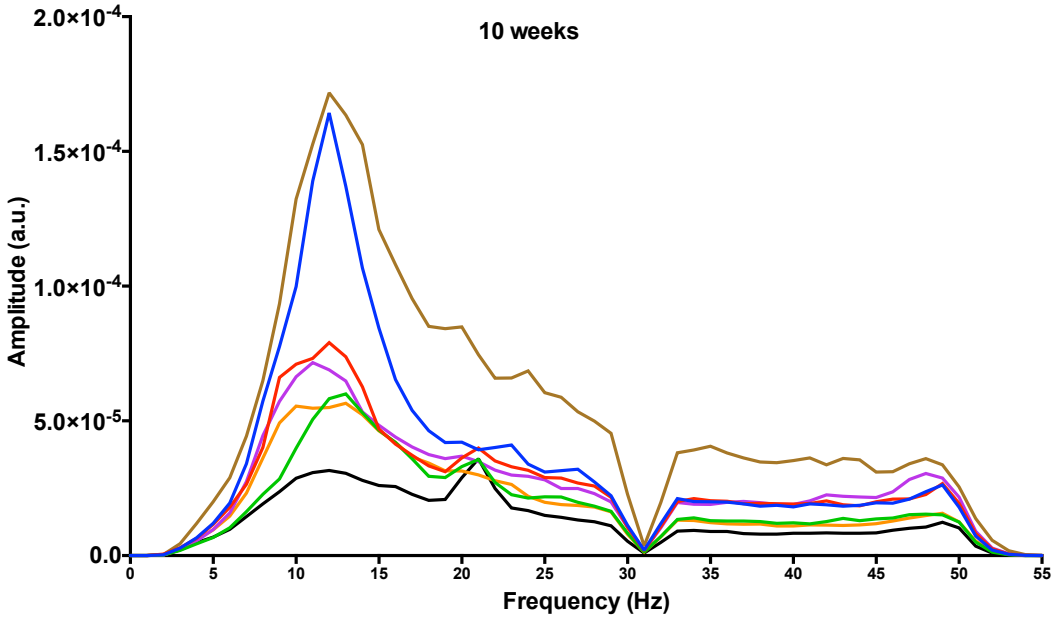
10 weeks
Amplitude (a.u.)
2.0×10-4
1.5×10-4
1.0×10-4
5.0×10-5
0.0
0
5
10
15
20
25
30
35
40
45
50
55
Frequency (Hz)

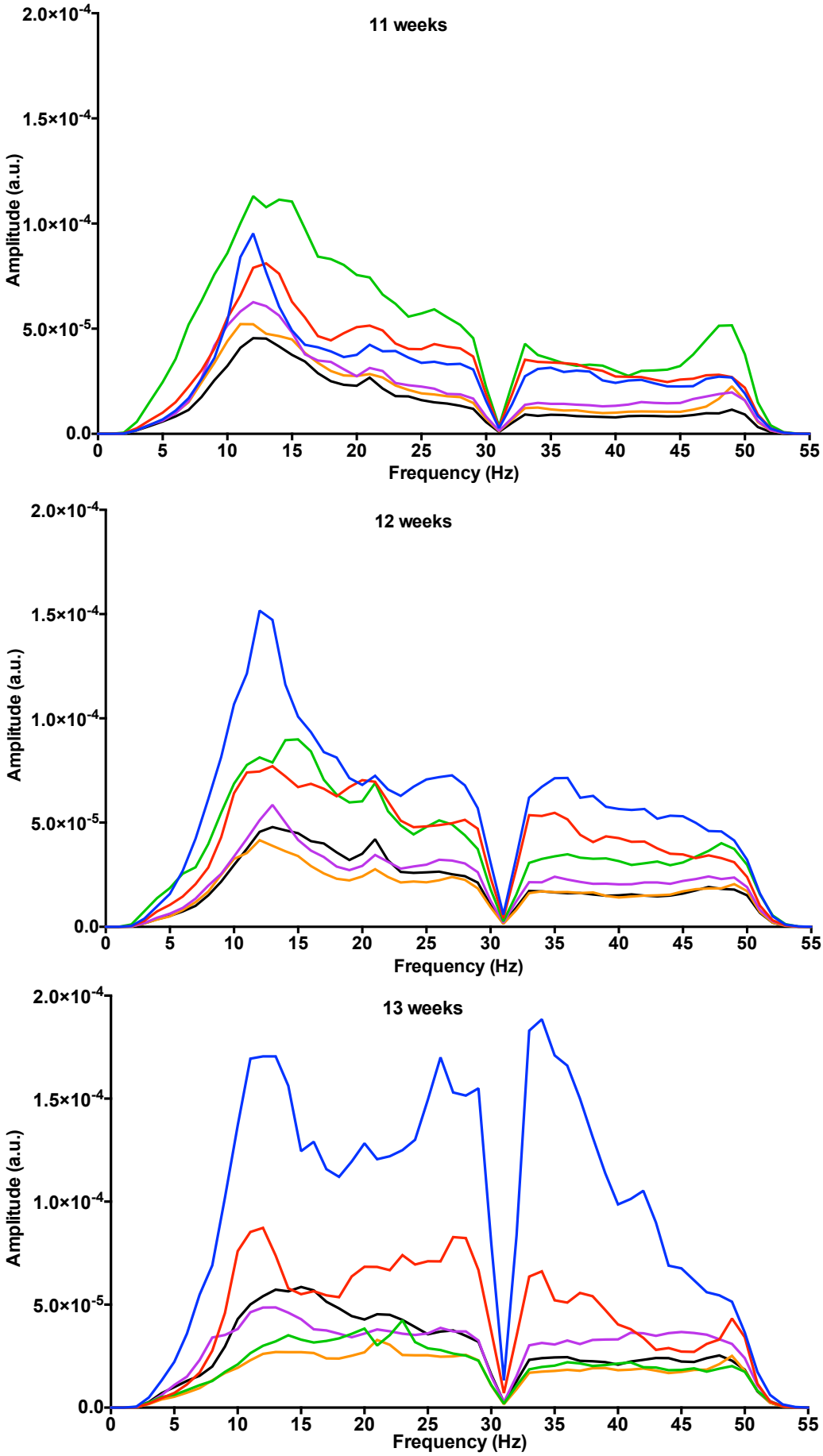

Figure 3.29. Effect of test compound on tremor of *Npc1*$^{-/-}$ mice. Data presented as mean tremor amplitude between 0 and 55 Hz (n=7).

At 10 weeks, only groups on *N*B-DGJ combinations had a lower fine tremor compared to UDCA alone (p=0.043 and 0.010 vs. *N*B-DGJ with UDCA and triple combination, respectively). By 11 weeks, high curcumin dose with UDCA group had higher fine tremor amplitude compared to UDCA with *N*B-DGJ group (p=0.013), to the *N*B-DGJ group alone (p=0.035) and to the triple combination group (p=0.003).

The effect of UDCA treatment on tremor appeared at 12 weeks, where mice treated with UDCA combined with *N*B-DGJ alone or with high dose curcumin had significantly lower tremor amplitude compared to untreated controls (p=0.030 and 0.028). While by 13 weeks, UDCA with curcumin, UDCA with *N*B-DGJ and *N*B-DGJ alone were successful in reducing fine tremor amplitude in *Npc1*$^{-/-}$ mice as well as the triple combination therapy, compared to untreated controls (p=0.002, 0.0001, 0.001 and 0.0003).

Although the lack of efficacy of *N*B-DGJ alone in preventing tremor has been previously reported in other LSD models using both imino sugars (106, 216). We have seen a positive effect at later at 13 weeks as well as a significant additive effect seen with the addition of UDCA.

UDCA treatment induced protection from acute ibuprofen toxicity **(Figure 3.30)**, although UDCA treatment on its own was associated with weight loss compared to untreated controls (p=0.025 and 0.013, at day 6 and 7, respectively), its addition prevented weight loss caused by the high dose ibuprofen starting from day 4 (p=0.042 and 0.035 and p<0.0001 for ibuprofen with UDCA vs. ibuprofen alone and ibuprofen vs. untreated controls at day 4 and 7, respectively).

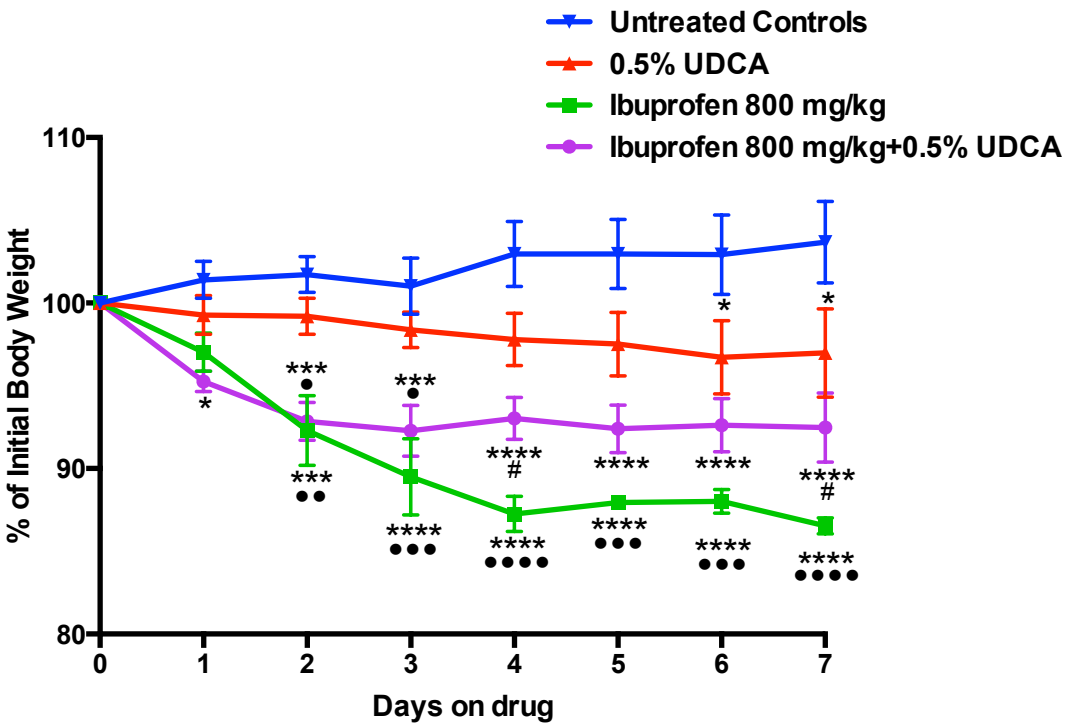

Figure 3.30. Acute effect of UDCA on ibuprofen toxicity in *Npc1*$^{-/-}$ mice. Data presented as mean (percent of initial body weight) ± SEM. **p*<0.05, ***p*<0.01 ****p*<0.001 and *****p*<0.0001, calculated using two-way ANOVA with Tukey's post hoc test (n=5). * denotes comparison vs. untreated controls, • denotes comparison vs. UDCA group and # denotes comparison vs. ibuprofen+UDCA group.

3.4. Discussion

Motor function tests assess the spontaneous activity of the mouse as it is a measure of locomotor function, strength, motivation, coordination, exploration and anxiety (217). It is a sensitive way of detecting functional deterioration, loss of strength and coordination (217). Rearing is a normal exploratory activity that requires strength, coordination and motivation to explore the environment. Centre rearing requires more strength and coordination than rearing with support and thus the ability to centre rear tends to get lost earlier in the course of the disease. With the relatively short life span of the *Npc1*$^{-/-}$ mouse, it is essential to take advantage of the available behavioural tests, developed and optimised to reflect functional changes with disease progression and to pick up any changes or improvement in response to treatment.

Tremor is a clinical feature of *Npc1*$^{-/-}$ mice (82) that is also present in the feline model (45) and patients (218). It is measurable using and automated commercial device, which records tremor amplitude over the range 0-64 Hz. *Npc1*$^{-/-}$ mice exhibit a characteristic tremor over two power ranges, low frequency tremor (5-30 Hz) that is normally associated with grooming activity and a fine high frequency tremor (31-51 Hz). Compared to wild-type mice, which have much lower tremor amplitude over the whole range with minimum variations, *Npc1*$^{-/-}$ mice present with a progressively higher tremor amplitude with considerable variation between different animals, a phenotype that was responsive to various treatments (92). Increased tremor is an established sign of drug toxicity (219, 220).

Multiple anti-inflammatory approaches have been assessed in *Npc1*$^{-/-}$ mice (92, 221) due to the major inflammatory component of NPC disease. The use of the NSAID ibuprofen in *Npc1*$^{-/-}$ mice alone and in combination with miglustat has produced a

significant additive effect significantly extending their life span and slowed down disease progression with marked improvement and reduction of inflammatory markers in the CNS (92). Ibuprofen is a cyclooxygenase inhibitor suppressing the production of pro-inflammatory prostaglandins (222). The outcome of these trials therefore encouraged investigating other anti-inflammatory therapies in NPC1 disease.

Since its discovery and marketing in 1978, vinpocetin (Cavinton) has been known for its use in cerebrovascular disorders and cognitive impairment (223). It acts as a vasodilator to enhance blood flow in the brain (224) and stimulates oxygen and glucose cerebral uptake from blood enhancing ATP production in neurons (225). It mediates these effects via multiple cellular targets including Ca^{2+}/calmodulin-stimulated cyclical nucleotide phosphodiesterase-1 (PDE-1) and voltage-dependent Na^{+} channels and Ca^{2+} channels (226).

Vinpocetine's anti-inflammatory properties were suggested from PDE inhibitory effect, which in turn is known to regulate inflammation through regulation of cyclic adenosine monophosphate (cAMP) and/or cyclic guanosine monophosphate (cGMP). Vinpocetine has been shown to exert its anti-inflammatory effect via NF-κB inhibition *in vitro* and *in vivo* through IKK direct inhibition rather than PDE **(Figure 3.31)** (208). Vinpocetine inhibits TNF–mediated NF-κB activation and proinflammatory mediators in many cell lines, as well as monocyte adhesion and chemotaxis. *In vivo* results using a mouse model of TNF- or LPS-induced lung inflammation, vinpocetine inhibits the induced up-regulation of the proinflammatory cytokines TNF and IL-1β and reduces interstitial polymorphonuclear leukocytes infiltration (208).

Although vinpocetine has not been reported to be associated, at its therapeutic doses, with adverse effects or toxicity (227), we have seen worsening of the tremor phenotype of treated mice, especially at the higher dose. This could be potentially attributed to it pharmacokinetics undergoing liver metabolism, since reducing the dose resulted in a significant increase in survival rate of treated mice.

The utilisation of both anti-inflammatory and cognitive improving effects of vinpocetine was suggested in neurodegenerative disease. The cognitive improvement effect in NPC disease needs to be addressed in the future and combined with bile acid treatment to try and minimise toxicity to allow higher dose treatment. Provided dose optimisation and possibly combination with miglustat, this compound might be a good candidate for a therapeutic intervention in NPC disease.

The improved neurological function of *Npc1*$^{-/-}$ mice in response to TNF-targeting biologics could be explained by direct anti-inflammatory effect in the periphery. The status of the blood-brain barrier in the *Npc1*$^{-/-}$ mice has not been assessed. However, we believe it may not be intact at late stage disease. These biologics do

not normally cross the blood-brain barrier but if the integrity is compromised, then a beneficiary effect reducing neuroinflammation could explains some of the improvements seen. The BBB is permeable in mouse models of other LSDs e.g. Sandhoff disease and neuronal ceroid lipofuscinoses (229).

Due to the nature of these biologics being either fully or partially humanised, they may elicit an immune response in the CNS that could have potentially further worsened the tremor phenotype without affecting motor function and coordination. Similarly, patients develop an antibody response towards those biologics with murine protein elements retained (not fully humanised) (230).

The differential responses we observed to the various biologics cold be explained by their mechanism of action, structure, pharmacokinetics and other factors. For instance, the two monoclonal antibodies (Humira and Remicade) bind two TNF molecules whereas Enbrel (TNF receptor fusion protein) only binds one TNF molecule (231). Furthermore, Enbrel has the ability to bind and neutralise both TNF and lymphotoxin-α (previously known as TNFβ), possibly making it less effective at neutralising TNF under conditions of elevated lymphotoxin-α (231). Anti-TNF biologics also have differential properties in terms of their affinity and binding capacities monomers vs. trimmers of TNF, so that unlike Humira and Remicade, Enbrel is only capable of binding TNF monomers (231). On the other hand, both Humira and Remicade have a relatively long plasma half-lives compared to Enbrel (232). However, Enbrel has shown to have higher binding capacity (232). The differences in the plasma half-life could explain the differential responses to these treatments in the *Npc1*$^{-/-}$ mice, especially in terms of rearing activity.

The differential response is also recognised in patients, the various biologics are preferably prescribed for different conditions of variable severity and patient often become refractory to one therapy and switch to a different product to regain efficacy (210).

The use of TNF-targeting biologics has the advantage over some small molecule therapies (NSAIDs and TNF inhibitors such as the xanthine derivative pentoxifylline (233)) of not being metabolised by the liver or the cytochrome P450 enzymes in particular (234, 235), therefore not adding extra burden on the liver or being associated with prolonged exposure. This would also make TNF-targeting biologics good candidates as an adjunctive therapy. However, small molecule anti-inflammatory drugs have the advantage of their ability to cross the blood-brain barrier and penetrating into other tissues, unlike these fusion proteins/antibodies. They are also much cheaper than the biologics. However, due to the possibility that blood-brain barrier integrity might be compromised at late stage *Npc1*$^{-/-}$ mice, this might not be an issue. In addition, TNF overproduction might contribute to the increased blood-brain barrier permeability (236).

Further optimisation of the dosing and potentially combination of these biologics with other therapies for example miglustat should be considered for future studies. Also, the increased risk of opportunistic infections associated with TNF-targeting biologics should be carefully considered (237), particularly that NPC1 patients have defective bacterial handling (Holm Uhlig, unpublished, personal communication).

Curcumin possesses anti-inflammatory effects via inhibition of TNF transcription and signalling (238). It also has antiproliferative and antioxidant effects with neuroprotective properties mediated by different mechanisms including anti-

protein-aggregate activities (239). These actions would therefore suggest other mechanisms by which curcumin would exert a beneficial effect in NPC1 disease.

Curcumin is a weak SERCA antagonist that although did not correct acidic store calcium levels, was successful in elevating cytosolic calcium compensating for the defective release form the acidic compartment. *In vitro* data also showed significant correction of NPC phenotypes in NPC deficient cells. *In vivo* study using the 150 mg/kg curcumin as a dry admix (powder) in *Npc1*$^{-/-}$ mice also showed marked improvement in survival rate, weight loss profile and motor function. These effects were accompanied by reduction in brain GSL storage (37).

Oral bioavailability of curcumin and therefore optimal dosing and delivery has been an issue possibly caused by its instability at neutral pH, increased auto-oxidation and metabolism with low intestinal permeation and bioavailability. These factors also make it difficult to attribute all its heterogeneous effects purely to the parent compound (240).

Three curcumin diets were assessed in *Npc1*$^{-/-}$ mice: 2% curcumin (99% pure curcumin, 3500 mg/kg), 0.17% curcumin (85% pure curcumin, 298 mg/kg), lipidated curcumin (0.05%curcumin, 88 mg/kg, at 20% in a stearic acid/phosphatidyl choline mix). Although bioavailability was enhanced upon consumption of the lipidated formula, none of these 3 dosages and formulations was successful in replicating the previous findings (113). The differences between the different studies probably lie in the dosage and purity of the curcumin used. We have seen less efficacy with a 300 mg/kg dose. It suggests toxic effect of the high dose possibly mediated by inefficient clearance as it is a known CYP450 inhibitor. Orally administered curcumin undergoes conjugation (glucuronidation and

sulphation), where as i.v. or i.p. administration results in the formation of curcumin reduction products in the liver and intestine (239, 241). Since all curcumin metabolites are not biologically active (242) and to overcome curcumin's low bioavailability, multiple approaches have been considered such as interference with glucuronidation (for instance using piperine (243)), the use of liposomal, nanoparticle and phospholipid complex formulations of curcumin and curcumin analogues (239).

Multiple studies have shown inhibition of the cytochrome P450 system by curcumin (200, 244, 245). While its effect on phase II GST enzyme seems to be dose-dependent with high dose being inhibitory (246-248). This could potentially have implications on administering curcumin with other liver metabolised compounds.

CNB 001 is a synthetic pyrazole derivative of curcumin (curcumin conjugated with cyclohexyl bisphenol A) that possesses neuroprotective effects of the two classes of compounds and is more stable than curcumin would be of potential interest to evaluate it the *Npc1*$^{-/-}$ mice (249-252).

The pelleted chow has been shown to be consumed more efficiently (206) and thus incorporating the test compound into this "formulation" insures maximal dosage (delivery/peak levels). Additionally, it has been reported that feeding mice on soft diet (powdered) after weaning has a negative effect on some of features of their neurological development, such as reducing synaptic formation in the cerebral cortex in addition to negatively influencing some cognitive skills such spatial learning in in the adult mice (253). This has been linked to reduced expression of BDNF in the hippocampus and cerebral cortex, the levels of which are have been found to highly correlate with the mastication activity during development. BDNF

in a main promoter of synaptic formation among other roles (254). The rate of neurogenesis has also been shown to be reduced in soft-diet fed weaning mice compared to their hard-fed littermates, this happens as a result of slower precursor cell proliferation in the hippocampus (255).

Formulation of diet into pellets is also thought to be associated with higher consumption and increased appetite compared to powdered diet (206) insuring better delivery of the therapeutic compound administered via this route.

The effect of genetic drifts in mouse colony on biomedical research (256, 257) in general and therapeutic trials in model of neurodegenerative diseases (258) is well established. Another factor related to the old colony that could have contributed to the discrepancy in the curcumin results, is the two infections occurred within the colony and their nature.

Helicobacter hepaticus, which results in liver disease and altered liver detoxifying capacity, (259) and *Pasteurella pneumotropica,* which is only of clinical significance in immunocompromised animals (260). The immunological status in response to either infection is known to be also altered (261, 262).

Inflammation (263) as well as infection (196) are factors that affect host susceptibility to xenobiotics and therefore affects their response to administered drugs. Similarly, environmental factors are equally as important in determining host detoxifying capacity and drug pharmacokinetics (264, 265), further contributing to the differential response to the high dose curcuimin we observed in the two colonies. These factors could explain the differences seen in response to the high curcumin doses between the two colonies.

UDCA although not a natural mouse BA, is less toxic than cholic acid and chenocholic acid (266), is known to induce CYP450 enzymes (267), its effect is not gender biased (268) and readily translatable into the clinic since it is FDA-approved for primary biliary cirrhosis (269). Indeed, NPC patients with cholestatic jaundice are transiently administered UDCA until their liver disease resolves. It may be argued that UDCA should be administered throughout the clinical course of NPC disease based on the findings in this chapter and **Chapter 2**.

The mechanism for the therapeutic effect of UDCA in liver disease is not fully known, however, multiple different mechanisms were proposed to contribute to protection from cholestatic liver disease including protection of both cholangiocytes and hepatocytes against toxic hydrophobic BAs ad BA induced apoptosis respectively as well as enhancing hepatobiliary secretion (269). UDCA protective effect on cholangiocytes is thought to be mediated through Ca^{2+} and PKCα pathways, affecting PKC redistribution between cytosol and plasma membrane increasing PKCα translocation to the membrane and increasing the membrane bound fraction (270). TUDCA stimulates both upregulation of PKCα and enhanced membrane translocation in a rat model of liver ischemia-reperfusion injury (271). PKCα upregulation should correct NPC cells, as sphingosine storage in NPC cells leads to reduction in the activity of PKCα (4, 130, 272). Upregulation of canalicular transporter proteins in UDCA fed mice has been reported but the effect is not specific for UDCA (273).

Multiple hepatic bile uptake (Ntcp and OatP2 and 4) and excretion transporters (conjugate export pumps Mrp1, 2, 3, 5 and bile salt export pump Bsep) were shown to be upregulated in *Npc1*$^{-/-}$ mice at baseline, while expression of Mrp excretory transporters was further enhanced upon high fat diet consumption the opposite

effect was seen with suppression of the expression of Ntcp, Bsep and OatP (274). Although the mechanism of these altered expression patterns under both conditions is not clear, this might have contributed to the altered BA composition and homeostasis in these mice suggesting a potential beneficial effect of BA supplementation in NPC1 disease.

The taurine conjugate of UDCA has shown to induce an elevation of cytosolic calcium in isolated rat liver *in vitro* in normal but not cholestatic cells supplemented with high extracellular calcium concentration (275), therefore, inducing hepatocyte exocytosis and membrane targeting and insertion of BA export transporters (269). UDCA may also play a role in elevating cytosolic calcium in NPC1 cells, similar to curcumin's action. Another mechanism partially responsible for mediating these effects is the activation of p38MAPK and of Erk-2 (276). Further evaluation of other BA supplementations with optimised dosing could add to our knowledge about this aspect of the disease.

The galactose analogue of miglustat, *N*B-DGJ, similarly inhibits the ceramide-specific glucosyltransferase which catalyses the first step in the GSL biosynthetic pathway (203, 214). As small molecule therapies, they have the advantage of crossing the blood-brain barrier, alleviating the central neurological symptoms (277). *N*B-DGJ is therefore a useful therapeutic approach whether on its own or in combination with other treatments.

Both imino sugars were tested in the mouse model of NPC1 disease with significant extension of the life span of treated mice, slowing disease progression (82). *N*B-DNJ therapy in the feline model of the disease was also associated with marked improvement (82). Moreover, the galactose analogue has the advantage of a better

side effect profile compared to *N*B-DNJ being a more selective inhibitor that does not cause weight loss or inhibits glycogen metabolism or disaccharidases (107). Intestinal disaccharidase inhibition could be the cause of the reported adverse effects observed in association with the high oral dose of miglustat, mainly GI manifestations (diarrhoea, weight loss and abdominal pain) (83, 278).

Many studies of therapeutic agents have used combination therapies with *N*B-DNJ (87, 92, 279). Combination of the various compounds, which target different steps in the pathological cascade should also be tested and may produce a more significant improvement (92). In this chapter several new candidates have been identified that merit further investigation with a view to clinical translation.

Chapter 4. Evaluation of Cogane and Myogane in Niemann-Pick Type C1 Disease, a Collaborative Study with Phytopharm

4.1. Introduction

Cogane (PYM50028) and Myogane (PYM50018) (Smilagenin and Sarsasapogenin, the lead compounds of Phytopharm, **Figure 4.1**) are small molecule compounds of the sapogenin family (the non-saccharide component of the natural products saponins). They occur naturally in a number of plants, such as *Asparagus* and *Anemarrhena* (280, 281), commonly used herbs for chronic neurological diseases in Chinese medicine (282). They are structurally related and orally bioavailable inducers of neurotrophic factors (glial cell-derived neurotrophic factor "GDNF" and brain derived neurotrophic factor "BDNF") capable of crossing the blood brain barrier (283). Their neuroprotective and neurotrophic effects make them of potential use for slowing neurodegeneration in common and orphan diseases. They have been suggested to be of therapeutic benefit in a range of neurodegenerative diseases (281).

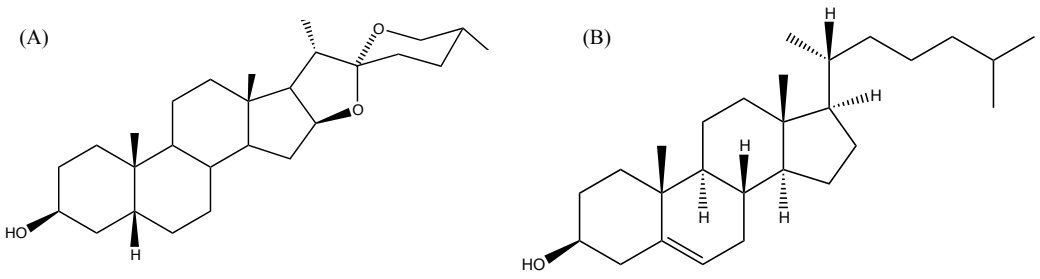

Figure 4.1. The structure of the compound PYM50028 (Cogane) (A) and cholesterol (B), Myogane is the (25*S*)-configuration epimer of Cogane.

Cogane and Myogane have undergone Phase I toxicology studies where they have shown good bioavailability and a good safety profile (284).

Efficacy in preclinical models of cognitive impairment (for example Cogane reversed cognitive deterioration in aged rats assessed using the Y-maze test and reversed neuronal loss in the chemically induced mouse model of Parkinson's disease (281, 283)) suggests a positive effect of these compounds in treating both motor and non-motor symptoms of neurodegenerative diseases such as Alzheimer's disease, ALS and Parkinson's disease. Cogane and Myogane efficacy in preclinical models of cognitive impairments also suggests a potential benefit in delaying disease progression in early-diagnosed cases.

Cogane has Orphan Drug status by the European Commission and by the US Food & Drug Administration for the treatment of ALS (http:// www.phytopharm.co.uk).

All information relevant to Cogane and Myogane trials were available from the company's web site (unless other references added) and is summarised in **Table 4.1**.

The table originally presented here cannot be made freely available via ORA because of 'copyright'.

Neurotrophic factors (GDNF and BDNF) are proteins that are synthesised and secreted in the striatum of the brain among other sites (288). They are known to play a role in neuronal regeneration (289). As these neurotrophic factors are

proteins they cannot be administered orally and do not cross the blood-brain barrier (290). Parenteral administration of GDNF and BDNF directly into the brain has shown significant clinical improvement in Parkinson's disease, however, it required very invasive administration (291). Whereas the use of Cogane or Myogane, which are orally bioavailable, administered once daily produce similar effect inducing the release of GDNF and BDNF in the brain (282).

As plant extracts identified as the active components of traditional Chinese medicinal herbs for age-related memory impairment, these compounds have been studied in aged animals and shown to improve memory, not through cholinesterase inhibition or glutamate receptor antagonism but the effect correlated with elevated density of muscarinic receptors (reduced in aged rat brain and transfected CHO cells) (286, 287, 292).

Whilst other sapogenins undergo Phase I drug metabolism in mice by hepatic microsomal cytochrome P450 (predominantly CYP3A4) and Phase II conjugation by UGT (293), in the sheep, smilagenin and sarsasapogenin have been shown to undergo glucoronidation in the liver (294). Other classes of sapogenins are also known to inhibit the activity of cytochrome P450 *in vitro* (295) which could influence the efficacy of these compounds in *Npc1*$^{-/-}$ mice.

Since NPC disease shares common neuropathological features with more common neurodegenerative disorders (150, 296, 297), we aimed to evaluate the potential neuroprotective effects of Cogane and Myogane as they cross the blood-brain barrier and have shown efficacy in animal models of other neurodegenerative disorders.

4.2. Methods

4.2.1. Test compounds

Cogane (PYM50028, 5β, 20α, 22α, 25R-spirostan-3β-ol) and Myogane (PYM50018, 5β, 20α, 22α, 25S-spirostan-3β-ol), (molecular weight 416.64) were provided by Phytopharm Plc. (Godmanchester, UK).

4.2.2. Cells

Since these compounds have not been tested *in vitro* in the context of NPC disease, they were initially assessed *in vitro* both in healthy and NPC1 deficient cells. RAW 264.7 (murine leukaemic macrophage cell line) cells were grown in Dulbecco's modified Eagle's medium (Sigma-Aldrich, Poole, UK) while NPC1-mutant CHO (Chinese hamster ovary) cells (NPC1 null, they are mutant CHO K1 cells with deleted NPC1 locus) (CT43, CHO M12) were grown in Ham's F-12/DMEM. All media were supplemented with 10% foetal bovine serum (Bio Sera, Ringmer, East Sussex, UK), 1% penicillin-streptomycin (Lonza Biologics, Sough, UK) and 1% L-glutamine (GIBCO Invitrogen, Paisley, UK). Cells were maintained at 37°C, 5% CO_2 and 100% relative humidity.

The required amounts of PYM50028 and PYM50018 were dissolved in dimethyl sulphoxide (DMSO; final concentration was 0.25% in all conditions). Cells were treated with two different concentrations of each compound; 1 and 5 μM for either 5 and 10 days or 5 and 20 days.

For a positive control (that induces NPC phenotype), RAW 264.7 cells were treated with U18666A (Merck, Poole, Dorset, UK), at a concentration of 2 μg/mL. Untreated control cells were included as a negative control.

4.2.2.1. Filipin Staining

Cells grown on glass coverslips were washed with PBS and fixed with 4% PFA for 30 minutes, quenched with complete medium for 15 minutes, washed with PBS and stained (incubated) with 25 mg/mL (final concentration is 187.5 μg/mL) of filipin (F9765, Sigma-Aldrich, Dorset, Poole, UK) for 30 minutes at room temperature. Coverslips were then mounted on glass slides using Mowiol, allowed to dry overnight.

4.2.2.2. Microscopy

Cells were imaged by fluorescence microscopy (Carl Zeiss fluorescence microscope), equipped with a QIMAGE camera (Empix Imaging Inc., Canada).

4.2.2.3. GSL analysis

Treated RAW 246.7 cells where harvested following 5 and 10 days treatment with both test compounds at 2 concentrations (1 and 5 μM). Harvested cells were re-suspended in mQH_2O and homogenised by 3 freeze-thaw cycles. The cell lysates were used for GSL extraction, purification and analysis as previously described (298). A bicinchoninic acid protein assay (BCA, Sigma) was performed in accordance with the manufacturer's instructions for the determination of the protein concentration in the cell lysates.

4.2.2.3.1. Svennerholm GSL extraction

Cell lysates were extracted at room temperature in 4 parts chloroform: methanol (1:2, v/v) for 3 hours. Samples were then centrifuged 3,000 rpm for 10 minutes. 1 part PBS and 1 part chloroform were added and spun at 1,000 x g for 5 min at room temperature. The lower phase was dried under nitrogen, resuspended in 50 μL chloroform: methanol (1:3, v/v), combined with the upper phase and applied to Isolute C18-EC columns (International Sorbent Technology, Mid Glamorgan, UK

Biotage) for further purification of GSLs and to remove any free oligosaccharides. The columns were pre-equilibrated 4 times with 1 mL methanol and twice with 1 mL water, after loading the samples, the columns were washed 3 times with 1 mL water and total GSL were then eluted by 0.5 mL chloroform: methanol (98:2, v/v), 2 x 0.5 mL chloroform: methanol (1:3, v/v) and 0.5 mL methanol.

4.2.2.3.2. Ceramide glycanase (CG) digestion

Samples were dried under nitrogen, re-suspended in 50 µL chloroform: methanol (2:1, v/v) and dried again under nitrogen. Samples were then resuspended in 17.5 µL CG buffer (50 mM sodium acetate pH 5.5 with 1 mg/mL sodium taurodeoxycholate), digested overnight at 37°C by adding 2.5 µL ceramide glycanase (CG, from *Hirudo medicinalis,* prepared in house).

4.2.2.3.3. 2AA labelling

Digested samples were made up to 30 µL with water and oligosaccharides were fluorescently labelled using 80 µL anthranilic acid (2AA) labelling mixture. The labelling mixture consisted of 2AA (30 mg/mL) and sodium cyanoborohydarate (45 mg/mL) in labelling buffer (4% sodium acetate trihydrate and 2% boric acid in methanol). Samples were kept at 80°C for 45-60 minutes for labelling.

After cooling to room temperature, samples were mixed with 1 mL acetonitrile: water (97: 3, v/v) and applied to Spe-ed SPE amide-2 columns (Applied Separations, Allentown, PA) columns pre-equilibrated with 1 mL acetonitrile, 2x1 mL water and 2x1 mL acetonitrile. Columns were washed with 2x1 mL acetonitrile: water (95:5, v/v). 2AA labelled oligosaccharides were eluted with 2x 0.75 mL water. 30 µL of the eluent was mixed with 70 µL acetonitrile (30: 70, v/v, sample: acetonitrile) and 2AA labelled oligosaccharides were then separated by NP-HPLC.

4.2.2.3.4. NP-HPLC Quantitation

The eluted 2AA labelled oligosaccharides were separated and quantified by normal phase high performance liquid chromatography (NP-HPLC) using TSK-amide 80 4.6 mm x 250 mm column with in-line 2 μm filter (Sigma). Separations carried out at 30°C, using Waters Alliance 2695 separations module with Ex_{λ} 360 nm, Em_{λ} 425 nm, using Waters 2475 Fluorescence detector.

Time (minutes)	0.0	6.0	35.0	37.0	39.0	41.0	42.0	54.0	60.0	61.0
Flow (mL/min)	0.8	0.8	0.8	0.8	0.8	0.8	1.2	1.2	0.8	0.1
Solvent A, %	71.6	71.6	52.8	23.0	23.0	71.6	71.6	71.6	71.6	71.6
Solvent B, %	8.4	8.4	27.2	57.0	57.0	8.4	8.4	8.4	8.4	8.4
Solvent C, %	20.0	20.0	20.0	20.0	20.0	20.0	20.0	20.0	20.0	20.0

Samples were injected 3:7 (milliQ water: acetonitrile, v/v) and sample injection volume was 50 μL. Solvent A was acetonitrile; solvent B was Milli-Q water and solvent C was 100 mM ammonium acetate hydroxide pH 3.85 with acetic acid. Gradient conditions are summarised in **Table 4.2**.

Table 4.2. Gradient conditions for NP-HPLC

Results were retrieved and processed using Empower software. A standard 2AA labelled glucose oligomer (from partial hydrolysis of dextran) was included to determine the glucose units (GU). Individual GSL species were identified by their GU values and quantified by comparison with a GSL standard mixture with known amount of GSLs. Results (pmol) were normalised to protein content.

4.2.2.4. Free cholesterol

Treated RAW 246.7 cells where harvested following 5 and 10 days treatment with both test compounds at 2 concentrations (1 and 5 μM). Harvested cells were re-suspended in PBS and homogenised by 3 freeze-thaw cycles. Free cholesterol levels

of the cell lysates were determined using the Amplex® Red cholesterol assay kit (Invitrogen, Paisley, UK) following manufacture's instructions.

4.2.3. Mice

Npc1$^{-/-}$ mice were generated, maintained and genotyped as described in **Chapter 2**. *Npc1*$^{-/-}$ mice at 3 weeks of age were fed with a diet of powdered chow (expanded Rat and Mouse Chow RM1, ground, SDS Ltd.) with or without the addition of Myogane (PYM50018) (Phytopharm Plc., Godmanchester, UK) according to published methods (105). Three doses were evaluated: 0.1 mg/kg/day (n=8) 1 mg/kg/day (n=14) and 10 mg/kg/day (n=4) (a dose of 10 mg/kg p.o. for 60 days resulted in significant neuroprotective and neurorestorative effects in a mouse model of Parkinson's disease where neuronal damage was induced by MPTP (283)).

4.2.3.1. Mouse behavioural analysis

Mice were monitored for functional improvement starting from 4 weeks of age (one week after treatment started) and throughout their life span using behavioural tests as described in **Chapter 3**.

4.2.3.2. Immunohistochemistry (IHC)

For immunohistochemistry; mice on the 10 mg/kg (n=3), 1 mg/kg (n=3) and 0.1 mg/kg (n=3) At 8 weeks of age, Myogane treated mice were euthanised by CO_2 asphyxiation, perfused through the left cardiac ventricle with 4% PFA and brains were post-fixed (24 hours) then cryoprotected (30% sucrose). Cerebellar tissues were freeze-embedded for cryostat-sectioning and parasagittal floating sections (10 μm) at 1 in 10 intervals were collected in PBS with 0.25% Triton ×100.

Sections were incubated at room temperature overnight with the following primary antibodies: Rat anti-mouse CD68 (1:100, Serotec) and rabbit polyclonal anti-calbindin D-28k (CB38, 1:3,000, SWANT). The primary antibodies were then detected using the following species-specific secondary antibodies incubated for 2-hour at room temperature: Alex Fluor 488 Donkey anti-rat IgG (L+H) (1:500, A-21208, Invitrogen) and DyLight 594 goat anti-rabbit IgG (L+H) (1:500, DI-1594, Vector Labs).

4.2.3.3. Image analysis

Images were taken using a Zeiss AXIO Imager A1 fluorescence microscope connected to a Zeiss AxioCamHRc digital camera. For each field, images of the FITC channel and the PE channel were merged in Adobe Photoshop, then analysed using ImageJ (NIH). For the molecular layer (ML), the area (in mm^2), and the number of $CD68^+$ cells were measured. The total number of cells and total area was calculated for each animal, and the results were expressed as the total number of $CD68^+$ cells per mm^2 of ML. Each treatment group consisted of three separate animals (n=3). For Purkinje cell survival, sections were stained with an antibody against calbindin, a specific marker for Purkinje cells in the cerebellum. The number of Purkinje cells per mm of Purkinje cell layer was counted in multiple sections and the mean calculated (n=3 per treatment group).

4.2.3.4. Biochemistry

For biochemistry, endstage mice (on the 1 mg/kg (n=5) and 0.1 mg/kg (n=5) Myogane) and age-matched control wild-type mice were killed by CO_2 asphyxiation, perfused through the left cardiac ventricle with PBS and whole brain, liver, spleen, lungs and kidneys were collected.

4.2.3.5. GSL analysis

Tissues (brain, liver, spleen, lungs and kidneys) were collected from the 1 mg/kg (n=5) and 0.1 mg/kg Myogane treated mice (n=5) at endstage and homogenised in milliQ water. Protein concentration was determined by the BCA assay as described. GSLs were extracted, separated, labelled and quantified as described in **section 4.2.2.3.**

4.2.3.6. Free cholesterol

Tissues (brain, liver, spleen, lungs and kidneys) were collected from the 1 mg/kg (n=5) and 0.1 mg/kg Myogane treated mice (n=5) at endstage and homogenised in milliQ water. Protein concentration was determined by the BCA assay as described. Free cholesterol levels of the endstage tissue homogenates were determined using the Amplex® Red cholesterol assay kit (Invitrogen, Paisley, UK) following manufacture's instructions and as described in **section 4.2.2.4**.

4.2.3.7. Thin-layer chromatography (TLC) analysis of Galactosylceramide

Glycolipids were extracted and purified from mouse brain homogenates as described in **section 4.2.2.3.** C18 purified glycolipids (corresponding to 100 μg protein) were dried under nitrogen, resuspended in chloroform: methanol 2:1 and spotted on a 20 cm x 20 cm TLC plate (HPTLC silica gel 60 plates, Merck). Lipids were separated on the TLC plate using a solvent system of chloroform: methanol: water, 160: 27: 3. GalCer standard (Galactocerebrosides from bovine brain, C4905, Sigma-Aldrich) was run alongside the samples. GalCer was detected by orcinol spray and the corresponding GalCer standard migration positions. GalCer levels were quantified with Image J software or ChemiDoc imaging system (BioRad).

4.2.4. Statistics

Data are expressed as mean ± SEM. Survival curves were created and analysed by the method of Kaplan and Meier. Quantitative data were statistically evaluated using one-way ANOVA followed by either Dunnet's or Tukey's post hoc test using GraphPad Prism version 6.0c (GraphPad Software, San Diego, California, USA). Differences were considered statistically significant when $p<0.05$.

4.3. Results

Initially, the two compounds (Cogane (PYM50028) and Myogane (PYM50018)) were tested *in vitro* at two concentrations (1 and 5 µM) and at two different time points (5 and 20, or 5 and 10 days) to rule out any potential negative effect on NPC1 function in healthy cells due to their structural resemblance to cholesterol. This is because certain amphiphiles of structural similarity to cholesterol are known inducers of NPC-like phenotypes (e.g. U18666A and progesterone) (36, 299). RAW cells were treated with these compounds for 5 and 20 days and filipin staining (intracellular free cholesterol probe) for free cholesterol did not show any significant increase in intracellular cholesterol levels compared to untreated cells and positive control treated with U18666A **(Figure 4.2).**

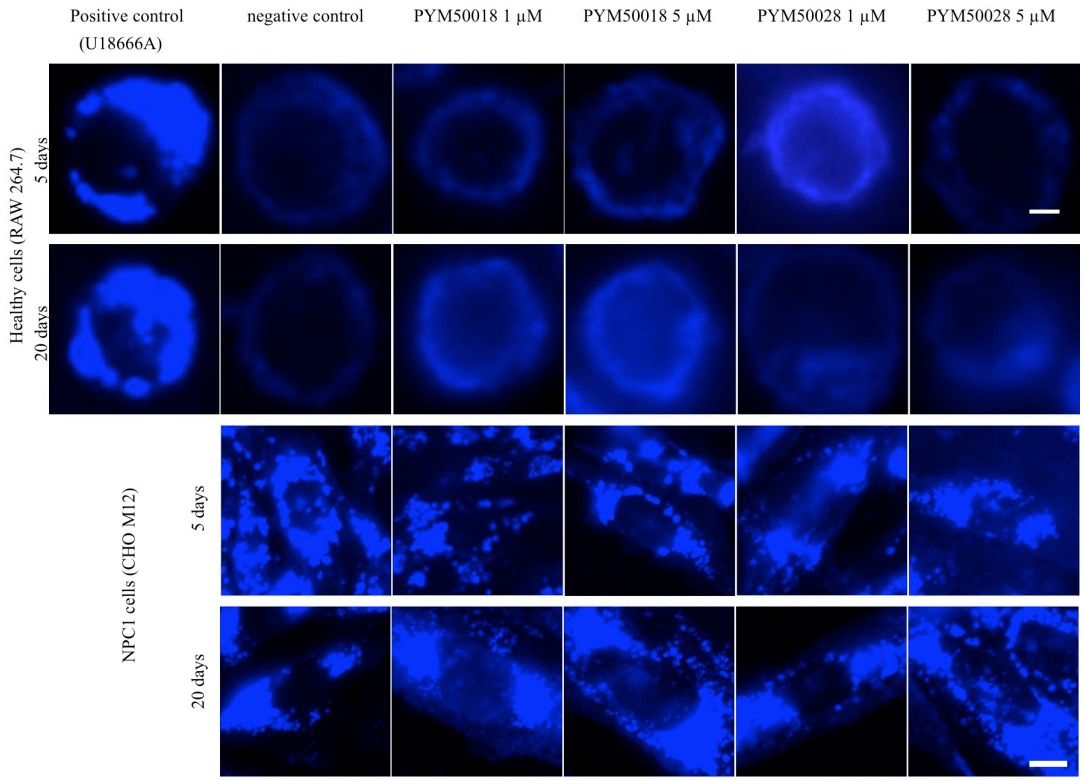

Figure 4.2. Visualisation of cholesterol with filipin. Scale bar 20 µm for the top panel and 2.5 µm for the bottom panel.

To confirm the absence of any inhibitory effect of these compounds on NPC1/NPC2, biochemical quantitation of intracellular free cholesterol **(Figure 4.3 A)** and GSL levels **(Figure 4.3 B)** following 5 and 10 day treatment with 1 and 5 μM of both compounds was also performed and there were no differences in the lipid levels compared to untreated cells, consistent with the *in vitro* filipin staining.

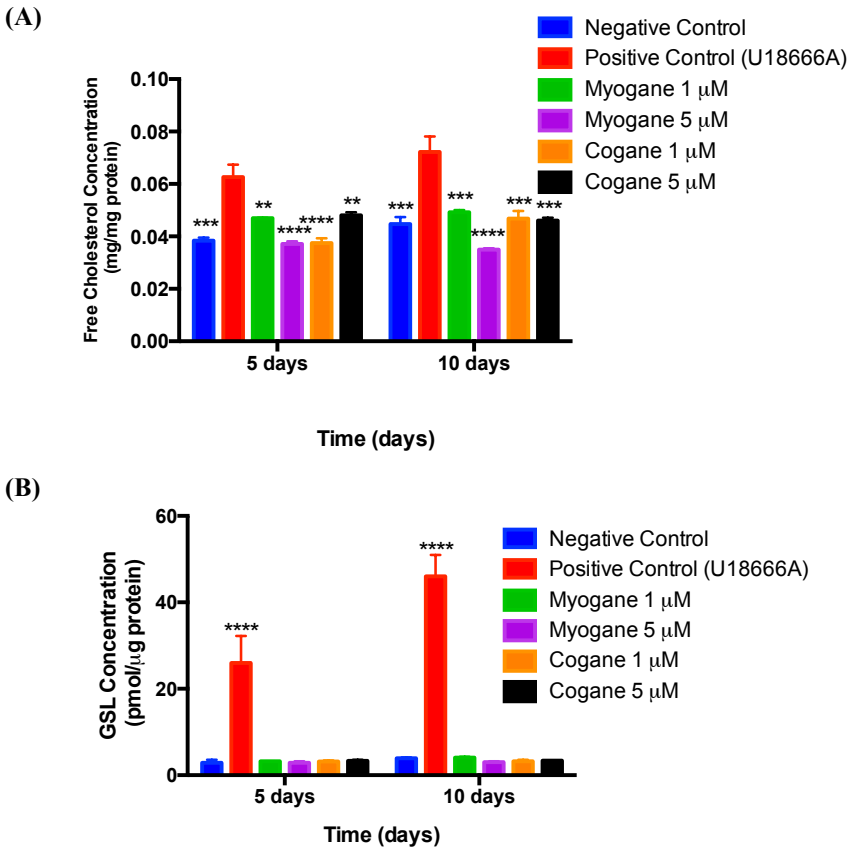

Figure 4.3. Effect of test compounds (Myogane and Cogane) at 1 and 5 μM on (A) free cholesterol concentration and (B) GSL concentration following treatment of RAW 264.7 cells for the indicated time points. Data presented as mean ± SEM, n=3. **p<0.01, ***p<0.001 and ****p< 0.0001, calculated using one-way ANOVA with Dunnett's post hoc test. Positive control is U18666A to inhibit the NPC pathway.

Both free cholesterol and GSL levels were significantly lower in both treatment groups in either concentration and both time points compared to U18666A treated cells (for free cholesterol at 5 days; p=0.005 and <0.0001 for Myogane 1 μM and 5 μM vs. U18666A and p<0.0001and p=0.086 for Cogane 1 μM and 5 μM vs. U18666A, at 10 days; p=0.0006 and <0.0001 for Myogane 1 μM and 5 μM vs.

U18666A and p=0.0003 and 0.0002 for Cogane 1 µM and 5 µM vs. U18666A, while for GSL p<0.0001 at 5 and 10 days for Myogane 1 µM and 5 µM and Cogane 1 µM and 5 µM vs. U18666A), suggesting no negative effect of Cogane and Myogane on NPC pathway in normal cells.

Myogane then progressed to *in vivo* evaluation of efficacy in *Npc1*$^{-/-}$ mice. Myogane was selected as Cogane at that time was in clinical trials and Phytopharm did not want investigational uses of the drug to be running during the clinical trial. Myogane was administered orally from weaning at doses of 0.1, 1 and 10 mg/kg/day. Treatment with Myogane at the three different doses was not associated with an increase in survival (p=0.997, 0.992 and 0.765 for 0.1, 1 and 10 mg/kg vs. untreated controls) **(Figure 4.4).**

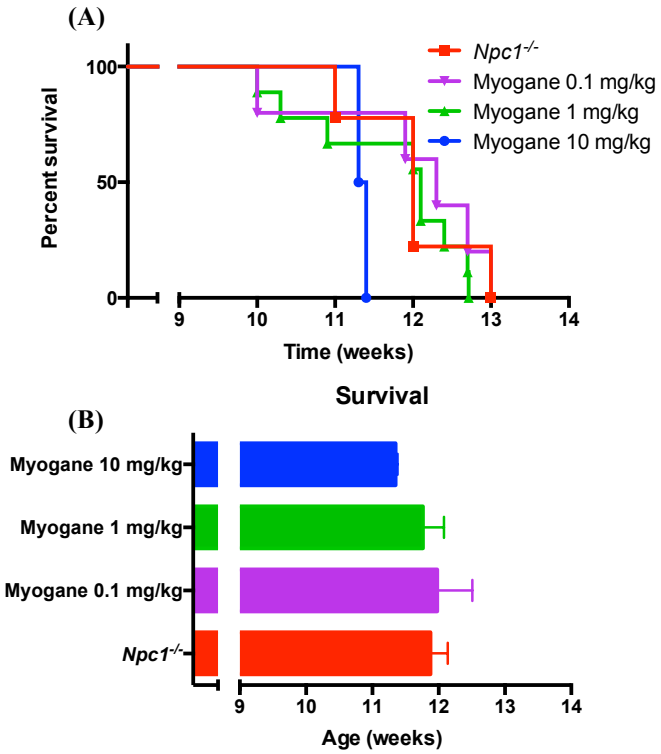

Figure 4.4. Effect of Myogane on survival of *Npc1*$^{-/-}$ mice. (A) Kaplan–Meier survival curve (percent survival) and (B) Average survival ages presented as mean ± SEM, n=4-10. One-way ANOVA with Tukey's post hoc test was performed.

Animals treated with the two lower doses did not lose as much weight as the untreated controls, their percentage of initial body weight was significantly higher than that of untreated controls starting from 5 up to 11 weeks of age for the 0.1 mg/kg group (also significantly higher than the 10 mg/kg group and the 1 mg/kg group only up to 8 weeks) and at 6 and 8 weeks of age for the 1 mg/kg group, these two doses seems to have successfully slowed the rate of weight loss **(Figure 4.5).** At 5 weeks the 0.1 mg/kg treated mice percentage body weight was significantly higher than the other 3 groups (p<0.0001, p=0.0004 and 0.0002 vs. untreated controls, 1mg/kg and 10 mg/kg groups, respectively). By 6 weeks the 1 mg/kg group percentage body weight became also significantly higher than the untreated controls (p=0.026). The 10 mg dose did not protect from weight loss, as the percentage body weight of treated mice was not different from that of untreated control throughout the course of the study (p=0.905, 0.846, 0.991, 0.999, 0.986, 0.944 and 0.358.at 5, 6, 7, 8, 9, 10 and 11 weeks, respectively).

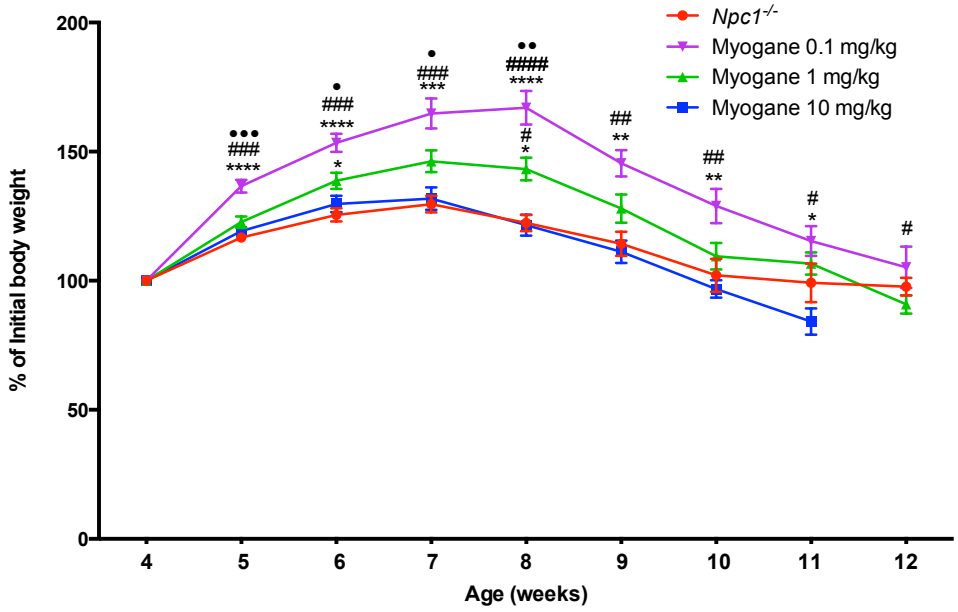

Figure 4.5. Effect of Myogane on weight loss in *Npc1*$^{-/-}$ mice. Data presented as mean (percent of initial body weight) ± SEM over the life span, n=7-14. *p<0.05, **p<0.01, ***p<0.001 and ****p<0.0001, calculated using one-way ANOVA with Tukey's post hoc test. * comparison vs. untreated *Npc1*$^{-/-}$, # comparison vs. 10 mg/kg group, ● comparison vs. the 1 mg/kg group.

Motor function in response to treatment was evaluated by measuring rearing activity in a five-minute open field test. Both lower doses were associated with improved rearing activity maintained from early symptomatic stage up to end stage compared to untreated controls, although did not reach statistical significance (only the 1 mg/kg group had a significantly higher rearing count compared to untreated controls at 10 weeks, p=0.005) **(Figure 4.6 A)**.

Interestingly, the lowest dose was associated with significant increase in the centre rearing activity compared to untreated group starting from 4 weeks of age (also compared to other treatment groups, p=0.0005, 0.0006 and 0.007 vs. untreated control, 1 mg/kg and 10 mg/kg groups, respectively), at 5 weeks (compared to untreated controls, p=0.011), 7 weeks (compared to untreated and 10 mg/kg treated groups, p=0.049 and 0.038, respectively) and 9 weeks (compared to untreated control group p=0.033). The 1 mg/kg treated group had a significant increase in centre rearing activity compared to untreated group at very late stage (11 weeks, p=0.037) **(Figure 4.6 B)**.

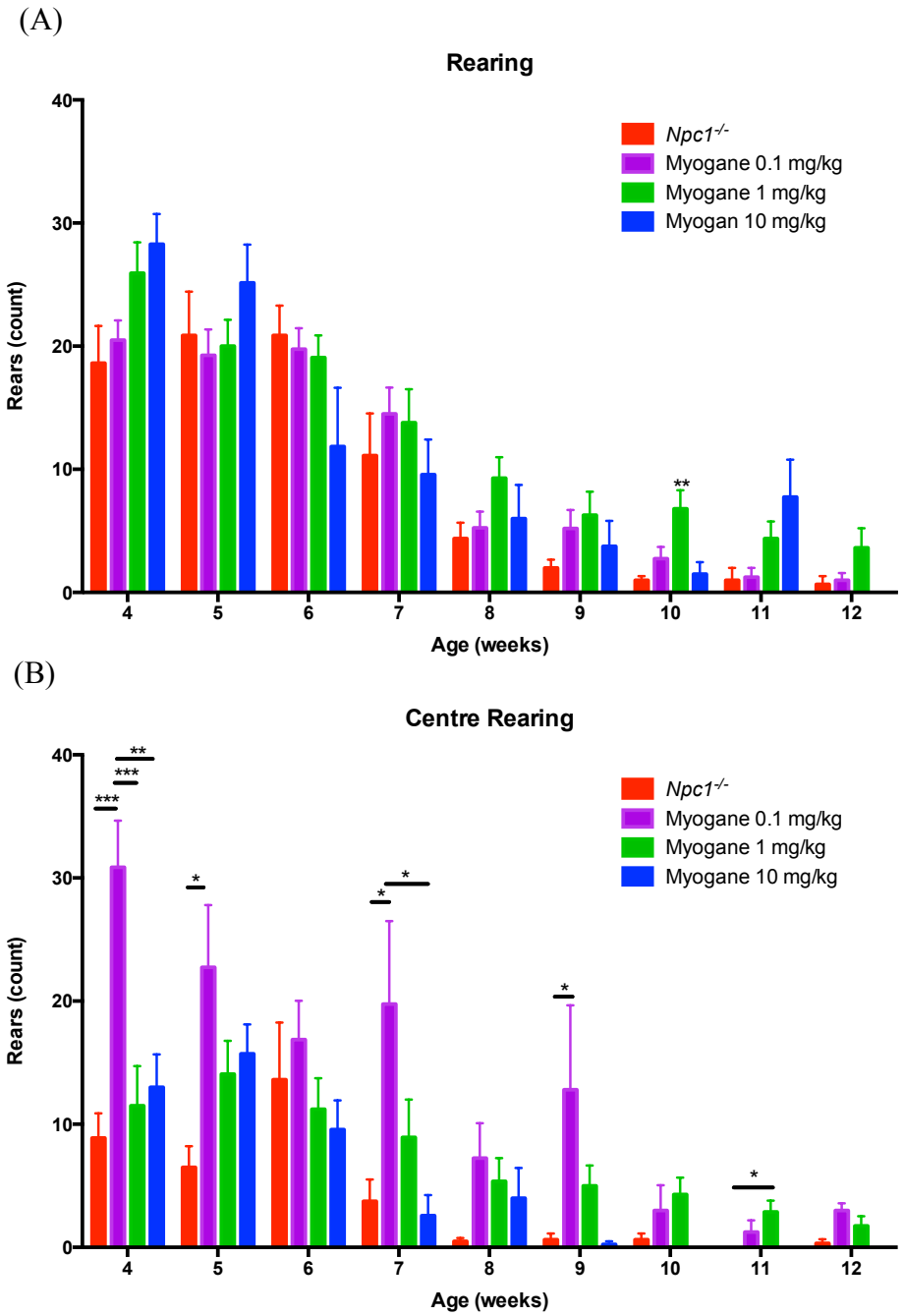

Figure 4.6. Effect of Myogane on (A) rearing and (B) centre rearing of *Npc1*$^{-/-}$ mice. Data presented as mean (rearing count) ± SEM, n=7-14. **p*<0.05, ***p*<0.01 and ****p*<0.001, calculated using one-way ANOVA with Tukey's post hoc test.

No significant reduction in tremor amplitude was observed with any of the doses at all disease stages **(Figure 4.7** and **Figure 4.8)**, in fact the high dose was associated with worsening of the tremor at the late symptomatic stage (10-11 weeks) possibly due to toxicity while the low dose may have been too low to produce any beneficial effect on the tremor amplitude.

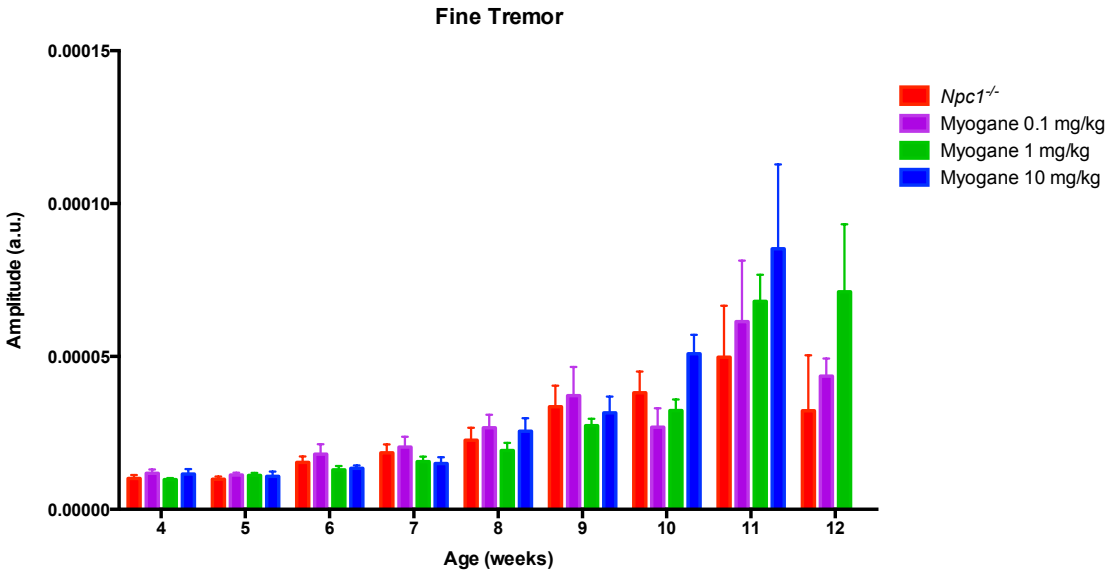

Figure 4.7. Effect of Myogane on fine tremor of *Npc1*$^{-/-}$ mice. Tremor amplitudes quantified as averaged fine tremor amplitude (over the range 31-51 Hz). Data presented as mean ± SEM, n=7-14. One-way ANOVA with Tukey's post hoc test was performed.

(A)

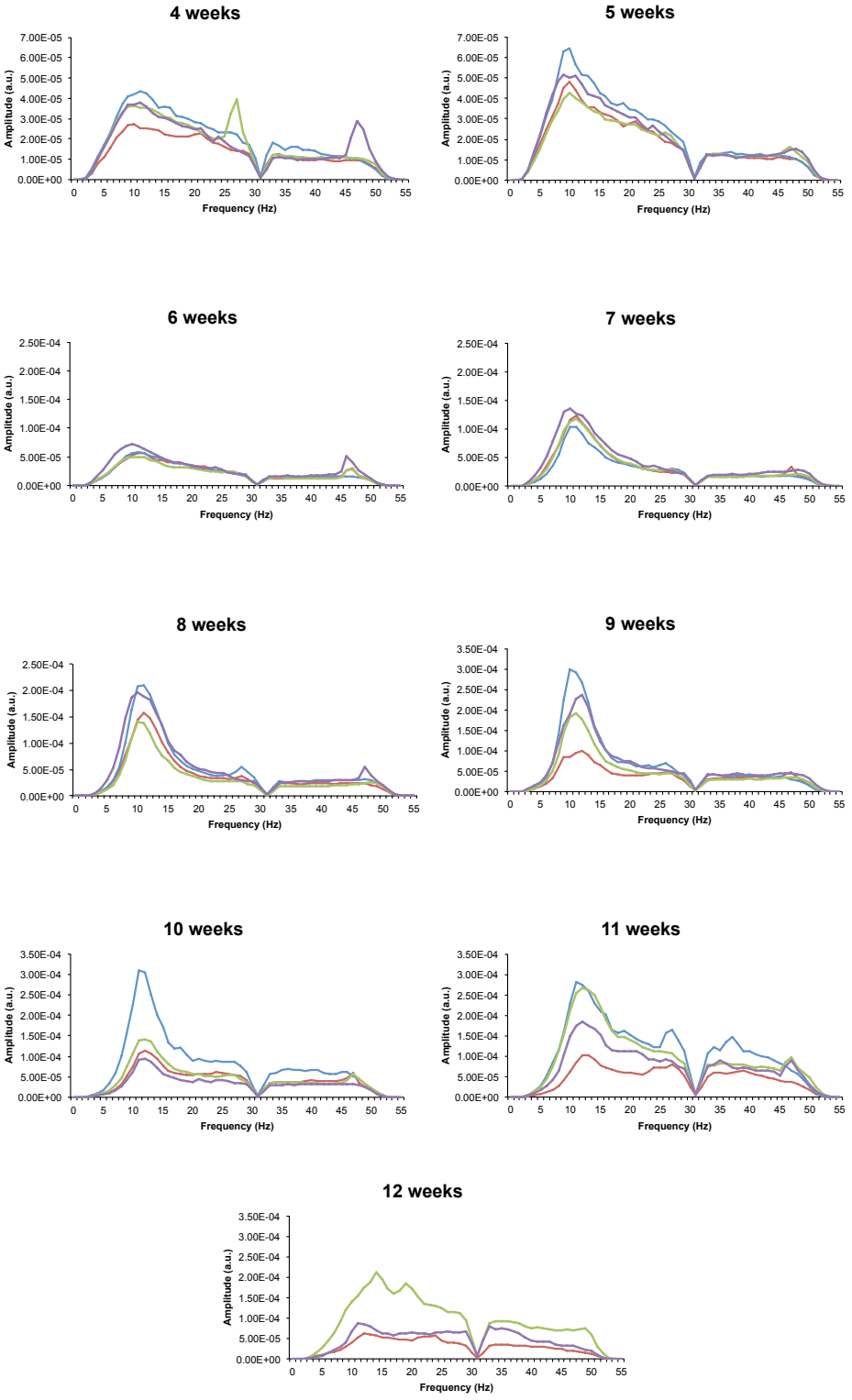
4 weeks
5 weeks
6 weeks
7 weeks
8 weeks
9 weeks
10 weeks
11 weeks
12 weeks
Amplitude (a.u.)
Frequency (Hz)

(B)

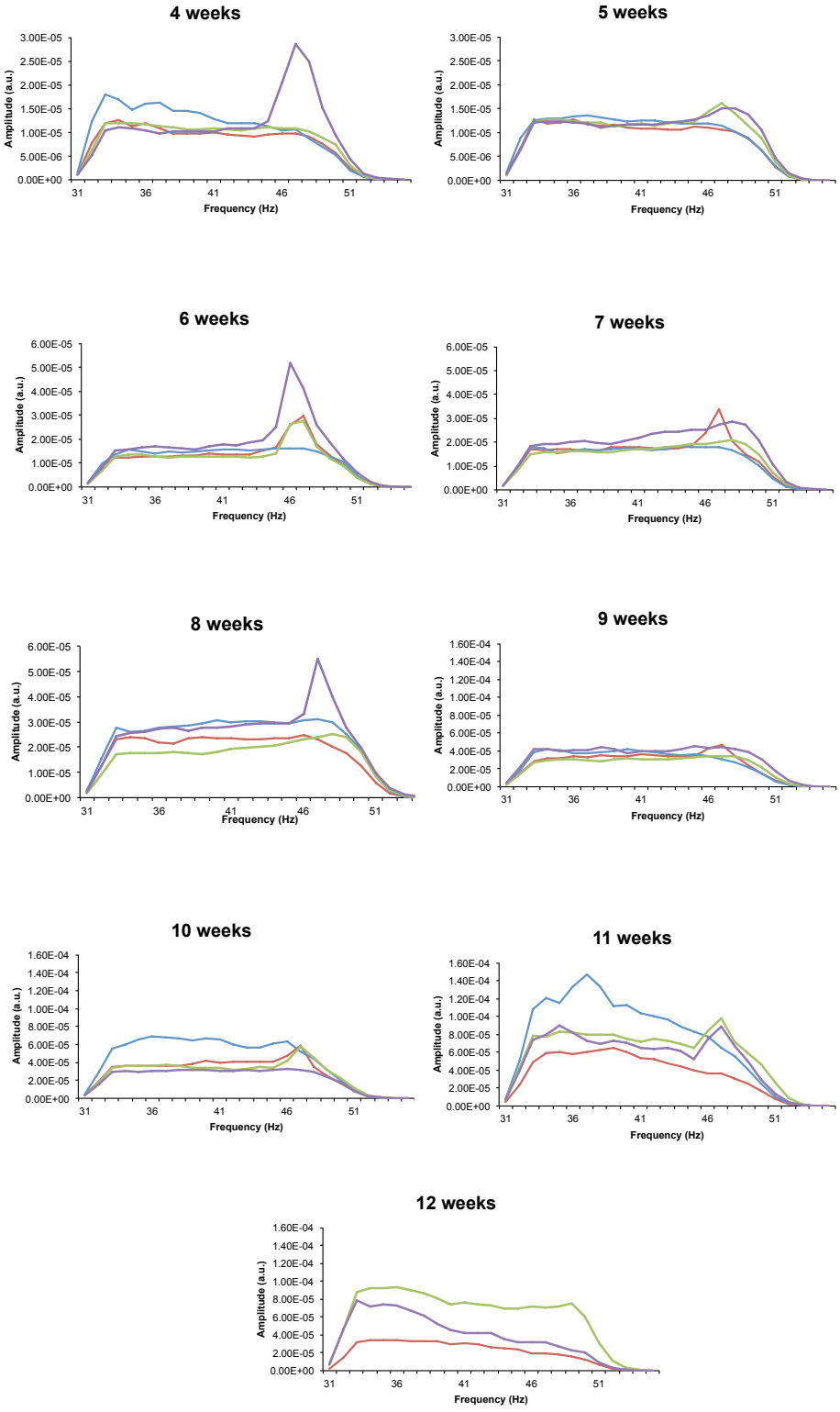

Figure 4.8. Effect of Myogane on tremor of *Npc1*$^{-/-}$ mice (A) overall tremor range and (B) fine tremor range. Data presented as mean tremor amplitude, n=7-14. Red; untreated *Npc1*$^{-/-}$ controls, purple; Myogane 0.1 mg/kg, green; Myogane 1 mg/kg and blue; Myogane 10 mg/kg.

Efficacy *in vivo* was further assessed at end-stage measuring GSL storage levels and free cholesterol concentrations in brain, lung, liver, kidney and spleen. There were no significant difference in the total levels of these lipids in the analysed tissues, however, 0.1 mg treatment was associated with an increase in some of the GSL species in the spleen and lung and that could be due to the heterogeneous nature of the spleen and the possibility that the measured total GSLs could also reflect macrophage storage in addition due to differential inflammatory infiltration that could have contributed to the increase in certain species in the low dose group **(Figure 4.9).**

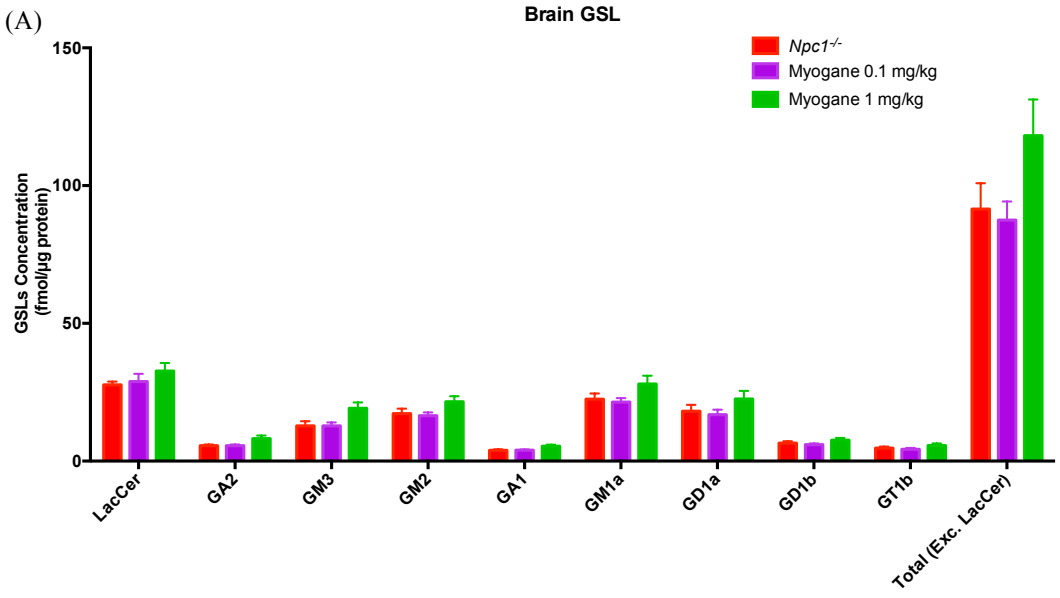

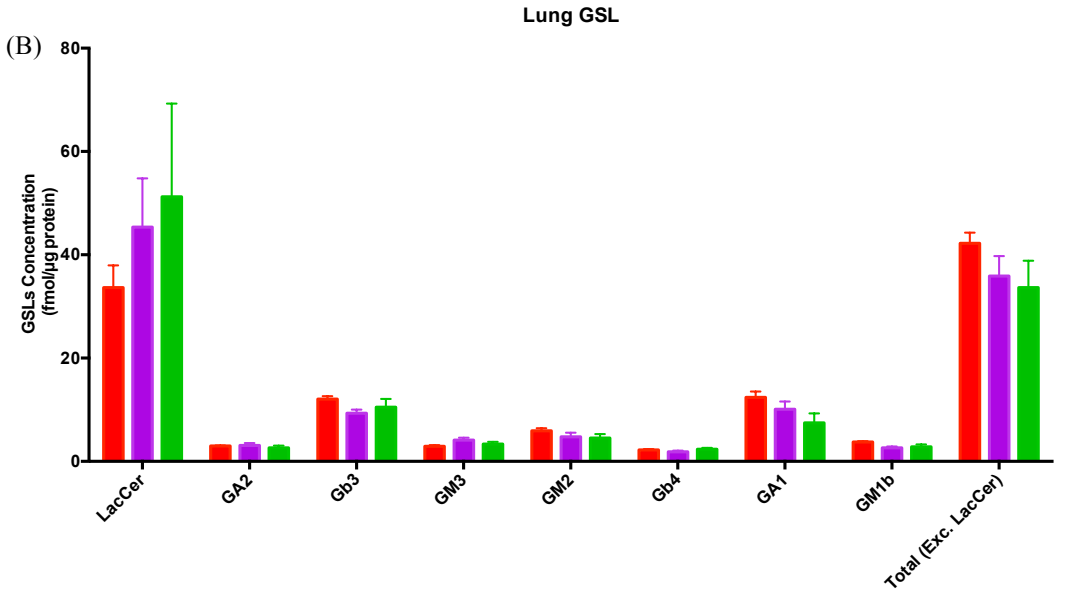
Lung GSL
(B)
GSLs Concentration (fmol/μg protein)
80
60
40
20
0
LacCer
GA2
Gb3
GM3
GM2
Gb4
GA1
GM1b
Total (Exc. LacCer)

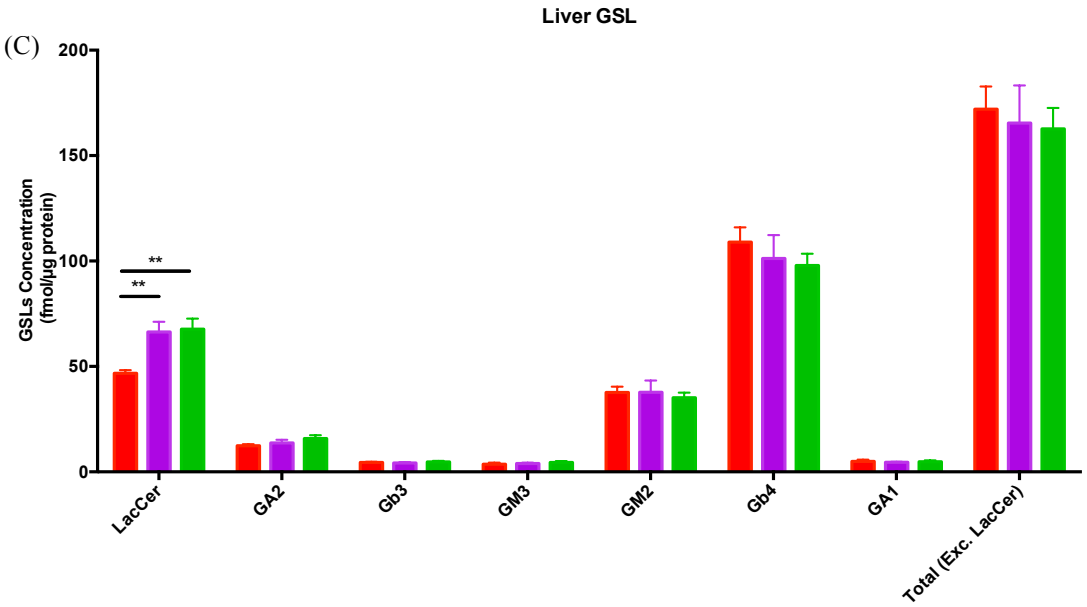
Liver GSL
(C)
GSLs Concentration (fmol/μg protein)
200
150
100
50
0
**
**
LacCer
GA2
Gb3
GM3
GM2
Gb4
GA1
Total (Exc. LacCer)

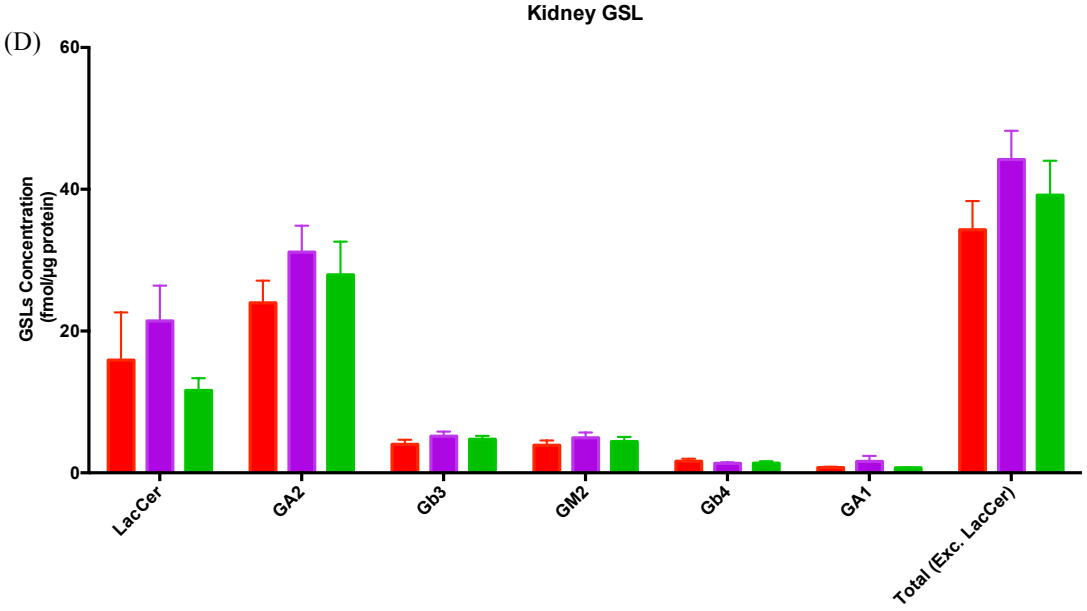
Kidney GSL
(D)
GSLs Concentration (fmol/μg protein)
60
40
20
0
LacCer
GA2
Gb3
GM2
Gb4
GA1
Total (Exc. LacCer)

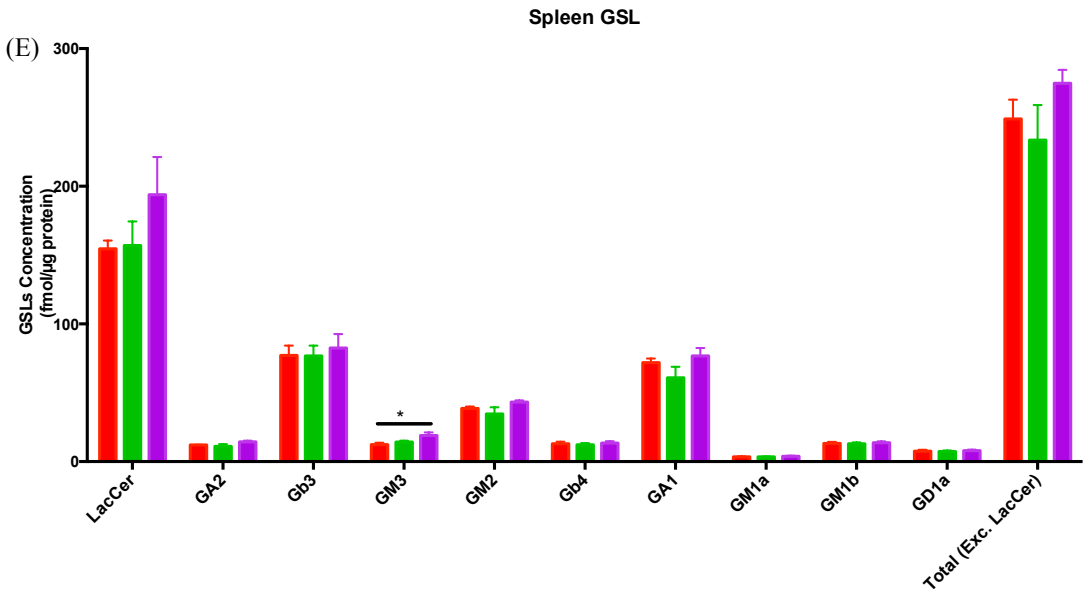

Figure 4.9. Effect of Myogane on *Npc1*$^{-/-}$ GSL levels in (A) Brain (B) Lung (C) Liver (D) Kidney and (E) Spleen of *Npc1*$^{-/-}$ mice vs Myogane treated *Npc1*$^{-/-}$ mice, at 0.1 mg and 01 mg measured at end point. Data presented as mean ± SEM, n=5. **p*<0.05 and ***p*<0.01, calculated using one-way ANOVA with Tukey's post hoc test.

In addition, the 1 mg group had a significantly lower free cholesterol level in the kidneys (p=0.007) **(Figure 4.10)**.

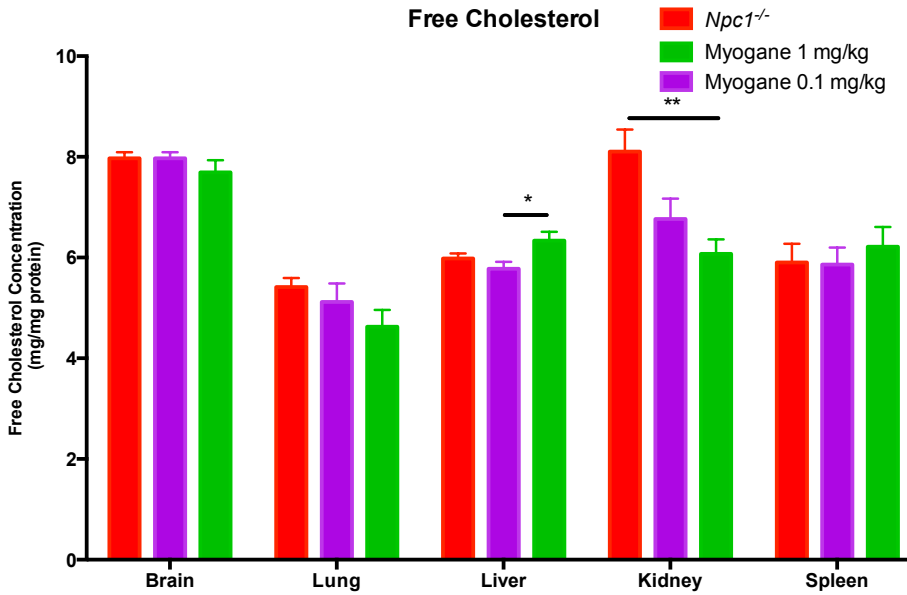

Figure 4.10. Effect of Myogane on free cholesterol levels in brain, lung, liver, kidney and spleen of *Npc1*$^{-/-}$ mice vs Myogane treated *Npc1*$^{-/-}$ mice, at 0.1 mg and 1 mg measured at end point. Data presented as mean ± SEM, n=5. **p*<0.05 and ***p*<0.01, calculated using one-way ANOVA with Tukey's post hoc test.

Cerebellar Purkinje cell loss is a main neuropathological feature of NPC1 disease (300). Although Purkinje cell survival in both lobule III and IV has not changed in response to treatment (for lobule III; p=0.993, 0.873 and 0.998 for 0.1, 1 and 10 mg/kg groups, respectively and for lobule VI; p=0.854, 0.989 and 0.935 for 0.1, 1 and 10 mg/kg groups, respectively) **(Figure 4.11** and **Figure 4.12)**, the pattern and count of Purkinje cells in cerebellar sections of all treatment groups were very consistent indicative of a neuroprotective effect unlike untreated controls where there has been a huge variation between the individual mice and the different sections of the same mouse.

Microglial activation appears to be a very early event in NPC1 pathogenesis, with increased microglial activation in most brain areas (including the cerebellum) from as early as 4 weeks of age before the onset of any symptoms and last to end-point (71). In NPC1 and other neurodegenerative diseases the mechanism of microglial activation is not fully understood, but results in oxidative stress in the brain. Activated microglia express the LE/Lys marker CD68 (92), member of the LAMP macrosialin family of hematopoietic mucin-like molecules (301).

Significant reduction in the number of activated microglia in the cerebellum was observed in all treatment groups with the lower dose (0.1 mg/kg) associated with the highest anti-inflammatory effect (for lobule III; p<0.0001, p=0.0004 and 0.002 for 0.1, 1 and 10 mg/kg groups, respectively and p= 0.024 for 0.1 mg/kg groups vs. 10 mg/kg group and for lobule IV; p<0.0001, p=0.007 and 0.0006 for 0.1, 1 and 10 mg/kg groups, respectively and p=0.014 for 0.1 mg/kg groups vs. 1 mg/kg group) **(Figure 4.11** and **Figure 4.12)**.

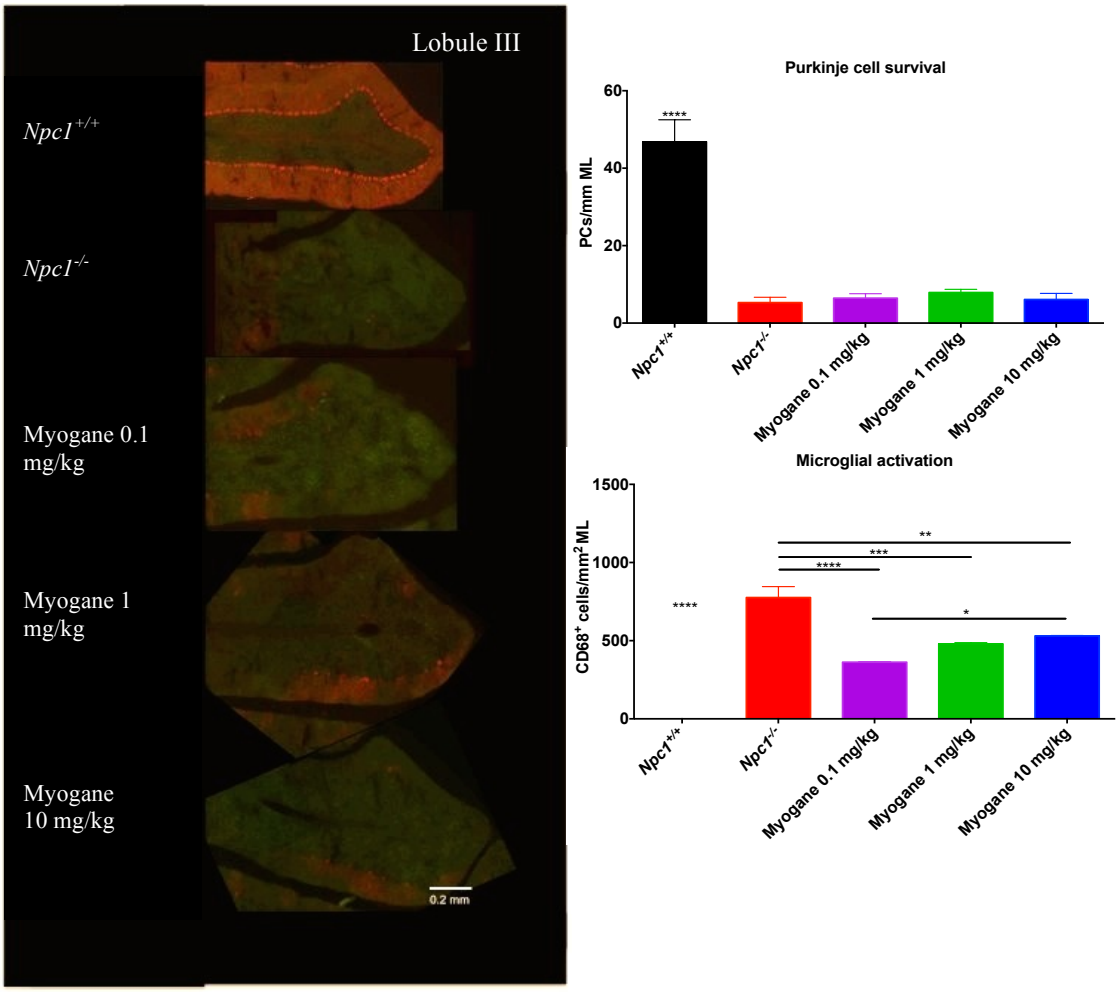

Figure 4.11. Effect of Myogane on *Npc1*$^{-/-}$ cerebellar lobule III microglial activation and Purkinje cell survival at 8 weeks of age. (A) Representative images of cerebellar sections double immunostained with anti-calbindin antibody and anti-CD68 antibody. The cerebellum of untreated *Npc1*$^{-/-}$ mice (untreated controls) was compared to Myogane treated mice at three different doses (0.1 mg, 1 mg and 10 mg), n=3 for each group. (B) The number of calbindin-labelled Purkinje cells in the Purkinje cell layer of cerebellar lobule IV was counted to evaluate the effect of Myogane treatment on Purkinje cell survival and compared to the untreated *Npc1*$^{-/-}$ animals. The number of Purkinje cells was calculated per m m of the Purkinje cell layer. The data is presented as mean of three different sections of three independent mice ± SEM. (C) The number of green CD68-labelled cells in the molecular layer (ML) of cerebellar lobule III of treated mice were counted and compared to the untreated *Npc1*$^{-/-}$ animals. The number of CD68^{+} cells was calculated per mm^2 of the molecular layer. Data presented as mean (of three different sections of three independent mice) ± SEM. $p<0.05$, $^{**}p<0.01$, $^{***}p<0.001$ and $^{****}p<0.0001$, calculated using one-way ANOVA with Tukey's post hoc test. Scale bar represents 0.2 mm.

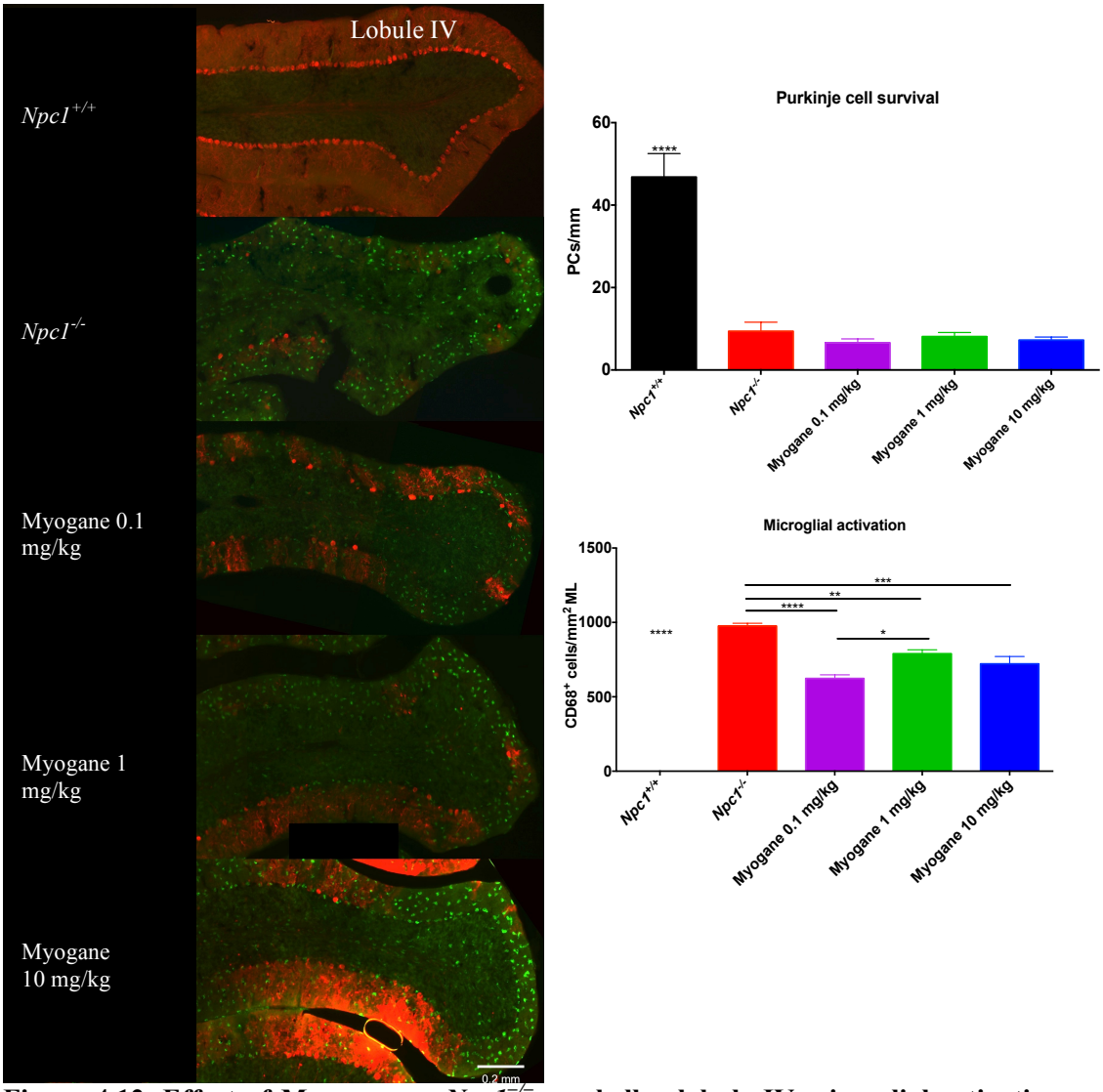

Figure 4.12. Effect of Myogane on *Npc1*$^{-/-}$ cerebellar lobule IV microglial activation and Purkinje cell survival at 8 weeks of age. (A) Representative images of cerebellar sections double immunostained with anti-calbindin antibody and anti-CD68 antibody. The cerebellum of untreated *Npc1*$^{-/-}$ mice (untreated controls) was compared to Myogane treated mice at three different doses (0.1 mg, 1 mg and 10 mg), n=3 for each group. (B) The number of calbindin-labelled Purkinje cells in the Purkinje cell layer of cerebellar lobule IV was counted to evaluate the effect of Myogane treatment on Purkinje cell survival and compared to the untreated *Npc1*$^{-/-}$ animals. The number of Purkinje cells was calculated per mm of the Purkinje cell layer. The data is presented as mean of three different sections of three independent mice ± SEM. (C) The number of green CD68-labelled cells in the molecular layer (ML) of cerebellar lobule IV of treated mice were counted and compared to the untreated *Npc1*$^{-/-}$ animals. The number of CD68^{+} cells was calculated per mm^2 of the molecular layer. Data presented as mean (of three different sections of three independent mice) ± SEM. ***p*<0.01, ****p*<0.001 and *****p*<0.0001, calculated using one-way ANOVA with Tukey's post hoc test. Scale bar represents 0.2 mm.

GalCer is the main sphingolipid component of myelin. In this study we used GalCer as surrogate marker of myelin content in *Npc1*$^{-/-}$ mouse brain to assess the effect of these neuroprotective agents on myelination. Upon separation on TLC plates, two GalCer bands were detected, the upper band corresponds to the non-hydroxy fatty acid-ceramide while the lower bans represents GalCer species with the hydroxylated fatty acids on the ceramide backbone.

Brain GalCer levels, revealed a significant reduction (by about 60% by postnatal day 14) in the *Npc1*$^{-/-}$ mice compared to wild-types in agreement with published studies (30, 302, 303). The non-hydroxy fatty acid fraction was particularly affected (normally accounts for about 35-40% of total galactosylceramide fraction). This is indicative of a myelination defect in NPC1 disease. The results also further confirmed our previous findings of a modest neuroprotective effect of this compound. In agreement with IHC results where the low doses were more effective, brains from the 1 mg/kg group had a trend towards higher levels of GalCer compared to untreated controls, however the difference did not reach statistical significance ($p=0.230$ and 0.097 for non-hydroxy and hydroxy fatty acid GalCer, respectively) **(Figure 4.13)**.

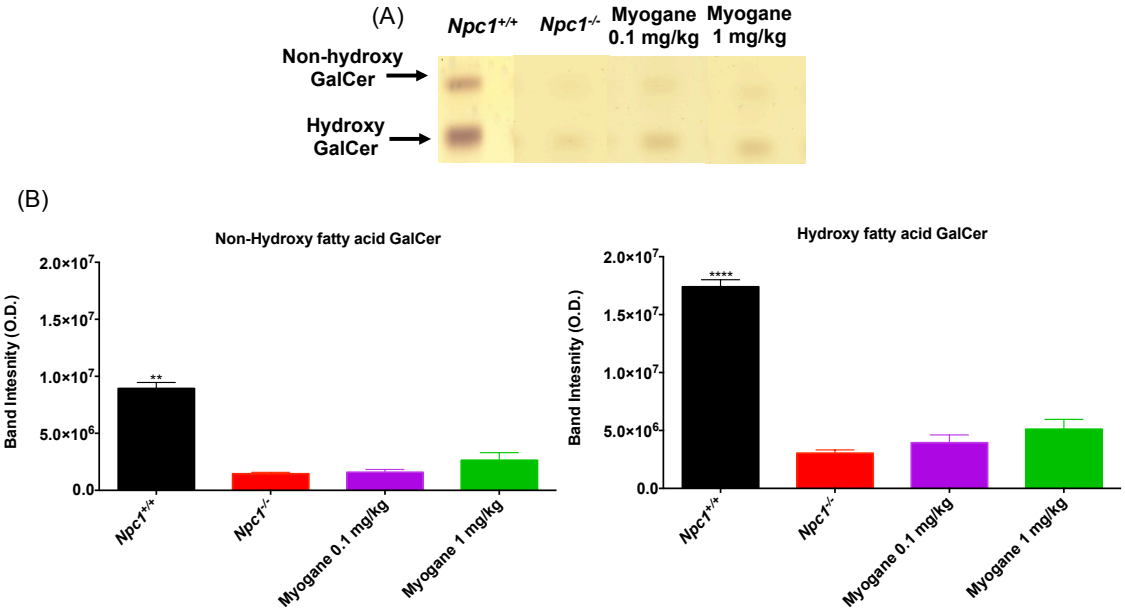

Figure 4.13. Effect of Myogane on *Npc1*$^{-/-}$ brain galactosylceramide levels as a surrogate marker of myelination. (A) Representative HPTLC plate of whole brain homogenates, extracted and separated on a HPTLC plate. Whole brain samples of wild-types (*Npc1*$^{+/+}$), untreated *Npc1*$^{-/-}$ mice were analysed and compared to Myogane treated mice at the two lower doses (0.1 mg/kg and 1 mg/kg), n=3-8 for each group, collected at end-point (10-13 weeks of age). (B) Absolute quantitation of the amounts of GalCer, both non-hydroxy (top band) and hydroxy (bottom band) fatty acid GalCer were quantified using ChemiDoc system. Data presented as mean ± SEM (n=3-8). One-way ANOVA with Tukey's post hoc test was performed.

4.4. Discussion

Since NPC disease shares common neuropathological features with other neurodegenerative disorders (150, 297), it is was logical to evaluate neuroprotective drugs (e.g. Cogane and Myogane) in NPC as they have shown efficacy in animal models of other neurodegenerative diseases (283). Cogane and Myogane are particularly attractive compounds as they cross the blood-brain barrier (283).

In this study we have examined the use of the two novel, orally bioavailable, non-peptide neurotrophic factor inducing compounds Cogane and Myogane. Initially, due to their structural similarities to cholesterol and the possibility that they could theoretically inhibit the function of NPC1 and/or NPC2 proteins (4), we investigated this by testing the effects of the two compounds in healthy cells. Neither drug induced any NPC disease cellular phenotypes. They were therefore progressed to a second *in vitro* study in order to assess their ability to correct NPC phenotypes in cells *in vitro*, which would then suggest another mechanism by which they mediated their beneficial effect, independent of their established neuroprotective effect that requires induction of neurotrophic factors. Neither of these compounds showed a significant effect on lipid storage burden in NPC1 deficient cells *in vitro*, ruling out the potentials of this other mechanistic approach suggested. Myogane then was tested in the mouse model of NPC disease in order to assess the magnitude of its neuroprotective effect in this disease.

We initially went from 30 mg/kg to 10 mg/kg in a pilot study to avoid masking any beneficial effects with adverse effects associated with toxicity potentially due to the reduced liver function in this mouse model. We then tested two lower doses; 1 and 0.1 mg/kg, which were functionally more beneficial than the 10 mg/kg dose.

The lower doses then progressed to biochemical and immunohistochemical analysis of lipid storage and cerebellar pathology in treated mice. No effect on storage (GSLs and cholesterol) was seen but the rate of brain demyelination may have been slowed (not significant) and interestingly exerting an anti-inflammatory effect in the cerebellum reducing microglial activation. This suggests that the functional benefit in the mice was mediated through the previously established neuroprotective and neurorestorative properties of Myogane. The anti-inflammatory effect of these compounds has not been reported previously and its unclear if this is a direct effect or the result of slowing the rate of neurodegeneration. The only published data on administration of these compounds in animal models of neurodegenerative diseases was by Visanji *et al.* (283), where 10 mg/kg Cogane was given orally to 5 week old MPTP (1-methyl-4-phenyl-1,2,3,6-tetrahydropyridine)-lesioned mice for 60 days, treated mice had a significant ~3-5 fold increase in the levels of the two neurotrophic factors in the striatum slowing the loss of striatal dopaminergic transporter levels, restoring dopaminergic transporter binding to almost levels seen in non-MPTP-lesioned mice and dopaminergic neurons in the substantia nigra. Cogane's neuroprotective effect included both cell body and terminal regions of dopaminergic neurons. Interestingly, a significant effect was also observed upon delayed administration of Cogane. The mechanism by which Cogane produced its effect is not known but inhibition of monoamine oxidase B and influencing MPTP metabolism in the brain affecting the levels of MPP^+ (1-methyl-4-phenylpyridinium) were ruled out *in vitro* and *in vivo* respectively.

Neurotrophic factors are secretory peptides, which play an important role in neuronal survival, maturation and differentiation during and after development. They act on specific neuronal populations (304). Neurotrophic factors bind to the p75 neurotrophin receptor (p75NR) and to their specific Trk receptor. Upon receptor binding, they induce autophosphorylation of the Trk receptor and subsequent activation of protein kinases with downstream activation of multiple signalling pathways including for example MAPK and PI3K pathways (305). Neurotrophic factors eventually stimulate the transcription of genes required for neuronal survival and differentiation during development and throughout adulthood as well. Neurotrophic factors have also shown to play a role in synaptic function (306).

Reduced BDNF levels are known to be associated with behavioural changes and susceptibility to psychiatric illness including depression and anxiety (307). It has also shown to reduce the release of NO from IFN-γ-activated microglia *in vitro* (308) which could explain the anti-inflammatory effect we observed suppressing microglial activation. BDNF mediates its effect on microglia via the high affinity neurotrophic receptor TrkB and to a lesser extent the p75 receptor with low affinity with subsequent upregulation of multiple proteins and suppression of iNOS (309). Furthermore, astrocyte derived-GDNF, but not BDNF, has shown to inhibit microglial activation in cultured midbrain and contribute to protection from nreurodegeneration and neuroinflammation (310). Although others have suggested regional differences in the expression of neurotrophic factors by microglia due to their differential properties in different brain regions and microenvironments, resulting in a constitutive expression of neurotrophic factors in some areas whereas in others the expression of neurotrophic factors is inducible (311).

Microglia activated by LPS (312) or IFN-γ have been shown to secrete BDNF, which in addition to its pro-survival role maintaining neurons, also induces the proliferation and activation of microglia *in vitro* (311, 313) and *in vivo* (314). Both BDNF secretion by activated microglia and BDNF interaction with microglia are mediated thorough the adenosine 2A receptors (A2AR) (315), antagonists to this receptor have shown beneficial in neurodegenerative conditions with a chronic neuroinflammation element (316, 317).

GDNF secretion by microglia has been reported to be inhibited upon stimulation with LPS, an effect of microglial activation at the secretory rather than the expression level (318). Activated microglia produce more BDNF than GDNF, indicative of a potentially neuroprotective effect of activated microglia in damaged

brain areas as opposed to the most common neurotoxic effect observed upon activation (319, 320).

Axonal spheroid formation and progressive cerebellar Purkinje cell loss is an established neuropathological feature of NPC1 disease and correlates with neurological presentation, motor dysfunction and clinical phenotype in both the mouse and cat models (321-323). Purkinje cell involvement is detected as an increase in parvalbumin-positive spheroids in *Npc1*$^{-/-}$ mice compared to controls, followed by diminishing number of spheroids in the cerebellum due to consequent Purkinje cell death. In particular, cerebellar lobules III and IV, which represent the early degenerating areas of the *Npc1*$^{-/-}$ cerebellum, as opposed to the late degenerating or non-degenerating area (lobule IX and X), which survive until very late stages of the disease (300). Purkinje cell loss starts with about 13% death by postnatal day 22 (324), and reaches 96% at very late stage at around 11 weeks of age (325). Preservation of Purkinje cells and delay in their death was observed in many therapeutics trialed in the *Npc1*$^{-/-}$ mouse including miglustat, ibuprofen and their combination (82, 92), allopregnanolone/cyclodextrin (121), cycodextrin and their combination with miglustat (87).

Galactosylceramide along with its sulphated derivative sulphogalactosylceramide are two specific glycolipid markers of oligodendrocytes and myelin. They are considered early surface markers and present on the surface of mature cells both *in vitro* (326) and *in vivo* and have been immunolocalised in oligodendrocytes and myelin sections (327), making it a useful surrogate marker of myelination. Galactosylceramide is the main component of myelin; its concentration is proportional to myelin amount in the brain (past early development stage). Galactosylceramide is both the most abundant and specific component of myelin

and accounts for about one fifth of the lipid dry weight of myelin. About 20% of myelin's galactolipid content is sulphated (328). Despite its abundance and specificity to myelin, galactosylceramide is not crucial for the synthesis or maintenance of myelin. Mice null for UDP-galactose:ceramide galactosyltransferase and therefore deficient in cerebrosides and sulphatides had a relatively normal myelin formation with minor structural alterations leading to progressive neurological deficit, suggestive of the dispensable role of galactosylceramide in myeline formation and maintenance (329).

Demyelination in *Npc1*$^{-/-}$ mice is observed at 7 weeks of age when myelination is normally complete in healthy mice, and is due to loss of both myelin protein and cholesterol (330). Demyelination in *Npc1*$^{-/-}$ mice has been proposed to be the cause of no overall cholesterol build-up in *Npc1*$^{-/-}$ brain, loss of myelin cholesterol could balance out neuronal cholesterol accumulation (331). Treatment with allopregnanolone/cyclodextrin was associated with significant delay in demyelination process in these mice as measured by CNPase (2', 3'-cyclic nucleotide 3'-phosphodiesterase) immunostaining (121).

In NPC disease, there is evidence of impaired myelination (to variable degrees) both in the CNS and peripheral nervous system (12). In the BALB/c *Npc1*$^{-/-}$ mouse there was a clear myelination defect in the CNS due to a primary myelinogenesis defect as opposed to a secondary defect (e.g. caused by myelin turnover or neurodegeneration) (332).

The underlying mechanism of myelination defect in NPC1 disease remains unknown, however, myelination defect is thought to be related to the dependence on *de novo* cholesterol biosynthesis in the brain (333). BDNF signalling via TrkB is

essential for normal myelinogenesis, BDNF signalling induces the expression of cholesterol synthesising enzymes stimulating *de novo* cholesterol synthesis in cultured cortical and hippocampal neurons (334). However, this pathway is potentially compromised in NPC disease. Striatal neurons from *Npc1*$^{-/-}$ mice are unresponsive to BDNF, unable to activate Trk receptors and to induce neurite outgrowth (335). Unresponsiveness to BDNF in NPC1 neurons seems to be caused by decreased BDNF signalling via TrkB, rather than underexpression of TrkB (335). The defective Trk signalling in NPC1 cells is possibly caused by alterations in membrane cholesterol levels, lipid raft integrity and ganglioside storage (GM2 and GM3). Neurotrophic factor signalling is dependent on lipid rafts and changes in membrane lipids (cholesterol and GSLs) have been suggested to interfere with BDNF and TrkB signalling (336). Lipid rafts appear to be important for the initiation of myelination (333). GM1, a ganglioside that is mistrafficked in NPC1 cells, is thought to mediate neuronal dysfunction. In neurons, GM1 is normally largely present in the synaptosomal membrane and mediates the effect of growth factors. It is known to stimulate neurite outgrowth and modulate the activity of Trk receptor (337). The defective Trk signalling in NPC1 cells could have contributed to the modest neuroprotective effect of Myogane in the mice.

Cholesterol depletion reduced TrkA autophosphorylation in the neuronal-like PC12 cell line (338). In another cell line, NBL-S cells GDNF signalling was affected by cholesterol depletion (339). The response to neurotrophic factors in NPC1 neurons is suggested to be receptor- and cell type-specific (333).

In neural stem cells from *Npc1*$^{-/-}$ mice, BDNF and TrkB expression was significantly lower and was upregulated in response to valproic acid, which is

suggested to be the mechanism by which valproic acid and HDACi mediate their neuroprotective effects enhancing neuronal survival and differentiation (96).

This is the first study testing these novel natural product compounds (Cogane and Myogane) in the mouse model of NPC1 disease, and the first study where treated animals were followed up thorough the course of the disease and monitored for functional benefit. The results obtained support the potential of using these compounds in combination with miglustat, with careful consideration of the dose intended. These compounds represent a class of compounds that have the potential to delay disease progression through both neuroprotective and neurorestorative effects and may synergise with other therapies that target different steps in the pathogenic cascade.

Chapter 5. Niemann-Pick Type C and Inflammatory Bowel Disease

5.1. Introduction

The two main inflammatory bowel diseases (IBD); ulcerative colitis and Crohn's disease are characterised by severe, chronic and relapsing inflammation of the gastrointestinal (GI) tract with the main common symptoms of diarrhoea and weigh loss (340). However, they vary anatomically in terms of the anatomical sites of inflammation in the GI tract and the histological features of the intestinal inflammation (340). Ulcerative colitis affects only the caecum, colon and/or rectum while Crohn's disease can present anywhere in the GI tract from the mouth to the anus (340). Generally, the terminal ileum and colon appear to be the most commonly affected regions (340). Histopathologically and microscopically, Crohn's disease is characterised by a transmural lesion, often discontinuous, while ulcerative colitis is a continuous lesion restricted to the intestinal mucosa (340).

Ulcerative colitis occurs at a worldwide incidence rate of 0.5–24.5/100,000 persons, while that of Crohn's disease is 0.1–16/100,000 individuals, with a combined prevalence rate of IBD of up to 396/100,000 (341). Males and females are almost equally affected with IBD with peak age of onset in early adulthood (342). It is however important to note that numbers of cases are increasing with industrialisation, which emphasises the role of environmental factors in the pathogenesis of these complex multifactorial diseases (343, 344). Although the underlying mechanisms of pathogenesis remain incompletely understood, they can be triggered by continuous and abnormal activation of immune response in the intestinal mucosa by the intestinal microbiota (intestinal microbial population) (345).

Approximately four cases have been reported in the literature of NPC patients presenting with IBD, more commonly Crohn's disease (109, 346-348).

There are two potential aspects of NPC disease that may predispose to Crohn's disease. Firstly, generalised inflammation is observed in NPC disease both in the CNS and periphery (71, 183) and seems to be TNF-dominated. This is due to the important role of both NPC proteins in normal immune cell (macrophages and lymphocytes) development and function thus initiating proper immunological response (349, 350). Also, NLRP3 inflammasome is dysregulated in NPC disease (Platt *et al.* unpublished observation). Abnormal immune responses driven by NPC dysfunction are believed to predispose to Crohn's disease, and therefore intestinal inflammation could be potentially one of these complications (349).

Secondly, we have shown that bile acid supplementation was effective in improving neurological function and partially correcting liver detoxifying capacity in the *Npc1*$^{-/-}$ mouse **(Chapter 2)**, this suggests that NPC1 disease is potentially associated with bile acid (BA) deficiency due to altered BA homeostasis affecting the composition/levels of BAs in NPC disease. Gut microbiota plays a crucial role in maintaining BA homeostasis, they are responsible for the biotransformation of the primary BA cholic acid (CA) and chenodeoxycholic acid (CDCA) synthesised and secreted from the liver to the intestinal lumen where they are transformed to secondary BAs by gut microbiota via two processes; deconjugation of the amino acids taurine or glycine (added to the primary BA after secretion into the biliary duct) by BA hydrolases followed by hydroxysteroid dehydrogenation to produce secondary BAs (351, 352). BAs undergo a very efficient enterohepatic circulation to generate the BA pool, in the gut; conjugated BAs undergo active reabsorption in the terminal ileum via specific transporters, transported back to the liver via the hepatic portal circulation (353).

Therefore dysbiosis (disturbance of the composition of gut microbiota) seen in IBD could impair BA metabolism and alter gut homeostasis **(Figure 5.1)**. BAs play an important role in gut mucosal defence through antimicrobial actions (354) and anti-inflammatory properties via down-regulating the synthesis of pro-inflammatory cytokines such as TNF (via inhibition NF-κB) (355). That is all suggestive of the crucial effect of BA homeostasis in maintaining gut integrity, and thus impaired BA homeostasis could further exacerbate the inflammatory status of the gut and contribute to the inflammatory phenotype.

We therefore aimed to study the potential association between these two disorders (NPC and Crohn's) and investigate whether loss of NPC function predisposes to IBD utilising the NPC1 mouse model.

5.2. Methods

The text originally presented here cannot be made freely available via ORA.

5.2.2. Animals

Npc1$^{-/-}$, *Npc1*$^{+/-}$ and *Npc1*$^{+/+}$ mice were generated, maintained and genotyped as described in **Chapter 2**.

GI tract from late end-stage (over 10 weeks of age) *Npc1*$^{-/-}$ and age- and sex-matched *Npc1*$^{+/+}$ mice were grossly examined (macroscopic) for bleeding and signs of inflammation/hypervascularisation.

5.2.3. Induction of colitis

Both studies were conducted in collaboration with Dr. George Song-Zhao and Dr. Kevin Maloy from the Sir William Dunn School of Pathology, University of Oxford and as described in **Sections 5.2.3.1 and 5.2.3.2.**

5.2.3.1. Dextran sodium sulphate (DSS)

Experimental colitis was chemically induced in mice of all three genotypes both males and females (n=4 per gender per genotype) aged 52-54 days of age (7.4 to 7.6 weeks old), by administrations of 4% (w/v; 40 g/L) DSS in drinking water *ad libitum* for 7 days. DSS (MP Biomedicals, Cat.: 160110) administered in the drinking water for 7 days will cause colitis and weight loss (357). DSS was renewed

on day 3 and replaced with water on day 7. Another group of untreated (control) mice of the 3 genotypes were included and were given water for 9 days, renewed at days 3 and 7. This dose was determined by a pilot study in this mouse strain (BALB/c) to establish the effective dose to induce colitis in wild-type mice.

Mice were monitored very closely and weighed and scored daily for adverse effects and IBD severity following the scoring scheme adapted form Wolfensohn and Lloyd, 2nd ed., p62 **(Table 5.1)**.

(A) General scoring scheme for assessment of mice

Appearance and behaviour	**Score**
Normal	0
General lack of grooming, less mobile	1
Ocular or nasal discharge, less alert, isolated	2
Piloerection, hunched up, very still	3
Food and water intake	
Normal (body condition score 3)	0
Body condition score 2-3 (weight loss 0-10%)	1
Body condition score 2 (weight loss 10-20%)	2
No intake, body condition score 1 (weight loss >20%)	6

Total Score	**Actions**
0-1	Normal
2-3	Ensure adequate access to food and fluids
4-5	Seek advice from NACWO and/or vet; administer fluids, heat, analgesics as necessary
6	Terminate

(B) Scoring scheme to assess the severity of IBD

No clinical signs of IBD	0
Weight loss below 20%, or loose faeces and mild inflammation of the anus	1
Weight loss below 20%, loose faeces and mild inflammation of the anus	2
Weight loss >20%, or prolapse sustained for a period of 48hr or prolapse associated with overt bleeding	3
Animals with grade 1 disease will be monitored carefully. Animals with grade 2 disease will be monitored daily; termination will be considered. At the first signs of grade 3 disease, animals will be killed and may be subjected to pathological examination.	

Table 5.1. Scoring scheme adapted for daily monitoring of mice on DSS, based on Wolfensohn and Lloyd, 2nd ed., p62. Mice were scored for any adverse effects (A) and severity of IBD (B).

5.2.3.2. *Citrobacter rodentium* Infection Study

The *Citrobacter rodentium* strain used was a nalidixic acid-resistant strain (ICC169, the mutant of the wild-type *C. rodentium* ICC168) which possesses similar infective properties (358), ICC168 was obtained from the original stocks by Barthold (359).

C. rodentium was grown aerobically overnight in Luria–Bertani (LB) broth supplemented with nalidixic acid (50 μg/mL) at 37°C to stationary phase, diluted the following day to an optical density of 0.1 and further grown to log phase, collected by centrifugation at 7,000 rpm for 10 minutes at 4°C, washed and resuspended in sterile phosphate-buffered saline (PBS) at a concentration of ~$2X10^{10}$ colony-forming units (CFU)/mL, so that 200 μL feeding volume gives ~$4X10^{9}$ CFU/mouse.

Twenty-four mice (8 of each genotype, 4 males and 4 females, either littermates or co-housed from weaning) were used for the infection study at 6 weeks of age.

At 6 weeks of age (day 0), mice were infected by oral gavage with 200 μL of the bacterial suspension (feeding dose ~$4x10^{9}$ CFU/mouse in a volume of 200 μL).

Infected mice were weighed daily and culled if they lost more than 20% of starting weight, monitored and scored daily for signs of IBD or any other adverse effects throughout the study. Two endpoints were used in this study, which corresponded to peak infection (assessed from bacterial load in the faeces), day 10 and day 19 post infection.

5.2.3.3. Enumerating faecal *C. rodentium*

Fecal shedding of *C. rodentium* was measured to assess bacterial infection in the caecum and colon. Faeces were collected daily into pre-weighed Eppendorf tubes with 500 μL sterile PBS and the weight of faecal pellet was determined. Faecal

pellets were vortexed for 1 minute before mashing using a 200 μL pipette, vortexed for another minute, spun down at the lowest centrifuge speed for 1-2 minutes. The supernatant was aspirated and then serially diluted before plating out onto nalidixic acid-supplemented LB plates. The number of colonies was counted and bacterial load was expressed as CFU/mg.

5.2.3.4. Enumerating tissue *C. rodentium*

To assess bacterial load in infected mice, about 3 mm sections of mid-, distal colon and caecum were collected. Tissues were weighed and then homogenised in 600 μL of PBS. Tissue homogenates were serially diluted and plated on nalidixic acid (Sigma-Aldrich, Gillingham, UK; final concentration 50 μg/mL) agar plates, incubated overnight at 37°C and colonies were counted the following day. The number of colonies (CFUs) were normalised to the weight of the tissue (CFU/mg).

5.2.3.5. Organ explant culture

For measuring secretory cytokine levels, about 3 mm sections of mid-, distal colon and caecum were collected. Tissues were weighed, washed in PBS (supplemented with antibiotics penicillin and streptomycin), incubated at 37°C overnight in complete RPMI. The next day, the supernatants were harvested and the levels of the following cytokines were measured using Flow Cytomix Cytokine Bead Assay (eBioscience, Vienna, Austria): interferon-γ (IFN-γ), IL-17A, IL-22, and TNF following manufacturer's instructions using a FACSCalibur instrument and CellQuest software (BD Biosciences) (360).

5.2.4. Tissue collection and preparation

For the DSS challenge; mice were sacrificed on day 9, whereas for the *C. rodentium* challenge; mice were sacrificed on day 10 post-infection (corresponding to peak

infection) by CO_2 asphyxiation. Another group of male mice were sacrificed at day 19 post-infection.

For DSS mice; the spleen and large intestine (mid-, and distal colon) were collected, while for *C. rodentium* infected mice large intestine only (Caecum, mid- and distal colon) were collected. Tissues were washed with PBS supplemented with 0.5% BSA and the faeces were flushed out. The following parameters were measure for DSS mice: spleen weight and length and weight of the colon weight and colon length (from the caeco-colic junction to the anus). Colon weight: length ratio was calculated and is indicative of colonic edema and/or hyperplasia and a measure of the degree of colonic inflammation. Only colon length was measured for *C. rodentium* mice. Colons and caeca were then fixed (overnight) by immersion in 4% PFA in 0.1 M phosphate buffer (pH 7.4).

Whole blood samples were collected by cardiac puncture from for *C. rodentium* infected mice, allowed to clot for about 30 minutes at room temperature, centrifuged at 3,000 rpm (1,000 x g) for 5 minutes and the sera separated and stored at -80°C until further processing for cytokine levels **(section 5.2.3.5).**

5.2.5. Histology

PFA fixed samples were processed using an automated Shandon Excelsior™ ES tissue processor (Thermo Fisher Scientific Inc., Fisher Scientific UK Ltd, Loughborough, Leicestershire) using following protocol: Formalin (30 minutes), 70% alcohol (1:30 hours), 90% alcohol (1:30 hours), 100% alcohol (1:30 hours), 100% alcohol (1:00 hour), 100% alcohol (1:30 hours), 100% alcohol (1:30 hours), histoclear (1:30 hours), histoclear (1:30 hours), histoclear (2:00 hours), wax (1:00 hour), wax (1:00 hour), wax (2:00 hours). Samples were then paraffin-embedded,

sectioned into 4-μm sections (Leica RM2126 microtome) and stained with haematoxylin and eosin (H&E). Samples were kindly processed by Richard Stillion from the Sir William Dunn School of Pathology, University of Oxford.

5.2.6. Imaging

Sections were photographed using a Zeiss AXIO Imager A1 light microscope equipped with a Zeiss AxioCamHRc digital camera.

5.2.7. Evaluation of histological sections

H&E-stained sections were scored blinded. For the DSS model, to evaluate the histological GI sections, four categories were considered and each scored 0-3. These categories are: epithelia (epithelial hyperplasia, goblet cell depletion and loss of epithelial cells), leukocyte infiltration in lamina propria, affected area and markers of severe inflammation (e.g. loss of crypt structure, submucosal inflammation, edema, and crypt abscesses) **(Table 5.2)**. These scores were added up (scores range between 0-12) and the sum results were plotted. DSS-induced inflammation is present mostly in mid- and distal colon, and therefore mid- and distal sections of the colon were analysed and the scores of the two segments were averaged to give the final colon score.

A	Epithelium	Hyperplasia	and/or	Goblet Cell Depletion	and/or	Loss of epithelial cells
	0	None		None		None
	1	Mild (1.5X)		Mild (25%)		Mild
	2	Moderate (2-3X)		Marked (25-50%)		Marked
	3	Severe (>3X)		Substantial (>50%)		Substantial

B	Inflammation in lamina propria
	0	None - few leucocytes
	1	Mild - some increase in leukocytes at tips of crypts OR many lymphoid follicles
	2	Moderate - marked infiltrate (notable broadening of crypt)
	3	Severe - dense infiltrate throughout

C	Area affected (% of section)
	0	None
	1	Up to 25%
	2	25-50%
	3	>50%

D	Markers of severe inflammation	Loss of crypt structure	and/or	Submucosal inflammation	and/or	Edema	and/or	Crypt abscesses
	0	None		None		None		None
	1	Mild		Mild		Mild		Few (<5)
	2	Marked		Marked		Marked		Many
	3	Substantial		-		-		-

Table 5.2. Summary of histological scoring for the DSS model. Each category is scored 0-3. High scores can be either due to additive scores of multiple factors (e.g.: moderate hyperplasia AND marked goblet cell depletion in category A) or due to the severe presentation (phenotype) of one factor in the category (e.g.: substantial crypt structure loss in category D).

For the *C. rodentium* model, caecum and distal colon sections were scored as follows: a total score of 0-15 was given to each section, based on 5 categories scored individually 0-3, these categories are: epithelial hyperplasia/damage and goblet cell depletion, leukocyte infiltration in lamina propria; submucosal inflammation and edema, area of tissue affected, and markers of severe inflammation such as bleeding, crypt abscesses, and necrosis/ulceration **(Table 5.3)** (361).

A	Epithelium	Hyperplasia	and/or	Goblet Cell Depletion	and/or	Damage
	0	None		None		None
	1	Mild (1.5X)		Mild (25%)		Mild
	2	Moderate (2-3X)		Marked (25-50%)		Marked
	3	Severe (>3X)		Substantial (>50%)		Substantial
B	Inflammation in lamina propria					
	0	None - few leucocytes				
	1	Mild - some increase in leukocytes at tips of crypts OR many lymphoid follicles				
	2	Moderate - marked infiltrate (notable broadening of crypt)				
	3	Severe - dense infiltrate throughout				
C	Submucosal	Oedema		Infiltration		Follicle
	0	None	and/or	None	and/or	None
	1	Mild	and/or	Mild	and/or	Enlarged
	2	Marked	OR	Marked		-
	3	Marked	AND	Marked		-
D	Area affected (% of section)					
	0	None				
	1	Up to 25%				
	2	25-50%				
	3	>50%				
E	Markers of severe inflammation	Bleeding	and/or	Crypt abscesses	and/or	Necrosis/ulceration
	0	None		None		None
	1	Some		Few		None
	2	Marked		Many		Few/small
	3	-		-		Large/many

Table 5.3. Summary of histological scoring for C. rodentium-induced colitis.

5.2.8. Statistics

For weight curves, data were analysed by two-way analysis of variance (ANOVA) with Bonferroni post-tests. For the other data, nonparametric Mann–Whitney test was performed to determine statistical significance using GraphPad Prism version 6.0c (GraphPad Software, San Diego, California, USA). Differences were considered statistically significant when $p<0.05$.

5.3. Results

The text and figures originally presented here cannot be made freely available via ORA.

To investigate the potential link between NPC and IBD, we looked for a spontaneous phenotype in late-end stage *Npc1*$^{-/-}$ mice compared to wild-type mice, we have observed differences macroscopically including enhanced vascularity in the ileo-colic junction as well as evidence of upper GI tract bleeding "haematochezia" **(Figure 5.4)**, however, microscopically, we could not detect any histological changes characteristic of Crohn's disease in symptomatic 9 week old mice, control mice for the DSS challenge (all three genotypes in the non-DSS groups) had normal baseline histopathology scores **(Figure 5.7)**.

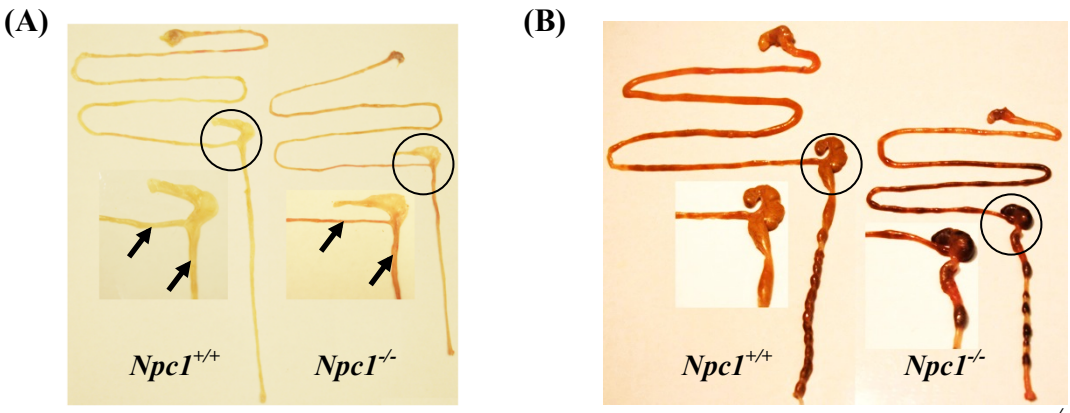

Figure 5.4. Macroscopic changes in the gastrointestinal tract of late end-stage *Npc1*$^{-/-}$ mice (over 10 weeks old) showing (A) enhanced vascularity in the ileo-colonic junction (circled areas and arrows) and (B) gastrointestinal tract bleeding (haematochezia) compared to age- and sex-matched wild-type.

The NPC1 mouse is on a BALB/c genetic background. We challenged these mice with the aim of inducing colitis experimentally either chemically (DSS model) or using an infectious model (*C. rodentium*) in order to detect any differences between the genotypes and whether NPC1 homozygous mice may present with an exacerbated response.

Upon DSS administration, female *Npc1*$^{-/-}$ mice started to show signs of weight loss by day 4 compared to wild-type and heterozygous mice **(Figure 5.5)**. However, at this stage this weight loss might have been part of the course of NPC1 disease and

not solely caused by DSS, as this weight loss was not statistically different compared to the non-DSS female *Npc1*$^{-/-}$ group. By day 5, the weight loss in the female *Npc1*$^{-/-}$ group became more significant compared to the wild-type and heterozygous mice and was sustained until the end of the experiment (day 8). Also, *Npc1*$^{-/-}$ males started to show severe weight loss in response to DSS, independent of their NPC1-associated weight loss (statistically significant difference between DSS and non-DSS male *Npc1*$^{-/-}$ mice at this point that became more profound towards the end of the course of the DSS challenge). By day 6, *Npc1*$^{-/-}$ females started to lose additional weight in response to DSS, a day later than the males. By day 7 following the challenge, male wild-type mice started to develop signs of inflammation with significant weight loss in comparison to controls (non-DSS) as well as to female wild-types on DSS which did not lose weight throughout the course (compared to their non-DSS controls). Also, male *Npc1*$^{-/-}$ on DSS lost significant weight starting from day 6 compared to *Npc1*$^{+/-}$ but not *Npc1*$^{+/+}$, consistent with the resistance to weight loss phenotype seen in NPC1 heterozygous mice (362). *Npc1* heterozygous males started to slowly lose weight from day 5 post-DSS; however, this was a much slower and less profound weight loss compared to wild-types. Although male heterozygotes weight loss in response to DSS was significant by day 8, male wild-type mice had a much more severe phenotype in this model as their weight loss by day 8 was significantly higher compared to their heterozygous controls on DSS. This suggests that *Npc1* heterozygosity confers partial protection to DSS-induced colitis and associated weight loss. *p*-values for the multiple comparisons are summarised in **Table 5.5**.

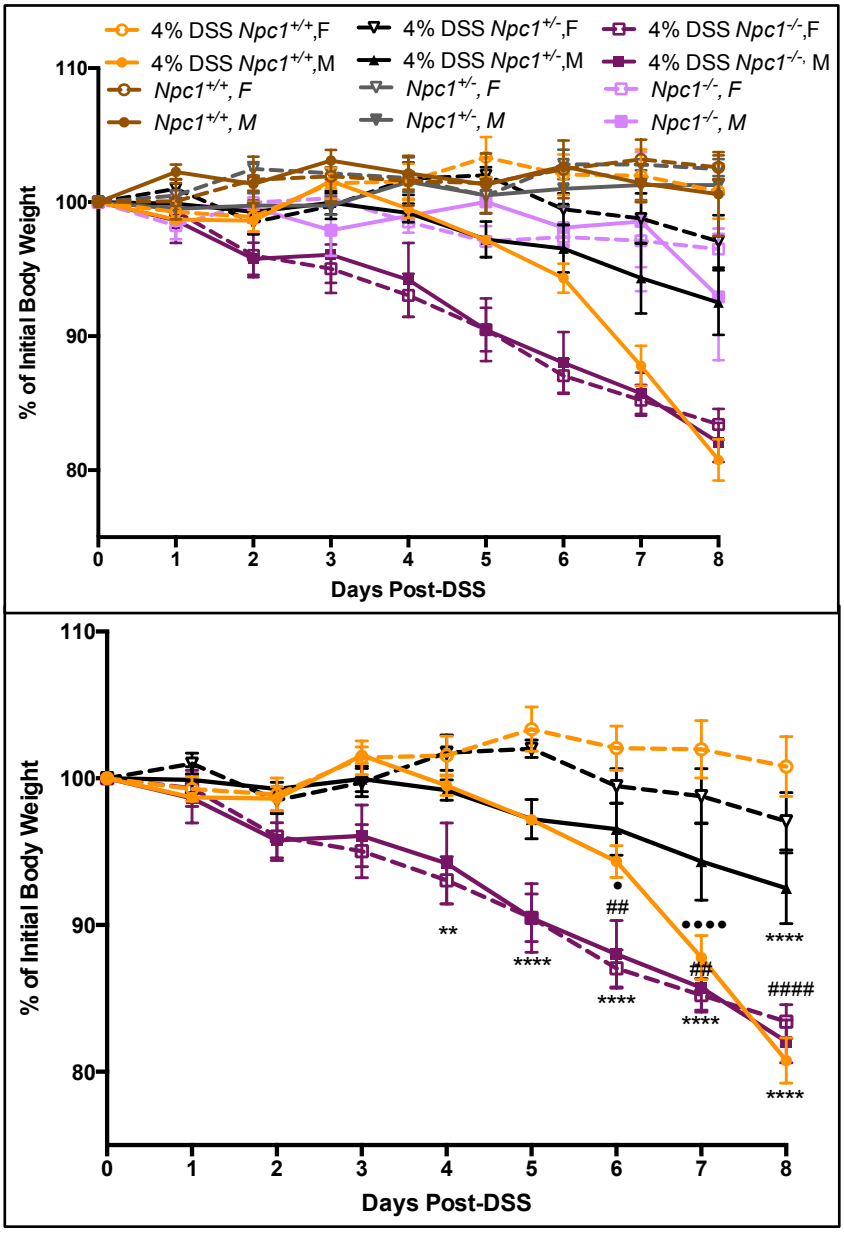
4% DSS Npc1+/+,F
4% DSS Npc1+/+,M
Npc1+/+, F
Npc1+/+, M
4% DSS Npc1+/-,F
4% DSS Npc1+/-,M
Npc1+/-, F
Npc1+/-, M
4% DSS Npc1-/-,F
4% DSS Npc1-/-, M
Npc1-/-, F
Npc1-/-, M
% of Initial Body Weight
Days Post-DSS
110
100
90
80
0
1
2
3
4
5
6
7
8
**
****
##
••••
####

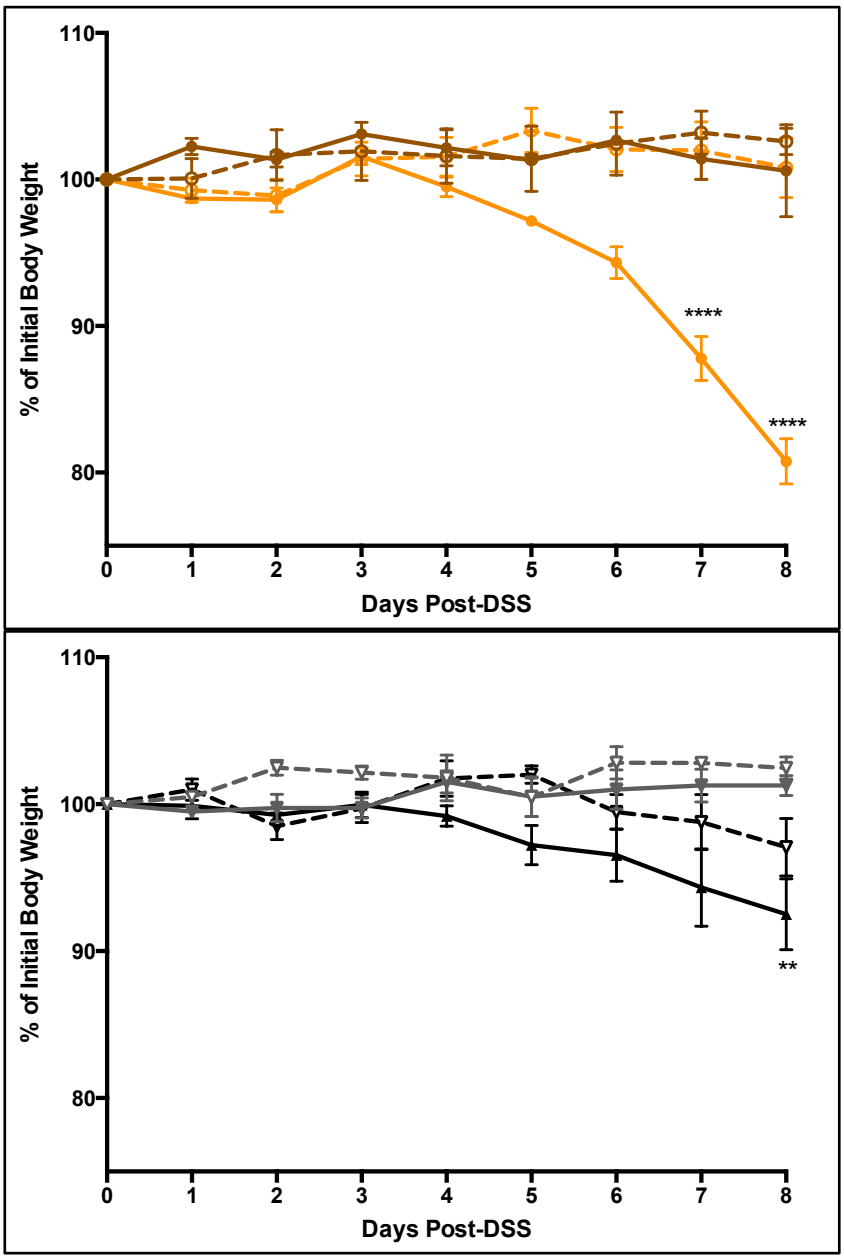
110
100
90
80
% of Initial Body Weight
****
****
0
1
2
3
4
5
6
7
8
Days Post-DSS
110
100
90
80
% of Initial Body Weight
**
0
1
2
3
4
5
6
7
8
Days Post-DSS

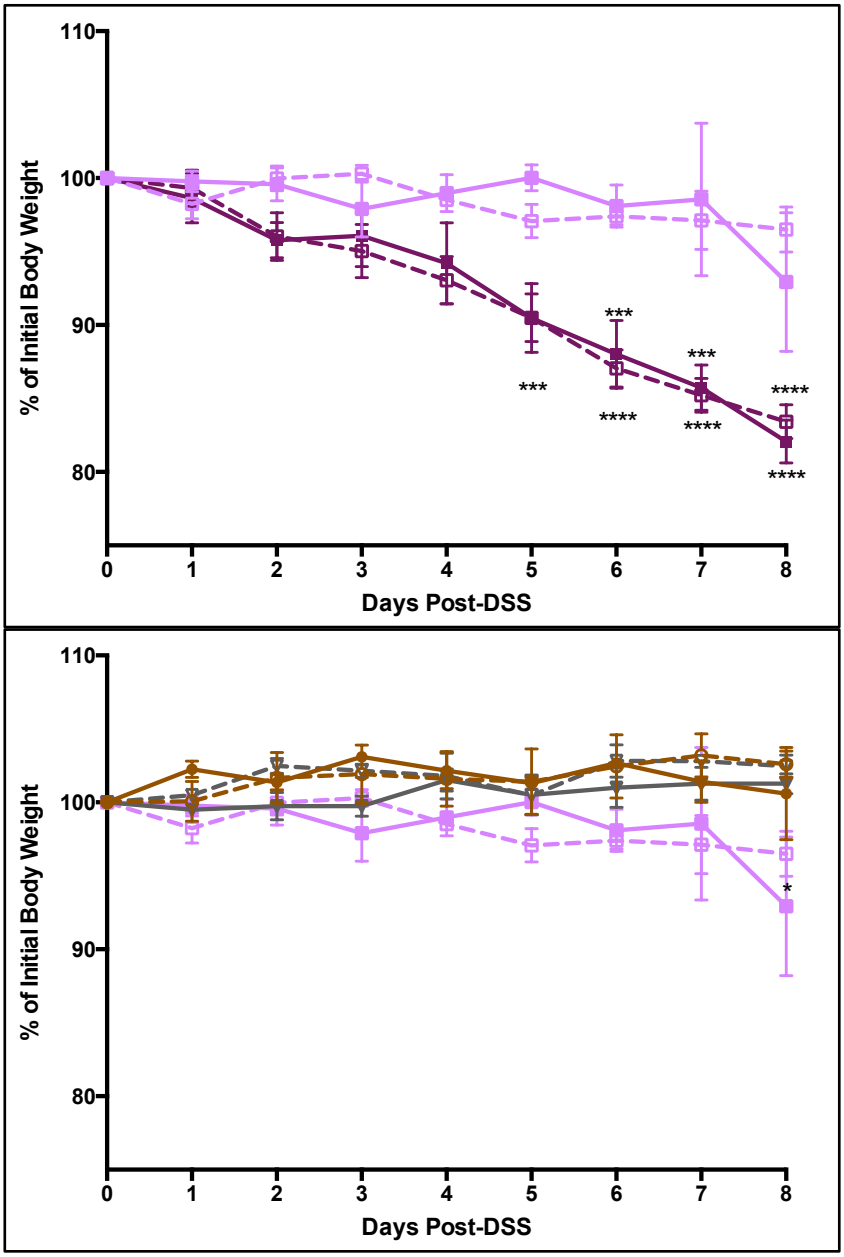

Figure 5.5. Changes in body weight during acute DSS-colitis in wild-type (*Npc1*$^{+/+}$), heterozygous (*Npc1*$^{+/-}$) and homozygous (*Npc1*$^{-/-}$) mice. Body weights presented as percentage of initial body weight, n=4 males and 4 females per group receiving 4% DSS in the drinking water (7 days on DSS followed by 2 days on sterile drinking water) and controls receiving sterile water for 9 days. Data are presented as means ± SEM (n=4). *p<0.05, **p<0.01, ***p<0.001 and **** p<0.0001, calculated using the two-way ANOVA with Bonferroni post-tests. * denotes comparison within same genotype and sex group for treated vs. untreated mice or within same sex and treatment group for one genotype vs. the other two genotypes, # denotes comparison within same sex and treatment group for *Npc1*$^{+/+}$ vs. *Npc1*$^{+/-}$ mice, • denotes comparison within same genotype and treatment group for female vs. male mice.

Comparison	Day 4		Day 5		Day 6		Day 7		Day 8	
	significance	*p*-value	significance	*p*-value	significance	*p*-value	significance	*p*-value	significance	*p*-value
4% DSS *Npc1*$^{+/+}$,F vs. 4% DSS *Npc1*$^{+/+}$,M	ns	> 0.9999	ns	0.2179	*	0.0171	****	< 0.0001	****	< 0.0001
4% DSS *Npc1*$^{+/+}$,F vs. 4% DSS *Npc1*$^{+/-}$,F	ns	> 0.9999	ns	> 0.9999	ns	> 0.9999	ns	> 0.9999	ns	> 0.9999
4% DSS *Npc1*$^{+/+}$,F vs. 4% DSS *Npc1*$^{-/-}$,F	**	0.004	****	< 0.0001	****	< 0.0001	****	< 0.0001	****	< 0.0001
4% DSS *Npc1*$^{+/+}$,F vs. *Npc1*$^{+/+}$, F	ns	> 0.9999	ns	> 0.9999	ns	> 0.9999	ns	> 0.9999	ns	> 0.9999
4% DSS *Npc1*$^{+/+}$,M vs. 4% DSS *Npc1*$^{+/-}$,M	ns	> 0.9999	ns	> 0.9999	ns	> 0.9999	ns	0.1251	****	< 0.0001
4% DSS *Npc1*$^{+/+}$,M vs. 4% DSS *Npc1*$^{-/-}$, M	ns	0.7752	ns	0.0986	ns	0.1757	ns	> 0.9999	ns	> 0.9999
4% DSS *Npc1*$^{+/+}$,M vs. *Npc1*$^{+/+}$, M	ns	> 0.9999	ns	> 0.9999	ns	0.0811	****	< 0.0001	****	< 0.0001
4% DSS *Npc1*$^{+/-}$,F vs. 4% DSS *Npc1*$^{-/-}$,F	**	0.0027	****	< 0.0001	****	< 0.0001	****	< 0.0001	****	< 0.0001
4% DSS *Npc1*$^{+/-}$,F vs. *Npc1*$^{+/-}$, F	ns	> 0.9999	ns	> 0.9999	ns	> 0.9999	ns	> 0.9999	ns	> 0.9999
4% DSS *Npc1*$^{+/-}$,M vs. 4% DSS *Npc1*$^{-/-}$, M	ns	> 0.9999	ns	0.0906	**	0.0037	**	0.0033	****	< 0.0001
4% DSS *Npc1*$^{+/-}$,M vs. *Npc1*$^{+/-}$, M	ns	> 0.9999	ns	> 0.9999	ns	> 0.9999	ns	0.1503	**	0.0083
4% DSS *Npc1*$^{-/-}$,F vs. 4% DSS *Npc1*$^{-/-}$, M	ns	> 0.9999	ns	> 0.9999	ns	> 0.9999	ns	> 0.9999	ns	> 0.9999
4% DSS *Npc1*$^{-/-}$,F vs. *Npc1*$^{-/-}$, F	ns	0.6078	ns	0.1178	****	< 0.0001	****	< 0.0001	****	< 0.0001
4% DSS *Npc1*$^{-/-}$, M vs. *Npc1*$^{-/-}$, M	ns	> 0.9999	***	0.0005	***	0.0001	****	< 0.0001	****	< 0.0001
Npc1$^{+/+}$, F vs. *Npc1*$^{+/+}$, M	ns	> 0.9999	ns	> 0.9999	ns	> 0.9999	ns	> 0.9999	ns	> 0.9999
Npc1$^{+/+}$, F vs. *Npc1*$^{+/-}$, F	ns	> 0.9999	ns	> 0.9999	ns	> 0.9999	ns	> 0.9999	ns	> 0.9999
Npc1$^{+/+}$, F vs. *Npc1*$^{-/-}$, F	ns	> 0.9999	ns	> 0.9999	ns	> 0.9999	ns	0.2591	ns	0.2498
Npc1$^{+/+}$, M vs. *Npc1*$^{+/-}$, M	ns	> 0.9999	ns	> 0.9999	ns	> 0.9999	ns	> 0.9999	ns	> 0.9999
Npc1$^{+/+}$, M vs. *Npc1*$^{-/-}$, M	ns	> 0.9999	ns	> 0.9999	ns	> 0.9999	ns	> 0.9999	ns	0.1926
Npc1$^{+/-}$, F vs. *Npc1*$^{+/-}$, M	ns	> 0.9999	ns	> 0.9999	ns	> 0.9999	ns	> 0.9999	ns	> 0.9999
Npc1$^{+/-}$, F vs. *Npc1*$^{-/-}$, F	ns	> 0.9999	ns	> 0.9999	ns	> 0.9999	ns	0.8128	ns	0.5646
Npc1$^{+/-}$, M vs. *Npc1*$^{-/-}$, M	ns	> 0.9999	ns	> 0.9999	ns	> 0.9999	ns	> 0.9999	*	0.0169
Npc1$^{-/-}$, F vs. *Npc1*$^{-/-}$, M	ns	> 0.9999	ns	> 0.9999	ns	> 0.9999	ns	> 0.9999	ns	> 0.9999

Table 5.5. Summary of *p*-values for the multiple comparisons of changes in body weight during acute DSS-colitis in wild-type (*Npc1*$^{+/+}$), heterozygous (*Npc1*$^{+/-}$) and homozygous (*Npc1*$^{-/-}$) mice.

In agreement with the weight loss profile, daily monitoring revealed a severe phenotype in male wild-type mice compare to female wild-type mice, and a slightly higher IBD score in this group compared to the other two genotypes, although all three groups started to show signs of IBD from day 5. Both groups of homozygous mice (males and females) behaved similarly with this regard **(Figure 5.6)**.

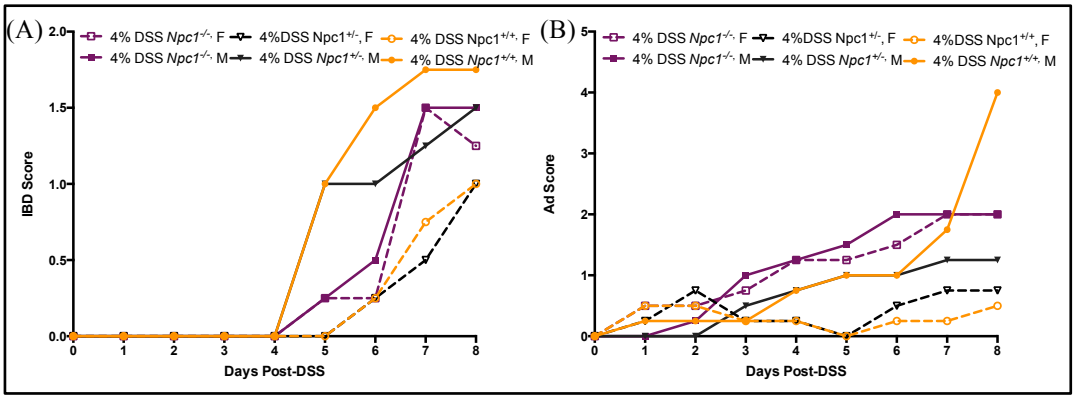

Figure 5.6. Disease severity during acute DSS-colitis in wild-type (*Npc1*$^{+/+}$), heterozygous (*Npc1*$^{+/-}$) and homozygous (*Npc1*$^{-/-}$) mice. (A) IBD scores and (B) adverse effects "Ad" scores, n=4 males and 4 females per group receiving 4% DSS in the drinking water (7 days on DSS followed by 2 days on sterile drinking water) and controls receiving sterile water for 9 days. Individual mice were monitored and scored daily for IBD and adverse effects as described in **section 5.2.3.1 (Table 5.1)**. Data are presented as means (n=4).

Following the same pattern, histopathology scores of distal colon sections (which is the most affected part of the GI tract in response to DSS (363)) from all challenged animals and their controls showed a trend of a potential phenotype penetrance in females in *Npc1* homozygotes and heterozygotes (similar to the trend recently observed NPC1 patients (Holm Uhlig, unpublished and personal communication), the opposite of the male bias of severe effect of DSS in male wild-type mice compared to females **(Figure 5.7 A and C)**. Significantly higher scores of intestinal pathology were seen in male wild-types, female heterozygotes and female homozygotes compared to their non-DSS age and sex-matched controls (p=0.029). Yet, amongst challenged groups, female wild-types had a significantly more severe

intestinal phenotype compared to both heterozygotes and homozygotes (p=0.029). Whereas in male homozygotes, although had signs of inflammation in the distal colon, the total score did not reach statistical significance compared to their baseline controls (p=0.057) but it was significantly lower than their matched wild-type DSS mice (p=0.029).

As for differences between genotypes, no clear signs of intestinal inflammation were detected in any of the control (non-DSS) groups, apart from minor histological changes that are normally seen at baseline in healthy mice (George Song-Zhao, Personal communication). Looking at mid-colon histopathology following DSS challenge, no clear differences were seen between genotypes (p>0.999, p=0.257 and 0.4571 for male *Npc1*$^{+/+}$ vs. *Npc1*$^{+/-}$, *Npc1*$^{+/+}$ vs. *Npc1*$^{-/-}$ and *Npc1*$^{+/-}$ vs. *Npc1*$^{-/-}$, respectively and >0.999, 0.400 and 0.200 for female *Npc1*$^{+/+}$ vs. *Npc1*$^{+/-}$, *Npc1*$^{+/+}$ vs. *Npc1*$^{-/-}$ and *Npc1*$^{+/-}$ vs. *Npc1*$^{-/-}$, respectively) **(Figure 5.7 A and B)**, however, in all genotypes, DSS-challenged animals had significantly higher scores compared to their sex-matched controls (except female heterozygous mice) (p=0.029) . We have looked at average mid- and distal colon scores to have a better overall assessment of more generalised phenotypes across the GI tract **(Figure 5.7 A and D)**. In all genotypes, DSS-challenged animals had a significantly worse phenotype compared to their sex-matched controls (p=0.029). While comparing across genotypes, DSS-wild-type animals had a significantly higher histopathology scores compared to their sex-matched DSS-homozygous *Npc1*$^{-/-}$ mice (p=0.029). When taken together, these data are consistent with partial protection from DSS-colitis conferred in the absence of a functional NPC1 protein (in *Npc1*$^{-/-}$ as well as *Npc1*$^{+/-}$ mice).

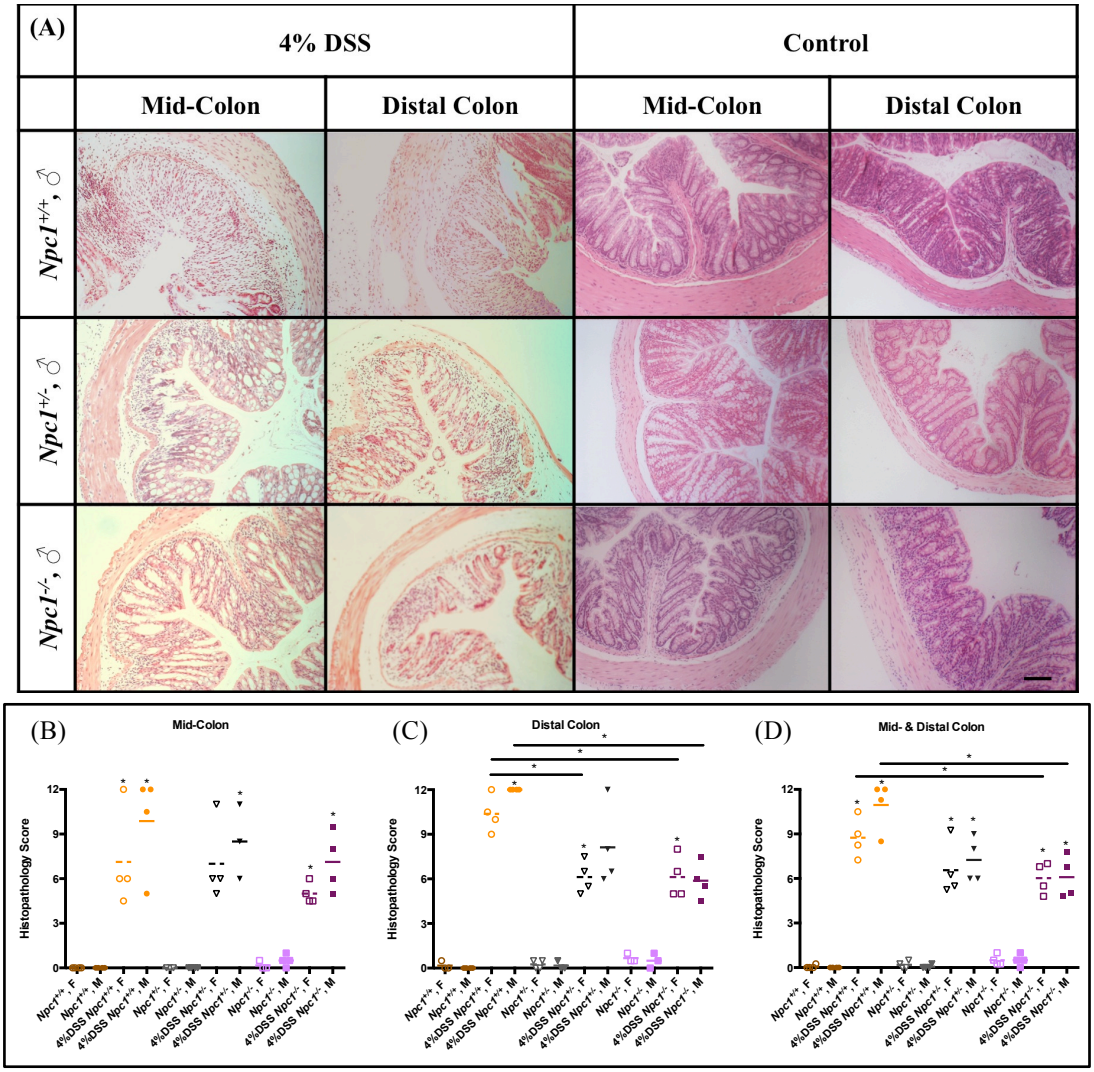

Figure 5.7. Histological assessment of disease severity during acute DSS-colitis in wild-type (*Npc1*$^{+/+}$), heterozygous (*Npc1*$^{+/-}$) and homozygous (*Npc1*$^{-/-}$) mice. (A) Representative H&E histological sections (original magnification x20), (B) histopathological scores of colitis in (B) mid-, (C) distal, and (D) average of mid- & distal colon, and collected on day 9, n=4 males and 4 females per group receiving 4% DSS in the drinking water (7 days on DSS followed by 2 days on sterile drinking water) and controls receiving sterile water for 9 days. Each symbol represents an individual animal and horizontal lines represent the mean of the group (n=4). *p<0.05, calculated using Mann–Whitney test. Scale bar represents 200 µm.

Other parameters of intestinal inflammation were measured at autopsy to assess the degree of DSS-induced damage/pathology. We observed significant shortening of the colon in response to DSS in wild-type and heterozygous animals, both males and females compared to their sex-matched non-DSS controls (p=0.029) **(Figure 5.8 A)**. Moreover, colon length was significantly lower in the DSS-male wild-types compare to the DSS-females (p=0.029), consistent with previous reports of male

bias in the susceptibility to DSS colitis (364). Only male homozygous DSS mice had a profound shortening of the colon upon DSS administration but not females (p=0.029 for male and p=0.143 for female mice, respectively). Colon weight as a measure of fluid retention and inflammation was only significantly increased in male heterozygous mice compared to their sex-matched controls (p=0.029) and to DSS challenged wild-type and homozygous male mice (p=0.029) **(Figure 5.8 B)**. As this difference could be to a large extent attributed to the weight of the heterozygous animals in general, we have also looked at a more accurate measure of intestinal inflammation, colon weight: length ratio, a measure of colonic edema and/or hyperplasia that correlates with the degree of colonic inflammation (365). The calculated ratios were also in agreement with the results so far in this model, with marked increase in colon weight: length ratio in all the male groups upon DSS administration (p=0.029), moreover, this increase was the least profound in the homozygous group (still significantly lower than the heterozygous males, p=0.029). Female heterozygous mice had a significant increase in the ratio upon DSS administration (p=0.029) **(Figure 5.8 C)**.

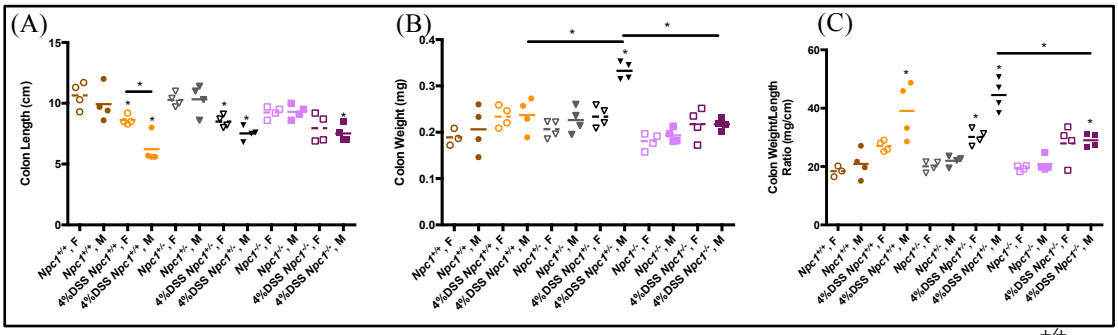

Figure 5.8. Disease severity during acute DSS-colitis in wild-type (*Npc1*$^{+/+}$), heterozygous (*Npc1*$^{+/-}$) and homozygous (*Npc1*$^{-/-}$) mice assessed by change in colon weight, length and weight/length ratio measured at autopsy. (A) Colon length (B) weight and (C) weight/length ratio measured on day 9, n=4 males and 4 females per group receiving 4% DSS in the drinking water (7 days on DSS followed by 2 days on sterile drinking water) and controls receiving sterile water for 9 days. Each symbol represents an individual animal and horizontal lines represent the mean of the group (n=4). **p*<0.05, calculated using Mann–Whitney test.

We have also assessed the level of systemic involvement in response to intestinal inflammation, where we measure spleen mass in all animals at autopsy. Progressive splenomegaly is a known feature of NPC1 disease in the mouse (366), no differences were observed except for a slight increase in spleen mass recorded in male heterozygous animals upon DSS administration (*p*=0.029) **(Figure 5.9)**.

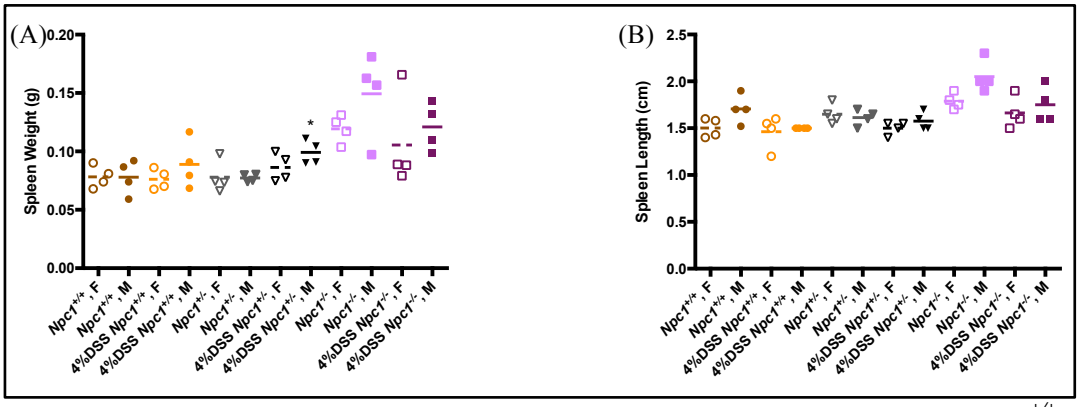

Figure 5.9. Disease severity during acute DSS-colitis in wild-type (*Npc1*$^{+/+}$), heterozygous (*Npc1*$^{+/-}$) and homozygous (*Npc1*$^{-/-}$) mice assessed by change in spleen weight and length measured at autopsy. (A) Spleen weight and (B) length measured on day 9, n=4 males and 4 females per group receiving 4% DSS in the drinking water (7 days on DSS followed by 2 days on sterile drinking water) and controls receiving sterile water for 9 days. Each symbol represents an individual animal and horizontal lines represent the mean of the group (n=4). **p*<0.05, calculated using Mann–Whitney test.

In a pilot infectious challenge study, following oral infection with *Citrobacter rodentium*, all three groups maintained body weight throughout the course of the

study apart from homozygous mice reaching disease endpoint, where significant progressive weight loss was observed irrespective of the bacterial infection or intestinal inflammation.

All groups developed similar phenotypes with minimum signs of intestinal inflammation as assessed at peak infection (day 10). Therefore, this second model of intestinal inflammation also failed to depict any detectable phenotype in *Npc1*$^{-/-}$ mice possibly due to the background of this mouse strain (BALB/c) being generally more resistant. BALB/c mice have a predominant Th2 response whereas C57BL/6 have the Th1 predominant response (367).

We also looked at bacterial load throughout the course of infection in order to assess any differences in bacterial handling affecting colonisation levels and bacterial clearance. *In vitro* data from cells treated with U18666A to mimic NPC cells have shown a defective bacterial handling (Holm Uhlig, unpublished, personal communication).

All groups followed the same pattern with peak infection at day 6 to 9 and have almost completely cleared the infection by day 19. Of interest, a group of homozygous mice followed completely different infection kinetics; they did not get infected until very late (peaked at day 19) and took much longer to clear bacteria from the GI tract (up to day 33). This was the only group that was infected pre-symptomatically.

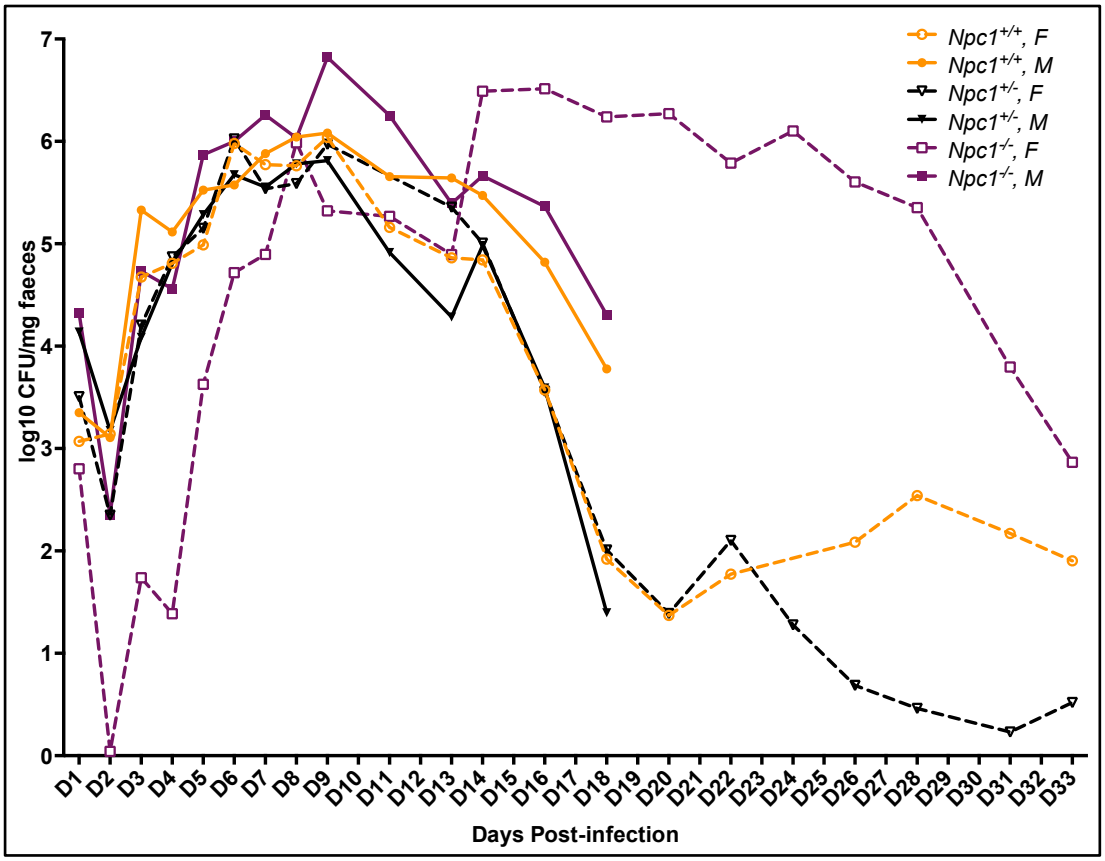

Figure 5.10. Host susceptibility to *C. rodentium* infection in wild-type (*Npc1*$^{+/+}$), heterozygous (*Npc1*$^{+/-}$) and homozygous (*Npc1*$^{-/-}$) mice. Mice (n=4 males and 4 females per group) were orally infected with *C. rodentium* at a dose of ~4x10^{9} cfu/mouse. *C. rodentium*-infected mice were killed at days 10 and 19.*C. rodentium* load in faeces measured from days 1 to 33 (D1-D33). Data are presented as means (n=4 up to D10 and n=2 from D11).

Bacterial burden in the infected sites (caecum and colon) did not show any marked difference between the groups either at day 10 (for caecum: p=0.829, 0.657 and >0.999 for *Npc1*$^{+/+}$ vs. *Npc1*$^{+/-}$, *Npc1*$^{+/+}$ vs. *Npc1*$^{-/-}$ and *Npc1*$^{+/-}$ vs. *Npc1*$^{-/-}$, respectively, for mid-colon: p=0.829, 0.114 and 0.343 for *Npc1*$^{+/+}$ vs. *Npc1*$^{+/-}$, *Npc1*$^{+/+}$ vs. *Npc1*$^{-/-}$ and *Npc1*$^{+/-}$ vs. *Npc1*$^{-/-}$, respectively and for distal colon: p=0.657, 0.209 and 0.057 for *Npc1*$^{+/+}$ vs. *Npc1*$^{+/-}$, *Npc1*$^{+/+}$ vs. *Npc1*$^{-/-}$ and *Npc1*$^{+/-}$ vs. *Npc1*$^{-/-}$, respectively) or day 19 **(Figure 5.11 A-C).**

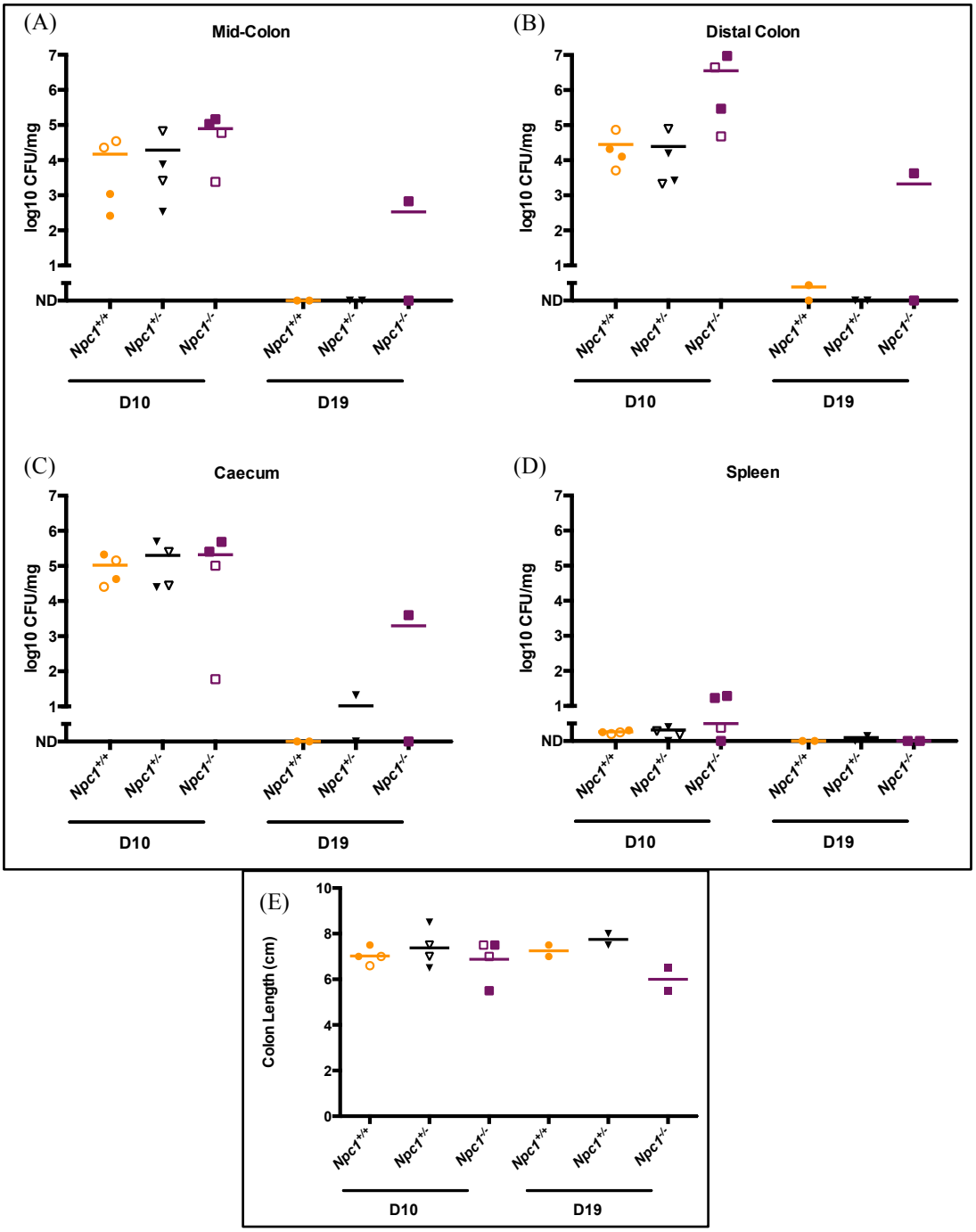

Figure 5.11. Host susceptibility to *C. rodentium* infection in wild-type (*Npc1*$^{+/+}$), heterozygous (*Npc1*$^{+/-}$) and homozygous (*Npc1*$^{-/-}$) mice. Mice were orally infected with *C. rodentium* at a dose of ~4x10^{9} cfu/mouse. *C. rodentium*-infected mice were killed at days 10 and 19. (A) *C. rodentium* load in mid- and (B) distal colon (C) caecum and (D) spleen, measured on day 10 and 19. (E) Colon length at day 10 and 19. Each symbol represents an individual animal and horizontal lines represent the mean of the group (D10; n=4, 2 males; filled symbols and 2 females; open symbols and D19; n=2 males; filled symbols). Mann–Whitney test was performed.

To assess the integrity of the intestinal barrier upon infection in all groups, we measured bacterial burden in the spleen to determine systemic involvement caused by bacterial translocation. At day 10 post-infection, we observed no translocation in the wild-type and heterozygous mice while two of the four infected *Npc1*$^{-/-}$ had detectable levels (9.5 vs. 0.4 and 0.7 CFU/mg for *Npc1*$^{-/-}$ vs. *Npc1*$^{+/+}$ and *Npc1*$^{+/-}$, respectively) **(Figure 5.11 D)**. Systemic involvement was observed in the symptomatic male homozygous mice as opposed to the two presymptomatic female homozygous mice and that corresponded with the highest infectious burden in the mid-colon and caecum. By day 19, all mice had no detectable bacteria in the spleen **(Figure 5.11 D)**. No differences were observed in colon length between genotypes **(Figure 5.11 E)**.

Histopathological assessment of sections from infected mice collected at day 10 (peak infection) did not shown significant difference between the three genotypes (p=0.829, p>0.999 and p=0.914 for *Npc1*$^{+/+}$ vs. *Npc1*$^{+/-}$, *Npc1*$^{+/+}$ vs. *Npc1*$^{-/-}$ and *Npc1*$^{+/-}$ vs. *Npc1*$^{-/-}$, respectively) **(Figure 5.12)**.

IL-22 is important for early protection against *C. rodentium*, it is produced by innate lymphoid tissue inducer cells and induces the production of antimicrobial peptides (368, 369). We have therefore measured the levels of secreted IL-22 in the colon, caecum and serum of infected animals at both time points and although there were no significant differences between the different genotypes (for caecum: p=0.486, 0.486 and 0.343 for *Npc1*$^{+/+}$ vs. *Npc1*$^{+/-}$, *Npc1*$^{+/+}$ vs. *Npc1*$^{-/-}$ and *Npc1*$^{+/-}$ vs. *Npc1*$^{-/-}$, respectively, for mid-colon: p=0.086, 0.086 and p>0.999 for *Npc1*$^{+/+}$ vs. *Npc1*$^{+/-}$, *Npc1*$^{+/+}$ vs. *Npc1*$^{-/-}$ and *Npc1*$^{+/-}$ vs. *Npc1*$^{-/-}$, respectively, for distal colon: p=0.343, 0.829 and 0.057 for *Npc1*$^{+/+}$ vs. *Npc1*$^{+/-}$, *Npc1*$^{+/+}$ vs. *Npc1*$^{-/-}$ and *Npc1*$^{+/-}$ vs. *Npc1*$^{-/-}$,

respectively and for serum: p=0.971, 0.914 and 0.914 for *Npc1*$^{+/+}$ vs. *Npc1*$^{+/-}$, *Npc1*$^{+/+}$ vs. *Npc1*$^{-/-}$ and *Npc1*$^{+/-}$ vs. *Npc1*$^{-/-}$, respectively), the caeca from the two female homozygous animals had elevated IL-22 levels compared to the females from the other two groups **(Figure 5.13)**.

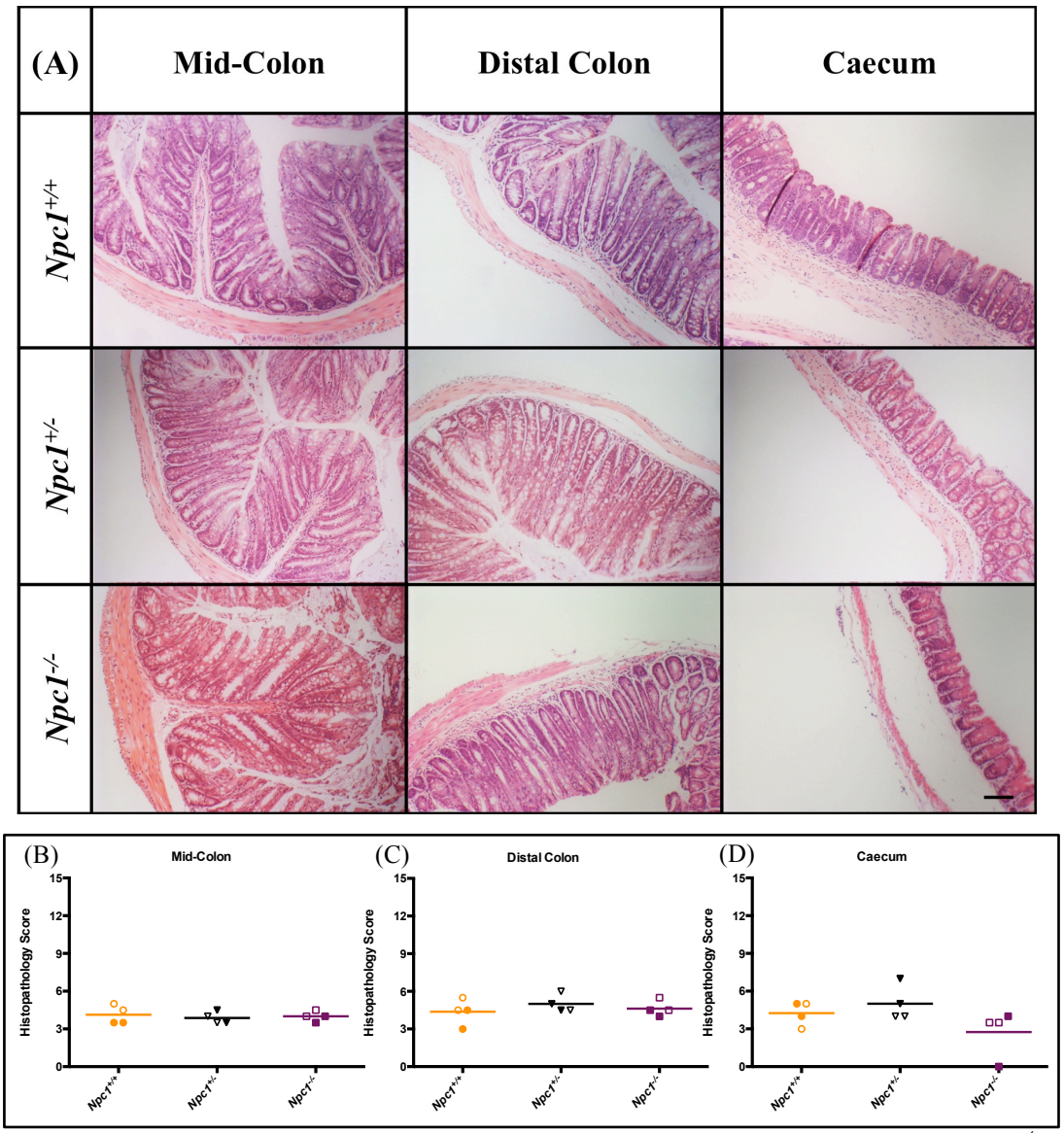

Figure 5.12. Host susceptibility to *C. rodentium* infection in wild-type (*Npc1*$^{+/+}$), heterozygous (*Npc1*$^{+/-}$) and homozygous (*Npc1*$^{-/-}$) mice. Mice were orally infected with *C. rodentium* at a dose of ~4x10^{9} cfu/mouse. *C. rodentium*-infected mice were killed at days 10 and 19. (A) Representative H&E photomicrographs of distal colon and caecum from *C. rodentium*-infected animals at day 10 (original magnification x50, Scale bar represents 200 µm). (B) Histological inflammation scores in the mid-colon, (C) distal colon and (D) cecum at days 10, assessed as described in the Methods **(Section 5.2.7).** Each symbol represents an individual animal and horizontal lines represent the mean of the group (n=4, 2 males; filled symbols and 2 females; open symbols). Mann–Whitney test was performed.

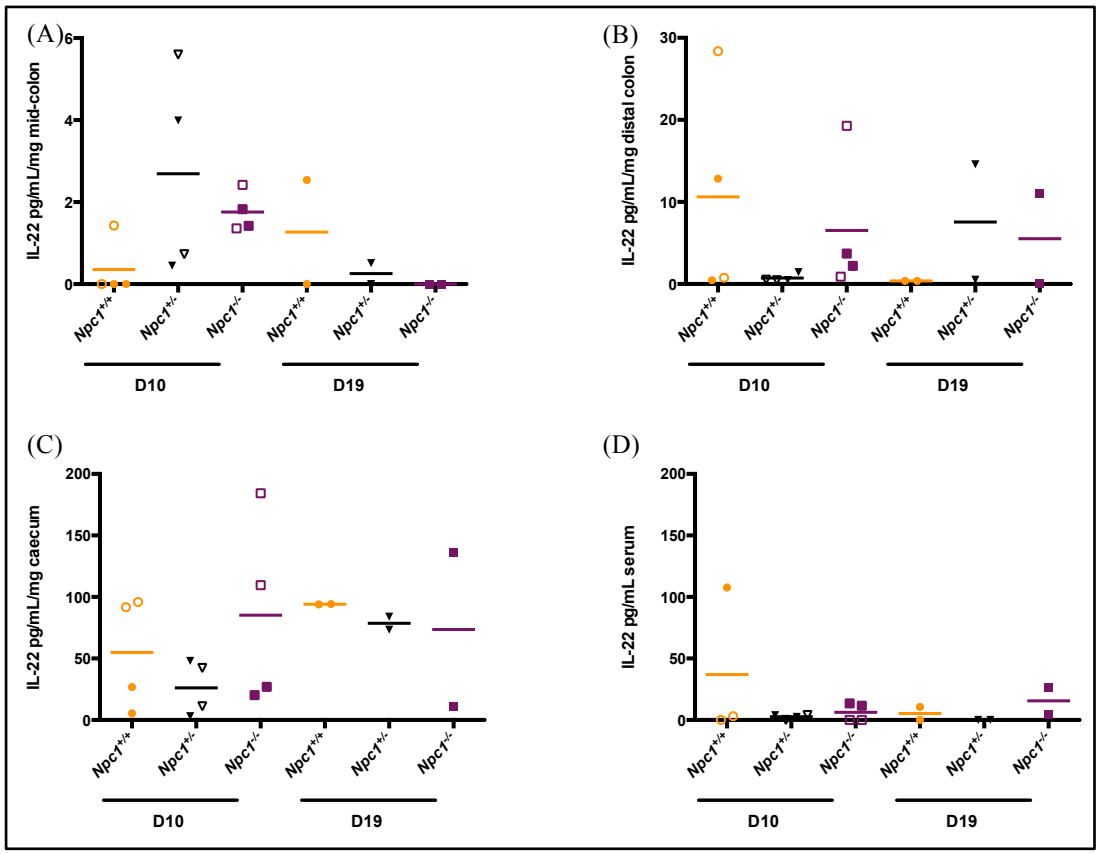

Figure 5.13. Effect of *C. rodentium* infection on inflammatory cytokines in wild-type (*Npc1*$^{+/+}$), heterozygous (*Npc1*$^{+/-}$) and homozygous (*Npc1*$^{-/-}$) mice. Mice were orally infected with *C. rodentium* at a dose of ~4x10^{9} cfu/mouse. *C. rodentium*-infected mice were killed at days 10 and 19. Mid-, distal colon and caeca were isolated and explants were cultured overnight before harvesting supernatants and analysed for IL-22 in: (A) mid-colon, (B) distal colon, (C) caecum and (D) serum. Each symbol represents an individual animal and horizontal lines represent the mean of the group (D10; n=4, 2 males; filled symbols and 2 females; open symbols and D19; n=2 males; filled symbols). Mann–Whitney test was performed.

Similarly, both IL-17 and IFN-γ are involved in mediating early protective response in *C. rodentium* infection (370, 371). IL-17 levels measured in organ explant cultures revealed a similar pattern in the caecum with the female homozygous mice having a trend towards an enhanced response **(Figure 5.14).**

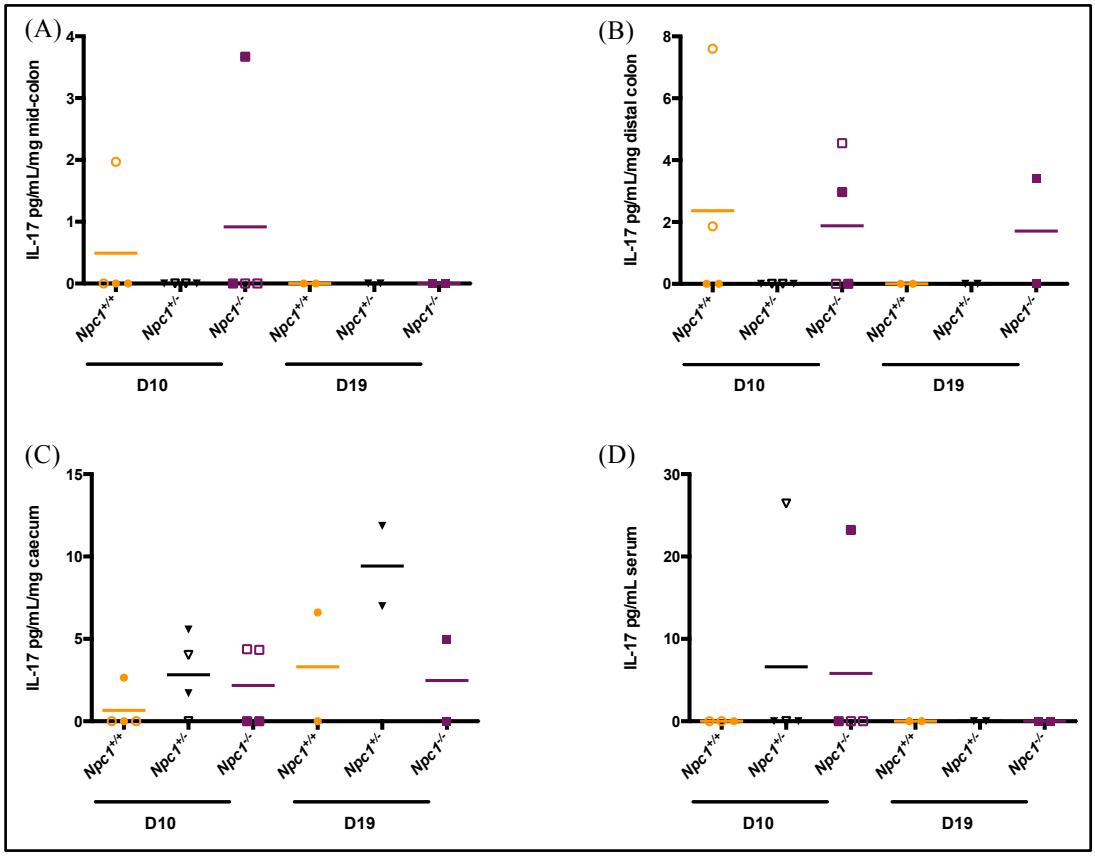

Figure 5.14. Effect of *C. rodentium* infection on inflammatory cytokines in wild-type (*Npc1*$^{+/+}$), heterozygous (*Npc1*$^{+/-}$) and homozygous (*Npc1*$^{-/-}$) mice. Mice were orally infected with *C. rodentium* at a dose of ~4x10^{9} cfu/mouse. *C. rodentium*-infected mice were killed at days 10 and 19. Mid-, distal colon and caeca were isolated and explants were cultured overnight before harvesting supernatants and analysed for IL-17 in: (A) mid-colon, (B) distal colon, (C) caecum and (D) serum. Each symbol represents an individual animal and horizontal lines represent the mean of the group (D10; n=4, 2 males; filled symbols and 2 females; open symbols and D19; n=2 males; filled symbols). Mann–Whitney test was performed.

However, IFN-γ levels at D10 (peak infection) were significantly higher of *Npc1*$^{-/-}$ compared to *Npc1*$^{+/+}$ in the caecum (p=0.029) and also in comparison to heterozygous animals when measured in the mid-colon (p=0.029). Similarly, female homozygotes had the highest response in caecal explants **(Figure 5.15).**

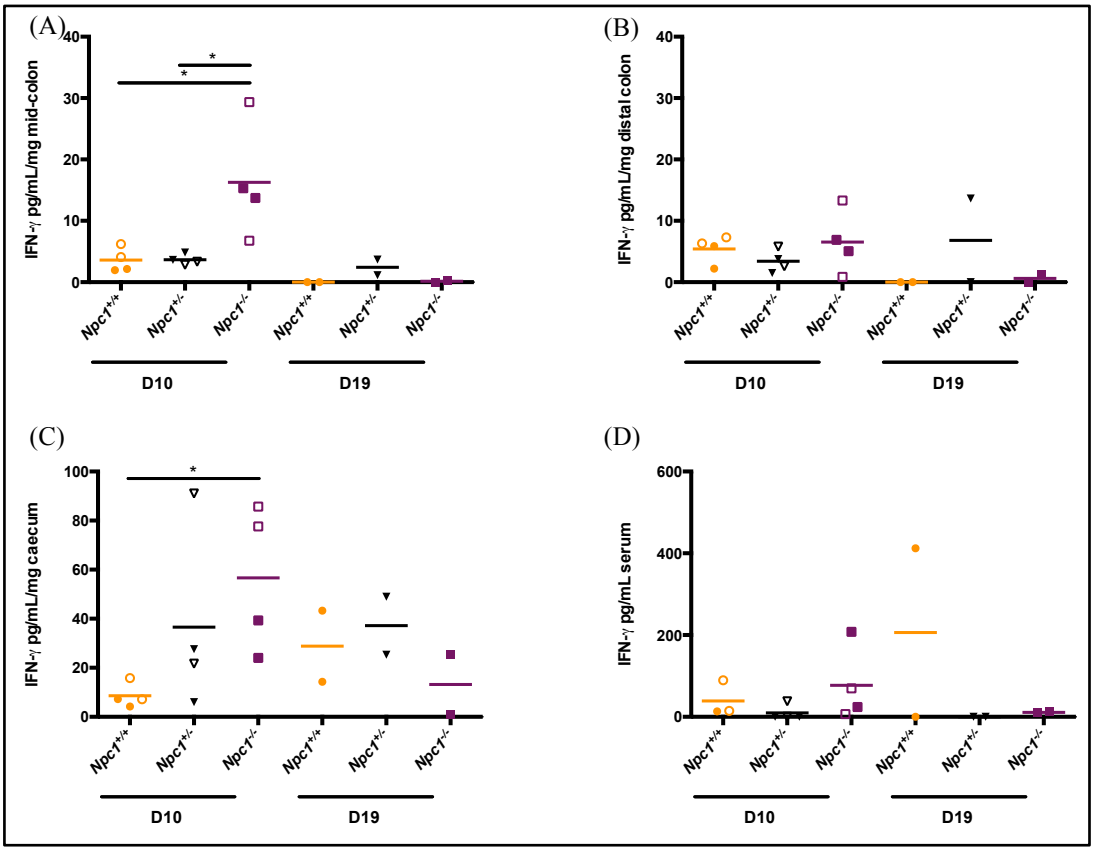

Figure 5.15. Effect of *C. rodentium* infection on inflammatory cytokines in wild-type (*Npc1*$^{+/+}$), heterozygous (*Npc1*$^{+/-}$) and homozygous (*Npc1*$^{-/-}$) mice. Mice were orally infected with *C. rodentium* at a dose of ~4x10^{9} cfu/mouse. *C. rodentium*-infected mice were killed at days 10 and 19. Mid-, distal colon and caeca were isolated and explants were cultured overnight before harvesting supernatants and analysed for IFN-γ in: (A) mid-colon, (B) distal colon, (C) caecum and (D) serum. Each symbol represents an individual animal and horizontal lines represent the mean of the group (D10; n=4, 2 males; filled symbols and 2 females; open symbols and D19; n=2 males; filled symbols). *p<0.05, calculated using Mann–Whitney test.

Unlike IL-22, IL-17 and IFN-γ; TNF is upregulated early in the course of *C. rodentium* infection as part of the Th1/Th17 elicited response (372) and reported to be associated with the enhanced pathology, where blockage using anti-TNF therapy was beneficial (373). *Npc1*$^{-/-}$ mice had significantly elevated levels of TNF in mid-colon explant cultures at D10 compared to *Npc1*$^{+/-}$ (p=0.029), similar pattern was seen in the distal colon and caecum, however, this did not reach statistical significance (p=0.057 and 0.343 for distal colon and caecum, respectively) **(Figure 5.16)**.

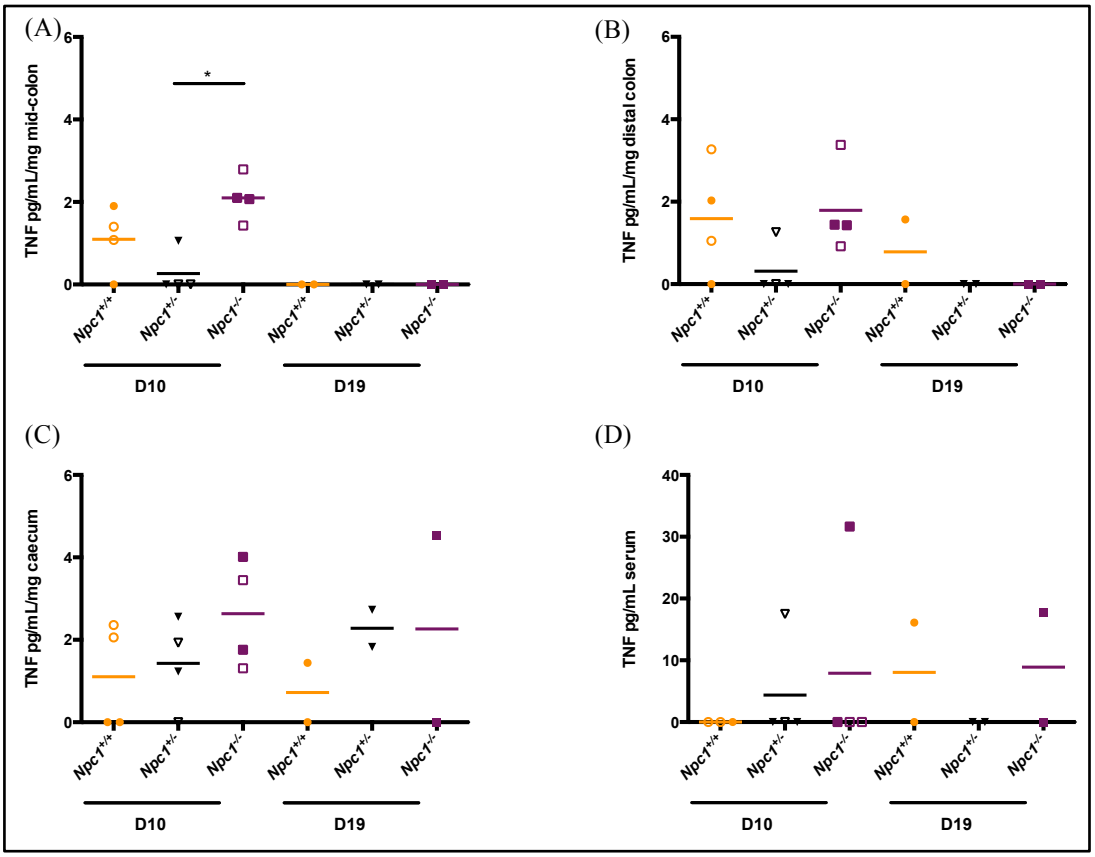

Figure 5.16. Effect of *C. rodentium* infection on inflammatory cytokines in wild-type (*Npc1*$^{+/+}$), heterozygous (*Npc1*$^{+/-}$) and homozygous (*Npc1*$^{-/-}$) mice. Mice were orally infected with *C. rodentium* at a dose of ~4x10^{9} cfu/mouse. *C. rodentium*-infected mice were killed at days 10 and 19. Mid-, distal colon and caeca were isolated and explants were cultured overnight before harvesting supernatants and analysed for TNF in: (A) mid-colon, (B) distal colon, (C) caecum and (D) serum. Each symbol represents an individual animal and horizontal lines represent the mean of the group (D10; n=4, 2 males; filled symbols and 2 females; open symbols and D19; n=2 males; filled symbols). *p<0.05, calculated using Mann–Whitney test.

Together, the secretory cytokine profile in response to infection suggests that *Npc1*$^{-/-}$ mice have an enhanced immune response. Although some elements of this enhanced immune response might be detrimental in other models while others are protective, the balance between these various elements may potentially have mediated protection in the various colitis models tested resulting in the less severe phenotype observed so far.

5.4. Discussion

A link between the lysosome and IBD has been suggested in Hermansky-Pudlak syndrome (HPS) (374). This is a rare, genetically heterogeneous autosomal recessive disease in which *HPS* gene mutations affect intracellular protein trafficking caused by a defect in the biogenesis and/or function of lysosome-related organelles (LRO) (including melanosomes and platelet dense granules) (375). The main features and clinical presentation of this disease include platelet dysfunction and prolonged bleeding times, oculocutaneous tyrosine-positive albinism in addition to systemic involvement caused by ceroid lipofuscin storage (375). Neutropenia with mild immunodeficiency and pulmonary fibrosis are associated with certain forms of the disease (375, 376). Significantly, Crohn's like granulomatous colitis develops in about 20% of HPS patients (377). It is, however, still unknown whether IBD in HPS develops as part of the disease process or as an independent disease entity (378).

Chemically induced models of intestinal inflammation are well established and commonly used to study IBD in experimental animals (357). DSS (363), trinitrobenzene sulfonic acid (379) and oxazolone (380) are used to induce colitis in rodents (357). DSS has the advantage of producing colitis that could be acute, chronic or relapsing depending on the dose and mouse strain studied (381). Other factors to consider for the differential responses seen in different studies include: DSS properties (molecular weight, degree of sulphation, manufacturer and batch), genetic factors (animal strain, sub-strain and gender), microbiological factors (microbiological state and intestinal microbiota composition), undetermined environmental factors as well as protocol and tissue processing-related factors (381-383). Gender differences in the susceptibility to DSS-colitis have been reported with

male mice being more susceptible and having a more severe response in the colon compared to females (364).

There are numerous reports of exaggerated response to DSS-induced colitis in immunodeficient mouse models (384, 385). Multiple inbred mouse strain with varying immune defects (either in both innate and adoptive immunity or are strains prone to autoimmune disease) have shown to be highly susceptible to DSS colitis (364).

Although the exact mechanism of action of DSS is not fully clear, it seems to mediate its effect via activation of macrophages and subsequent macrophage-mediated immune response, direct toxic effects on the gut epithelia, compromising the integrity of the mucosal barrier and upsetting luminal microbiota composition (357, 363, 381). A potential explanation of the partial protection seen in *Npc1*$^{-/-}$ mice against DSS damage could be that lipid storage in intestinal epithelial cells provided protection against DSS directed toxicity.

C. rodentium (formerly known as *Cirtobacter ferundii* biotype 4280), a gram negative aerophilic bacterium, is a pathogenic bacterial species that colonises mice and cause transmissible murine colonic hyperplasia (TMCH) (386) characterised by colonic epithelial cell hyperplasia and proliferation mainly in the distal colon, and is a common naturally occurring disease in laboratory mice (387, 388). *C. rodentium* infection also induces colitis and causes murine GI disease that clinically resembles human enteropathogenic *E. coli* (EPEC) and enterohemorrhagic *E. coli* (EHEC) (387). Symptoms start with diarrhoea and weight loss and histological features include crypt hyperplasia, proliferation of epithelial cells, infiltration of immune cells, goblet cell depletion and mucosal thickening (388). Bacteria mostly colonise

the distal colon attaching to the epithelial surface and effacing the brush border resulting in attaching and effacing (A/E) lesion characteristic of this infection and the similar human homologues EPEC and EHEC (389, 390). *C. rodentium* is non-invasive and uses a type III secretion system to deliver bacterial protein effector into the host cell (387), making this a useful model to investigate in *Npc1*$^{-/-}$ mice for a potentially differential response compared to wild-type animals. Onset of the earliest signs occurs at day 4 following oral infection with *C. rodentium* and some signs peak with maximal mucosal thickening at day 10-12. (386). Although there is a significant inflammatory component in this infection; this has not been fully studied. The infection triggers a Th1 immune response with elevated IL-12, IFN-γ and TNF, characteristic of IBD (Crohn's disease) (372). Recovery is normally achieved after 3-4 weeks (maximum 2 to 3 months post infection) and provides life long immunity in immunocompetent mice, whereas immunocompromised animals fail to clear the bacteria and die after 20 days. *C. rodentium* clearance and eradication is B cell dependent and is mediated via IgG (391). The *C. rodentium* model can serve as a surrogate model of human E. coli being self-limiting (no high mortality or morbidity associated) in most adult mice (386).

The outcome of the infection in mice is dependent on multiple factors including the host genetic background (392). Some outbred and inbred strains presented with an exaggerated response to the bacterial challenge resulting in an accelerated severe manifestation of the different disease elements (hyperplasia, ulceration and inflammation) associated with higher mortality (392). Also, diet and host microbiota composition can influence the host response to bacterial infection (387), all of which are important factors to consider and might be influenced in *Npc1*$^{-/-}$ mice, contributing to the outcome of this challenge.

C. rodentium provides a useful model to study and characterise colitis and infection in the mouse. The link between infection and IBD is related to the multifactorial nature of these diseases and the interaction between abnormal host immune response triggered in response to exposure to enteric bacteria in a genetically susceptible host (388), several elements in NPC1 disease could therefore potentially trigger an abnormal response to this bacterial challenge, including autophagy and bacterial handling defects as well as abnormal immune response (inflammasome defect and TNF overproduction).

The aim of this study was to characterise *C. rodentium* infection-associated intestinal inflammation in NPC1 homozygous and heterozygous mice in comparison to the outcome and severity of the inflammation in the wild-type controls for a potentially exaggerated/protective response/phenotype associated with *Npc1* mutation to add more power to the outcome of the DSS-colitis challenge and to seek a differential response to a different model of colitis that acts via a different mechanism.

A previous study in *Npc1*$^{-/-}$ mice has shown that *Npc1*$^{-/-}$ mice infected with *C. rodentium* presented with delayed and less severe response to the bacterial infection (393). Significantly longer time was required for bacterial colonisation of the colonic mucosa and formation of the characteristic A/E lesion in the *Npc1*$^{-/-}$ mice (12 vs. 6 days) compared to their matched wild-type controls (393). *Npc1*$^{-/-}$ mice also failed to reach significant colonic epithelial hyperplasia compared to the infected controls with significantly lower production of the pro-inflammatory cytokine IFN-γ and elevation of the anti-inflammatory cytokine IL-10 in response to the infection (393). This partial protection against *C. rodentium* in the *Npc1*$^{-/-}$ mice has been suggested to be related to the reduced cholesterol in membrane lipid rafts

in NPC compared to wild-types not allowing A/E lesion formation (393). These findings suggest the role of host cholesterol content in the membrane lipid rafts in the formation of A/E lesion and initiation and maintenance of A/E bacterial infection as shown in NPC1 patients derived fibroblasts being resistant to A/E *E. coli*-induced cytoskeleton rearrangements because of the lower cholesterol rich microdomain in the plasma membrane where the NPC1 fibroblasts failed to form characteristic cytoskeletal rearrangement (protein foci) at bacterial adherence site with microcolonies adhering) in response to EHEP and EPEC infection, suggesting an important role of cholesterol in these membrane lipid rafts for the A/E lesion formation following EHEC and *C. rodentium* infection *in vitro* illustrating the role of membrane cholesterol in the pathogenesis of bacterial infectious diseases (394).

In the current study we did not observe any difference between the three genotypes apart from the homozygous mice infected pre-symptomatically (at ~4 weeks of age), where it took them much longer to reach peak infection and longer to clear infection. In the previous study (393) homozygous mice were infected at 4 weeks but were not allowed to reach peak infection as the study had two very early time points (6 and 12 days) which might have corresponded to peak infection in the wild-types. However, infection course was not long enough to reach peak infection in the homozygous mice (393) (mice started getting highly infected on day 14 in our study, **Figure 5.10**). Also in that previous study, inflammatory cytokine levels were measured from cultured splenocytes, which are not necessarily the most accurate reflection of intestinal inflammation (393).

In most animal models of intestinal inflammation, as well as in IBD patients, inflammation is driven by IL-12/IL-23 activated Th1/Th17, which subsequently stimulate the production of the pro-inflammatory cytokines IFN-γ, TNF and IL-17,

the latter two are key mediators of intestinal inflammation in the mouse (also in human) (395). Immunosuppressive therapy that acts via the inhibition of IL-17 attenuated intestinal inflammation in a chronic DSS colitis model (396).

There are currently two opposing and conflicting theories about the role of the inflammasome in the pathogenesis of IBD and DSS colitis. Recent studies proposed a detrimental effect of NLRP3 inflammasome in the susceptibility and severity of chemically induced colitis (397-400), whereas others have shown evidence of the protective role of NLRP3 (401-403).

Nlrp3$^{-/-}$ mice as well as pharmacological inhibition of caspase-1 by pralnacasan (inhibitor of IL-1β converting enzyme, ICE) were associated with significantly lower susceptibility to DSS colitis demonstrated by lower cytokine levels in the colon and peritoneal macrophages and lower histopathologiacal and clinical scores compared to their wild-type and untreated littermates (397). The reduced severity of colitis was more profound earlier in disease, thus Bauer *et al.* suggested the implication of NLRP3 in the early stages of the initiation of intestinal inflammation (397).

Nlrp3$^{-/-}$, *Pycard*$^{-/-}$ (lacking the adaptor protein component of the inflammasome; ASC) and *Casp1*$^{-/-}$ mice have shown to be more susceptible to DSS colitis due to failure to produce the biologically active form of IL-18 leading to loss of intestinal epithelial integrity therefore commensal bacteria dissemination resulting in leukocyte infiltration and stimulation of chemokine release in the colon (401). This study by Zaki *et al.* highlights the important role of NLRP3 and NLRP3-derived IL-18 in maintaining gut homeostasis in terms of epithelial integrity, barrier permeability and preventing commensal bacterial overgrowth (401).

Another line of evidence in support of the crucial role of the inflammasome in maintaining gut integrity arose from using several models of *Nlrp3*$^{-/-}$, *Acs*$^{-/-}$ and *Nlrc4*$^{-/-}$ mice showing increased susceptibility to *C. rodentium* infectious model of colitis suggesting the protective role of these inflammasome components in IBD (361, 404).

The conflicting role of the NLRP3 inflammasome in the development of IBD, whether it has a protective or a detrimental effect in response to DSS, could also be explained by the type of cells where inflammasome activation takes place, for example in macrophages, inflammasome activation (as occurs in chronic exposure to insult or DSS) in intestinal immune cells results in subsequent activation of the biologically active pro-inflammatory cytokine IL-1 and IL-18 and further tissue damage. Whereas in response to acute injury (as in acute DSS), inflammasome activation occurs in the intestinal epithelia cells with the subsequent release of active cytokines such as IL-18 for intestinal epithelial cells proliferation and repair **(Figure 5.17)** (http://www.rndsystems.com).

IL-1β production both in murine *Npc1*$^{-/-}$ resident peritoneal macrophages and in U18666A cellular model of NPC has been shown to be impaired compared to wild-type cells. In both models (murine *Npc1*$^{-/-}$ resident peritoneal macrophages and U18666A cellular model), the priming step of NLRP3 inflammasome activation seems to be partially impaired with affecting pro-IL-1β and pro-caspase-1 expression in drug treated cells compared to untreated cells. Similarly, LPS-induced pro-IL-1β and pro-caspase-1 expression was also impaired by pre-treatment with U18666A. The inflammasome-independent cytokine TNF was elevated by LPS in U18666A-treated macrophages (Nick Platt, personal communication).

Gut microbiota play a role in maintaining brain function and many studies have shown that disturbances of gut microbiota composition are associated with CNS pathology, manifested in psychological and behavioural changes (405). The communication between the brain and the gut is bidirectional (406). Intestinal microbiota mainly affect stress-related behaviour and manipulation of microbiota composition can induce a state of anxiety, depression and behavioural changes in animals (407). IBD-associated anxiety and depression are quite common and more profound in active disease, with about 50-90% of IBD patients presenting with psychiatric manifestations as well (408). These observations raised the interest in the link between these anatomically distinct systems. Studies in germ-free mice have shown that the composition of gut microbiota influences post-natal brain development and the development of the pituitary-hypothalamic-adrenal axis (409), affecting behaviour, stress and pain response (410-412). The link between the two systems is postulated to be via regulation of immune cells and inflammatory response in the gut affecting brain development and neural plasticity (413). The link between the two systems could suggest that in NPC diseae; CNS disease could potentially predispose to IBD through the interaction between the two systmes.

The NPC1 protein is thought to be a sphingosine transporter moving sphingosine from the lysosomal lumen to the cytosol where it can be then phosphorylated to sphingosine-1-phosphate (S1P) (4). It is therefore plausible to suggest that there would be a reduction in the intracellular content of S1P in NPC1-deficient cells and subsequent down regulation and disruption of S1P signalling pathways. Sphingolipid metabolism is induced by cytokines, which activate sphingosine kinase (SK) (414). S1P is a pro-inflammatory lipid and its role in inflammatory bowel disease was illustrated by challenging *Sk1*$^{-/-}$ mice with DSS (415). TNF

stimulates SK1, which is in turn is essential for mediating TNF's effects (415). *Sk1*$^{-/-}$ mice had a significantly less severe phenotype in response to DSS compared to wild-type mice (415). This highlights the potential use of SK1 inhibitors as therapeutic agent for managing diseases with inflammatory components whether systemic or localised and implicates sphingosine and its metabolites in predisposition to IBD in NPC disease (415, 416).

NPC1 patients have an abnormal bile acid composition with an increased excretion of sulfated and conjugated forms of 3β-hydroxy-, 3β-hydroxy-7-oxo-, and 3β,7α/β-dihydroxy-5-cholenoic acids (417, 418). Such abnormal composition could precipitate for further downstream defects (such as dysbiosis and synthesis of endogenous compounds via regulation of gene expression).

The role of bile acid composition in the maintaining normal gut microbiota has been demonstrated in a study by Devkota *et al.* (419). This study has implicated the consumption of diet high in saturated fats (milk fats) as a risk factor for the development of IBD (419). Saturated fats altered the composition of BAs with subsequent dysbiosis (419). This in turn resulted in defective immune status in conventional and specific pathogen free (SPF) mice, leading to the development of colitis in genetically susceptible host (immunodeficient mice, *Il10*$^{-/-}$) compared to wild-types (419). Saturated fats, being hydrophobic, stimulate the taurine conjugation of bile acids (420) producing more sulphur to be used by pathogenic suphur-reducing bacteria *B. wadsworthia* (of the Deltaproteobacteria phylum), which expand under these conditions (419). Similarly, colitis developed in the *Il10*$^{-/-}$ mice fed normal diet supplemented with taurocholic acid (419). There is also a possibility that by-product of this process, hydrogen sulphide (H_2S) also potentially thought to have detrimental effect on intestinal mucosal barrier, eliciting a

synergistic immune response (419). Together, these events can lead to intestinal inflammation in genetically susceptible host shifting immune response toward an unbalanced chronic localised intestinal inflammation **(Figure 5.18** and **Figure 5.19).** BA dyshomeostasis (altered composition with abnormal BAs present and other main BAs deficient) and dysbiosis in NPC disease could therefore lead to IBD.

Dietary-animal model of colitis has been also proposed further supporting the role of diet and BA in the development of IBD (422). Since high fat diet was associated with elevated levels of the secondary BA deoxycholate in human faeces (423) (potentially also elevated in the colon), this property was utilised to induce colitis in normal wild-type mice (422). Mice fed diet supplemented with 0.2% deoxycholate for 8 months developed colitis, with characteristic gene expression changes, molecular and cellular changes similar to those seen in IBD (422) **(Figure 5.20).**

In addition, studies on patients with active and remission Crohn's disease or ulcerative colitis have shown similar findings with regard to the role of gut BA homeostasis in intestinal integrity (356). Patients with active IBD have altered gut luminal BA composition with higher faecal conjugated and sulphated BAs and lower levels of secondary BAs (also in the serum), due to IBD-associated dysbiosis and subsequent BA dysmetabolism (impaired deconjugation, transformation and desulphation) (356). The most abundant bacteria in human intestinal lumen include Bacteroidetes and Firmicutes, (424), which are the major BA deconjugating species (425). In IBD patients, bacteria of the Firmicutes phylum are reduced (356).

The antimicrobial function of bile acids has been an area of great interest (426-428). Conjugated bile acids in the lumen of the small intestine are known inhibitors of bacterial growth both *in vitro* (427) and *in vivo*, via regulating the expression of intestinal innate immunity (428). Unconjugated BAs, however, have more potent antimicrobial effects than conjugated BAs (426). Furthermore, the antimicrobial

effects of conjugated BAs, have been suggested to be rather exerted by the associated long chain fatty acids (429) present in the mixed micelle (430). Conjugated BAs effect is mediated via the FXR, upregulating genes involved in maintaining intestinal epithelial integrity and preventing bacterial overgrowth (428) such as nitric oxide synthetase (iNOS), nitric oxide in turn also possess antimicrobial activity (430). Ligation of bile duct in wild-type animals was associated with a massive increase in intestinal bacterial growth and dissemination (431), which was responsive to FXR agonist and unlike FXR deficient mice (428).

BAs are thought to mediate their antibacterial effect via two different mechanisms; in the duodenum and jejunum where the concentration are relatively higher, conjugated BA and associated fatty acids exert their effects utilising their pharmacological properties, whereas in the ileum where conjugated BAs are actively absorbed and there should be virtually no fatty acids, absorbed conjugated BAs act through activation of nuclear receptors (FXR) in the enterocytes (430) **(Figure 5.21).**

The figure originally presented here cannot be made freely available via ORA because of 'copyright'.

BAs and associated fatty acids are therefore additional components of intestinal innate immunity along with gastric acidity, bile and intestinal epithelium IgA, gut motility and Paneth cell-secreted anti-microbial peptides such as defensin (430, 432). The potential lack of the anti-microbial action of BAs in NPC disease (due to BA dyshomeostasis) could therefore also be contributing to the development of IBD in NPC.

It is an appealing mechanism to propose that due to cholesterol sequestration in the lysosome in NPC disease, and subsequent down-regulation of BA synthetic enzymes, BA dysmetabolism and altered intestinal BA homeostasis could possibly lead to the development of Crohn's-like pathology in this disease. This could be accomplished via two related mechanisms which feed into each-other leading to a continuous loop; defective BA homeostasis in the gut promote the flourishing of pathogenic bacteria possibly causing localised inflammation (provided host is

genetically predisposed, which is believed to be the case with impaired immune response as part of NPC disease, manifested in peripheral and CNS inflammation). This dysbiosis in turn results in further BA dysmetabolism with more conjugated and sulphated BAs, further promoting the expansion of the pathogenic sulphur-reducing microorganisms. Additionally, altered BA homeostasis may result in the loss of their anti-inflammatory actions (a property of secondary BA (355)).

There are multiple components of NPC disease that could be responsible for the lack of the anticipated exaggerated response to induced colitis models, as seen in normal mice. The lipid profile of NPC1 deficient cells could have exerted an effect of which cholesterol sequestering in the LE/Lys (156) seems to be of major contribution, although this requires investigating experimentally.

The ATP binding cassette transporter A1 (ABCA1) plays a role in glucocorticoid production and therefore confers protection against IBD and was identified as a susceptibility gene in human genome screening of families with IBD (433). Over-expression of ABCA1 in active ulcerative colitis has been reported and suggested to play a role in reducing intracellular cholesterol and oxidised molecules (ROS) (434), these effects are known to be exerted by intracellular cholesterol among other lipids as cholesterol has been shown to induce an inflammatory response (435). IBD patients have significantly elevated levels of ROS compared to healthy controls (more pronounced in Crohn's disease than ulcerative colitis) and oxidative stress seems to be an active component during the course of active IBD (436). A similar observation has been made in mice lacking anti-oxidative enzymes where they developed a characteristic crypt lesion and colitis similar to what is seen in ulcerative colitis (437). Oxidative stress in NPC disease could therefore be another predisposing factor to IBD, especially with the similarities between NPC cells and

ABCA1 deficient (Tangier) cells. Tangier disease, an autosomal recessive disease, is caused by mutations in ABCA1 and is characterised by high-density lipoprotein (HDL) deficiency, sterol deposition in tissue macrophages, and atherosclerosis. ABCA1 is responsible for reverse cholesterol transport (438). Tangier disease has recently shown multiple cellular and molecular aspects in common with NPC disease. Tangier patient fibroblasts exhibited enlarged lysosomal compartments, disrupted endocytic trafficking, cholesterol accumulation, increased sphingomyelin and GSL levels, and defective calcium levels in the acidic stores similar to phenotypes observed in NPC patient fibroblasts. Indeed, an adult Tangier patient was responsive to miglustat with significant neurological and systemic improvement (Colaco *et al.* unpublished data, manuscript in preparation).

The role of cholesterol in IBD is further illustrated by the role of ApoA4, a component of intestine-derived lipoprotein that is involved in ABCA1-mediated cholesterol reverse transport (439, 440). Intracellular cholesterol is transported via ABCA1 to the ApoA1-4 component of HDL (440). Its anti-atherogenic properties have been attributed to this role in reverse cholesterol transport, in addition to its anti-oxidative properties (441). ApoA4 has been also reported to have anti-inflammatory activity evident from its ability to markedly alleviate DSS colitis in mice given i.p. injection of human recombinant ApoA4 (442). In contrast, ApoA4 KO mice have a significantly worsening of the phenotype amenable to improvement upon administration of exogenous ApoA4 (442). These anti-inflammatory properties were attributed to P-selectin inhibition by ApoA4 (442). Inhibition of P-selectin prevented subsequent leukocyte and platelet adhesion (442). However, some of the anti-inflammatory effects of ApoA4 could also be attributed to its anti-atherogentic actions (442). ApoA4 stimulates the efflux of intracellular cholesterol

therefore reducing its pro-inflammatory effects (442). It could be a primary effect or secondary effect via its cholesterol modulating activity.

Inflammation, as well as other harmful cellular processes, requires cholesterol trafficking into the ER (from the lysosome) (435, 443). It is therefore possible that cholesterol trapping into the lysosome (whether full or partial) produces a beneficial blockage of these intracellular pathways with subsequent anti-inflammatory and anti-atherogenic effects. Again, heterozygosity of the *Npc1* mutation seems to maintain the best balance between beneficial pro- and anti-inflammatory activities (443). Several studies have reported an intermediate phenotype in the *Npc1* heterozygotes including an abnormal intermediate metabolite profile, for instance in the feline model (444).

As NPC1-deficient cells have under-expression of some LXR target genes and associated products (445), these cells might share similar properties with proliferative cells (446). However, with cholesterol being trapped in the LE/Lys and not converted to active LXR ligands, LXR activation, and subsequent cholesterol metabolism and lack of its proliferative action won't be achieved. On the other hand, sequestered free cholesterol in the LE/Lys won't be available intracellularly to exert its proliferative effects conferring a degree of protection (446).

Interestingly, the main innate immune response regulator genes associated with Crohn's disease, but not ulcerative colitis, are two autophagy regulating genes: ATG16L1 and IRGM and NOD2 (which has shown to form a complex with ATG16L1 at the cytoplasmic membrane) emphasising the role of bacterial recognition and intracellular processing in the pathogenesis of Crohn's disease which is also in favor of the hypothesis of a defective autophagy in Crohn's disease

with inefficient handling of intracellular pathogens. LRRK2 is another IBD susceptibility genes involved in regulating autophagy (447). With the role of bacterial recognition, handling and autophagy in the pathogenesis of IBD; defecs in these pathways in NPC disease could potentially increase the susceptibility to IBD.

These GWAS studies have highlighted the potential link between IBD and the associated extra-intestinal inflammation conditions (i.e. ankylosing spondylitis, non-drug induced osteoporosis) and autoimmune diseases (i.e. asthma, multiple sclerosis, type 1 diabetes, autoimmune thyroid disease, and coeliac disease) sharing susceptibility loci (448). This could support the hypothesis that generalised extra-intestinal inflammation seen in NPC1 disease could predispose to IBD.

NOD2/CARD15 (also IBD1) was the first identified susceptibility gene loci in Crohn's disease followed by IBD5, IL23R and ATG16L1, all validated in multiple studies (449-458). Gene loci implicated in Crohn's disease play a crucial role in innate immunity, autophagy and phagocytosis highlighting the contribution of these pathways in Crohn's disease pathogenesis (455, 456). Although functional gene network analysis did not reveal a direct interaction/overlap between NPC and key IBD and IBD-like monogenic genes (Holm Uhlig, unpublished), several pathways implicated in the pathogenesis of IBD (and their associated gene were identified as susceptibility loci), are also defective to certain degree in NPC disease (such as TNF overproduction and autophagy defect) (454, 455, 459).

Recent studies have reported defective bacterial handling and phagocytosis in NPC1 cells, also NPC1 dysfunction is associated with increased basal autophagy, as shown in both *Npc1*$^{-/-}$ mice and patient-derived fibroblasts thorough upregulation of class III phosphoinositide 3-kinase and beclin-1 but not Akt-mTOR-p70 S6K

pathway (460-462). However, this upregulation of autophagy is coupled with failure to clear autophagosomes and lysosomes in NPC disease (195).

Autophagy is crucial for host defense against *C. rodentium* and in regulating intestinal resistance to *C. rodentium* infection. Mice with conditional deletion of the autophagy protein Atg7 in the intestinal epithelium had an exacerbated response to *C. rodentium* infection with upregulation of the proinflammatory cytokines in the large intestine. Moreover, clearance of *C. rodentium* was significantly reduced in *Atg7* knonckout mice (463). Also, mice deficient in the autophagy protein Atg16L1 (chimeric mice with Atg16L1 deficient haematopoietic cells) presented with a more severe phenotype (significant weight loss and mortality) in response to DSS with significantly elevated levels of the proinflammatory cytokines IL-1β and IL-18 compared to the control chimeric mice expressing the wild-type Agt16L1 protein (464). This phenotype was responsive to IL-1β and IL-18 neutralising antibodies with marked improvement (464). On the other hand the role of autophagy in chemically induced colitis is not clear. Mice with *Atg7* deletion in intestinal epithelial did not show to have an abnormal response to DSS induced colitis compared to the control mice and deletion of this autophagy protein did not affect their susceptibility to DSS colitis and only affected Paneth cell granule formation (mice only had smaller granules and less lysozymes in Paneth cells) suggesting the dispensable nature of this protein in the host intestinal immune defense/homeostasis (465).

Natural killer (NK) cells emphasise the role of innate immunity in clearing enteric pathogens including *C. rodentium* infection. NK cell depleted mice had a higher bacterial load with disseminated infection to other organs, higher colonic bacterial

colonisation associated with milder inflammation caused by less cytokine production and immune cell recruitment due to the lack of NK cells. NK cells also exert a direct cytotoxic effect against *C. rodentium in vitro* (466). Marked systemic reduction in NK cell frequency is seen in *Npc1*$^{-/-}$ mice and patients, due to sphingosine misstrafficking in the lysosome and subsequent reduction in S1P levels affecting S1P gradient formation required for migration of NK cells from lymphoid tissues to other systemic organs (467). This NK cell defect in *Npc1*$^{-/-}$ mice could therefore have contributed to the phenotype observed in both challenges (DSS and *C. rodentium* infection) with prolonged infection period and less severe inflammation with lower cytokine levels seen in the *Npc1*$^{-/-}$ and *Npc1*$^{+/-}$ mice.

Although NPC1 disease is associated with a chronic overproduction of TNF, it would be important to identify the mechanism by which the overproduction of this proinflammatory cytokine is induced. Several animal models with characteristic overproduction of TNF present with varying phenotypes depending on the mechanism and kinetics of TNF overexpression (468). For instance, TNF ARE-deficient mice have both rheumatoid arthritis and IBD phenotypes due to the functional mutation of the regulatory ARE (conferring stability and overexpression of TNF mRNA systematically including synovial sites) (469). TTP KO mice (tristetraprolin, a TNF ARE regulatory binding protein that inhibits TNF overexpression in macrophages) have rheumatoid arthritis (470). TIA1-deficient mice (T-cell intracellular antigen, which also binds to TNF ARE and inhibits the translation of TNF mRNA) present with no inflammatory condition as a result (471). This is mainly attributed to the kinetics and nature of the defect, ARE mutation also confers loss of responsiveness to anti-inflammatory mechanisms (thus resulting in chronic inflammatory condition; IBD) which is intact in TTP KO mice

leading to anti-inflammatory response and quick drop in TNF levels (468).

The effects of the overexpression of TNF and TNF receptor death pathway genes in *Npc1*$^{-/-}$ mice (in brain and liver and contributes to liver disease) (69, 153, 472) could imply the potential enhanced susceptibility to IBD in this disease. The link between abnormal cytokine levels and IBD has been defined (473), with TNF being the most implicated in the pathogenesis of IBD (373) and the reported efficacy of anti-TNF therapy in IBD patients (474). TNF affects both innate (475) and adaptive (476) immune responses and also targets both immune (477) and non-immune (478) cell types in the intestine leading to sustained intestinal inflammation. The *Tnf*$^{\Delta ARE}$ mouse, engineered with a post-translational defect in the regulation of TNF mRNA, presents with a Crohn's like intestinal inflammation and has been a useful model for studying the contribution of TNF and the underlying mechanisms (469). It appears that regardless of the mechanism of TNF overproduction, TNF-mediated IBD results form the activation of Th1 CD8+ T cell response with subsequent production of IL-12 and IFN-γ via the activation of two kinases Tpl2 and JNK2 but not MK2 (479). Pathogenic differences between myeloid and T cell driven TNF have also been suggested. The CD8+ T cell model of intestinal inflammation as seen in the *Tnf*$^{\Delta ARE}$ mouse is characterised by an ileal localisation of inflammation as opposed to the CD4+ T cell model of colonic inflammation (473).

PBMCs and human monocyte derived macrophage treated with U18666A to induce NPC1 phenotypes produced much lower levels of TNF in response to LPS challenge compared to DMSO treated cells (Holm Uhlig, unpublished, personal communication). This might explain the differential susceptibility to induced colitis in *Npc1*$^{-/-}$ mice compared to wild-types and heterozygotes, since these mice have a

constitutive overproduction/overexpression of TNF but potentially a defect in inducible production.

The role of intracellular calcium in IBD pathogenesis has not been investigated, however, we believe it might play a role as mice with defective acidic store calcium release (two-pore channel 2 knockout, TPC2 KO mice) presented with an exaggerated response to DSS challenge compared to wild-types (Nicoli *et al.*, unpublished data). This would implicate acidic store calcium filling defect in NPC cells in the potential pathogenesis of IBD in NPC disease, as it leads to subsequent impaired calcium release in common with TPC2 deficient cells **(Figure 5.22).** Predisposition factors to IBD in NPC could therefore potentially be an early cellular event such as reduced acidic store calcium release, which would need further investigation.

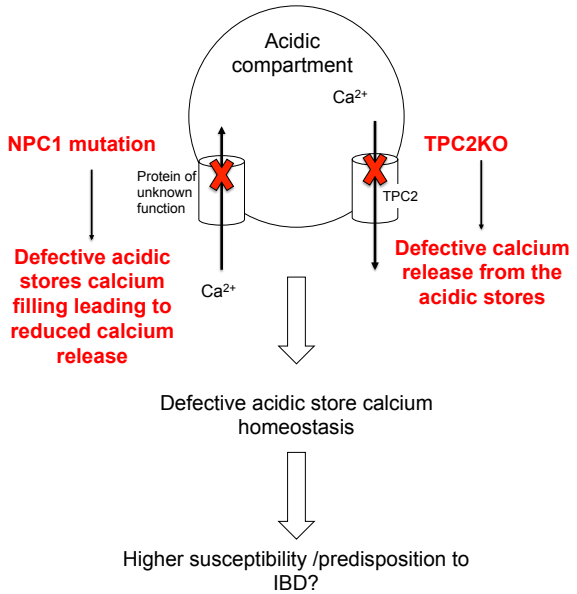

Figure 5.22. Proposed mechanism of the link between lysosomal calcium homeostasis and IBD.

Although functional gene network analysis did not reveal a direct interaction between NPC and IBD, patients' data along with the increasing incidence of

Crohn's-like intestinal inflammation in NPC patients support the existence of real link between the two diseases. Excluding miglustat as a precipitating factor, there are other key elements of NPC disease which could potentially predispose to IBD, including altered immune regulation and BA dyshomeostasis **(Table 5.6)**. Targeting these elements, for example using anti-inflammatory therapy (small molecule or TNF-targeting biologics) and BA supplementation could represent a promising therapeutic approach to alleviate Crohn's-like intestinal inflammation in NPC patients. Due to the chronic, debilitating nature of Crohn's disease, early diagnosis as well as early intervention would be crucial and might affect prognosis.

Summary of potential predisposing factors that could lead to Crohn's-like intestinal inflammation in NPC
• IBD in other LRO disease (HPS). • Cholesterol intracellular pro-inflammatory effects. • NLRP3 inflammasome defect. • The link between the gut and the CNS. • BA dyshomeostasis and subsequent dysbiosis. • Oxidative stress and ROS. • Generalised TNF-dominated extra-intestinal inflammation. • Autophagy/phagocytosis/bacterial handling and clearing defect. • Impaired innate immunity (NK cells defect). • Acidic store calcium filling defect (insight from the TPC2 KO mouse).

Table 5.6. Summary of potential predisposing factors to IBD in NPC disease.

Chapter 6. Concluding Remarks

6.1. General discussion and conclusions

In this thesis I aimed to study novel approaches to treating NPC disease, based on targeting unique steps in the pathogenic cascade. In the course of these studies I uncovered a novel drug metabolism defect in *Npc1*$^{-/-}$ mice that in turn has suggested some new approaches to treating NPC disease.

The defect in the CYP450 system in NPC disease **(Chapter 2)** came to light when evaluating liver metabolised drugs such as curcumin and ibuprofen in these mice. Efficacy of treatment in *Npc1*$^{-/-}$ mice using compound at doses tolerated in other strains and models was investigated. We observed toxicity of these drugs in *Npc1*$^{-/-}$ mice at doses that were well tolerated in other mouse strains suggesting a potential defect in xenobiotic metabolising capacity. We found a reduction in multiple CYP450 catalysed reactions in the mouse and cat models of NPC1 disease and also post-mortem liver samples from NPC patients.

Impaired drug metabolism could potentially have implications for both animal studies trialling liver metabolised compounds, but also the treatment and management of NPC patients as well as careful consideration of whether carriers have full drug metabolism function. Interestingly a similar phenotype has been previously reported in other

neurodegenerative disease (Parkinson's disease), affecting both Phase I and Phase II metabolism with subgroups of patients having reduced capacity of sulphur metabolism (S-oxidation) and altered substrate specificity (480, 481).

The field of experimental therapeutics in NPC disease has grown extensively over the past decade (reviewed in **Chapter 1**). We therefore aimed to assess a range of therapeutic approaches in the mouse model that targets multiple steps in the pathogenic cascade **(Chapter 3)**. A main focus of this thesis was the inflammatory aspect of the disease, as well as the potential use of curcumin as a calcium modulating compound to compensate for insufficient calcium release from the lysosome in NPC disease. A compound (vinpocetine) with a previously unappreciated anti-inflammatory properties was investigated at two doses and different effects were seen, although functional benefit was seen with the higher dose, the lower dose resulted in a marked increase in the life span of the mice.

TNF-targeting biologics were tested in the NPC1 mouse model for the first time. NPC has a TNF-dominated pro-inflammatory cytokine profile and as an antibody-based therapy, it offers the advantage of avoiding the drug metabolism defect. The anti-TNF biologics are in human use in other diseases (e.g. Remicade for Crohn's disease intestinal inflammation (482)). Four of these biologics were tested and were all beneficial at the early symptomatic stage; however, saline injected mice were also improved illustrating the benefit of rehydration on its own (particularly when given i.p.). However, at a later disease stages Humira (and to some extent Enbrel) had an additional functional benefit over the PBS injected controls, suggesting an effect of the treatment itself (antibody or protein). This suggests the anti-inflammatory effect potentially penetrating the CNS and improving neurological function. The efficacy of Humira pointed to the possibility that blood-brain barrier

integrity is potentially compromised at later disease stage, which would need further investigating and could have major implications to the therapeutic side.

Calcium modulating agents were then evaluated (curcumin-related analogues) in various doses and in two colonies (old colony environmentally exposed, the new colony barrier maintained). Initial results in the old colony with the optimal determined dose (37) were consistent with the reported findings of efficacy of this treatment. The reformulation into pellets to increase consumption was beneficial in terms of motor function and slight increase in survival but it did not produce a beneficial effect on tremor. A curcuminoid mixture consisting of curcumin, desmethoxycurcumin and bisdesmethoxycurcumin was also reformulated into pellets and administered at the same dose, this treatment was associated with a similar effect as the pure curcumin pelleted diet, except for its lack of efficacy on the life span of treated mice. A slightly higher dose of curcumin appeared to be toxic to mice from the old colony (with weight loss and loss of activity very early on).

All treated animals from this colony had a worsening of tremor (except for the initial trial with the optimum dose), suggestive of a negative effect in the "old" colony treated with high curcumin doses. Revisiting the higher dose of curcumin in the new colony resulted in tolerability, to some extent, to the 250 mg/kg dose, but possibly not he 300 mg/kg dose. Interestingly, neither treatment increases the tremor of the treated mice, in the new colony, possibly due to reduced environmental exposure to xenobiotics and infections. Two issues appeared with respect to curcumin therapy in terms of dosing and purity. The use of an optimum dose that would have efficacy with no toxicity as well as using the most pure curcumin form would possibly be the best approach. Curcumin's clear benefit as a

calcium modulator is offset by this compound being a liver metabolised, and not only that it is a known inhibitor of the cytochrome P450 system so its negative effects at high doses are not surprising in light of our discovery that the CYP450 system is compromised in NPC. The question was could a strategy be developed to improve its tolerability?

While using UDCA supplementation to upregulate CYP450 gene expression and successfully compensated for the CYP450 defect, the functional benefit of this treatment led to the assessment of this treatment in combination with the high dose curcumin (to assess whether this approach would provide protection from toxicity *in vivo*) and combination with *N*B-DGJ was also performed. Apart from weight loss associated with UDCA, the combination of curcumin with UDCA resulted in partial protection form the negative effect of either compound alone and the addition of *N*B-DGJ added significant benefit to the combination therapy.

In the context of evaluating therapeutic agents in NPC disease, two neuroprotective and neurorestorative compounds, cogane and myogane **(Chapter 4)**, were assessed *in vitro*, and had no effects at the cellular level in terms of inducing or correcting NPC disease cellular phenotypes. Myogane was also tested in the NPC1 mouse where it showed functional benefit at the lower doses as well as a significant anti-inflammatory effect in the CNS and slight protection from demyelination. With their ability to readily cross the blood-brain barrier and their safety and tolerability established in pre-clinical models of other neurodegenerative conditions, these compounds might represent another class of therapeutics for NPC disease, which are the subject of interest and development by a small pharmaceutical company (Phytopharm). Comparison of the efficacy of the various treatments investigated in this thesis is summarised in **Table 6.1.**

Therapy	Survival	Body weight	Rearing activity	Tremor
Vinpocetine, 10 mg/kg	---	↓	↑	↓ at early stage (not significant) --- ↑ at later sage
Vinpocetine, 2 mg/kg	↑	↓	---	↓ at early stage (not significant) --- ↑ at later sage
Humira	↑ compared to untreated controls	---	↑	↓ at later stage
Enbrel	---	---	↑ at later stage (not significant)	↓ at later stage (not significant)
Remicade	---	↓ transient at 8 and 9 weeks	↑ at later stage (not significant)	↓ at later stage (not significant)
Curcumin, 150 mg/kg	↑	---	---	↓
Curcumin, 250 mg/kg	↑ (not significant)	↓ (not significant)	↓ at later stage (not significant)	---
Curcumin (P), 150 mg/kg	↑ (not significant)	---	↑	↑ at later stage (not significant)
Curcuminoids (P), 150 mg/kg	↑ (not significant)	---	↑	↑ at later stage (not significant)
Curcumin, 250 mg/kg	↑ (not significant)	↓ (not significant)	↓ at later stage (not significant)	---
Curcumin, 250 mg/kg (new colony)	---	↑ early stage (not significant)	↑	---
Curcumin, 300 mg/kg	---	↑ early stage (not significant), loss delayed by 1 week	---	---
*N*B-DGJ	↑	↑	↑ (not significant)	↓ at later stage
UDCA	---	↓	↑	↑
UDCA+Curcumin 300 mg/kg	---	---	↑ (not significant)	↓ at later stage (↓ vs. curcumin alone, not significant)
UDCA+*N*B-DGJ	↑	↑	↑	↓ (↓ vs. *N*B-DGJ alone, not significant)
UDCA+*N*B-DGJ+Curcumin 300 mg/kg	↑	↑	↑	↓
Myogane 0.1 mg/kg	---	↑	↑	↓ at 10 weeks (not significant) ↑ (not significant)
Myogane 1 mg/kg	---	↑	↑	↓ at early stage (not significant) ↑ at late stage (not significant)
Myogane 10 mg/kg	↓ (not significant)	---	↑ (not significant)	---

Table 6.1. Summary of the outcome of the various therapeutics trialled in this thesis.

The outcome of therapeutic trials in mouse models is highly dependent on multiple practical factors. The discrepancies in outcome arising between the same trials conducted at different times or on different colonies could have been the result of variations in the mouse model, affecting the mouse phenotype and thus trial outcome, caused by genetic drift, microbial/immunological status of the mice (highly dependent on the animal facility) and also differences in procedure conducted between different labs/places to replicate/conduct similar trials. All these factors could possibly contribute to the variations reported in results between different studies (in different research groups and different countries). Even simple factors like dietary composition can change xenobiotic exposure which considering the CYP450 defect could influence toxicity (483). Infection and resulting inflammation (196) could also be a factor and further inhibit drug metabolism and enhance tremor.

In our hands we have conducted the same trials using the same agents over a long period of time and have encountered differences in the outcome. A major contributing factor was an outbreak of *Pasteurella pneumotropica* and *Helicobacter hepaticus* (261). *Helicobacter hepaticus* is known to influence liver detoxifying capacity (259) affecting the pharmacokinetics of administered compounds and hence the end result of the therapeutic intervention in these mice. The infection is also associated with altered circulating bile acid composition (261). While both infections affect immunological state of the infected animals (261, 262), *Pasteurella pneumotropica* has been recognised as having minimal effects in immunocompetent mice. However, with immunocompromised mice that is not the case (260).

Additionally, genetic drift in the colony was another main factor, as results obtained in mice from a long established old colony varied from those we had for mice

generated form a new "ultraclean" colony. Curcumin, in particular, has given variable results in *Npc1*$^{-/-}$ mice over the years, between the two colonies we had and between our colony and other lab's (37, 113). Susceptibility to the dose variation was also different. Comparison with normal (wild-type) and untreated homozygous mice should help highlight these differences and make interpretation and comparison of results easier. As curcumin is a CYP450 inhibitor it may well exacerbate the CYP450 defect in NPC1 mice and at CYP450 inhibitory doses its negative effects will outweigh its beneficial effects at lower doses. Another approach of testing curcumin in NPC disease would be in the cat model to avoid mouse colony-related variations and have a reliable assessment of efficacy.

The increasing number of reported cases of Crohn's-like intestinal inflammation in NPC patients necessitated the investigation of this disease aspect in the mouse model **(Chapter 5)**, as it seemed to be independent of migulstat treatment in NPC patients (84). Although the two diseases do not overlap genetically, signs of upper GI bleeding in very late end stage homozygous mice were recorded in our NPC1 mouse colony (old and new colonies). SPF mice did not have histopathological features of intestinal inflammation at baseline. Unexpectedly, partial protection from intestinal inflammation was observed in both homozygous and heterozygous mice compared to wild-type BALB/c mice in response to two models of colitis (chemical and infectious). Two distinct features were however seen in the *Npc1*$^{-/-}$ mice: different infection kinetics with longer time to reach peak infection as well as to clear infection, in particular in animals infected presymptomatically. The other main finding was the enhanced secretion of inflammatory cytokines in response to infection. However, in all cases GI tract from homozygous and heterozygous animals were at the microscopic level indistinguishable form wild-type mice.

These two findings would require further investigation to establish and fully characterise the phenotype in the *Npc1*$^{-/-}$ mice. The other direction to take would be to investigate this again at baseline in another NPC1 mouse model that is not on a BALB/c background, due to the resistance of the BALB/c mice and their Th1-dominated immune response to induction of IBD (367). We would possibly need to induce colitis experimentally in case of absence of a spontaneous phenotype. The outcome of this would help understand this element in the patients, establish proper treatment and aid early diagnosis and early intervention. With the majority of the reported findings being associated with the NPC1 defect, at least one NPC2 patient has presented with Crohn's-like intestinal inflammation.

An interesting phenotype was observed in heterozygotes. They potentially have an intermediate phenotype when it comes to the drug metabolism defect, the pharmacokinetic functional study of midazolam in the mouse model and the findings in the mouse would possibly suggest human carriers may have impaired CYP450 function. The partial protection of NPC1 heterozygosity in the mice against induced colitis is quite interesting and could have other implications for microbial handling and cytokine production.

Heterozygotes are often not included in NPC research even though they have been studied and found to develop late onset disease in the feline model. Heterozygous animals should not therefore be used as controls, only wild-type mice are suitable true controls. The disease status of the heterozygotes is of particular interest due to the high carrier frequency in the population and the apparent defect in drug metabolism. Whether human heterozygous carriers also have more Crohn's disease would also merit further investigation.

6.2. Future work

Detailed analysis of BA homeostasis in bile, circulation and liver as well as urinary excretion would add more to our understanding of the nature and effect of this aspect of NPC disease. The prediction would be that the products of the classical ER biosynthetic pathway would be affected by cholesterol storage, as cholesterol transport to mitochondria is normal in NPC **(Figure 6.1)**.

That would include assessment in the murine and feline models as well as looking at patient derived samples. Identifying the precise changes in this system would help tailor other approaches to target this defect, which could translate into simple dietary supplementation of a potentially already approved BA used in other hepatic diseases. This element of NPC disease has the potential of improving neurological function by reducing xenobiotic neurotoxicity, liver disease as well as intestinal inflammation and could be rapidly translated to clinical practice.

The discovery of a previously unappreciated anti-inflammatory properties of other classes of drugs (such as vinpocetine) would potentially allow further assessment of the effect of targeting inflammation in NPC disease. Drugs with better pharmacokinetic and safety profile with less undesirable side effects would be of particular interest.

Moreover, drugs which possess multiple pharmacological effects or target more than one pathological element/mechanism of NPC disease would also be good candidates as they would be combination therapies in their own right.

More attention should be directed at reformulating and optimised dosing of compounds already trialled in NPC disease, such as curcumin, to enhance their bioavailability and half-life, therefore optimise their delivery, reduce their impact on the CYP450 system and maximise their therapeutic effects. Other approaches to increasing cytosolic calcium with other drugs should also be explored.

The use of TNF-targeting biologics also has the potentials of transition to the clinic, if neurological efficacy is seen in patients. TNF-targeting biologics should also be tested in other neurodegenerative diseases with inflammatory component such as

Sandhoff disease, possibly combined with anti-IL-1β therapies as GM2 gangliosidoses involve TNF and IL-1β driven inflammation.

The potential of combining these therapeutic agents with miglustat and other therapies should also be carefully considered as they might have additive or synergistic benefits when combined but care will need to be applied to appropriate dosing particularly with liver metabolised drugs.

As the pharmaceutical industry develops neuroprotective and neurorestorative compounds for more common neurodegenerative disorders such as Parkinson's disease and Alzheimer's disease, new candidates should also be evaluated in the *Npc1*$^{-/-}$ mice and other LSDs.

It is important to appreciate the translatable aspects of this research. With cyclodextrin, for instance, having progressed to evaluation in the feline model and then trialled in NPC patients. Similarly, this would be the next step for interesting candidate therapies.

Developing other tools to assess the efficacy of therapeutics in *Npc1*$^{-/-}$ mice would also be of great value to this research. This includes additional functional assessments such as those for cognition, motor function and coordination. They would need careful validation in this mouse model and optimisation of the methods.

For the GI tract aspect of the disease, the differences between the human disease and the mouse model should be appreciated; the mouse model used is an acute model that resembles severe NPC disease in patients (26). Taking this into consideration along with the effect of the genetic background of the mouse (on the

immune status in particular (367)) would suggest investigating intestinal pathology in the other mouse models of NPC disease on C57BL/6 background is needed.

Taken together, the research in this thesis has evaluated multiple new approaches to therapy in the NPC1 mouse, identified a drug metabolism defect previously unknown in NPC disease, determined the probable mechanisms leading to this defect and developed new leads for rapid translation into the clinic.

Chapter 7. Bibliography

1. Niemann A. Ein unbekanntes krankheitsbild. Jahrb Kinderheilkd 1914;79(1).

2. Crocker AC. The cerebral defect in Tay-Sachs disease and Niemann-Pick disease. J Neurochem 1961;7:69-80.

3. Brady RO, Kanfer JN, Mock MB, Fredrickson DS. The metabolism of sphingomyelin. II. Evidence of an enzymatic deficiency in Niemann-Pick diseae. Proc Natl Acad Sci U S A 1966;55(2):366-369.

4. Lloyd-Evans E, Platt FM. Lipids on trial: the search for the offending metabolite in Niemann-Pick type C disease. Traffic 2010;11(4):419-428.

5. Vanier MT. Niemann-Pick disease type C. Orphanet J Rare Dis 2010;5:16.

6. Carstea ED, Polymeropoulos MH, Parker CC, Detera-Wadleigh SD, O'Neill RR, Patterson MC, Goldin E, Xiao H, Straub RE, Vanier MT, et al. Linkage of Niemann-Pick disease type C to human chromosome 18. Proc Natl Acad Sci U S A 1993;90(5):2002-2004.

7. Naureckiene S, Sleat DE, Lackland H, Fensom A, Vanier MT, Wattiaux R, Jadot M, Lobel P. Identification of HE1 as the second gene of Niemann-Pick C disease. Science 2000;290(5500):2298-2301.

8. Vance JE. Lipid imbalance in the neurological disorder, Niemann-Pick C disease. FEBS Lett 2006;580(23):5518-5524.

9. Trendelenburg G, Vanier MT, Maza S, Millat G, Bohner G, Munz DL, Zschenderlein R. Niemann-Pick type C disease in a 68-year-old patient. J Neurol Neurosurg Psychiatry 2006;77(8):997-998.

10. Iturriaga C, Pineda M, Fernandez-Valero EM, Vanier MT, Coll MJ. Niemann-Pick C disease in Spain: clinical spectrum and development of a disability scale. J Neurol Sci 2006;249(1):1-6.

11. Imrie J, Dasgupta S, Besley GT, Harris C, Heptinstall L, Knight S, Vanier MT, Fensom AH, Ward C, Jacklin E, Whitehouse C, Wraith JE. The natural history of Niemann-Pick disease type C in the UK. J Inherit Metab Dis 2007;30(1):51-59.

12. Walterfang M, Fietz M, Fahey M, Sullivan D, Leane P, Lubman DI, Velakoulis D. The neuropsychiatry of Niemann-Pick type C disease in adulthood. J Neuropsychiatry Clin Neurosci 2006;18(2):158-170.

13. Sevin M, Lesca G, Baumann N, Millat G, Lyon-Caen O, Vanier MT, Sedel F. The adult form of Niemann-Pick disease type C. Brain 2007;130(Pt 1):120-133.

14. Spiegel R, Raas-Rothschild A, Reish O, Regev M, Meiner V, Bargal R, Sury V, Meir K, Nadjari M, Hermann G, Iancu TC, Shalev SA, Zeigler M. The clinical spectrum of fetal Niemann-Pick type C. Am J Med Genet A 2009;149A(3):446-450.

15. Vanier MT, Wenger DA, Comly ME, Rousson R, Brady RO, Pentchev PG. Niemann-Pick disease group C: clinical variability and diagnosis based on defective

cholesterol esterification. A collaborative study on 70 patients. Clin Genet 1988;33(5):331-348.

16. Bjurulf B, Spetalen S, Erichsen A, Vanier MT, Strom EH, Stromme P. Niemann-Pick disease type C2 presenting as fatal pulmonary alveolar lipoproteinosis: morphological findings in lung and nervous tissue. Medical science monitor : international medical journal of experimental and clinical research 2008;14(8):CS71-75.

17. Fink JK, Filling-Katz MR, Sokol J, Cogan DG, Pikus A, Sonies B, Soong B, Pentchev PG, Comly ME, Brady RO. Clinical spectrum of Niemann-Pick disease type C. Neurology 1989;39(8):1040-1049.

18. Millat G, Marcais C, Tomasetto C, Chikh K, Fensom AH, Harzer K, Wenger DA, Ohno K, Vanier MT. Niemann-Pick C1 disease: correlations between NPC1 mutations, levels of NPC1 protein, and phenotypes emphasize the functional significance of the putative sterol-sensing domain and of the cysteine-rich luminal loop. Am J Hum Genet 2001;68(6):1373-1385.

19. Frohlich E, Harzer K, Heller T, Ruhl U. Ultrasound echogenic splenic tumors: nodular manifestation of type C Niemann-Pick disease. Ultraschall Med 1990;11(3):119-122.

20. Fensom AH, Grant AR, Steinberg SJ, Ward CP, Lake BD, Logan EC, Hulman G. An adult with a non-neuronopathic form of Niemann-Pick C disease. J Inherit Metab Dis 1999;22(1):84-86.

21. Dvorakova L, Sikora J, Hrebicek M, Hulkova H, Bouckova M, Stolnaja L, Elleder M. Subclinical course of adult visceral Niemann-Pick type C1 disease. A rare or underdiagnosed disorder? J Inherit Metab Dis 2006;29(4):591.

22. Carstea ED, Morris JA, Coleman KG, Loftus SK, Zhang D, Cummings C, Gu J, Rosenfeld MA, Pavan WJ, Krizman DB, Nagle J, Polymeropoulos MH, Sturley SL, Ioannou YA, Higgins ME*, et al.* Niemann-Pick C1 disease gene: homology to mediators of cholesterol homeostasis. Science 1997;277(5323):228-231.

23. Higgins ME, Davies JP, Chen FW, Ioannou YA. Niemann-Pick C1 is a late endosome-resident protein that transiently associates with lysosomes and the trans-Golgi network. Mol Genet Metab 1999;68(1):1-13.

24. Davies JP, Ioannou YA. Topological analysis of Niemann-Pick C1 protein reveals that the membrane orientation of the putative sterol-sensing domain is identical to those of 3-hydroxy-3-methylglutaryl-CoA reductase and sterol regulatory element binding protein cleavage-activating protein. J Biol Chem 2000;275(32):24367-24374.

25. Ioannou YA. The structure and function of the Niemann-Pick C1 protein. Mol Genet Metab 2000;71(1-2):175-181.

26. Maue RA, Burgess RW, Wang B, Wooley CM, Seburn KL, Vanier MT, Rogers MA, Chang CC, Chang TY, Harris BT, Graber DJ, Penatti CA, Porter DM,

Szwergold BS, Henderson LP*, et al.* A novel mouse model of Niemann-Pick type C disease carrying a D1005G-Npc1 mutation comparable to commonly observed human mutations. Hum Mol Genet 2012;21(4):730-750.

27. Davies JP, Chen FW, Ioannou YA. Transmembrane molecular pump activity of Niemann-Pick C1 protein. Science 2000;290(5500):2295-2298.

28. Tseng TT, Gratwick KS, Kollman J, Park D, Nies DH, Goffeau A, Saier MH, Jr. The RND permease superfamily: an ancient, ubiquitous and diverse family that includes human disease and development proteins. Journal of molecular microbiology and biotechnology 1999;1(1):107-125.

29. Scott C, Ioannou YA. The NPC1 protein: structure implies function. Biochim Biophys Acta 2004;1685(1-3):8-13.

30. Sleat DE, Wiseman JA, El-Banna M, Price SM, Verot L, Shen MM, Tint GS, Vanier MT, Walkley SU, Lobel P. Genetic evidence for nonredundant functional cooperativity between NPC1 and NPC2 in lipid transport. Proc Natl Acad Sci U S A 2004;101(16):5886-5891.

31. Millat G, Marcais C, Rafi MA, Yamamoto T, Morris JA, Pentchev PG, Ohno K, Wenger DA, Vanier MT. Niemann-Pick C1 disease: the I1061T substitution is a frequent mutant allele in patients of Western European descent and correlates with a classic juvenile phenotype. Am J Hum Genet 1999;65(5):1321-1329.

32. Millat G, Bailo N, Molinero S, Rodriguez C, Chikh K, Vanier MT. Niemann-Pick C disease: use of denaturing high performance liquid chromatography for the detection of NPC1 and NPC2 genetic variations and impact on management of patients and families. Mol Genet Metab 2005;86(1-2):220-232.

33. Chikh K, Rodriguez C, Vey S, Vanier MT, Millat G. Niemann-Pick type C disease: subcellular location and functional characterization of NPC2 proteins with naturally occurring missense mutations. Hum Mutat 2005;26(1):20-28.

34. Vanier MT. Lipid changes in Niemann-Pick disease type C brain: personal experience and review of the literature. Neurochem Res 1999;24(4):481-489.

35. Walkley SU, Suzuki K. Consequences of NPC1 and NPC2 loss of function in mammalian neurons. Biochim Biophys Acta 2004;1685(1-3):48-62.

36. Liscum L, Faust JR. The intracellular transport of low density lipoprotein-derived cholesterol is inhibited in Chinese hamster ovary cells cultured with 3-beta-[2-(diethylamino)ethoxy]androst-5-en-17-one. J Biol Chem 1989;264(20):11796-11806.

37. Lloyd-Evans E, Morgan AJ, He X, Smith DA, Elliot-Smith E, Sillence DJ, Churchill GC, Schuchman EH, Galione A, Platt FM. Niemann-Pick disease type C1 is a sphingosine storage disease that causes deregulation of lysosomal calcium. Nat Med 2008;14(11):1247-1255.

38. Infante RE, Wang ML, Radhakrishnan A, Kwon HJ, Brown MS, Goldstein JL. NPC2 facilitates bidirectional transfer of cholesterol between NPC1 and lipid bilayers, a step in cholesterol egress from lysosomes. Proc Natl Acad Sci U S A 2008;105(40):15287-15292.

39. Pentchev PG, Boothe AD, Kruth HS, Weintroub H, Stivers J, Brady RO. A genetic storage disorder in BALB/C mice with a metabolic block in esterification of exogenous cholesterol. J Biol Chem 1984;259(9):5784-5791.

40. Miyawaki S, Mitsuoka S, Sakiyama T, Kitagawa T. Sphingomyelinosis, a new mutation in the mouse: a model of Niemann-Pick disease in humans. The Journal of heredity 1982;73(4):257-263.

41. Miyawaki S, Yoshida H, Mitsuoka S, Enomoto H, Ikehara S. A mouse model for Niemann-Pick disease. Influence of genetic background on disease expression in spm/spm mice. J Hered 1986;77(6):379-384.

42. Park WD, O'Brien JF, Lundquist PA, Kraft DL, Vockley CW, Karnes PS, Patterson MC, Snow K. Identification of 58 novel mutations in Niemann-Pick disease type C: correlation with biochemical phenotype and importance of PTC1-like domains in NPC1. Hum Mutat 2003;22(4):313-325.

43. Lowenthal AC, Cummings JF, Wenger DA, Thrall MA, Wood PA, de Lahunta A. Feline sphingolipidosis resembling Niemann-Pick disease type C. Acta Neuropathol 1990;81(2):189-197.

44. Somers KL, Royals MA, Carstea ED, Rafi MA, Wenger DA, Thrall MA. Mutation analysis of feline Niemann-Pick C1 disease. Mol Genet Metab 2003;79(2):99-103.

45. Brown DE, Thrall MA, Walkley SU, Wenger DA, Mitchell TW, Smith MO, Royals KL, March PA, Allison RW. Feline Niemann-Pick disease type C. Am J Pathol 1994;144(6):1412-1415.

46. Vanier MT, Rodriguez-Lafrasse C, Rousson R, Gazzah N, Juge MC, Pentchev PG, Revol A, Louisot P. Type C Niemann-Pick disease: spectrum of phenotypic variation in disruption of intracellular LDL-derived cholesterol processing. Biochim Biophys Acta 1991;1096(4):328-337.

47. Patterson MC. A riddle wrapped in a mystery: understanding Niemann-Pick disease, type C. Neurologist 2003;9(6):301-310.

48. Vanier MT, Rodriguez-Lafrasse C, Rousson R, Duthel S, Harzer K, Pentchev PG, Revol A, Louisot P. Type C Niemann-Pick disease: biochemical aspects and phenotypic heterogeneity. Dev Neurosci 1991;13(4-5):307-314.

49. Patterson MC, Hendriksz CJ, Walterfang M, Sedel F, Vanier MT, Wijburg F, Group N-CGW. Recommendations for the diagnosis and management of Niemann-Pick disease type C: an update. Mol Genet Metab 2012;106(3):330-344.

50. Porter FD, Scherrer DE, Lanier MH, Langmade SJ, Molugu V, Gale SE, Olzeski D, Sidhu R, Dietzen DJ, Fu R, Wassif CA, Yanjanin NM, Marso SP, House

J, Vite C*, et al.* Cholesterol oxidation products are sensitive and specific blood-based biomarkers for Niemann-Pick C1 disease. Sci Transl Med 2010;2(56):56ra81.

51. Jiang X, Sidhu R, Porter FD, Yanjanin NM, Speak AO, te Vruchte DT, Platt FM, Fujiwara H, Scherrer DE, Zhang J, Dietzen DJ, Schaffer JE, Ory DS. A sensitive and specific LC-MS/MS method for rapid diagnosis of Niemann-Pick C1 disease from human plasma. J Lipid Res 2011;52(7):1435-1445.

52. Lachmann RH, te Vruchte D, Lloyd-Evans E, Reinkensmeier G, Sillence DJ, Fernandez-Guillen L, Dwek RA, Butters TD, Cox TM, Platt FM. Treatment with miglustat reverses the lipid-trafficking defect in Niemann-Pick disease type C. Neurobiol Dis 2004;16(3):654-658.

53. Te Vruchte D, Speak AO, Wallom KL, Al Eisa N, Smith DA, Hendriksz CJ, Simmons L, Lachmann RH, Cousins A, Hartung R, Mengel E, Runz H, Beck M, Amraoui Y, Imrie J*, et al.* Relative acidic compartment volume as a lysosomal storage disorder-associated biomarker. J Clin Invest 2014.

54. Hollak CE, van Weely S, van Oers MH, Aerts JM. Marked elevation of plasma chitotriosidase activity. A novel hallmark of Gaucher disease. J Clin Invest 1994;93(3):1288-1292.

55. Guo Y, He W, Boer AM, Wevers RA, de Bruijn AM, Groener JE, Hollak CE, Aerts JM, Galjaard H, van Diggelen OP. Elevated plasma chitotriosidase activity in various lysosomal storage disorders. J Inherit Metab Dis 1995;18(6):717-722.

56. Imrie J, Vijayaraghaven S, Whitehouse C, Harris S, Heptinstall L, Church H, Cooper A, Besley GT, Wraith JE. Niemann-Pick disease type C in adults. J Inherit Metab Dis 2002;25(6):491-500.

57. Ries M, Schaefer E, Luhrs T, Mani L, Kuhn J, Vanier MT, Krummenauer F, Gal A, Beck M, Mengel E. Critical assessment of chitotriosidase analysis in the rational laboratory diagnosis of children with Gaucher disease and Niemann-Pick disease type A/B and C. J Inherit Metab Dis 2006;29(5):647-652.

58. Baggiolini M. Chemokines and leukocyte traffic. Nature 1998;392(6676):565-568.

59. Chang KL, Hwu WL, Yeh HY, Lee NC, Chien YH. CCL18 as an alternative marker in Gaucher and Niemann-Pick disease with chitotriosidase deficiency. Blood Cells Mol Dis 2010;44(1):38-40.

60. Wyss-Coray T, Mucke L. Inflammation in neurodegenerative disease--a double-edged sword. Neuron 2002;35(3):419-432.

61. Lucas SM, Rothwell NJ, Gibson RM. The role of inflammation in CNS injury and disease. Br J Pharmacol 2006;147 Suppl 1:S232-240.

62. Amor S, Puentes F, Baker D, van der Valk P. Inflammation in neurodegenerative diseases. Immunology 2010;129(2):154-169.

63. Liu B, Hong JS. Role of microglia in inflammation-mediated neurodegenerative diseases: mechanisms and strategies for therapeutic intervention. J Pharmacol Exp Ther 2003;304(1):1-7.

64. Glass CK, Saijo K, Winner B, Marchetto MC, Gage FH. Mechanisms underlying inflammation in neurodegeneration. Cell 2010;140(6):918-934.

65. Cluzeau CV, Watkins-Chow DE, Fu R, Borate B, Yanjanin N, Dail MK, Davidson CD, Walkley SU, Ory DS, Wassif CA, Pavan WJ, Porter FD. Microarray expression analysis and identification of serum biomarkers for Niemann-Pick disease, type C1. Hum Mol Genet 2012;21(16):3632-3646.

66. Cologna SM, Cluzeau CV, Yanjanin NM, Blank PS, Dail MK, Siebel S, Toth CL, Wassif CA, Lieberman AP, Porter FD. Human and mouse neuroinflammation markers in Niemann-Pick disease, type C1. J Inherit Metab Dis 2014;37(1):83-92.

67. Liao G, Wen Z, Irizarry K, Huang Y, Mitsouras K, Darmani M, Leon T, Shi L, Bi X. Abnormal gene expression in cerebellum of Npc1-/- mice during postnatal development. Brain Res 2010;1325:128-140.

68. Li H, Repa JJ, Valasek MA, Beltroy EP, Turley SD, German DC, Dietschy JM. Molecular, anatomical, and biochemical events associated with neurodegeneration in mice with Niemann-Pick type C disease. J Neuropathol Exp Neurol 2005;64(4):323-333.

69. Wu YP, Mizukami H, Matsuda J, Saito Y, Proia RL, Suzuki K. Apoptosis accompanied by up-regulation of TNF-alpha death pathway genes in the brain of Niemann-Pick type C disease. Mol Genet Metab 2005;84(1):9-17.

70. Vitner EB, Salomon R, Farfel-Becker T, Meshcheriakova A, Ali M, Klein AD, Platt FM, Cox TM, Futerman AH. RIPK3 as a potential therapeutic target for Gaucher's disease. Nat Med 2014;20(2):204-208.

71. Baudry M, Yao Y, Simmons D, Liu J, Bi X. Postnatal development of inflammation in a murine model of Niemann-Pick type C disease: immunohistochemical observations of microglia and astroglia. Exp Neurol 2003;184(2):887-903.

72. Pressey SN, Smith DA, Wong AM, Platt FM, Cooper JD. Early glial activation, synaptic changes and axonal pathology in the thalamocortical system of Niemann-Pick type C1 mice. Neurobiol Dis 2012;45(3):1086-1100.

73. Schwartz M, Baruch K. The resolution of neuroinflammation in neurodegeneration: leukocyte recruitment via the choroid plexus. EMBO J 2014;33(1):7-22.

74. Kandt RS, Emerson RG, Singer HS, Valle DL, Moser HW. Cataplexy in variant forms of Niemann-Pick disease. Ann Neurol 1982;12(3):284-288.

75. Mignot E, Lammers GJ, Ripley B, Okun M, Nevsimalova S, Overeem S, Vankova J, Black J, Harsh J, Bassetti C, Schrader H, Nishino S. The role of

cerebrospinal fluid hypocretin measurement in the diagnosis of narcolepsy and other hypersomnias. Arch Neurol 2002;59(10):1553-1562.

76. Madra M, Sturley SL. Niemann-Pick type C pathogenesis and treatment: from statins to sugars. Clinical lipidology 2010;5(3):387-395.

77. Hsu YS, Hwu WL, Huang SF, Lu MY, Chen RL, Lin DT, Peng SS, Lin KH. Niemann-Pick disease type C (a cellular cholesterol lipidosis) treated by bone marrow transplantation. Bone Marrow Transplant 1999;24(1):103-107.

78. Bonney DK, O'Meara A, Shabani A, Imrie J, Bigger BW, Jones S, Wraith JE, Wynn RF. Successful allogeneic bone marrow transplant for Niemann-Pick disease type C2 is likely to be associated with a severe 'graft versus substrate' effect. J Inherit Metab Dis 2010.

79. Sakiyama T, Tsuda M, Owada M, Joh K, Miyawaki S, Kitagawa T. Bone marrow transplantation for Niemann-Pick mice. Biochem Biophys Res Commun 1983;113(2):605-610.

80. Patterson MC, Di Bisceglie AM, Higgins JJ, Abel RB, Schiffmann R, Parker CC, Argoff CE, Grewal RP, Yu K, Pentchev PG. The effect of cholesterol-lowering agents on hepatic and plasma cholesterol in Niemann-Pick disease type C. Neurology 1993;43(1):61-64.

81. Erickson RP, Garver WS, Camargo F, Hossain GS, Heidenreich RA. Pharmacological and genetic modifications of somatic cholesterol do not substantially alter the course of CNS disease in Niemann-Pick C mice. J Inherit Metab Dis 2000;23(1):54-62.

82. Zervas M, Somers KL, Thrall MA, Walkley SU. Critical role for glycosphingolipids in Niemann-Pick disease type C. Curr Biol 2001;11(16):1283-1287.

83. Patterson MC, Vecchio D, Prady H, Abel L, Wraith JE. Miglustat for treatment of Niemann-Pick C disease: a randomised controlled study. Lancet Neurol 2007;6(9):765-772.

84. Wraith JE, Vecchio D, Jacklin E, Abel L, Chadha-Boreham H, Luzy C, Giorgino R, Patterson MC. Miglustat in adult and juvenile patients with Niemann-Pick disease type C: long-term data from a clinical trial. Mol Genet Metab 2010;99(4):351-357.

85. Alvarez AR, Klein A, Castro J, Cancino GI, Amigo J, Mosqueira M, Vargas LM, Yevenes LF, Bronfman FC, Zanlungo S. Imatinib therapy blocks cerebellar apoptosis and improves neurological symptoms in a mouse model of Niemann-Pick type C disease. FASEB J 2008;22(10):3617-3627.

86. Griffin LD, Gong W, Verot L, Mellon SH. Niemann-Pick type C disease involves disrupted neurosteroidogenesis and responds to allopregnanolone. Nat Med 2004;10(7):704-711.

87. Davidson CD, Ali NF, Micsenyi MC, Stephney G, Renault S, Dobrenis K, Ory DS, Vanier MT, Walkley SU. Chronic cyclodextrin treatment of murine Niemann-Pick C disease ameliorates neuronal cholesterol and glycosphingolipid storage and disease progression. PloS one 2009;4(9):e6951.

88. Liu B, Turley SD, Burns DK, Miller AM, Repa JJ, Dietschy JM. Reversal of defective lysosomal transport in NPC disease ameliorates liver dysfunction and neurodegeneration in the npc1-/- mouse. Proc Natl Acad Sci U S A 2009;106(7):2377-2382.

89. Repa JJ, Li H, Frank-Cannon TC, Valasek MA, Turley SD, Tansey MG, Dietschy JM. Liver X receptor activation enhances cholesterol loss from the brain, decreases neuroinflammation, and increases survival of the NPC1 mouse. J Neurosci 2007;27(52):14470-14480.

90. Kaptzan T, West SA, Holicky EL, Wheatley CL, Marks DL, Wang T, Peake KB, Vance J, Walkley SU, Pagano RE. Development of a Rab9 transgenic mouse and its ability to increase the lifespan of a murine model of Niemann-Pick type C disease. Am J Pathol 2009;174(1):14-20.

91. Zhang M, Li J, Chakrabarty P, Bu B, Vincent I. Cyclin-dependent kinase inhibitors attenuate protein hyperphosphorylation, cytoskeletal lesion formation, and motor defects in Niemann-Pick Type C mice. Am J Pathol 2004;165(3):843-853.

92. Smith D, Wallom KL, Williams IM, Jeyakumar M, Platt FM. Beneficial effects of anti-inflammatory therapy in a mouse model of Niemann-Pick disease type C1. Neurobiol Dis 2009;36(2):242-251.

93. Vincent M, Sayre NL, Graham MJ, Crooke RM, Shealy DJ, Liscum L. Evaluation of an anti-tumor necrosis factor therapeutic in a mouse model of Niemann-Pick C liver disease. PloS one 2010;5(9):e12941.

94. Bascunan-Castillo EC, Erickson RP, Howison CM, Hunter RJ, Heidenreich RH, Hicks C, Trouard TP, Gillies RJ. Tamoxifen and vitamin E treatments delay symptoms in the mouse model of Niemann-Pick C. Journal of applied genetics 2004;45(4):461-467.

95. Kirkegaard T, Roth AG, Petersen NH, Mahalka AK, Olsen OD, Moilanen I, Zylicz A, Knudsen J, Sandhoff K, Arenz C, Kinnunen PK, Nylandsted J, Jaattela M. Hsp70 stabilizes lysosomes and reverts Niemann-Pick disease-associated lysosomal pathology. Nature 2010;463(7280):549-553.

96. Kim SJ, Lee BH, Lee YS, Kang KS. Defective cholesterol traffic and neuronal differentiation in neural stem cells of Niemann-Pick type C disease improved by valproic acid, a histone deacetylase inhibitor. Biochem Biophys Res Commun 2007;360(3):593-599.

97. Devlin C, Pipalia NH, Liao X, Schuchman EH, Maxfield FR, Tabas I. Improvement in lipid and protein trafficking in Niemann-Pick C1 cells by correction of a secondary enzyme defect. Traffic 2010;11(5):601-615.

98. Takaura N, Yagi T, Maeda M, Nanba E, Oshima A, Suzuki Y, Yamano T, Tanaka A. Attenuation of ganglioside GM1 accumulation in the brain of GM1 gangliosidosis mice by neonatal intravenous gene transfer. Gene Ther 2003;10(17):1487-1493.

99. Norflus F, Tifft CJ, McDonald MP, Goldstein G, Crawley JN, Hoffmann A, Sandhoff K, Suzuki K, Proia RL. Bone marrow transplantation prolongs life span and ameliorates neurologic manifestations in Sandhoff disease mice. J Clin Invest 1998;101(9):1881-1888.

100. Patterson MC, Platt F. Therapy of Niemann-Pick disease, type C. Biochim Biophys Acta 2004;1685(1-3):77-82.

101. Sands MS, Davidson BL. Gene therapy for lysosomal storage diseases. Molecular therapy : the journal of the American Society of Gene Therapy 2006;13(5):839-849.

102. Ponder KP. Immune response hinders therapy for lysosomal storage diseases. J Clin Invest 2008;118(8):2686-2689.

103. Dickson P, McEntee M, Vogler C, Le S, Levy B, Peinovich M, Hanson S, Passage M, Kakkis E. Intrathecal enzyme replacement therapy: successful treatment of brain disease via the cerebrospinal fluid. Mol Genet Metab 2007;91(1):61-68.

104. Koudinov AR, Koudinova NV. Cholesterol homeostasis failure as a unifying cause of synaptic degeneration. J Neurol Sci 2005;229-230:233-240.

105. Platt FM, Neises GR, Reinkensmeier G, Townsend MJ, Perry VH, Proia RL, Winchester B, Dwek RA, Butters TD. Prevention of lysosomal storage in Tay-Sachs mice treated with N-butyldeoxynojirimycin. Science 1997;276(5311):428-431.

106. Jeyakumar M, Butters TD, Cortina-Borja M, Hunnam V, Proia RL, Perry VH, Dwek RA, Platt FM. Delayed symptom onset and increased life expectancy in Sandhoff disease mice treated with N-butyldeoxynojirimycin. Proc Natl Acad Sci U S A 1999;96(11):6388-6393.

107. Andersson U, Butters TD, Dwek RA, Platt FM. N-butyldeoxygalactonojirimycin: a more selective inhibitor of glycosphingolipid biosynthesis than N-butyldeoxynojirimycin, in vitro and in vivo. Biochem Pharmacol 2000;59(7):821-829.

108. Weinreb NJ, Barranger JA, Charrow J, Grabowski GA, Mankin HJ, Mistry P. Guidance on the use of miglustat for treating patients with type 1 Gaucher disease. Am J Hematol 2005;80(3):223-229.

109. Patterson MC, Vecchio D, Jacklin E, Abel L, Chadha-Boreham H, Luzy C, Giorgino R, Wraith JE. Long-term miglustat therapy in children with Niemann-Pick disease type C. J Child Neurol 2010;25(3):300-305.

110. Pineda M, Wraith JE, Mengel E, Sedel F, Hwu WL, Rohrbach M, Bembi B, Walterfang M, Korenke GC, Marquardt T, Luzy C, Giorgino R, Patterson MC.

Miglustat in patients with Niemann-Pick disease Type C (NP-C): a multicenter observational retrospective cohort study. Mol Genet Metab 2009;98(3):243-249.

111. Piper RC, Luzio JP. CUPpling calcium to lysosomal biogenesis. Trends Cell Biol 2004;14(9):471-473.

112. Bilmen JG, Khan SZ, Javed MH, Michelangeli F. Inhibition of the SERCA Ca^{2+} pumps by curcumin. Curcumin putatively stabilizes the interaction between the nucleotide-binding and phosphorylation domains in the absence of ATP. Eur J Biochem 2001;268(23):6318-6327.

113. Borbon IA, Hillman Z, Duran E, Jr., Kiela PR, Frautschy SA, Erickson RP. Lack of efficacy of curcumin on neurodegeneration in the mouse model of Niemann-Pick C1. Pharmacol Biochem Behav 2012;101(1):125-131.

114. Cole GM, Teter B, Frautschy SA. Neuroprotective effects of curcumin. Adv Exp Med Biol 2007;595:197-212.

115. Jacobs WB, Walsh GS, Miller FD. Neuronal survival and p73/p63/p53: a family affair. The Neuroscientist : a review journal bringing neurobiology, neurology and psychiatry 2004;10(5):443-455.

116. Tsai KK, Yuan ZM. c-Abl stabilizes p73 by a phosphorylation-augmented interaction. Cancer Res 2003;63(12):3418-3424.

117. Capdeville R, Buchdunger E, Zimmermann J, Matter A. Glivec (STI571, imatinib), a rationally developed, targeted anticancer drug. Nat Rev Drug Discov 2002;1(7):493-502.

118. Mellon S, Gong W, Griffin LD. Niemann pick type C disease as a model for defects in neurosteroidogenesis. Endocr Res 2004;30(4):727-735.

119. Mellon SH, Gong W, Schonemann MD. Endogenous and synthetic neurosteroids in treatment of Niemann-Pick Type C disease. Brain Res Rev 2008;57(2):410-420.

120. Langmade SJ, Gale SE, Frolov A, Mohri I, Suzuki K, Mellon SH, Walkley SU, Covey DF, Schaffer JE, Ory DS. Pregnane X receptor (PXR) activation: a mechanism for neuroprotection in a mouse model of Niemann-Pick C disease. Proc Natl Acad Sci U S A 2006;103(37):13807-13812.

121. Ahmad I, Lope-Piedrafita S, Bi X, Hicks C, Yao Y, Yu C, Chaitkin E, Howison CM, Weberg L, Trouard TP, Erickson RP. Allopregnanolone treatment, both as a single injection or repetitively, delays demyelination and enhances survival of Niemann-Pick C mice. J Neurosci Res 2005;82(6):811-821.

122. Liu B, Li H, Repa JJ, Turley SD, Dietschy JM. Genetic variations and treatments that affect the lifespan of the NPC1 mouse. J Lipid Res 2008;49(3):663-669.

123. Vite C, Mauldin E, Ward S, Stein V, Prociuk M, Haskins ME, Strattan R, Kao M, Ory D, Walkley SU, Vanier MT. Intrathecal cyclodextrin therapy of feline Niemann-Pick Type C disease. Mol Genet Metab 2011;102(2):S44.

124. Ward S, O'Donnell P, Fernandez S, Vite CH. 2-hydroxypropyl-beta-cyclodextrin raises hearing threshold in normal cats and in cats with Niemann-Pick type C disease. Pediatr Res 2010;68(1):52-56.

125. Repa JJ, Mangelsdorf DJ. The role of orphan nuclear receptors in the regulation of cholesterol homeostasis. Annu Rev Cell Dev Biol 2000;16:459-481.

126. Whitney KD, Watson MA, Collins JL, Benson WG, Stone TM, Numerick MJ, Tippin TK, Wilson JG, Winegar DA, Kliewer SA. Regulation of cholesterol homeostasis by the liver X receptors in the central nervous system. Mol Endocrinol 2002;16(6):1378-1385.

127. Gofflot F, Chartoire N, Vasseur L, Heikkinen S, Dembele D, Le Merrer J, Auwerx J. Systematic gene expression mapping clusters nuclear receptors according to their function in the brain. Cell 2007;131(2):405-418.

128. Lombardi D, Soldati T, Riederer MA, Goda Y, Zerial M, Pfeffer SR. Rab9 functions in transport between late endosomes and the trans Golgi network. EMBO J 1993;12(2):677-682.

129. Walter M, Davies JP, Ioannou YA. Telomerase immortalization upregulates Rab9 expression and restores LDL cholesterol egress from Niemann-Pick C1 late endosomes. J Lipid Res 2003;44(2):243-253.

130. Walter M, Chen FW, Tamari F, Wang R, Ioannou YA. Endosomal lipid accumulation in NPC1 leads to inhibition of PKC, hypophosphorylation of vimentin and Rab9 entrapment. Biology of the cell / under the auspices of the European Cell Biology Organization 2009;101(3):141-152.

131. Hanks SK, Hunter T. Protein kinases 6. The eukaryotic protein kinase superfamily: kinase (catalytic) domain structure and classification. FASEB J 1995;9(8):576-596.

132. Angelo M, Plattner F, Giese KP. Cyclin-dependent kinase 5 in synaptic plasticity, learning and memory. J Neurochem 2006;99(2):353-370.

133. Jope RS, Johnson GV. The glamour and gloom of glycogen synthase kinase-3. Trends Biochem Sci 2004;29(2):95-102.

134. Yamaguchi H, Ishiguro K, Uchida T, Takashima A, Lemere CA, Imahori K. Preferential labeling of Alzheimer neurofibrillary tangles with antisera for tau protein kinase (TPK) I/glycogen synthase kinase-3 beta and cyclin-dependent kinase 5, a component of TPK II. Acta Neuropathol 1996;92(3):232-241.

135. Engmann O, Giese KP. Crosstalk between Cdk5 and GSK3beta: Implications for Alzheimer's Disease. Frontiers in molecular neuroscience 2009;2:2.

136. Bi X, Liu J, Yao Y, Baudry M, Lynch G. Deregulation of the phosphatidylinositol-3 kinase signaling cascade is associated with neurodegeneration in Npc1-/- mouse brain. Am J Pathol 2005;167(4):1081-1092.

137. Bu B, Li J, Davies P, Vincent I. Deregulation of cdk5, hyperphosphorylation, and cytoskeletal pathology in the Niemann-Pick type C murine model. J Neurosci 2002;22(15):6515-6525.

138. Noble W, Planel E, Zehr C, Olm V, Meyerson J, Suleman F, Gaynor K, Wang L, LaFrancois J, Feinstein B, Burns M, Krishnamurthy P, Wen Y, Bhat R, Lewis J*, et al.* Inhibition of glycogen synthase kinase-3 by lithium correlates with reduced tauopathy and degeneration in vivo. Proc Natl Acad Sci U S A 2005;102(19):6990-6995.

139. Koh CH, Whiteman M, Li QX, Halliwell B, Jenner AM, Wong BS, Laughton KM, Wenk M, Masters CL, Beart PM, Bernard O, Cheung NS. Chronic exposure to U18666A is associated with oxidative stress in cultured murine cortical neurons. J Neurochem 2006;98(4):1278-1289.

140. Zampieri S, Mellon SH, Butters TD, Nevyjel M, Covey DF, Bembi B, Dardis A. Oxidative stress in NPC1 deficient cells: protective effect of allopregnanolone. Journal of cellular and molecular medicine 2009;13(9B):3786-3796.

141. Fu R, Yanjanin NM, Bianconi S, Pavan WJ, Porter FD. Oxidative stress in Niemann-Pick disease, type C. Mol Genet Metab 2010;101(2-3):214-218.

142. Nylandsted J, Gyrd-Hansen M, Danielewicz A, Fehrenbacher N, Lademann U, Hoyer-Hansen M, Weber E, Multhoff G, Rohde M, Jaattela M. Heat shock protein 70 promotes cell survival by inhibiting lysosomal membrane permeabilization. J Exp Med 2004;200(4):425-435.

143. Gevry NY, Lalli E, Sassone-Corsi P, Murphy BD. Regulation of niemann-pick c1 gene expression by the 3'5'-cyclic adenosine monophosphate pathway in steroidogenic cells. Mol Endocrinol 2003;17(4):704-715.

144. Pipalia NH, Cosner CC, Huang A, Chatterjee A, Bourbon P, Farley N, Helquist P, Wiest O, Maxfield FR. Histone deacetylase inhibitor treatment dramatically reduces cholesterol accumulation in Niemann-Pick type C1 mutant human fibroblasts. Proc Natl Acad Sci U S A 2011;108(14):5620-5625.

145. Munkacsi AB, Chen FW, Brinkman MA, Higaki K, Gutierrez GD, Chaudhari J, Layer JV, Tong A, Bard M, Boone C, Ioannou YA, Sturley SL. An "exacerbate-reverse" strategy in yeast identifies histone deacetylase inhibition as a correction for cholesterol and sphingolipid transport defects in human Niemann-Pick type C disease. J Biol Chem 2011;286(27):23842-23851.

146. Harzer K, Massenkeil G, Frohlich E. Concurrent increase of cholesterol, sphingomyelin and glucosylceramide in the spleen from non-neurologic Niemann-Pick type C patients but also patients possibly affected with other lipid trafficking disorders. FEBS Lett 2003;537(1-3):177-181.

147. Pentchev PG, Gal AE, Booth AD, Omodeo-Sale F, Fouks J, Neumeyer BA, Quirk JM, Dawson G, Brady RO. A lysosomal storage disorder in mice characterized by a dual deficiency of sphingomyelinase and glucocerebrosidase. Biochim Biophys Acta 1980;619(3):669-679.

148. Thomas GH, Tuck-Muller CM, Miller CS, Reynolds LW. Correction of sphingomyelinase deficiency in Niemann-Pick type C fibroblasts by removal of lipoprotein fraction from culture media. J Inherit Metab Dis 1989;12(2):139-151.

149. Lachmann RH. Miglustat. Oxford GlycoSciences/Actelion. Curr Opin Investig Drugs 2003;4(4):472-479.

150. Vanier MT, Millat G. Niemann-Pick disease type C. Clin Genet 2003;64(4):269-281.

151. Kelly DA, Portmann B, Mowat AP, Sherlock S, Lake BD. Niemann-Pick disease type C: diagnosis and outcome in children, with particular reference to liver disease. The Journal of pediatrics 1993;123(2):242-247.

152. Frolov A, Zielinski SE, Crowley JR, Dudley-Rucker N, Schaffer JE, Ory DS. NPC1 and NPC2 regulate cellular cholesterol homeostasis through generation of low density lipoprotein cholesterol-derived oxysterols. The Journal of biological chemistry 2003;278(28):25517-25525.

153. Beltroy EP, Richardson JA, Horton JD, Turley SD, Dietschy JM. Cholesterol accumulation and liver cell death in mice with Niemann-Pick type C disease. Hepatology 2005;42(4):886-893.

154. Sayre NL, Rimkunas VM, Graham MJ, Crooke RM, Liscum L. Recovery from liver disease in a Niemann-Pick type C mouse model. J Lipid Res 2010;51(8):2372-2383.

155. Hafner M, Reen T, Rozma D. Regulation of hepatic cytochromes p450 by lipids and cholesterol. Curr Drug Metab 2011;12(2):173-185.

156. te Vruchte D, Lloyd-Evans E, Veldman RJ, Neville DC, Dwek RA, Platt FM, van Blitterswijk WJ, Sillence DJ. Accumulation of glycosphingolipids in Niemann-Pick C disease disrupts endosomal transport. J Biol Chem 2004;279(25):26167-26175.

157. Loftus SK, Morris JA, Carstea ED, Gu JZ, Cummings C, Brown A, Ellison J, Ohno K, Rosenfeld MA, Tagle DA, Pentchev PG, Pavan WJ. Murine model of Niemann-Pick C disease: mutation in a cholesterol homeostasis gene. Science 1997;277(5323):232-235.

158. Nerurkar PV, Park SS, Thomas PE, Nims RW, Lubet RA. Methoxyresorufin and benzyloxyresorufin: substrates preferentially metabolized by cytochromes P4501A2 and 2B, respectively, in the rat and mouse. Biochem Pharmacol 1993;46(5):933-943.

159. Namkung MJ, Yang HL, Hulla JE, Juchau MR. On the substrate specificity of cytochrome P450IIIA1. Mol Pharmacol 1988;34(5):628-637.

160. Roe AL, Howard G, Blouin R, Snawder JE. Characterization of cytochrome P450 and glutathione S-transferase activity and expression in male and female ob/ob mice. Int J Obes Relat Metab Disord 1999;23(1):48-53.

161. Burke MD, Thompson S, Weaver RJ, Wolf CR, Mayer RT. Cytochrome P450 specificities of alkoxyresorufin O-dealkylation in human and rat liver. Biochem Pharmacol 1994;48(5):923-936.

162. Perkins S, Verschoyle RD, Hill K, Parveen I, Threadgill MD, Sharma RA, Williams ML, Steward WP, Gescher AJ. Chemopreventive efficacy and pharmacokinetics of curcumin in the min/+ mouse, a model of familial adenomatous polyposis. Cancer Epidemiol Biomarkers Prev 2002;11(6):535-540.

163. Lim GP, Chu T, Yang F, Beech W, Frautschy SA, Cole GM. The curry spice curcumin reduces oxidative damage and amyloid pathology in an Alzheimer transgenic mouse. The Journal of neuroscience : the official journal of the Society for Neuroscience 2001;21(21):8370-8377.

164. Appiah-Opong R, Commandeur JN, van Vugt-Lussenburg B, Vermeulen NP. Inhibition of human recombinant cytochrome P450s by curcumin and curcumin decomposition products. Toxicology 2007;235(1-2):83-91.

165. Jalbert G, Castonguay A. Effects of NSAIDs on NNK-induced pulmonary and gastric tumorigenesis in A/J mice. Cancer Lett 1992;66(1):21-28.

166. Keim KL, Hall PC. General neuropharmacology of vinpocetine: A putative cerebral activator. Drug Dev Res 1987;11(2):107-115.

167. Nelson DR, Zeldin DC, Hoffman SM, Maltais LJ, Wain HM, Nebert DW. Comparison of cytochrome P450 (CYP) genes from the mouse and human genomes, including nomenclature recommendations for genes, pseudogenes and alternative-splice variants. Pharmacogenetics 2004;14(1):1-18.

168. Guengerich FP. Cytochrome P-450 3A4: regulation and role in drug metabolism. Annu Rev Pharmacol Toxicol 1999;39:1-17.

169. Camargo F, Erickson RP, Garver WS, Hossain GS, Carbone PN, Heidenreich RA, Blanchard J. Cyclodextrins in the treatment of a mouse model of Niemann-Pick C disease. Life Sci 2001;70(2):131-142.

170. Ishikawa M, Yoshii H, Furuta T. Interaction of modified cyclodextrins with cytochrome P-450. Biosci Biotechnol Biochem 2005;69(1):246-248.

171. van Herwaarden AE, Smit JW, Sparidans RW, Wagenaar E, van der Kruijssen CM, Schellens JH, Beijnen JH, Schinkel AH. Midazolam and cyclosporin a metabolism in transgenic mice with liver-specific expression of human CYP3A4. Drug Metab Dispos 2005;33(7):892-895.

172. Gandhi AS, Guo T, Shah P, Moorthy B, Chow DS, Hu M, Ghose R. CYP3A-dependent drug metabolism is reduced in bacterial inflammation in mice. Br J Pharmacol 2012;166(7):2176-2187.

173. Kronbach T, Mathys D, Umeno M, Gonzalez FJ, Meyer UA. Oxidation of midazolam and triazolam by human liver cytochrome P450IIIA4. Mol Pharmacol 1989;36(1):89-96.

174. Seo KA, Bae SK, Choi YK, Choi CS, Liu KH, Shin JG. Metabolism of 1'- and 4-hydroxymidazolam by glucuronide conjugation is largely mediated by UDP-glucuronosyltransferases 1A4, 2B4, and 2B7. Drug Metab Dispos 2010;38(11):2007-2013.

175. Kim KH, Bae JH, Cha SW, Han SS, Park KH, Jeong TC. Role of metabolic activation by cytochrome P450 in thioacetamide-induced suppression of antibody response in male BALB/c mice. Toxicol Lett 2000;114(1-3):225-235.

176. Ueda A, Hamadeh HK, Webb HK, Yamamoto Y, Sueyoshi T, Afshari CA, Lehmann JM, Negishi M. Diverse roles of the nuclear orphan receptor CAR in regulating hepatic genes in response to phenobarbital. Mol Pharmacol 2002;61(1):1-6.

177. Orrenius S, Ericsson JL, Ernster L. Phenobarbital-induced synthesis of the microsomal drug-metabolizing enzyme system and its relationship to the proliferation of endoplasmic membranes. A morphological and biochemical study. J Cell Biol 1965;25(3):627-639.

178. Schacter BA, Mason JI. The effect of phenobarbital, 3-methylcholanthrene, 3,4-benzpyrene, and pregnenolone-16α-carbonitrile on microsomal heme oxygenase and splenic cytochrome P-450. Arch Biochem Biophys 1974;160(1):274-278.

179. Porter TD. The roles of cytochrome b5 in cytochrome P450 reactions. J Biochem Mol Toxicol 2002;16(6):311-316.

180. Ono T, Bloch K. Solubilization and partial characterization of rat liver squalene epoxidase. J Biol Chem 1975;250(4):1571-1579.

181. Ilan Z. Evidence for a new physiological role of hepatic NADPH: ferricytochrome (P-450) oxidoreductase. Direct electron input to the microsomal fatty acid chain elongation system. J Biol Chem 1981;256(19):10066.

182. Gu J, Weng Y, Zhang Q-Y, Cui H, Behr M, Wu L, Yang W, Zhang L, Ding X. Liver-specific Deletion of the NADPH-Cytochrome P450 Reductase Gene. J Biol Chem 2003;278(28):25895-25901.

183. Rimkunas VM, Graham MJ, Crooke RM, Liscum L. TNF-{alpha} plays a role in hepatocyte apoptosis in Niemann-Pick type C liver disease. J Lipid Res 2009;50(2):327-333.

184. Handschin C, Podvinec M, Amherd R, Looser R, Ourlin JC, Meyer UA. Cholesterol and bile acids regulate xenosensor signaling in drug-mediated induction of cytochromes P450. J Biol Chem 2002;277(33):29561-29567.

185. Pascussi JM, Gerbal-Chaloin S, Duret C, Daujat-Chavanieu M, Vilarem MJ, Maurel P. The tangle of nuclear receptors that controls xenobiotic metabolism and transport: crosstalk and consequences. Annu Rev Pharmacol Toxicol 2008;48:1-32.

186. Handschin C, Meyer UA. Induction of drug metabolism: the role of nuclear receptors. Pharmacol Rev 2003;55(4):649-673.

187. Riddick DS, Lee C, Bhathena A, Timsit YE, Cheng PY, Morgan ET, Prough RA, Ripp SL, Miller KK, Jahan A, Chiang JY. Transcriptional suppression of cytochrome P450 genes by endogenous and exogenous chemicals. Drug metabolism and disposition: the biological fate of chemicals 2004;32(4):367-375.

188. Janowski BA, Grogan MJ, Jones SA, Wisely GB, Kliewer SA, Corey EJ, Mangelsdorf DJ. Structural requirements of ligands for the oxysterol liver X receptors LXRalpha and LXRbeta. Proc Natl Acad Sci U S A 1999;96(1):266-271.

189. Janowski BA, Willy PJ, Devi TR, Falck JR, Mangelsdorf DJ. An oxysterol signalling pathway mediated by the nuclear receptor LXR alpha. Nature 1996;383(6602):728-731.

190. Spencer TA, Li D, Russel JS, Collins JL, Bledsoe RK, Consler TG, Moore LB, Galardi CM, McKee DD, Moore JT, Watson MA, Parks DJ, Lambert MH, Willson TM. Pharmacophore analysis of the nuclear oxysterol receptor LXRalpha. J Med Chem 2001;44(6):886-897.

191. Chawla A, Repa JJ, Evans RM, Mangelsdorf DJ. Nuclear receptors and lipid physiology: opening the X-files. Science 2001;294(5548):1866-1870.

192. Amigo L, Mendoza H, Castro J, Quinones V, Miquel JF, Zanlungo S. Relevance of Niemann-Pick type C1 protein expression in controlling plasma cholesterol and biliary lipid secretion in mice. Hepatology 2002;36(4 Pt 1):819-828.

193. Xie C, Turley SD, Dietschy JM. Centripetal cholesterol flow from the extrahepatic organs through the liver is normal in mice with mutated Niemann-Pick type C protein (NPC1). J Lipid Res 2000;41(8):1278-1289.

194. Lim YP, Huang JD. Interplay of pregnane X receptor with other nuclear receptors on gene regulation. Drug metabolism and pharmacokinetics 2008;23(1):14-21.

195. Pacheco CD, Lieberman AP. The pathogenesis of Niemann-Pick type C disease: a role for autophagy? Expert Rev Mol Med 2008;10:e26.

196. Morgan ET. Regulation of cytochromes P450 during inflammation and infection. Drug Metab Rev 1997;29(4):1129-1188.

197. Muntane-Relat J, Ourlin JC, Domergue J, Maurel P. Differential effects of cytokines on the inducible expression of CYP1A1, CYP1A2, and CYP3A4 in human hepatocytes in primary culture. Hepatology 1995;22(4 Pt 1):1143-1153.

198. Morgan ET. Regulation of cytochrome p450 by inflammatory mediators: why and how? Drug Metab Dispos 2001;29(3):207-212.

199. Jackson H, Solaymani-Dodaran M, Card TR, Aithal GP, Logan R, West J. Influence of ursodeoxycholic acid on the mortality and malignancy associated with

primary biliary cirrhosis: a population-based cohort study. Hepatology 2007;46(4):1131-1137.

200. Thapliyal R, Maru GB. Inhibition of cytochrome P450 isozymes by curcumins in vitro and in vivo. Food Chem Toxicol 2001;39(6):541-547.

201. Kearns GL, Abdel-Rahman SM, Alander SW, Blowey DL, Leeder JS, Kauffman RE. Developmental pharmacology--drug disposition, action, and therapy in infants and children. N Engl J Med 2003;349(12):1157-1167.

202. Storch J, Xu Z. Niemann-Pick C2 (NPC2) and intracellular cholesterol trafficking. Biochim Biophys Acta 2009;1791(7):671-678.

203. Platt FM, Neises GR, Dwek RA, Butters TD. N-butyldeoxynojirimycin is a novel inhibitor of glycolipid biosynthesis. J Biol Chem 1994;269(11):8362-8365.

204. Koca SS, Isik A, Ozercan IH, Ustundag B, Evren B, Metin K. Effectiveness of etanercept in bleomycin-induced experimental scleroderma. Rheumatology (Oxford) 2008;47(2):172-175.

205. Deveci F, Muz MH, Ilhan N, Kirkil G, Turgut T, Akpolat N. Evaluation of the anti-inflammatory effect of infliximab in a mouse model of acute asthma. Respirology 2008;13(4):488-497.

206. Priestman DA, van der Spoel AC, Butters TD, Dwek RA, Platt FM. N-butyldeoxynojirimycin causes weight loss as a result of appetite suppression in lean and obese mice. Diabetes, obesity & metabolism 2008;10(2):159-166.

207. Perry VH, Cunningham C, Holmes C. Systemic infections and inflammation affect chronic neurodegeneration. Nat Rev Immunol 2007;7(2):161-167.

208. Jeon KI, Xu X, Aizawa T, Lim JH, Jono H, Kwon DS, Abe J, Berk BC, Li JD, Yan C. Vinpocetine inhibits NF-kappaB-dependent inflammation via an IKK-dependent but PDE-independent mechanism. Proc Natl Acad Sci U S A 2010;107(21):9795-9800.

209. Tabas I, Glass CK. Anti-inflammatory therapy in chronic disease: challenges and opportunities. Science 2013;339(6116):166-172.

210. Tracey D, Klareskog L, Sasso EH, Salfeld JG, Tak PP. Tumor necrosis factor antagonist mechanisms of action: a comprehensive review. Pharmacol Ther 2008;117(2):244-279.

211. Genovese MC, Bathon JM, Fleischmann RM, Moreland LW, Martin RW, Whitmore JB, Tsuji WH, Leff JA. Longterm safety, efficacy, and radiographic outcome with etanercept treatment in patients with early rheumatoid arthritis. J Rheumatol 2005;32(7):1232-1242.

212. Seminerio JL, Loftus EV, Jr., Colombel JF, Thapa P, Sandborn WJ. Infliximab for Crohn's disease: the first 500 patients followed up through 2009. Dig Dis Sci 2013;58(3):797-806.

213. Croft M, Benedict CA, Ware CF. Clinical targeting of the TNF and TNFR superfamilies. Nat Rev Drug Discov 2013;12(2):147-168.

214. Platt FM, Neises GR, Karlsson GB, Dwek RA, Butters TD. N-butyldeoxygalactonojirimycin inhibits glycolipid biosynthesis but does not affect N-linked oligosaccharide processing. J Biol Chem 1994;269(43):27108-27114.

215. Drack AV, Dumitrescu AV, Bhattarai S, Gratie D, Stone EM, Mullins R, Sheffield VC. TUDCA slows retinal degeneration in two different mouse models of retinitis pigmentosa and prevents obesity in Bardet-Biedl syndrome type 1 mice. Invest Ophthalmol Vis Sci 2012;53(1):100-106.

216. Andersson U, Smith D, Jeyakumar M, Butters TD, Borja MC, Dwek RA, Platt FM. Improved outcome of N-butyldeoxygalactonojirimycin-mediated substrate reduction therapy in a mouse model of Sandhoff disease. Neurobiol Dis 2004;16(3):506-515.

217. van Abeelen JHF. Mouse mutants studied by means of ethological methods. Genetica 1964;34(1):270-286.

218. Coleman RJ, Robb SA, Lake BD, Brett EM, Harding AE. The diverse neurological features of Niemann-Pick disease type C: a report of two cases. Mov Disord 1988;3(4):295-299.

219. Maekawa A, Matsushima Y, Onodera H, Shibutani M, Ogasawara H, Kodama Y, Kurokawa Y, Hayashi Y. Long-term toxicity/carcinogenicity of musk xylol in B6C3F1 mice. Food Chem Toxicol 1990;28(8):581-586.

220. Chen J, Dong X, Zhao J, Tang G. In vivo acute toxicity of titanium dioxide nanoparticles to mice after intraperitioneal injection. J Appl Toxicol 2009;29(4):330-337.

221. Fu R, Wassif CA, Yanjanin NM, Watkins-Chow DE, Baxter LL, Incao A, Liscum L, Sidhu R, Firnkes S, Graham M, Ory DS, Porter FD, Pavan WJ. Efficacy of N-acetylcysteine in phenotypic suppression of mouse models of Niemann-Pick disease, type C1. Hum Mol Genet 2013;22(17):3508-3523.

222. McIntyre BA, Philp RB. Effect of three nonsteroidal anti-inflammatory agents on platelet function and prostaglandin synthesis in vitro. Thromb Res 1978;12(1):67-77.

223. Bagoly E, Feher G, Szapary L. The role of vinpocetine in the treatment of cerebrovascular diseases based in human studies. Orv Hetil 2007;148(29):1353-1358.

224. Tamaki N, Kusunoki T, Matsumoto S. The effect of vinpocetine on cerebral blood flow in patients with cerebrovascular disorders. Ther Hung 1985;33(1):13-21.

225. Szobor A, Klein M. Ethyl apovincaminate therapy in neurovascular diseases. Arzneimittelforschung 1976;26(10a):1984-1989.

226. Bonoczk P, Gulyas B, Adam-Vizi V, Nemes A, Karpati E, Kiss B, Kapas M, Szantay C, Koncz I, Zelles T, Vas A. Role of sodium channel inhibition in neuroprotection: effect of vinpocetine. Brain Res Bull 2000;53(3):245-254.

227. Balestreri R, Fontana L, Astengo F. A double-blind placebo controlled evaluation of the safety and efficacy of vinpocetine in the treatment of patients with chronic vascular senile cerebral dysfunction. J Am Geriatr Soc 1987;35(5):425-430.

228. Medina AE. Vinpocetine as a potent antiinflammatory agent. Proc Natl Acad Sci U S A 2010;107(22):9921-9922.

229. Jeyakumar M, Thomas R, Elliot-Smith E, Smith DA, van der Spoel AC, d'Azzo A, Perry VH, Butters TD, Dwek RA, Platt FM. Central nervous system inflammation is a hallmark of pathogenesis in mouse models of GM1 and GM2 gangliosidosis. Brain 2003;126(Pt 4):974-987.

230. Baert F, Noman M, Vermeire S, Van Assche G, G DH, Carbonez A, Rutgeerts P. Influence of immunogenicity on the long-term efficacy of infliximab in Crohn's disease. N Engl J Med 2003;348(7):601-608.

231. Scallon B, Cai A, Solowski N, Rosenberg A, Song XY, Shealy D, Wagner C. Binding and functional comparisons of two types of tumor necrosis factor antagonists. J Pharmacol Exp Ther 2002;301(2):418-426.

232. Kaymakcalan Z, Sakorafas P, Bose S, Scesney S, Xiong L, Hanzatian DK, Salfeld J, Sasso EH. Comparisons of affinities, avidities, and complement activation of adalimumab, infliximab, and etanercept in binding to soluble and membrane tumor necrosis factor. Clin Immunol 2009;131(2):308-316.

233. Marques LJ, Zheng L, Poulakis N, Guzman J, Costabel U. Pentoxifylline inhibits TNF-alpha production from human alveolar macrophages. Am J Respir Crit Care Med 1999;159(2):508-511.

234. Lee SH, Slattery JT. Cytochrome P450 isozymes involved in lisofylline metabolism to pentoxifylline in human liver microsomes. Drug Metab Dispos 1997;25(12):1354-1358.

235. Lobo ED, Hansen RJ, Balthasar JP. Antibody pharmacokinetics and pharmacodynamics. J Pharm Sci 2004;93(11):2645-2668.

236. Tsao N, Hsu HP, Wu CM, Liu CC, Lei HY. Tumour necrosis factor-alpha causes an increase in blood-brain barrier permeability during sepsis. J Med Microbiol 2001;50(9):812-821.

237. Weisman MH. What are the risks of biologic therapy in rheumatoid arthritis? An update on safety. J Rheumatol Suppl 2002;65:33-38.

238. Aggarwal BB, Gupta SC, Sung B. Curcumin: an orally bioavailable blocker of TNF and other pro-inflammatory biomarkers. Br J Pharmacol 2013;169(8):1672-1692.

239. Aggarwal BB, Sung B. Pharmacological basis for the role of curcumin in chronic diseases: an age-old spice with modern targets. Trends Pharmacol Sci 2009;30(2):85-94.

240. Metzler M, Pfeiffer E, Schulz SI, Dempe JS. Curcumin uptake and metabolism. Biofactors 2013;39(1):14-20.

241. Garcea G, Berry DP, Jones DJ, Singh R, Dennison AR, Farmer PB, Sharma RA, Steward WP, Gescher AJ. Consumption of the putative chemopreventive agent curcumin by cancer patients: assessment of curcumin levels in the colorectum and their pharmacodynamic consequences. Cancer Epidemiol Biomarkers Prev 2005;14(1):120-125.

242. Sandur SK, Pandey MK, Sung B, Ahn KS, Murakami A, Sethi G, Limtrakul P, Badmaev V, Aggarwal BB. Curcumin, demethoxycurcumin, bisdemethoxycurcumin, tetrahydrocurcumin and turmerones differentially regulate anti-inflammatory and anti-proliferative responses through a ROS-independent mechanism. Carcinogenesis 2007;28(8):1765-1773.

243. Shoba G, Joy D, Joseph T, Majeed M, Rajendran R, Srinivas PS. Influence of piperine on the pharmacokinetics of curcumin in animals and human volunteers. Planta Med 1998;64(4):353-356.

244. Firozi PF, Aboobaker VS, Bhattacharya RK. Action of curcumin on the cytochrome P450-system catalyzing the activation of aflatoxin B1. Chem Biol Interact 1996;100(1):41-51.

245. Ciolino HP, Daschner PJ, Wang TT, Yeh GC. Effect of curcumin on the aryl hydrocarbon receptor and cytochrome P450 1A1 in MCF-7 human breast carcinoma cells. Biochem Pharmacol 1998;56(2):197-206.

246. Piper JT, Singhal SS, Salameh MS, Torman RT, Awasthi YC, Awasthi S. Mechanisms of anticarcinogenic properties of curcumin: the effect of curcumin on glutathione linked detoxification enzymes in rat liver. Int J Biochem Cell Biol 1998;30(4):445-456.

247. Iersel ML, Ploemen JP, Struik I, van Amersfoort C, Keyzer AE, Schefferlie JG, van Bladeren PJ. Inhibition of glutathione S-transferase activity in human melanoma cells by alpha,beta-unsaturated carbonyl derivatives. Effects of acrolein, cinnamaldehyde, citral, crotonaldehyde, curcumin, ethacrynic acid, and trans-2-hexenal. Chem Biol Interact 1996;102(2):117-132.

248. Oetari S, Sudibyo M, Commandeur JN, Samhoedi R, Vermeulen NP. Effects of curcumin on cytochrome P450 and glutathione S-transferase activities in rat liver. Biochem Pharmacol 1996;51(1):39-45.

249. Lapchak PA, Schubert DR, Maher PA. Delayed treatment with a novel neurotrophic compound reduces behavioral deficits in rabbit ischemic stroke. J Neurochem 2011;116(1):122-131.

250. Liu Y, Dargusch R, Maher P, Schubert D. A broadly neuroprotective derivative of curcumin. J Neurochem 2008;105(4):1336-1345.

251. Lapchak PA. Neuroprotective and neurotrophic curcuminoids to treat stroke: a translational perspective. Expert Opin Investig Drugs 2011;20(1):13-22.

252. Chen Q, Prior M, Dargusch R, Roberts A, Riek R, Eichmann C, Chiruta C, Akaishi T, Abe K, Maher P, Schubert D. A novel neurotrophic drug for cognitive enhancement and Alzheimer's disease. PloS one 2011;6(12):e27865.

253. Yamamoto T, Hirayama A. Effects of soft-diet feeding on synaptic density in the hippocampus and parietal cortex of senescence-accelerated mice. Brain Res 2001;902(2):255-263.

254. Yamamoto T, Hirayama A, Hosoe N, Furube M, Hirano S. Effects of soft-diet feeding on BDNF expression in hippocampus of mice. The Bulletin of Tokyo Dental College 2008;49(4):185-190.

255. Yamamoto T, Hirayama A, Hosoe N, Furube M, Hirano S. Soft-diet feeding inhibits adult neurogenesis in hippocampus of mice. The Bulletin of Tokyo Dental College 2009;50(3):117-124.

256. Fahey JR, Katoh H, Malcolm R, Perez AV. The case for genetic monitoring of mice and rats used in biomedical research. Mamm Genome 2013;24(3-4):89-94.

257. Festing MF. Genetic reliability of commercially-bred laboratory mice. Lab Anim 1974;8(3):265-270.

258. Ferrante RJ. Mouse models of Huntington's disease and methodological considerations for therapeutic trials. Biochim Biophys Acta 2009;1792(6):506-520.

259. Chomarat P, Sipowicz MA, Diwan BA, Fornwald LW, Awasthi YC, Anver MR, Rice JM, Anderson LM, Wild CP. Distinct time courses of increase in cytochromes P450 1A2, 2A5 and glutathione S-transferases during the progressive hepatitis associated with Helicobacter hepaticus. Carcinogenesis 1997;18(11):2179-2190.

260. Boot R, van Herck H, van der Logt J. Mutual viral and bacterial infections after housing rats of various breeders within an experimental unit. Lab Anim 1996;30(1):42-45.

261. Ward JM, Anver MR, Haines DC, Benveniste RE. Chronic active hepatitis in mice caused by Helicobacter hepaticus. Am J Pathol 1994;145(4):959-968.

262. Patten CC, Jr., Myles MH, Franklin CL, Livingston RS. Perturbations in cytokine gene expression after inoculation of C57BL/6 mice with Pasteurella pneumotropica. Comparative medicine 2010;60(1):18-24.

263. Ganey PE, Roth RA. Concurrent inflammation as a determinant of susceptibility to toxicity from xenobiotic agents. Toxicology 2001;169(3):195-208.

264. Vesell ES. Genetic and environmental factors affecting hexobarbital metabolism in mice. Ann N Y Acad Sci 1968;151(2):900-912.

265. Denison MS, Whitlock JP, Jr. Xenobiotic-inducible transcription of cytochrome P450 genes. J Biol Chem 1995;270(31):18175-18178.

266. Song P, Zhang Y, Klaassen CD. Dose-response of five bile acids on serum and liver bile Acid concentrations and hepatotoxicty in mice. Toxicol Sci 2011;123(2):359-367.

267. Paolini M, Pozzetti L, Montagnani M, Potenza G, Sabatini L, Antelli A, Cantelli-Forti G, Roda A. Ursodeoxycholic acid (UDCA) prevents DCA effects on male mouse liver via up-regulation of CYP [correction of CXP] and preservation of BSEP activities. Hepatology 2002;36(2):305-314.

268. Zhang Y, Klaassen CD. Effects of feeding bile acids and a bile acid sequestrant on hepatic bile acid composition in mice. J Lipid Res 2010;51(11):3230-3242.

269. Paumgartner G, Beuers U. Ursodeoxycholic acid in cholestatic liver disease: mechanisms of action and therapeutic use revisited. Hepatology 2002;36(3):525-531.

270. Beuers U, Bilzer M, Chittattu A, Kullak-Ublick GA, Keppler D, Paumgartner G, Dombrowski F. Tauroursodeoxycholic acid inserts the apical conjugate export pump, Mrp2, into canalicular membranes and stimulates organic anion secretion by protein kinase C-dependent mechanisms in cholestatic rat liver. Hepatology 2001;33(5):1206-1216.

271. Baiocchi L, Tisone G, Russo MA, Longhi C, Palmieri G, Volpe A, Almerighi C, Telesca C, Carbone M, Toti L, De Leonardis F, Angelico M. TUDCA prevents cholestasis and canalicular damage induced by ischemia-reperfusion injury in the rat, modulating PKCalpha-ezrin pathway. Transpl Int 2008;21(8):792-800.

272. Rodriguez-Lafrasse C, Rousson R, Valla S, Antignac P, Louisot P, Vanier MT. Modulation of protein kinase C by endogenous sphingosine: inhibition of phorbol dibutyrate binding in Niemann-Pick C fibroblasts. The Biochemical journal 1997;325 (Pt 3):787-791.

273. Fickert P, Zollner G, Fuchsbichler A, Stumptner C, Pojer C, Zenz R, Lammert F, Stieger B, Meier PJ, Zatloukal K, Denk H, Trauner M. Effects of ursodeoxycholic and cholic acid feeding on hepatocellular transporter expression in mouse liver. Gastroenterology 2001;121(1):170-183.

274. Erickson RP, Bhattacharyya A, Hunter RJ, Heidenreich RA, Cherrington NJ. Liver disease with altered bile acid transport in Niemann-Pick C mice on a high-fat, 1% cholesterol diet. American journal of physiology Gastrointestinal and liver physiology 2005;289(2):G300-307.

275. Beuers U, Nathanson MH, Isales CM, Boyer JL. Tauroursodeoxycholic acid stimulates hepatocellular exocytosis and mobilizes extracellular Ca^{++} mechanisms defective in cholestasis. J Clin Invest 1993;92(6):2984-2993.

276. Kurz AK, Graf D, Schmitt M, Vom Dahl S, Haussinger D. Tauroursodesoxycholate-induced choleresis involves p38(MAPK) activation and

translocation of the bile salt export pump in rats. Gastroenterology 2001;121(2):407-419.

277. Brady RO. Emerging strategies for the treatment of hereditary metabolic storage disorders. Rejuvenation research 2006;9(2):237-244.

278. Fischl MA, Resnick L, Coombs R, Kremer AB, Pottage JC, Jr., Fass RJ, Fife KH, Powderly WG, Collier AC, Aspinall RL. The safety and efficacy of combination N-butyl-deoxynojirimycin (SC-48334) and zidovudine in patients with HIV-1 infection and 200-500 CD4 cells/mm3. J Acquir Immune Defic Syndr 1994;7(2):139-147.

279. Williams IM, Wallom KL, Smith DA, Al Eisa N, Smith C, Platt FM. Improved neuroprotection using miglustat, curcumin and ibuprofen as a triple combination therapy in Niemann-Pick disease type C1 mice. Neurobiol Dis 2014;67C:9-17.

280. Xia Z, Rubin I, Whittle B, Gunning P, Hu Y, Brostoff J, Wang W. Smilagenin and its use. Google Patents; 2001.

281. Xia Z, Hu Y, Rubin I, Brostoff J, Whittle B, Wang W, Gunning P. Sarsasapogenin and smilagenin for treating cognitive dysfunctions. Google Patents; 2011.

282. Zhang Y, Xia Z, Hu Y, Orsi A, Rees D. Role of glial cell derived neurotrophic factor in the protective effect of smilagenin on rat mesencephalic dopaminergic neurons damaged by MPP+. FEBS Lett 2008;582(6):956-960.

283. Visanji NP, Orsi A, Johnston TH, Howson PA, Dixon K, Callizot N, Brotchie JM, Rees DD. PYM50028, a novel, orally active, nonpeptide neurotrophic factor inducer, prevents and reverses neuronal damage induced by MPP+ in mesencephalic neurons and by MPTP in a mouse model of Parkinson's disease. FASEB J 2008;22(7):2488-2497.

284. Wessels DH, Grover R, Frend A, Levene S, Potgieter L. A randomised, double blind, placebo controlled single ascending dose study of PYM50018, with an open label cross-over stage to assess food effect. Clin Pharmacol Ther 2005;77(2):P67-P67.

285. Zhang R, Wang Z, Howson PA, Xia Z, Zhou S, Wu E, Xia Z, Hu Y. Smilagenin attenuates beta amyloid (25-35)-induced degeneration of neuronal cells via stimulating the gene expression of brain-derived neurotrophic factor. Neuroscience 2012;210:275-285.

286. Hu Y, Xia Z, Sun Q, Orsi A, Rees D. A new approach to the pharmacological regulation of memory: Sarsasapogenin improves memory by elevating the low muscarinic acetylcholine receptor density in brains of memory-deficit rat models. Brain Res 2005;1060(1-2):26-39.

287. Hu Y, Wang Z, Zhang R, Wu P, Xia Z, Orsi A, Rees D. Regulation of M1-receptor mRNA stability by smilagenin and its significance in improving memory of aged rats. Neurobiol Aging 2010;31(6):1010-1019.

288. Connor B, Dragunow M. The role of neuronal growth factors in neurodegenerative disorders of the human brain. Brain Res Brain Res Rev 1998;27(1):1-39.

289. Rosenblad C, Kirik D, Bjorklund A. Sequential administration of GDNF into the substantia nigra and striatum promotes dopamine neuron survival and axonal sprouting but not striatal reinnervation or functional recovery in the partial 6-OHDA lesion model. Exp Neurol 2000;161(2):503-516.

290. Oiwa Y, Nakai K, Itakura T. Histological effects of intraputaminal infusion of glial cell line-derived neurotrophic factor in Parkinson disease model macaque monkeys. Neurol Med Chir (Tokyo) 2006;46(6):267-275; discussion 275-266.

291. Gill SS, Patel NK, Hotton GR, O'Sullivan K, McCarter R, Bunnage M, Brooks DJ, Svendsen CN, Heywood P. Direct brain infusion of glial cell line-derived neurotrophic factor in Parkinson disease. Nat Med 2003;9(5):589-595.

292. Hu H, Zhang R, Zhang Y, Xia Z, Hu Y. Role of CREB in the regulatory action of sarsasapogenin on muscarinic M1 receptor density during cell aging. FEBS Lett 2010;584(8):1549-1552.

293. Wang YZ, Wang YS, Chu SF, Chen NH, Zhang JT. Protopanaxatriol metabolites identified by LC-MS/MS after oral administration in mice. Int J Clin Pharmacol Ther 2010;48(4):282-290.

294. Flaoyen A, Wilkins AL. Metabolism of saponins from Narthecium ossifragum--a plant implicated in the aetiology of alveld, a hepatogenous photosensitization of sheep. Vet Res Commun 1997;21(5):335-345.

295. Hao M, Zhao Y, Chen P, Huang H, Liu H, Jiang H, Zhang R, Wang H. Structure-activity relationship and substrate-dependent phenomena in effects of ginsenosides on activities of drug-metabolizing P450 enzymes. PloS one 2008;3(7):e2697.

296. Wraith JE, Baumgartner MR, Bembi B, Covanis A, Levade T, Mengel E, Pineda M, Sedel F, Topcu M, Vanier MT, Widner H, Wijburg FA, Patterson MC. Recommendations on the diagnosis and management of Niemann-Pick disease type C. Mol Genet Metab 2009;98(1-2):152-165.

297. Jeyakumar M, Dwek RA, Butters TD, Platt FM. Storage solutions: treating lysosomal disorders of the brain. Nature reviews Neuroscience 2005;6(9):713-725.

298. Neville DC, Coquard V, Priestman DA, te Vruchte DJ, Sillence DJ, Dwek RA, Platt FM, Butters TD. Analysis of fluorescently labeled glycosphingolipid-derived oligosaccharides following ceramide glycanase digestion and anthranilic acid labeling. Anal Biochem 2004;331(2):275-282.

299. Butler JD, Blanchette-Mackie J, Goldin E, O'Neill RR, Carstea G, Roff CF, Patterson MC, Patel S, Comly ME, Cooney A, et al. Progesterone blocks cholesterol translocation from lysosomes. J Biol Chem 1992;267(33):23797-23805.

300. Sarna JR, Larouche M, Marzban H, Sillitoe RV, Rancourt DE, Hawkes R. Patterned Purkinje cell degeneration in mouse models of Niemann-Pick type C disease. J Comp Neurol 2003;456(3):279-291.

301. Holness CL, da Silva RP, Fawcett J, Gordon S, Simmons DL. Macrosialin, a mouse macrophage-restricted glycoprotein, is a member of the lamp/lgp family. J Biol Chem 1993;268(13):9661-9666.

302. Liu Y, Wu YP, Wada R, Neufeld EB, Mullin KA, Howard AC, Pentchev PG, Vanier MT, Suzuki K, Proia RL. Alleviation of neuronal ganglioside storage does not improve the clinical course of the Niemann-Pick C disease mouse. Hum Mol Genet 2000;9(7):1087-1092.

303. Reid PC, Lin S, Vanier MT, Ohno-Iwashita Y, Harwood HJ, Jr., Hickey WF, Chang CC, Chang TY. Partial blockage of sterol biosynthesis with a squalene synthase inhibitor in early postnatal Niemann-Pick type C npcnih null mice brains reduces neuronal cholesterol accumulation, abrogates astrogliosis, but may inhibit myelin maturation. J Neurosci Methods 2008;168(1):15-25.

304. Henderson CE. Role of neurotrophic factors in neuronal development. Curr Opin Neurobiol 1996;6(1):64-70.

305. Kaplan DR, Miller FD. Neurotrophin signal transduction in the nervous system. Curr Opin Neurobiol 2000;10(3):381-391.

306. Lu B. BDNF and activity-dependent synaptic modulation. Learn Mem 2003;10(2):86-98.

307. Lyons WE, Mamounas LA, Ricaurte GA, Coppola V, Reid SW, Bora SH, Wihler C, Koliatsos VE, Tessarollo L. Brain-derived neurotrophic factor-deficient mice develop aggressiveness and hyperphagia in conjunction with brain serotonergic abnormalities. Proc Natl Acad Sci U S A 1999;96(26):15239-15244.

308. Mizoguchi Y, Monji A, Kato T, Seki Y, Gotoh L, Horikawa H, Suzuki SO, Iwaki T, Yonaha M, Hashioka S, Kanba S. Brain-derived neurotrophic factor induces sustained elevation of intracellular Ca2+ in rodent microglia. J Immunol 2009;183(12):7778-7786.

309. Nakajima K, Kikuchi Y, Ikoma E, Honda S, Ishikawa M, Liu Y, Kohsaka S. Neurotrophins regulate the function of cultured microglia. Glia 1998;24(3):272-289.

310. Rocha SM, Cristovao AC, Campos FL, Fonseca CP, Baltazar G. Astrocyte-derived GDNF is a potent inhibitor of microglial activation. Neurobiol Dis 2012;47(3):407-415.

311. Elkabes S, DiCicco-Bloom EM, Black IB. Brain microglia/macrophages express neurotrophins that selectively regulate microglial proliferation and function. J Neurosci 1996;16(8):2508-2521.

312. Nakajima K, Honda S, Tohyama Y, Imai Y, Kohsaka S, Kurihara T. Neurotrophin secretion from cultured microglia. J Neurosci Res 2001;65(4):322-331.

313. Zhang J, Geula C, Lu C, Koziel H, Hatcher LM, Roisen FJ. Neurotrophins regulate proliferation and survival of two microglial cell lines in vitro. Exp Neurol 2003;183(2):469-481.

314. Jiang Y, Wei N, Lu T, Zhu J, Xu G, Liu X. Intranasal brain-derived neurotrophic factor protects brain from ischemic insult via modulating local inflammation in rats. Neuroscience 2011;172:398-405.

315. Gomes C, Ferreira R, George J, Sanches R, Rodrigues DI, Goncalves N, Cunha RA. Activation of microglial cells triggers a release of brain-derived neurotrophic factor (BDNF) inducing their proliferation in an adenosine A2A receptor-dependent manner: A2A receptor blockade prevents BDNF release and proliferation of microglia. Journal of neuroinflammation 2013;10:16.

316. Chen JF, Sonsalla PK, Pedata F, Melani A, Domenici MR, Popoli P, Geiger J, Lopes LV, de Mendonca A. Adenosine A2A receptors and brain injury: broad spectrum of neuroprotection, multifaceted actions and "fine tuning" modulation. Prog Neurobiol 2007;83(5):310-331.

317. Gomes CV, Kaster MP, Tome AR, Agostinho PM, Cunha RA. Adenosine receptors and brain diseases: neuroprotection and neurodegeneration. Biochim Biophys Acta 2011;1808(5):1380-1399.

318. Matsushita Y, Nakajima K, Tohyama Y, Kurihara T, Kohsaka S. Activation of microglia by endotoxin suppresses the secretion of glial cell line-derived neurotrophic factor (GDNF) through the action of protein kinase C alpha (PKCalpha) and mitogen-activated protein kinases (MAPKS). J Neurosci Res 2008;86(9):1959-1971.

319. Batchelor PE, Liberatore GT, Wong JY, Porritt MJ, Frerichs F, Donnan GA, Howells DW. Activated macrophages and microglia induce dopaminergic sprouting in the injured striatum and express brain-derived neurotrophic factor and glial cell line-derived neurotrophic factor. J Neurosci 1999;19(5):1708-1716.

320. Suzuki H, Imai F, Kanno T, Sawada M. Preservation of neurotrophin expression in microglia that migrate into the gerbil's brain across the blood-brain barrier. Neurosci Lett 2001;312(2):95-98.

321. March PA, Thrall MA, Brown DE, Mitchell TW, Lowenthal AC, Walkley SU. GABAergic neuroaxonal dystrophy and other cytopathological alterations in feline Niemann-Pick disease type C. Acta Neuropathol 1997;94(2):164-172.

322. Walkley SU. Cellular pathology of lysosomal storage disorders. Brain Pathol 1998;8(1):175-193.

323. Zervas M, Dobrenis K, Walkley SU. Neurons in Niemann-Pick disease type C accumulate gangliosides as well as unesterified cholesterol and undergo dendritic and axonal alterations. J Neuropathol Exp Neurol 2001;60(1):49-64.

324. German DC, Liang CL, Song T, Yazdani U, Xie C, Dietschy JM. Neurodegeneration in the Niemann-Pick C mouse: glial involvement. Neuroscience 2002;109(3):437-450.

325. German DC, Quintero EM, Liang CL, Ng B, Punia S, Xie C, Dietschy JM. Selective neurodegeneration, without neurofibrillary tangles, in a mouse model of Niemann-Pick C disease. J Comp Neurol 2001;433(3):415-425.

326. Raff MC, Fields KL, Hakomori SI, Mirsky R, Pruss RM, Winter J. Cell-type-specific markers for distinguishing and studying neurons and the major classes of glial cells in culture. Brain Res 1979;174(2):283-308.

327. Zalc B, Monge M, Dupouey P, Hauw JJ, Baumann NA. Immunohistochemical localization of galactosyl and sulfogalactosyl ceramide in the brain of the 30-day-old mouse. Brain Res 1981;211(2):341-354.

328. Baumann N, Pham-Dinh D. Biology of oligodendrocyte and myelin in the mammalian central nervous system. Physiol Rev 2001;81(2):871-927.

329. Marcus J, Popko B. Galactolipids are molecular determinants of myelin development and axo-glial organization. Biochim Biophys Acta 2002;1573(3):406-413.

330. Xie C, Burns DK, Turley SD, Dietschy JM. Cholesterol is sequestered in the brains of mice with Niemann-Pick type C disease but turnover is increased. J Neuropathol Exp Neurol 2000;59(12):1106-1117.

331. Dietschy JM, Turley SD. Cholesterol metabolism in the brain. Curr Opin Lipidol 2001;12(2):105-112.

332. Weintraub H, Abramovici A, Sandbank U, Pentchev PG, Brady RO, Sekine M, Suzuki A, Sela B. Neurological mutation characterized by dysmyelination in NCTR-Balb/C mouse with lysosomal lipid storage disease. J Neurochem 1985;45(3):665-672.

333. Paul CA, Boegle AK, Maue RA. Before the loss: neuronal dysfunction in Niemann-Pick Type C disease. Biochim Biophys Acta 2004;1685(1-3):63-76.

334. Suzuki S, Kiyosue K, Hazama S, Ogura A, Kashihara M, Hara T, Koshimizu H, Kojima M. Brain-derived neurotrophic factor regulates cholesterol metabolism for synapse development. J Neurosci 2007;27(24):6417-6427.

335. Henderson LP, Lin L, Prasad A, Paul CA, Chang TY, Maue RA. Embryonic striatal neurons from niemann-pick type C mice exhibit defects in cholesterol metabolism and neurotrophin responsiveness. J Biol Chem 2000;275(26):20179-20187.

336. Guirland C, Suzuki S, Kojima M, Lu B, Zheng JQ. Lipid rafts mediate chemotropic guidance of nerve growth cones. Neuron 2004;42(1):51-62.

337. Mutoh T, Tokuda A, Miyadai T, Hamaguchi M, Fujiki N. Ganglioside GM1 binds to the Trk protein and regulates receptor function. Proc Natl Acad Sci U S A 1995;92(11):5087-5091.

338. Peiro S, Comella JX, Enrich C, Martin-Zanca D, Rocamora N. PC12 cells have caveolae that contain TrkA. Caveolae-disrupting drugs inhibit nerve growth

factor-induced, but not epidermal growth factor-induced, MAPK phosphorylation. J Biol Chem 2000;275(48):37846-37852.

339. Tansey MG, Baloh RH, Milbrandt J, Johnson EM, Jr. GFRalpha-mediated localization of RET to lipid rafts is required for effective downstream signaling, differentiation, and neuronal survival. Neuron 2000;25(3):611-623.

340. Baumgart DC, Sandborn WJ. Inflammatory bowel disease: clinical aspects and established and evolving therapies. Lancet 2007;369(9573):1641-1657.

341. Lakatos PL. Recent trends in the epidemiology of inflammatory bowel diseases: up or down? World journal of gastroenterology : WJG 2006;12(38):6102-6108.

342. Cosnes J, Gower-Rousseau C, Seksik P, Cortot A. Epidemiology and natural history of inflammatory bowel diseases. Gastroenterology 2011;140(6):1785-1794.

343. Ogunbi SO, Ransom JA, Sullivan K, Schoen BT, Gold BD. Inflammatory bowel disease in African-American children living in Georgia. J Pediatr 1998;133(1):103-107.

344. Matricon J, Barnich N, Ardid D. Immunopathogenesis of inflammatory bowel disease. Self/Nonself 2010;1(4):299-309.

345. Podolsky DK. Inflammatory bowel disease. N Engl J Med 2002;347(6):417-429.

346. Jolliffe DS, Sarkany I. Niemann-Pick type III and Crohn's disease. J R Soc Med 1983;76(4):307-308.

347. Steven LC, Driver CP. Niemann-pick disease type C and Crohn's disease. Scott Med J 2005;50(2):80-81.

348. Heron B, Valayannopoulos V, Baruteau J, Chabrol B, Ogier H, Latour P, Dobbelaere D, Eyer D, Labarthe F, Maurey H, Cuisset JM, de Villemeur TB, Sedel F, Vanier MT. Miglustat therapy in the French cohort of paediatric patients with Niemann-Pick disease type C. Orphanet J Rare Dis 2012;7:36.

349. Lopez ME, Klein AD, Hong J, Dimbil UJ, Scott MP. Neuronal and epithelial cell rescue resolves chronic systemic inflammation in the lipid storage disorder Niemann-Pick C. Hum Mol Genet 2012;21(13):2946-2960.

350. Sagiv Y, Hudspeth K, Mattner J, Schrantz N, Stern RK, Zhou D, Savage PB, Teyton L, Bendelac A. Cutting edge: impaired glycosphingolipid trafficking and NKT cell development in mice lacking Niemann-Pick type C1 protein. J Immunol 2006;177(1):26-30.

351. Ridlon JM, Kang DJ, Hylemon PB. Bile salt biotransformations by human intestinal bacteria. J Lipid Res 2006;47(2):241-259.

352. Batta AK, Salen G, Arora R, Shefer S, Batta M, Person A. Side chain conjugation prevents bacterial 7-dehydroxylation of bile acids. J Biol Chem 1990;265(19):10925-10928.

353. Dawson PA, Lan T, Rao A. Bile acid transporters. J Lipid Res 2009;50(12):2340-2357.

354. Hylemon PB, Zhou H, Pandak WM, Ren S, Gil G, Dent P. Bile acids as regulatory molecules. J Lipid Res 2009;50(8):1509-1520.

355. Greve JW, Gouma DJ, Buurman WA. Bile acids inhibit endotoxin-induced release of tumor necrosis factor by monocytes: an in vitro study. Hepatology 1989;10(4):454-458.

356. Duboc H, Rajca S, Rainteau D, Benarous D, Maubert M-A, Quervain E, Thomas G, Barbu V, Humbert L, Despras G, Bridonneau C, Dumetz F, Grill J-P, Masliah J, Beaugerie L*, et al.* Connecting dysbiosis, bile-acid dysmetabolism and gut inflammation in inflammatory bowel diseases. Gut 2013;62(4):531-539.

357. Wirtz S, Neufert C, Weigmann B, Neurath MF. Chemically induced mouse models of intestinal inflammation. Nat Protoc 2007;2(3):541-546.

358. Wiles S, Clare S, Harker J, Huett A, Young D, Dougan G, Frankel G. Organ specificity, colonization and clearance dynamics in vivo following oral challenges with the murine pathogen Citrobacter rodentium. Cellular microbiology 2004;6(10):963-972.

359. Barthold SW, Osbaldiston GW, Jonas AM. Dietary, bacterial, and host genetic interactions in the pathogenesis of transmissible murine colonic hyperplasia. Lab Anim Sci 1977;27(6):938-945.

360. Ahern PP, Schiering C, Buonocore S, McGeachy MJ, Cua DJ, Maloy KJ, Powrie F. Interleukin-23 drives intestinal inflammation through direct activity on T cells. Immunity 2010;33(2):279-288.

361. Song-Zhao GX, Srinivasan N, Pott J, Baban D, Frankel G, Maloy KJ. Nlrp3 activation in the intestinal epithelium protects against a mucosal pathogen. Mucosal immunology 2013.

362. Jelinek DA, Maghsoodi B, Borbon IA, Hardwick RN, Cherrington NJ, Erickson RP. Genetic variation in the mouse model of Niemann Pick C1 affects female, as well as male, adiposity, and hepatic bile transporters but has indeterminate effects on caveolae. Gene 2012;491(2):128-134.

363. Okayasu I, Hatakeyama S, Yamada M, Ohkusa T, Inagaki Y, Nakaya R. A novel method in the induction of reliable experimental acute and chronic ulcerative colitis in mice. Gastroenterology 1990;98(3):694-702.

364. Mähler M, Bristol IJ, Leiter EH, Workman AE, Birkenmeier EH, Elson CO, Sundberg JP. Differential susceptibility of inbred mouse strains to dextran sulfate sodium-induced colitis. American Journal of Physiology - Gastrointestinal and Liver Physiology 1998;274(3):G544-G551.

365. Morteau O, Morham SG, Sellon R, Dieleman LA, Langenbach R, Smithies O, Sartor RB. Impaired mucosal defense to acute colonic injury in mice lacking cyclooxygenase-1 or cyclooxygenase-2. J Clin Invest 2000;105(4):469-478.

366. Xie C, Turley SD, Pentchev PG, Dietschy JM. Cholesterol balance and metabolism in mice with loss of function of Niemann-Pick C protein. Am J Physiol 1999;276(2 Pt 1):E336-344.

367. Locksley RM, Heinzel FP, Sadick MD, Holaday BJ, Gardner KD, Jr. Murine cutaneous leishmaniasis: susceptibility correlates with differential expansion of helper T-cell subsets. Ann Inst Pasteur Immunol 1987;138(5):744-749.

368. Zheng Y, Valdez PA, Danilenko DM, Hu Y, Sa SM, Gong Q, Abbas AR, Modrusan Z, Ghilardi N, de Sauvage FJ, Ouyang W. Interleukin-22 mediates early host defense against attaching and effacing bacterial pathogens. Nat Med 2008;14(3):282-289.

369. Sonnenberg GF, Monticelli LA, Elloso MM, Fouser LA, Artis D. CD4(+) lymphoid tissue-inducer cells promote innate immunity in the gut. Immunity 2011;34(1):122-134.

370. Ishigame H, Kakuta S, Nagai T, Kadoki M, Nambu A, Komiyama Y, Fujikado N, Tanahashi Y, Akitsu A, Kotaki H, Sudo K, Nakae S, Sasakawa C, Iwakura Y. Differential roles of interleukin-17A and -17F in host defense against mucoepithelial bacterial infection and allergic responses. Immunity 2009;30(1):108-119.

371. Shiomi H, Masuda A, Nishiumi S, Nishida M, Takagawa T, Shiomi Y, Kutsumi H, Blumberg RS, Azuma T, Yoshida M. Gamma interferon produced by antigen-specific CD4+ T cells regulates the mucosal immune responses to Citrobacter rodentium infection. Infect Immun 2010;78(6):2653-2666.

372. Higgins LM, Frankel G, Douce G, Dougan G, MacDonald TT. Citrobacter rodentium infection in mice elicits a mucosal Th1 cytokine response and lesions similar to those in murine inflammatory bowel disease. Infect Immun 1999;67(6):3031-3039.

373. Neurath MF, Fuss I, Pasparakis M, Alexopoulou L, Haralambous S, Meyer zum Buschenfelde KH, Strober W, Kollias G. Predominant pathogenic role of tumor necrosis factor in experimental colitis in mice. Eur J Immunol 1997;27(7):1743-1750.

374. HERMANSKY F, PUDLAK P. Albinism Associated with Hemorrhagic Diathesis and Unusual Pigmented Reticular Cells in the Bone Marrow: Report of Two Cases with Histochemical Studies. Blood 1959;14(2):162-169.

375. Wei ML. Hermansky–Pudlak syndrome: a disease of protein trafficking and organelle function. Pigment Cell Res 2006;19(1):19-42.

376. Di Pietro SM, Dell'Angelica EC. The Cell Biology of Hermansky–Pudlak Syndrome: Recent Advances. Traffic 2005;6(7):525-533.

377. Schinella RA, Greco MA, Cobert BL, Denmark LW, Cox RP. Hermansky-Pudlak Syndrome with Granulomatous Colitis. Ann Intern Med 1980;92(1):20-23.

378. Hussain N, Quezado M, Huizing M, Geho D, White JG, Gahl W, Mannon P. Intestinal disease in Hermansky-Pudlak syndrome: occurrence of colitis and relation to genotype. Clinical gastroenterology and hepatology : the official clinical practice journal of the American Gastroenterological Association 2006;4(1):73-80.

379. Neurath MF, Fuss I, Kelsall BL, Stuber E, Strober W. Antibodies to interleukin 12 abrogate established experimental colitis in mice. J Exp Med 1995;182(5):1281-1290.

380. Boirivant M, Fuss IJ, Chu A, Strober W. Oxazolone colitis: A murine model of T helper cell type 2 colitis treatable with antibodies to interleukin 4. J Exp Med 1998;188(10):1929-1939.

381. Perse M, Cerar A. Dextran sodium sulphate colitis mouse model: traps and tricks. Journal of biomedicine & biotechnology 2012;2012:718617.

382. Moolenbeek C, Ruitenberg EJ. The 'Swiss roll': a simple technique for histological studies of the rodent intestine. Lab Anim 1981;15(1):57-59.

383. Cooper HS, Murthy SN, Shah RS, Sedergran DJ. Clinicopathologic study of dextran sulfate sodium experimental murine colitis. Laboratory investigation; a journal of technical methods and pathology 1993;69(2):238-249.

384. Araki A, Kanai T, Ishikura T, Makita S, Uraushihara K, Iiyama R, Totsuka T, Takeda K, Akira S, Watanabe M. MyD88-deficient mice develop severe intestinal inflammation in dextran sodium sulfate colitis. J Gastroenterol 2005;40(1):16-23.

385. Axelsson LG, Landström E, Goldschmidt TJ, Grönberg A, Bylund-Fellenius AC. Dextran sulfate sodium (DSS) induced experimental colitis in immunodeficient mice: Effects in CD4+-cell depleted, athymic and NK-cell depleted SCID mice. Inflamm Res 1996;45(4):181-191.

386. Barthold SW, Coleman GL, Jacoby RO, Livestone EM, Jonas AM. Transmissible murine colonic hyperplasia. Vet Pathol 1978;15(2):223-236.

387. Luperchio SA, Schauer DB. Molecular pathogenesis of Citrobacter rodentium and transmissible murine colonic hyperplasia. Microbes and infection / Institut Pasteur 2001;3(4):333-340.

388. Mundy R, MacDonald TT, Dougan G, Frankel G, Wiles S. Citrobacter rodentium of mice and man. Cellular microbiology 2005;7(12):1697-1706.

389. Moon HW, Whipp SC, Argenzio RA, Levine MM, Giannella RA. Attaching and effacing activities of rabbit and human enteropathogenic Escherichia coli in pig and rabbit intestines. Infect Immun 1983;41(3):1340-1351.

390. Donnenberg MS, Tzipori S, McKee ML, O'Brien AD, Alroy J, Kaper JB. The role of the eae gene of enterohemorrhagic Escherichia coli in intimate attachment in vitro and in a porcine model. J Clin Invest 1993;92(3):1418-1424.

391. Maaser C, Housley MP, Iimura M, Smith JR, Vallance BA, Finlay BB, Schreiber JR, Varki NM, Kagnoff MF, Eckmann L. Clearance of Citrobacter rodentium requires B cells but not secretory immunoglobulin A (IgA) or IgM antibodies. Infect Immun 2004;72(6):3315-3324.

392. Vallance BA, Deng W, Jacobson K, Finlay BB. Host susceptibility to the attaching and effacing bacterial pathogen Citrobacter rodentium. Infect Immun 2003;71(6):3443-3453.

393. Shen-Tu G, Schauer DB, Jones NL, Sherman PM. Detergent-resistant microdomains mediate activation of host cell signaling in response to attaching-effacing bacteria. Lab Invest 2009;90(2):266-281.

394. Riff JD, Callahan JW, Sherman PM. Cholesterol-Enriched Membrane Microdomains Are Required for Inducing Host Cell Cytoskeleton Rearrangements in Response to Attaching-Effacing Escherichia coli. Infect Immun 2005;73(11):7113-7125.

395. Wirtz S, Neurath MF. Mouse models of inflammatory bowel disease. Advanced Drug Delivery Reviews 2007;59(11):1073-1083.

396. Fitzpatrick LR, Deml L, Hofmann C, Small JS, Groeppel M, Hamm S, Lemstra S, Leban J, Ammendola A. 4SC-101, a novel immunosuppressive drug, inhibits IL-17 and attenuates colitis in two murine models of inflammatory bowel disease. Inflamm Bowel Dis 2010;16(10):1763-1777.

397. Bauer C, Duewell P, Mayer C, Lehr HA, Fitzgerald KA, Dauer M, Tschopp J, Endres S, Latz E, Schnurr M. Colitis induced in mice with dextran sulfate sodium (DSS) is mediated by the NLRP3 inflammasome. Gut 2010;59(9):1192-1199.

398. Bauer C, Loher F, Dauer M, Mayer C, Lehr HA, Schonharting M, Hallwachs R, Endres S, Eigler A. The ICE inhibitor pralnacasan prevents DSS-induced colitis in C57BL/6 mice and suppresses IP-10 mRNA but not TNF-alpha mRNA expression. Dig Dis Sci 2007;52(7):1642-1652.

399. Siegmund B, Lehr HA, Fantuzzi G, Dinarello CA. IL-1 beta -converting enzyme (caspase-1) in intestinal inflammation. Proc Natl Acad Sci U S A 2001;98(23):13249-13254.

400. Sivakumar PV, Westrich GM, Kanaly S, Garka K, Born TL, Derry JM, Viney JL. Interleukin 18 is a primary mediator of the inflammation associated with dextran sulphate sodium induced colitis: blocking interleukin 18 attenuates intestinal damage. Gut 2002;50(6):812-820.

401. Zaki MH, Boyd KL, Vogel P, Kastan MB, Lamkanfi M, Kanneganti T-D. The NLRP3 Inflammasome Protects against Loss of Epithelial Integrity and Mortality during Experimental Colitis. Immunity 2010;32(3):379-391.

402. Dupaul-Chicoine J, Yeretssian G, Doiron K, Bergstrom KS, McIntire CR, LeBlanc PM, Meunier C, Turbide C, Gros P, Beauchemin N, Vallance BA, Saleh M. Control of intestinal homeostasis, colitis, and colitis-associated colorectal cancer by the inflammatory caspases. Immunity 2010;32(3):367-378.

403. Allen IC, TeKippe EM, Woodford RM, Uronis JM, Holl EK, Rogers AB, Herfarth HH, Jobin C, Ting JP. The NLRP3 inflammasome functions as a negative regulator of tumorigenesis during colitis-associated cancer. J Exp Med 2010;207(5):1045-1056.

404. Nordlander S, Pott J, Maloy KJ. NLRC4 expression in intestinal epithelial cells mediates protection against an enteric pathogen. Mucosal immunology 2013.

405. Bercik P, Denou E, Collins J, Jackson W, Lu J, Jury J, Deng Y, Blennerhassett P, Macri J, McCoy KD, Verdu EF, Collins SM. The intestinal microbiota affect central levels of brain-derived neurotropic factor and behavior in mice. Gastroenterology 2011;141(2):599-609, 609 e591-593.

406. Rabin BS, Cohen S, Ganguli R, Lysle DT, Cunnick JE. Bidirectional interaction between the central nervous system and the immune system. Crit Rev Immunol 1989;9(4):279-312.

407. Foster JA, McVey Neufeld KA. Gut-brain axis: how the microbiome influences anxiety and depression. Trends Neurosci 2013;36(5):305-312.

408. Walker JR, Ediger JP, Graff LA, Greenfeld JM, Clara I, Lix L, Rawsthorne P, Miller N, Rogala L, McPhail CM, Bernstein CN. The Manitoba IBD cohort study: a population-based study of the prevalence of lifetime and 12-month anxiety and mood disorders. Am J Gastroenterol 2008;103(8):1989-1997.

409. Sudo N, Chida Y, Aiba Y, Sonoda J, Oyama N, Yu XN, Kubo C, Koga Y. Postnatal microbial colonization programs the hypothalamic-pituitary-adrenal system for stress response in mice. The Journal of physiology 2004;558(Pt 1):263-275.

410. Lyte M, Varcoe JJ, Bailey MT. Anxiogenic effect of subclinical bacterial infection in mice in the absence of overt immune activation. Physiol Behav 1998;65(1):63-68.

411. Collins SM, Surette M, Bercik P. The interplay between the intestinal microbiota and the brain. Nature reviews Microbiology 2012;10(11):735-742.

412. Dinan TG, Cryan JF. Regulation of the stress response by the gut microbiota: implications for psychoneuroendocrinology. Psychoneuroendocrinology 2012;37(9):1369-1378.

413. Hooper LV, Littman DR, Macpherson AJ. Interactions between the microbiota and the immune system. Science 2012;336(6086):1268-1273.

414. Xia P, Wang L, Gamble JR, Vadas MA. Activation of sphingosine kinase by tumor necrosis factor-alpha inhibits apoptosis in human endothelial cells. J Biol Chem 1999;274(48):34499-34505.

415. Snider AJ, Kawamori T, Bradshaw SG, Orr KA, Gilkeson GS, Hannun YA, Obeid LM. A role for sphingosine kinase 1 in dextran sulfate sodium-induced colitis. FASEB J 2009;23(1):143-152.

416. Chumanevich AA, Poudyal D, Cui X, Davis T, Wood PA, Smith CD, Hofseth LJ. Suppression of colitis-driven colon cancer in mice by a novel small molecule inhibitor of sphingosine kinase. Carcinogenesis 2010;31(10):1787-1793.

417. Alvelius G, Hjalmarson O, Griffiths WJ, Bjorkhem I, Sjovall J. Identification of unusual 7-oxygenated bile acid sulfates in a patient with Niemann-Pick disease, type C. J Lipid Res 2001;42(10):1571-1577.

418. Iida T, Kakiyama G, Hibiya Y, Miyata S, Inoue T, Ohno K, Goto T, Mano N, Goto J, Nambara T, Hofmann AF. Chemical synthesis of the 3-sulfooxy-7-N-acetylglucosaminyl-24-amidated conjugates of 3beta,7beta-dihydroxy-5-cholen-24-oic acid, and related compounds: unusual, major metabolites of bile acid in a patient with Niemann-Pick disease type C1. Steroids 2006;71(1):18-29.

419. Devkota S, Wang Y, Musch MW, Leone V, Fehlner-Peach H, Nadimpalli A, Antonopoulos DA, Jabri B, Chang EB. Dietary-fat-induced taurocholic acid promotes pathobiont expansion and colitis in Il10-/- mice. Nature 2012;487(7405):104-108.

420. Lindstedt S, Avigan J, Goodman DS, Sjovall J, Steinberg D. The effect of dietary fat on the turnover of cholic acid and on the composition of the biliary bile acids in man. J Clin Invest 1965;44(11):1754-1765.

421. Sartor RB. Gut microbiota: Diet promotes dysbiosis and colitis in susceptible hosts. Nat Rev Gastroenterol Hepatol 2012;9(10):561-562.

422. Bernstein H, Holubec H, Bernstein C, Ignatenko N, Gerner E, Dvorak K, Besselsen D, Ramsey L, Dall'Agnol M, Ann Blohm-Mangone K, Padilla-Torres J, Cui H, Garewal H, Payne CM. Unique dietary-related mouse model of colitis. Inflamm Bowel Dis 2006;12(4):278-293.

423. Reddy BS. Diet and excretion of bile acids. Cancer Res 1981;41(9 Pt 2):3766-3768.

424. Eckburg PB, Bik EM, Bernstein CN, Purdom E, Dethlefsen L, Sargent M, Gill SR, Nelson KE, Relman DA. Diversity of the human intestinal microbial flora. Science 2005;308(5728):1635-1638.

425. Jones BV, Begley M, Hill C, Gahan CG, Marchesi JR. Functional and comparative metagenomic analysis of bile salt hydrolase activity in the human gut microbiome. Proc Natl Acad Sci U S A 2008;105(36):13580-13585.

426. Sung JY, Shaffer EA, Costerton JW. Antibacterial activity of bile salts against common biliary pathogens. Effects of hydrophobicity of the molecule and in the presence of phospholipids. Dig Dis Sci 1993;38(11):2104-2112.

427. Binder HJ, Filburn B, Floch M. Bile acid inhibition of intestinal anaerobic organisms. Am J Clin Nutr 1975;28(2):119-125.

428. Inagaki T, Moschetta A, Lee YK, Peng L, Zhao G, Downes M, Yu RT, Shelton JM, Richardson JA, Repa JJ, Mangelsdorf DJ, Kliewer SA. Regulation of antibacterial defense in the small intestine by the nuclear bile acid receptor. Proc Natl Acad Sci U S A 2006;103(10):3920-3925.

429. Zheng CJ, Yoo JS, Lee TG, Cho HY, Kim YH, Kim WG. Fatty acid synthesis is a target for antibacterial activity of unsaturated fatty acids. FEBS Lett 2005;579(23):5157-5162.

430. Hofmann AF, Eckmann L. How bile acids confer gut mucosal protection against bacteria. Proc Natl Acad Sci U S A 2006;103(12):4333-4334.

431. Slocum MM, Sittig KM, Specian RD, Deitch EA. Absence of intestinal bile promotes bacterial translocation. Am Surg 1992;58(5):305-310.

432. Macfarlane S, Macfarlane GT. Bacterial diversity in the human gut. Adv Appl Microbiol 2004;54:261-289.

433. Satsangi J, Parkes M, Louis E, Hashimoto L, Kato N, Welsh K, Terwilliger JD, Lathrop GM, Bell JI, Jewell DP. Two stage genome-wide search in inflammatory bowel disease provides evidence for susceptibility loci on chromosomes 3, 7 and 12. Nat Genet 1996;14(2):199-202.

434. Verma N, Ahuja V, Paul J. Profiling of ABC Transporters During Active Ulcerative Colitis and In Vitro Effect of Inflammatory Modulators. Dig Dis Sci 2013;58(8):2282-2292.

435. Tabas I. Macrophage death and defective inflammation resolution in atherosclerosis. Nat Rev Immunol 2010;10(1):36-46.

436. Rezaie A, Parker R, Abdollahi M. Oxidative Stress and Pathogenesis of Inflammatory Bowel Disease: An Epiphenomenon or the Cause? Dig Dis Sci 2007;52(9):2015-2021.

437. Esworthy RS, Aranda R, Martín MG, Doroshow JH, Binder SW, Chu F-F. Mice with combined disruption of Gpx1 andGpx2 genes have colitis. American Journal of Physiology - Gastrointestinal and Liver Physiology 2001;281(3):G848-G855.

438. Oram JF. Tangier disease and ABCA1. Biochim Biophys Acta 2000;1529(1-3):321-330.

439. Karathanasis SK, Oettgen P, Haddad IA, Antonarakis SE. Structure, evolution, and polymorphisms of the human apolipoprotein A4 gene (APOA4). Proc Natl Acad Sci U S A 1986;83(22):8457-8461.

440. Stein O, Stein Y, Lefevre M, Roheim PS. The role of apolipoprotein A-IV in reverse cholesterol transport studied with cultured cells and liposomes derived from an ether analog of phosphatidylcholine. Biochim Biophys Acta 1986;878(1):7-13.

441. Ostos MA, Conconi M, Vergnes L, Baroukh N, Ribalta J, Girona J, Caillaud JM, Ochoa A, Zakin MM. Antioxidative and antiatherosclerotic effects of human

apolipoprotein A-IV in apolipoprotein E-deficient mice. Arterioscler Thromb Vac Biol 2001;21(6):1023-1028.

442. Vowinkel T, Mori M, Krieglstein CF, Russell J, Saijo F, Bharwani S, Turnage RH, Davidson WS, Tso P, Granger DN, Kalogeris TJ. Apolipoprotein A-IV inhibits experimental colitis. J Clin Invest 2004;114(2):260-269.

443. Feng B, Zhang D, Kuriakose G, Devlin CM, Kockx M, Tabas I. Niemann-Pick C heterozygosity confers resistance to lesional necrosis and macrophage apoptosis in murine atherosclerosis. Proceedings of the National Academy of Sciences 2003;100(18):10423-10428.

444. Brown DE, Thrall MA, Walkley SU, Wurzelmann S, Wenger DA, Allison RW, Just CA. Metabolic abnormalities in feline Niemann-Pick type C heterozygotes. J Inherit Metab Dis 1996;19(3):319-330.

445. De Windt A, Rai M, Kytomaki L, Thelen KM, Lutjohann D, Bernier L, Davignon J, Soini J, Pandolfo M, Laaksonen R. Gene set enrichment analyses revealed several affected pathways in Niemann-pick disease type C fibroblasts. DNA Cell Biol 2007;26(9):665-671.

446. Lo Sasso G, Bovenga F, Murzilli S, Salvatore L, Di Tullio G, Martelli N, D'Orazio A, Rainaldi S, Vacca M, Mangia A, Palasciano G, Moschetta A. Liver X receptors inhibit proliferation of human colorectal cancer cells and growth of intestinal tumors in mice. Gastroenterology 2013;144(7):1497-1507, 1507 e1491-1413.

447. Barrett JC, Hansoul S, Nicolae DL, Cho JH, Duerr RH, Rioux JD, Brant SR, Silverberg MS, Taylor KD, Barmada MM, Bitton A, Dassopoulos T, Datta LW, Green T, Griffiths AM*, et al.* Genome-wide association defines more than 30 distinct susceptibility loci for Crohn's disease. Nat Genet 2008;40(8):955-962.

448. Baumgart DC, Sandborn WJ. Crohn's disease. Lancet 2012;380(9853):1590-1605.

449. Okazaki T, Wang MH, Rawsthorne P, Sargent M, Datta LW, Shugart YY, Bernstein CN, Brant SR. Contributions of IBD5, IL23R, ATG16L1, and NOD2 to Crohn's disease risk in a population-based case-control study: evidence of gene-gene interactions. Inflamm Bowel Dis 2008;14(11):1528-1541.

450. Hugot JP, Chamaillard M, Zouali H, Lesage S, Cezard JP, Belaiche J, Almer S, Tysk C, O'Morain CA, Gassull M, Binder V, Finkel Y, Cortot A, Modigliani R, Laurent-Puig P*, et al.* Association of NOD2 leucine-rich repeat variants with susceptibility to Crohn's disease. Nature 2001;411(6837):599-603.

451. Ogura Y, Bonen DK, Inohara N, Nicolae DL, Chen FF, Ramos R, Britton H, Moran T, Karaliuskas R, Duerr RH, Achkar JP, Brant SR, Bayless TM, Kirschner BS, Hanauer SB*, et al.* A frameshift mutation in NOD2 associated with susceptibility to Crohn's disease. Nature 2001;411(6837):603-606.

452. Rioux JD, Daly MJ, Silverberg MS, Lindblad K, Steinhart H, Cohen Z, Delmonte T, Kocher K, Miller K, Guschwan S, Kulbokas EJ, O'Leary S,

Winchester E, Dewar K, Green T*, et al.* Genetic variation in the 5q31 cytokine gene cluster confers susceptibility to Crohn disease. Nat Genet 2001;29(2):223-228.

453. Yamazaki K, McGovern D, Ragoussis J, Paolucci M, Butler H, Jewell D, Cardon L, Takazoe M, Tanaka T, Ichimori T, Saito S, Sekine A, Iida A, Takahashi A, Tsunoda T*, et al.* Single nucleotide polymorphisms in TNFSF15 confer susceptibility to Crohn's disease. Hum Mol Genet 2005;14(22):3499-3506.

454. Hampe J, Franke A, Rosenstiel P, Till A, Teuber M, Huse K, Albrecht M, Mayr G, De La Vega FM, Briggs J, Gunther S, Prescott NJ, Onnie CM, Hasler R, Sipos B*, et al.* A genome-wide association scan of nonsynonymous SNPs identifies a susceptibility variant for Crohn disease in ATG16L1. Nat Genet 2007;39(2):207-211.

455. Parkes M, Barrett JC, Prescott NJ, Tremelling M, Anderson CA, Fisher SA, Roberts RG, Nimmo ER, Cummings FR, Soars D, Drummond H, Lees CW, Khawaja SA, Bagnall R, Burke DA*, et al.* Sequence variants in the autophagy gene IRGM and multiple other replicating loci contribute to Crohn's disease susceptibility. Nat Genet 2007;39(7):830-832.

456. Rioux JD, Xavier RJ, Taylor KD, Silverberg MS, Goyette P, Huett A, Green T, Kuballa P, Barmada MM, Datta LW, Shugart YY, Griffiths AM, Targan SR, Ippoliti AF, Bernard EJ*, et al.* Genome-wide association study identifies new susceptibility loci for Crohn disease and implicates autophagy in disease pathogenesis. Nat Genet 2007;39(5):596-604.

457. Wellcome Trust Case Control C. Genome-wide association study of 14,000 cases of seven common diseases and 3,000 shared controls. Nature 2007;447(7145):661-678.

458. Duerr RH, Taylor KD, Brant SR, Rioux JD, Silverberg MS, Daly MJ, Steinhart AH, Abraham C, Regueiro M, Griffiths A, Dassopoulos T, Bitton A, Yang H, Targan S, Datta LW*, et al.* A genome-wide association study identifies IL23R as an inflammatory bowel disease gene. Science 2006;314(5804):1461-1463.

459. Hampe J, Schreiber S, Shaw SH, Lau KF, Bridger S, Macpherson AJ, Cardon LR, Sakul H, Harris TJ, Buckler A, Hall J, Stokkers P, van Deventer SJ, Nurnberg P, Mirza MM*, et al.* A genomewide analysis provides evidence for novel linkages in inflammatory bowel disease in a large European cohort. Am J Hum Genet 1999;64(3):808-816.

460. Marchiando AM, Ramanan D, Ding Y, Gomez LE, Hubbard-Lucey VM, Maurer K, Wang C, Ziel JW, van Rooijen N, Nunez G, Finlay BB, Mysorekar IU, Cadwell K. A deficiency in the autophagy gene Atg16L1 enhances resistance to enteric bacterial infection. Cell host & microbe 2013;14(2):216-224.

461. Pacheco CD, Kunkel R, Lieberman AP. Autophagy in Niemann-Pick C disease is dependent upon Beclin-1 and responsive to lipid trafficking defects. Hum Mol Genet 2007;16(12):1495-1503.

462. Pacheco CD, Lieberman AP. Lipid trafficking defects increase Beclin-1 and activate autophagy in Niemann-Pick type C disease. Autophagy 2007;3(5):487-489.

463. Inoue J, Nishiumi S, Fujishima Y, Masuda A, Shiomi H, Yamamoto K, Nishida M, Azuma T, Yoshida M. Autophagy in the intestinal epithelium regulates Citrobacter rodentium infection. Arch Biochem Biophys 2012;521(1-2):95-101.

464. Saitoh T, Fujita N, Jang MH, Uematsu S, Yang BG, Satoh T, Omori H, Noda T, Yamamoto N, Komatsu M, Tanaka K, Kawai T, Tsujimura T, Takeuchi O, Yoshimori T*, et al.* Loss of the autophagy protein Atg16L1 enhances endotoxin-induced IL-1beta production. Nature 2008;456(7219):264-268.

465. Wittkopf N, Gunther C, Martini E, Waldner M, Amann KU, Neurath MF, Becker C. Lack of intestinal epithelial atg7 affects paneth cell granule formation but does not compromise immune homeostasis in the gut. Clinical & developmental immunology 2012;2012:278059.

466. Hall LJ, Murphy CT, Hurley G, Quinlan A, Shanahan F, Nally K, Melgar S. Natural killer cells protect against mucosal and systemic infection with the enteric pathogen Citrobacter rodentium. Infect Immun 2013;81(2):460-469.

467. Speak AO, Te Vruchte D, Davis LC, Morgan AJ, Smith DA, Yanjanin NM, Simmons L, Hartung R, Runz H, Mengel E, Beck M, Imrie J, Jacklin E, Wraith JE, Hendriksz C*, et al.* Altered distribution and function of natural killer cells in murine and human Niemann-Pick disease type C1. Blood 2014;123(1):51-60.

468. Kollias G. TNF pathophysiology in murine models of chronic inflammation and autoimmunity. Semin Arthritis Rheum 2005;34(5 Suppl1):3-6.

469. Kontoyiannis D, Pasparakis M, Pizarro TT, Cominelli F, Kollias G. Impaired on/off regulation of TNF biosynthesis in mice lacking TNF AU-rich elements: implications for joint and gut-associated immunopathologies. Immunity 1999;10(3):387-398.

470. Taylor GA, Carballo E, Lee DM, Lai WS, Thompson MJ, Patel DD, Schenkman DI, Gilkeson GS, Broxmeyer HE, Haynes BF, Blackshear PJ. A pathogenetic role for TNF alpha in the syndrome of cachexia, arthritis, and autoimmunity resulting from tristetraprolin (TTP) deficiency. Immunity 1996;4(5):445-454.

471. Phillips K, Kedersha N, Shen L, Blackshear PJ, Anderson P. Arthritis suppressor genes TIA-1 and TTP dampen the expression of tumor necrosis factor alpha, cyclooxygenase 2, and inflammatory arthritis. Proc Natl Acad Sci U S A 2004;101(7):2011-2016.

472. Rimkunas VM, Graham MJ, Crooke RM, Liscum L. In vivo antisense oligonucleotide reduction of NPC1 expression as a novel mouse model for Niemann Pick type C- associated liver disease. Hepatology 2008;47(5):1504-1512.

473. Strober W, Fuss IJ, Blumberg RS. The immunology of mucosal models of inflammation. Annu Rev Immunol 2002;20:495-549.

474. Papadakis KA, Targan SR. Tumor necrosis factor: biology and therapeutic inhibitors. Gastroenterology 2000;119(4):1148-1157.

475. Podolsky DK. Inflammatory bowel disease (1). N Engl J Med 1991;325(13):928-937.

476. Kollias G, Douni E, Kassiotis G, Kontoyiannis D. On the role of tumor necrosis factor and receptors in models of multiorgan failure, rheumatoid arthritis, multiple sclerosis and inflammatory bowel disease. Immunol Rev 1999;169:175-194.

477. Van Deventer SJ. Tumour necrosis factor and Crohn's disease. Gut 1997;40(4):443-448.

478. Piguet PF, Vesin C, Guo J, Donati Y, Barazzone C. TNF-induced enterocyte apoptosis in mice is mediated by the TNF receptor 1 and does not require p53. Eur J Immunol 1998;28(11):3499-3505.

479. Kontoyiannis D, Boulougouris G, Manoloukos M, Armaka M, Apostolaki M, Pizarro T, Kotlyarov A, Forster I, Flavell R, Gaestel M, Tsichlis P, Cominelli F, Kollias G. Genetic dissection of the cellular pathways and signaling mechanisms in modeled tumor necrosis factor-induced Crohn's-like inflammatory bowel disease. J Exp Med 2002;196(12):1563-1574.

480. Steventon GB, Heafield MT, Waring RH, Williams AC. Xenobiotic metabolism in Parkinson's disease. Neurology 1989;39(7):883-887.

481. Steventon GB, Sturman S, Waring RH, Williams AC. A review of xenobiotic metabolism enzymes in Parkinson's disease and motor neuron disease. Drug Metabol Drug Interact 2001;18(2):79-98.

482. Baldassano R, Braegger CP, Escher JC, DeWoody K, Hendricks DF, Keenan GF, Winter HS. Infliximab (REMICADE) therapy in the treatment of pediatric Crohn's disease. Am J Gastroenterol 2003;98(4):833-838.

483. Yang CS, Brady JF, Hong JY. Dietary effects on cytochromes P450, xenobiotic metabolism, and toxicity. FASEB J 1992;6(2):737-744.

484. Sundaram SS, Bove KE, Lovell MA, Sokol RJ. Mechanisms of disease: Inborn errors of bile acid synthesis. Nat Clin Pract Gastroenterol Hepatol 2008;5(8):456-468.

Appendix

Publications of material related to this thesis

Technical advance

Relative acidic compartment volume as a lysosomal storage disorder–associated biomarker

Danielle te Vruchte,[1] Anneliese O. Speak,[1] Kerri L. Wallom,[1] Nada Al Eisa,[1] David A. Smith,[1] Christian J. Hendriksz,[2] Louise Simmons,[2] Robin H. Lachmann,[3] Alison Cousins,[3] Ralf Hartung,[4] Eugen Mengel,[5] Heiko Runz,[4] Michael Beck,[4] Yasmina Amraoui,[4] Jackie Imrie,[6] Elizabeth Jacklin,[6] Kate Riddick,[6] Nicole M. Yanjanin,[7] Christopher A. Wassif,[1,7] Arndt Rolfs,[8] Florian Rimmele,[8] Naomi Wright,[9] Clare Taylor,[9] Uma Ramaswami,[9] Timothy M. Cox,[10] Caroline Hastings,[11] Xuntian Jiang,[12] Rohini Sidhu,[12] Daniel S. Ory,[12] Begona Arias,[13] Mylvaganam Jeyakumar,[1] Daniel J. Sillence,[14] James E. Wraith,[6] Forbes D. Porter,[7] Mario Cortina-Borja,[15] and Frances M. Platt[1]

[1]Department of Pharmacology, University of Oxford, Oxford, United Kingdom. [2]Birmingham Children's Hospital, Birmingham, United Kingdom. [3]National Hospital for Neurology and Neurosurgery, London, United Kingdom. [4]Department of Lysosomal Storage Disorder, Villa Metabolica, Center for Paediatric and Adolescent Medicine, University Medical Center Mainz, Mainz, Germany. [5]Children's Hospital, University of Mainz Medical Centre, Mainz, Germany. [6]Genetic Medicine, St. Mary's Hospital, Manchester, United Kingdom. [7]Eunice Kennedy Shriver National Institute of Child Health and Human Development, NIH, Bethesda, Maryland, USA. [8]Albrecht-Kossel-Institute for Neuroregeneration, University of Rostock, Rostock, Germany. [9]Paediatric Metabolic Unit, Addenbrooke's Hospital, Cambridge, United Kingdom. [10]National Institute for Health Research, University of Cambridge Biomedical Research Centre (Metabolic theme), Cambridge, United Kingdom. [11]Children's Hospital and Research Center, Oakland, California, USA. [12]Washington University School of Medicine, St. Louis, Missouri, USA. [13]Hospital Sanitas la Zarzuela, Madrid, Spain. [14]School of Pharmacy, De Montfort University, Leicester, United Kingdom. [15]MRC Centre of Epidemiology for Child Health, Institute of Child Health, University College London, United Kingdom.

Lysosomal storage disorders (LSDs) occur at a frequency of 1 in every 5,000 live births and are a common cause of pediatric neurodegenerative disease. The relatively small number of patients with LSDs and lack of validated biomarkers are substantial challenges for clinical trial design. Here, we evaluated the use of a commercially available fluorescent probe, Lysotracker, that can be used to measure the relative acidic compartment volume of circulating B cells as a potentially universal biomarker for LSDs. We validated this metric in a mouse model of the LSD Niemann-Pick type C1 disease (NPC1) and in a prospective 5-year international study of NPC patients. Pediatric NPC subjects had elevated acidic compartment volume that correlated with age-adjusted clinical severity and was reduced in response to therapy with miglustat, a European Medicines Agency–approved drug that has been shown to reduce NPC1-associated neuropathology. Measurement of relative acidic compartment volume was also useful for monitoring therapeutic responses of an NPC2 patient after bone marrow transplantation. Furthermore, this metric identified a potential adverse event in NPC1 patients receiving i.v. cyclodextrin therapy. Our data indicate that relative acidic compartment volume may be a useful biomarker to aid diagnosis, clinical monitoring, and evaluation of therapeutic responses in patients with lysosomal disorders.

Introduction

Lysosomal storage disorders (LSDs) are a group of more than 60 inborn errors of metabolism that result in the expansion of the late endosomal/lysosomal (LE/Lys) compartment in cells (1–3). We therefore hypothesized that measuring relative LE/Lys volume could serve as a potentially universal biomarker for this family of disorders. To test this hypothesis, we developed an assay using the fluorescent probe Lysotracker, a weakly basic amine that selectively builds up in the acidic compartment (i.e., LE/Lys). This probe can be visualized and quantified in circulating cells and has previously been reported in a single clinical case study of a patient with adult-onset Niemann-Pick type C disease (NPC) (3). NPC1 is a progressive neurodegenerative LSD caused by mutations in either *NPC1* or *NPC2* (4). Diagnosis of NPC, which is technically challenging, is often delayed. There is currently 1 European Medical Association–approved disease-modifying therapy, miglustat, which is licensed for treating the CNS manifestations of NPC1, combined with symptomatic management (5, 6). At the time of the clinical trial of miglustat, there were no validated biomarkers for NPC that could be used as secondary endpoints in support of clinical data. Recently, oxysterols emerged as the first validated biochemical biomarker for NPC (7, 8).

In this study, we optimized the Lysotracker assay and validated it in a prospective study of more than 100 NPC patients derived from multiple independent clinical cohorts to ensure statistical power. We used this disorder as proof of concept for its use in other LSDs, due to the relatively large number of patients available to study with this specific lysosomal disorder. We applied this

Authorship note: Danielle te Vruchte and Anneliese O. Speak contributed equally to this work. James E. Wraith is deceased.

Conflict of interest: Michael Beck receives unrestricted grants, travel support, and honoraria from Genzyme, Shire, Biomarin, and Actelion. Forbes D. Porter receives speaker honoraria, consultancy, and unrestricted grants from Actelion. Christian J. Hendriksz receives unrestricted grants, research agreements, travel support, and/or honoraria from Genzyme, Shire, Biomarin, Synegeva, GlaxoSmithKline, Amicus, and Actelion. Eugen Mengel and Frances M. Platt receive speaker fees, research grants, and consultant fees from Actelion.

Citation for this article: *J Clin Invest.* 2014;124(3):1320–1328. doi:10.1172/JCI72835.

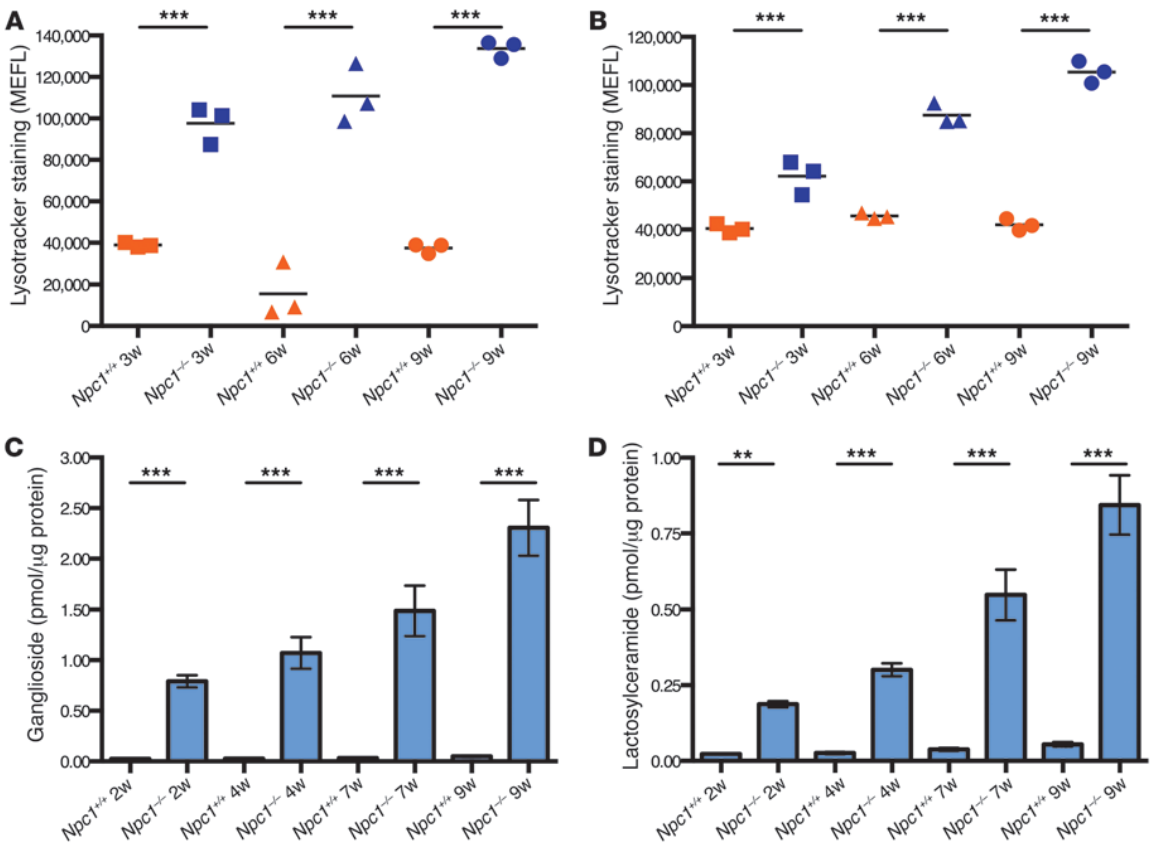

Figure 1

Relative LE/Lys volume increases progressively in B cells in a mouse model of NPC1 disease and parallels the rate of GSL storage in the brain. (**A** and **B**) Splenic (**A**) and circulating (**B**) B cells were analyzed by flow cytometry over the lifespan of the *Npc1*$^{-/-}$ mouse (3 weeks, presymptomatic; 6 weeks, early symptomatic; 9 weeks, late symptomatic) and compared with wild-type *Npc1*$^{+/+}$ controls. A pan–B cell marker was detected using an anti-CD19 monoclonal antibody conjugated to PE, and cells were costained with Lysotracker green. Analysis was performed on gated B cells (CD19^{+}), and Lysotracker staining levels were standardized to fluorescent microbeads conjugated to defined numbers of fluorescent molecules/bead to linearize the logarithmic data collected by the cytometer. There was progressive elevation in B cell MEFL at each time point relative to the previous age point ($P < 0.01$, spleen, all ages, and blood, 6 and 9 weeks). (**C** and **D**) GSL analysis, performed by HPLC, of GM2 ganglioside (**C**) and lactosylceramide (**D**) in the forebrain of 2-, 4-, 7-, and 9-week-old *Npc1*$^{-/-}$ mice compared with wild-type controls. $^{**}P < 0.01$; $^{***}P < 0.001$.

assay to small, resting, circulating B cells because they can readily be identified as a uniform population using the CD19 marker and do not change in response to infection. Circulating B cells are therefore a suitable cell type to analyze in longitudinal studies. We found here that this biomarker correlated with age-adjusted clinical severity scores and was responsive to miglustat therapy. It also correlated with levels of oxysterol (an NPC-specific biochemical biomarker; ref. 7) in the same patient samples. This biomarker also showed utility in monitoring response to bone marrow transplantation (BMT) in an NPC2 patient and identified an unanticipated adverse event in NPC patients receiving cyclodextrin therapy with i.v. 2-hydroxypropyl-β-cyclodextrin (HPβCD). Taken together, our data support the use of this biomarker in clinical monitoring of NPC. In addition, this assay has the potential to be a universal monitoring tool for any disease with lysosomal hypertrophy.

Results

Assay validation in a mouse model. We first validated the assay in resting B cells (splenic and circulating) from *Npc1*$^{-/-}$ mutant mice using the minimal group size to provide statistically valid results with enough power (in this case, 3 mice per group per time point). We quantified Lysotracker fluorescence — calibrated using fluorescent microbead standards and expressed as mean equivalent of fluorescence (MEFL) — and observed a progressive increase in relative acidic compartment volume (Figure 1, A and B). This expansion of LE/Lys was seen at all ages compared with age-matched controls and was highly significant at each time point in both splenic and circulating B cells ($P < 0.001$). We have previously shown that B cells from *Npc1*$^{-/-}$ store high levels of glycosphingolipids (GSLs) when measured by HPLC (9). A key finding was that peripheral B cell storage, as indicated by MEFL, paralleled progressive ganglioside and lactosylceramide storage in the brain, as measured by HPLC (Figure 1, C and D), which indicates that the rate of storage in B cells in the periphery parallels storage in the CNS. The probe LipidTOX, which detects phospholipid storage, detected phospholipids in control and *Npc1*$^{-/-}$ B cells, but did not show enhanced staining in *Npc1*$^{-/-}$ relative to wild-type B cells (Supplemental Figure 1B; supplemental material available online with this article; doi:10.1172/JCI72835DS1), and thus was not further evaluated.

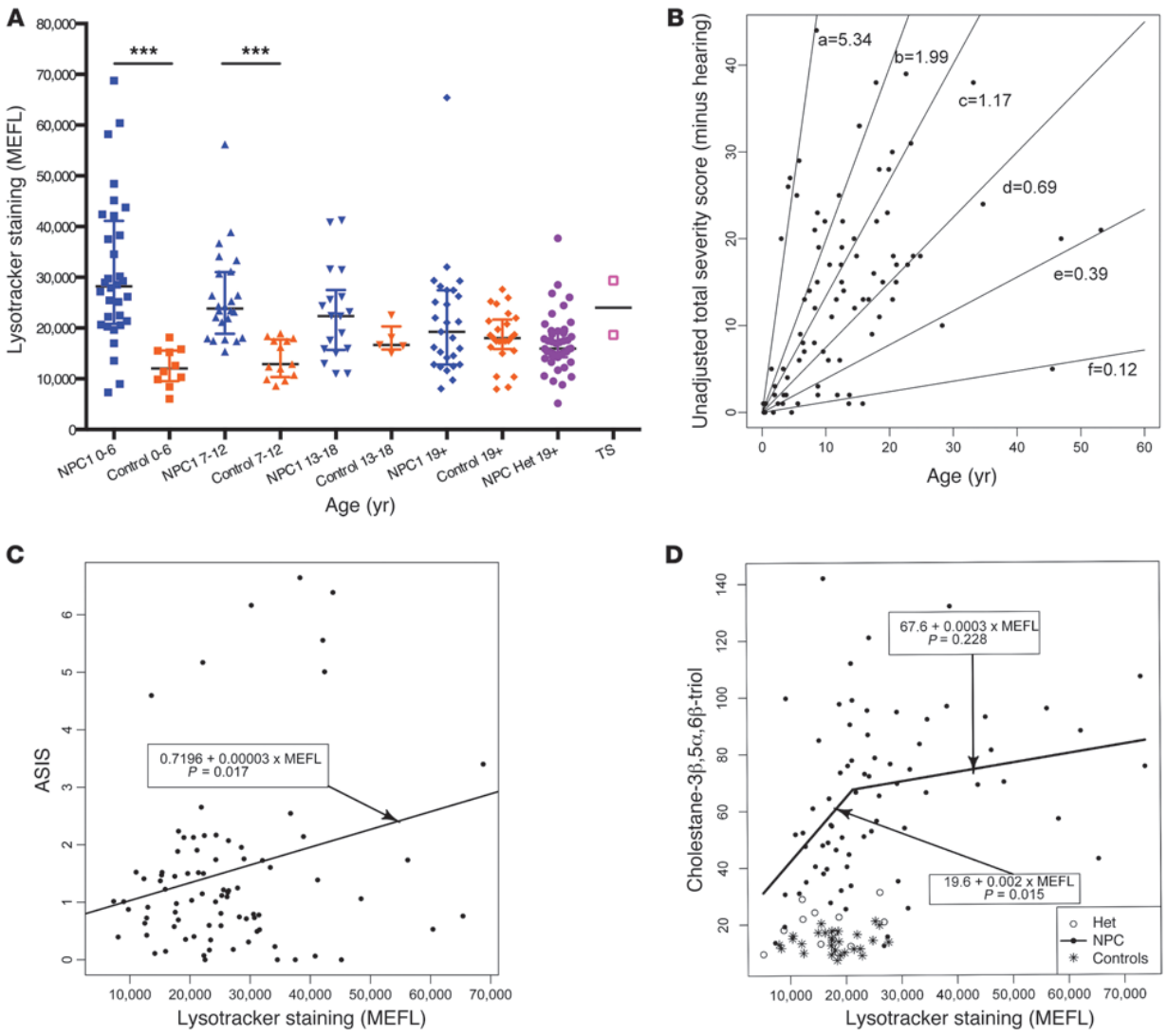

Figure 2

Relative LE/Lys volume identifies pediatric patients with NPC1 disease. Data were collected prospectively on NPC1 patients (n = 97, aged 2 months to 53 years), heterozygous carriers (NPC Het; n = 40, aged 23 to 76 years), age-matched controls (n = 53, aged 4 months to 64 years), and 2 pediatric patients with Tay-Sachs disease (TS). (**A**) Lysotracker values from circulating B cells were measured by flow cytometry and plotted against patient age. Each patient only appears once, standardized to the first sample analyzed for each patient. ***P < 0.01. (**B**) When the same patients' data were plotted as unadjusted severity score (with higher value denoting greater disease burden) against age, multiple subgroups were identified. These were designated according to decreasing severity, from the severest (subgroup a) to the mildest (subgroup f). Rate of change per year is indicated for each subgroup. (**C**) Total severity score (without hearing, as this was not measured by all clinical centers) for each patient was divided by patient age to generate ASIS. When plotted against MEFL, a statistically significant correlation was found (P = 0.017). (**D**) When each patient's plasma cholestane-3β,5α,6β-triol level was plotted against their MEFL value, a statistically significant correlation was observed in all patients (P < 0.01). A piecewise linear model significantly improved the goodness-of-fit with respect to a single linear model (P < 0.001); in this model, the initial slope was significant (P = 0.015), and the second was not (P = 0.228), with the estimated change point being 21,269 MEFL.

Assay validation in patient blood samples. The Lysotracker assay was then applied to peripheral blood B cells from NPC patients. Although this assay would in practice be used for monitoring individual patients over time, we had the opportunity here to evaluate this biomarker at the population level. We found that MEFL values were significantly elevated in B cells from the majority of pediatric NPC1 patients (aged 0–12 years; P < 0.001; Figure 2A); only 4 cases in the 0–6 year age range and 6 cases in the 7–12 year age range overlapped with control values. 2 infantile Tay-Sachs disease patients also had elevated levels of MEFL above the age-matched control range. The youngest NPC1 subjects with significant clinical manifestations had the highest MEFL values (P < 0.05, 0–6 years vs. 13–18 years; P < 0.01, 0–6 years vs. ≥19 years). In contrast, the adult NPC1 patients (with later onset and slower disease progression) and the heterozygous carriers did not differ significantly from age-matched controls at the population level (Figure 2A).

Characterization of the study cohort. To better characterize the study cohort, clinical severity scores (for which higher scores denote

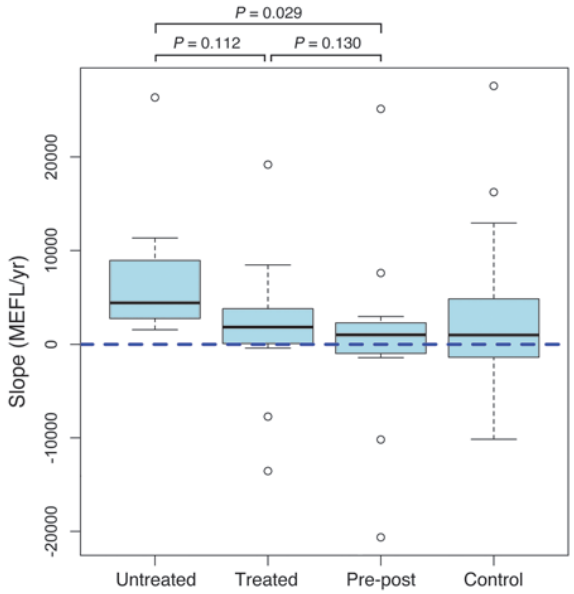

Figure 3
Miglustat treatment reduces lysosomal storage in NPC1 patients' B cells. Box plots summarizing progression of storage for untreated ($n = 7$), chronic miglustat ($n = 17$), and pre-post miglustat ($n = 14$) patient groups as well as adult controls ($n = 14$) analyzed over time. The box is limited by the 1st and 3rd quartiles (Q1 and Q3), and the median is indicated by a bar inside the box; whiskers and outliers are defined in terms of 2 unmarked boundaries defined using Tukey's rule as Q1 – 1.5 IQR and Q3 + 1.5 IQR (IQR, interquartile range, i.e., Q3 – Q1). Whiskers extend to the smallest and largest observed values within the boundaries, and outliers are defined as points outside the boundaries. Adjusted pairwise multiple comparisons are shown (Wilcoxon-Mann-Whitney test). See Table 1 and Supplemental Figure 7.

increasing severity; ref. 10) were plotted against patient age. Hearing was excluded, as it was not measured in all clinical centers. There was no simple linear or nonlinear model that adequately represented the complete data distribution (Supplemental Figure 2). We therefore looked for discrete subpopulations of patients and identified 6 subgroups (denoted a–f), with subgroups b, c, and d defined by latent class mixture modeling (Figure 2B). The study cohort included miglustat-treated patients, which were represented in all 6 subgroups (Supplemental Figures 3 and 4). Seizures are a common feature in the most severely affected patients; consistent with this, patients with seizures were almost exclusively present in subgroups a–c (Supplemental Figure 5). When a small number of untreated patients were plotted longitudinally, they remained within the same subgroup (Supplemental Figure 6), which suggests that these subgroups may have prognostic value. When MEFL values were plotted against total clinical severity score, no significant correlation was observed in the group as a whole or in subgroups a–f (data not shown). As disease progression has been reported to be linear in NPC disease (10), and different patients achieved their severity scores over variable numbers of years (Figure 2B), total severity scores were divided by age to give an annual severity increment score (ASIS). When ASIS was plotted against MEFL, a significant correlation was observed for the total NPC1 population ($P = 0.017$; Figure 2C), but not after stratifying by latent subgroups a–f, as these were individually underpowered (data not shown).

Relationship to oxysterols. Oxysterols have been validated as NPC-specific biochemical biomarkers (7, 8). We therefore measured cholestane-3β,5α,6β-triol and MEFL in matched plasmas and found a significant correlation in NPC1 patients ($P = 0.015$), but not in controls or heterozygous carriers (Figure 2D).

Response to treatment with miglustat. Longitudinal data were collected on 38 patients that were untreated, chronically treated with miglustat (>6 months; ref. 5), or analyzed both before and after miglustat therapy, with the first point being pretreatment (referred to herein as pre-post analysis) (Table 1). There were no significant differences in median ages for the 3 groups ($P = 0.09$). Of the untreated patients, 86% had positive slopes (progression of storage), compared with 71% in the chronically miglustat-treated group and 43% in the pre-post group (Table 1 and Figure 3). Untreated adult controls (variable MEFL values) with repeat measures were analyzed, and no significant slopes were detected (Figure 3 and Supplemental Figure 7).

Response to BMT in an NPC2 patient. An NPC2 patient was analyzed before and after BMT. Prior to BMT (and before immunosuppressive conditioning), the patient's MEFL value approximated the

Table 1
Miglustat treatment slows the rate of storage in NPC1 patients

Treatment and clinical status	Median age at first measurement (yr)	Subjects analyzed (*n*)	Positive slope (*n*)	Negative slope (*n*)	No slope (*n*)	Median slope (MEFL/yr)
NPC1 untreated	9.8	7	6	0	1	4,436
NPC1 chronic miglustat	10.9	17	12	3	2	1,849[A]
NPC1 pre-post miglustat	9.5	14	6	4	4	1,010[B,C]
Untreated adult controls	43.0	14	6	4	4	998

There was no significant difference in the median ages for the 3 NPC1 patient groups ($P = 0.65$, Kruskal-Wallis test). Ages were not available for all adult controls, but were >18 and <65 years; median based on $n = 6$. Slopes were calculated from each patient's longitudinal data, based on ≥2 repeat measures (untreated, 2–4; pre-post, 2–5; chronic miglustat, 2–6) over time up to 3.0 years (median, last measurement up to 10.92 months after first sample analyzed). Given the small number of repeat measurements, rather than calculating a P value for each individual slope, subjects with a ±10% difference between first and last MEFL were defined as stable (no slope). A logistic regression model showed a significant difference between the proportion of positive slopes (NPC1 untreated, 86%; NPC1 chronic miglustat, 71%; NPC1 pre-post miglustat, 43%) and nonpositive slopes between the untreated and pre-post groups ($P = 0.05$). Overall, median slopes from the 3 patient groups were significantly not homogeneous ($P = 0.03$, Kruskal-Wallis test). [A]$P = 0.11$ vs. untreated; [B]$P = 0.029$ vs. untreated; [C]$P = 0.13$ vs. treated; Wilcoxon-Mann-Whitney tests with Benjamini-Hochberg correction for multiple comparisons.

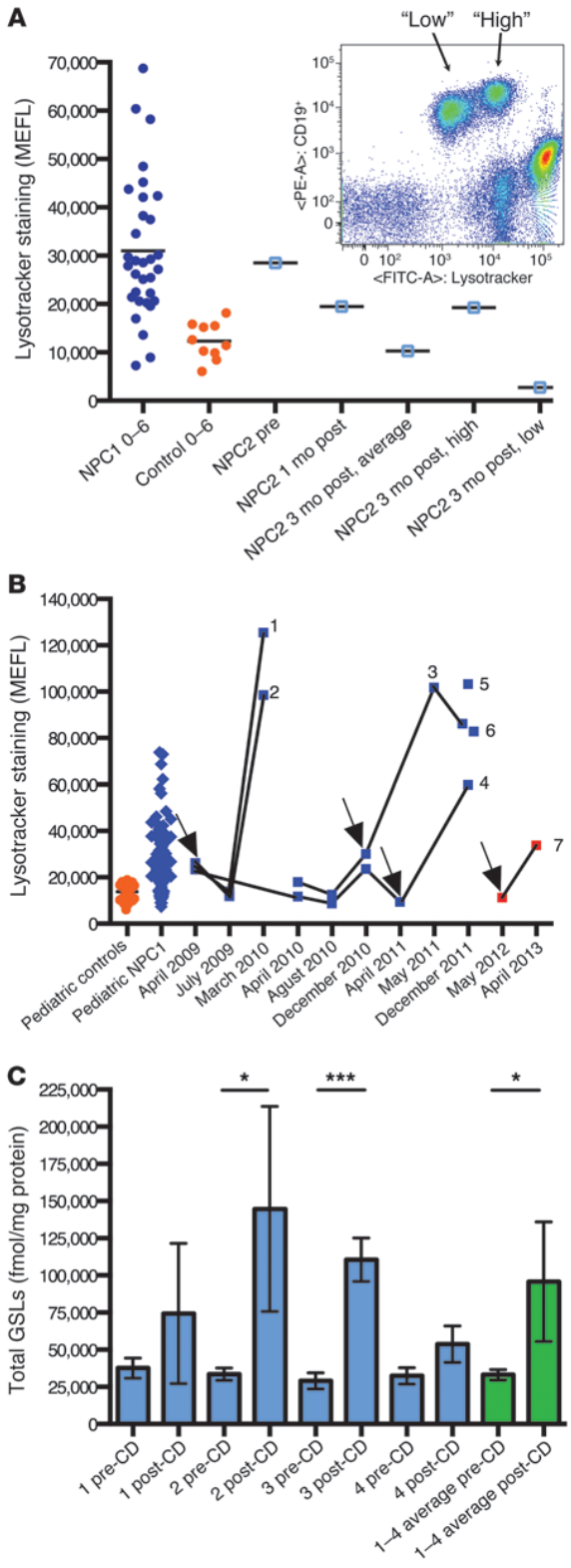

Figure 4

Relative LE/Lys volume is a sensitive measure of response and potentially adverse response to NPC disease therapeutics. (**A**) Pre-post analysis of an NPC2 patient with BMT, using Lysotracker analysis of circulating B cells. MEFL was reduced 1 month after BMT, and by 3 months was within the pediatric control range. At 3 months after BMT, donor chimerism developed and was detected by the presence of 2 B cell populations (inset; gated on mononuclear cells). The populations had high or low Lysotracker fluorescence, with a 50:50 distribution of B cells between the 2 populations. HLA typing confirmed the development of 50% donor chimerism (not shown). (**B**) 7 patients on HPβCD therapy (individual use INDs) were analyzed. Patients 1–4 were analyzed pre-post i.v. HPβCD (arrows denote therapy initiation points), patients 5 and 6 were analyzed after HPβCD only, and patient 7 was analyzed pre-post intrathecal HPβCD delivery (no i.v. administration throughout the treatment period). (**C**) B cells isolated from the blood of patients 1–4 were analyzed to determine their levels of GSL storage. Total GSL levels were compared before and after HPβCD delivery for each patient and plotted individually (blue; error bars derived from 3 independent HPLC analytical runs of the same samples). An average of the 4 patients was also plotted (green; error bars derived from the mean values for each patient). $^{*}P < 0.05$; $^{***}P < 0.001$.

average for NPC1 patients of a similar age (Figure 4A). At 1 month after BMT, the B cell MEFL was reduced, and by 3 months after BMT, it had moved into the control range (Figure 4A), suggestive of cross correction and/or cell replacement with donor cells. At this point, 2 equally abundant (50:50) subpopulations of B cells were detected, which were classified as high or low MEFL staining (Figure 4A). This coincided with the development of 50% donor chimerism, based on human leukocyte analysis (data not shown).

Unanticipated potential adverse response to HPβCD treatment. Finally, we investigated the effects of HPβCD therapy on B cell MEFL, both pre-post i.v. HPβCD therapy in 4 pediatric NPC1 patients (patients 1–4) and after i.v. HPβCD therapy in 2 additional individuals (patients 5 and 6); all 6 were being treated under individual patient Investigational New Drug (IND) provisions (Figure 4B). In patients 1–4, pre-post analysis showed a dramatic increase in B cell MEFL values in response to HPβCD treatment, with patients 1–3 exceeding the NPC patient range. Analysis of patients 5 and 6 after HPβCD therapy showed MEFL values similar to those of patients 1–3. In patients 1–4, B cells were isolated, and all 4 had increased levels of GSL storage after HPβCD treatment (Figure 4C). We also analyzed a single patient pre-post approximately 1 year of intrathecal HPβCD therapy (patient 7). Despite being well managed on miglustat, with a MEFL value in the normal pediatric range prior to intrathecal HPβCD treatment, patient 7 also showed increased MEFL values in response to HPβCD, albeit not as great as those in patients 1–6 with i.v. administration (Figure 4B).

Discussion

In addition to disease-specific biomarkers (7), it would be useful to have a general biomarker for measuring the degree of storage in all lysosomal disorders, regardless of the biochemical nature of the stored macromolecule(s). We therefore selected the probe Lysotracker to study, as it measures relative acidic compartment volume in live cells. An increased Lysotracker value could reflect lysosome enlargement, increased number of lysosomes, or both.

We first validated this assay in *Npc1*$^{-/-}$ mutant mice and found that the rate of storage in the brain and circulating B cells mirrored each other; thus, measuring storage in circulating B cells is a suitable surrogate for measuring progression of storage in the brain. This suggests that although absolute amounts of lipid storage differ in different cell types in NPC, the rate of storage is similar in

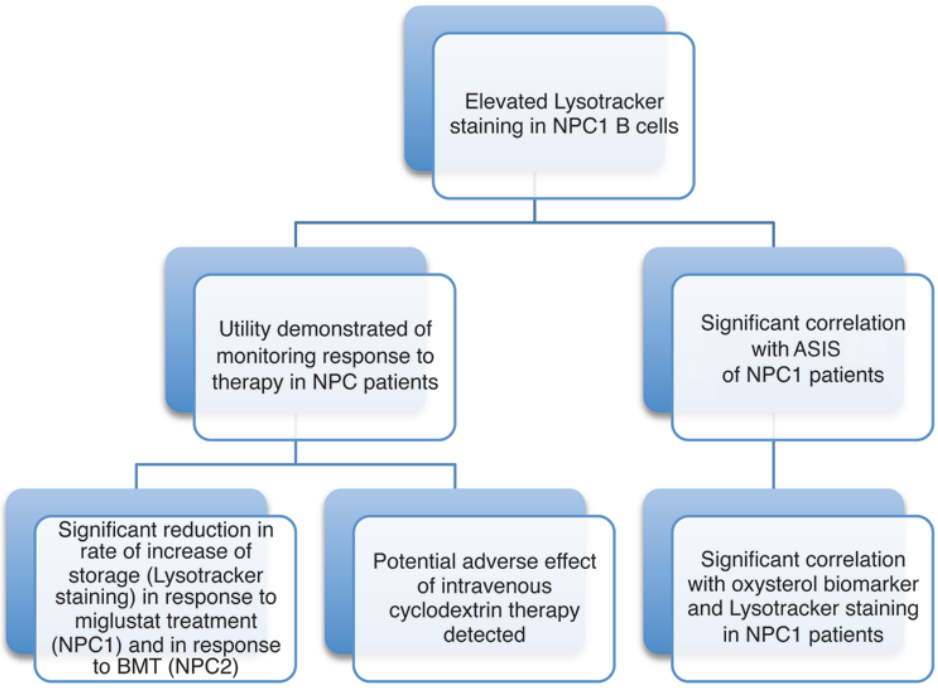

Figure 5
Summary of major findings in the study.

different tissues as disease progresses, so the use of peripheral biomarkers is still informative and also minimally invasive for patients.

We then applied this assay to a multicenter, international prospective study of 106 NPC patients, spanning a 5-year period. To our knowledge, this is the largest prospective study ever undertaken in a neurodegenerative lysosomal disorder. Typically, biomarker validation involves analysis of multiple independent clinical cohorts, each of sufficient size to provide sufficient statistical power, in order to draw conclusions about the biomarker's practical utility. In the case of a rare lysosomal disease such as NPC, this is clearly not possible, due to small patient numbers. Instead, we combined patients from 3 independent clinical cohorts from 3 countries to sufficiently power this study. Although this biomarker would be used in practice at the individual patient level, in the present study we began with population-based analysis to define the study cohort. We found that the clinical severity of the total NPC study cohort spanned the severity range, and additionally revealed 6 discrete subgroups with differential rates of disease progression. Individual untreated patients longitudinally tracked an individual subgroup, which suggests that simply plotting total severity against age may have prognostic value, particularly in patients older than 5 years.

At the population level, the clear finding was that pediatric NPC patients had significantly elevated levels of Lysotracker staining in circulating B cells, minimally overlapping those of age-matched controls. Similar findings were made in 2 18-month-old Tay-Sachs disease patients compared with pediatric controls 0–6 years of age. As lysosomal hypertrophy is a universal feature of LSDs, it is logical to hypothesize, based on our data in more than 100 NPC1 patients and 2 Tay-Sachs patients, that relative LE/Lys volume could represent a universal biomarker for lysosomal disorders. The trend in NPC1 patients was for older patients to have lower average MEFL values at the population level than pediatric NPC1 patients, implying a milder disease burden in older patients, as might be predicted. In contrast, the controls had a very tight distribution in pediatric individuals, which broadened over time to a diverse range of values in the adult group. This may suggest that some individuals develop impaired lysosomal flux as they age, leading to an expansion of the lysosomal system. There was no simple age relationship, which suggests that this is not an inevitable consequence of aging. Alternatively, an expanded lysosomal system in some adults in the general population may reflect an increased rate of substrate flux through the lysosomal compartment. This unexpected observation merits further investigation in the general population in order to better understand its basis and potential clinical significance.

However, the Lysotracker assay was useful in adults for monitoring individual changes over time, with patients serving as their own controls (Table 1 and ref. 3). As the biomarker would be used in clinical practice for monitoring individual patients over time, not for population-based studies, this underscores its practical utility. When Lysotracker was compared with the NPC disease-specific oxysterol biochemical biomarker, there was a significant correlation with patients with lower MEFL values. Interestingly, a subset of patients with very high Lysotracker values did not have the predicted high level of triol species (assuming a linear relationship), suggestive of potentially attenuated oxidative stress responses in these individuals and highlighting the need to use multiple biomarkers in NPC. Control and heterozygous carriers could be distinguished on the basis of mildly elevated oxysterol levels, whereas Lysotracker values overlapped between these 2 genotypes.

We calculated ASIS and found it to be significantly correlated with relative lysosomal volume. Scoring with ASIS may also represent a simple tool for stratifying patients for clinical trials or for monitoring disease progression. As the severity score used to calculate ASIS is derived from multiple neurological clinical measures (10), these data, in agreement with our findings in the *Npc1*$^{-/-}$ mouse (Figure 1), are suggestive of an association between storage in the CNS and in the hematopoietic system. Therefore, monitoring B cell lysosomal volume is a valid minimally invasive surrogate for storage levels in the CNS in NPC. These data also suggest that human B cell progenitors store progressively, such that this is reflected in the mature circulating B cell population, as the half-life of B cells in the blood is only 36 days (11). Most untreated NPC patients had increased relative lysosomal volumes over time, but significant decreases were observed in the miglustat-treated groups, consistent with miglustat stabilizing/slowing the

rate of disease progression in NPC1 patients (5, 12–14). Patients in whom pre-post analysis was performed exhibited the most marked decrease in storage, relative to the chronically miglustat treated group, which was relatively stable at the initiation of the study.

We also investigated the effects of 2 experimental therapies on this biomarker. NPC2 constitutes 5% of NPC cases (15) and is appropriate for BMT, as the NPC2 protein is a soluble, mannose-6-phosphorylated protein amenable to secretion/recapture cross-correction (16, 17). The efficacy of BMT was recently reported in an NPC2 patient (18). We therefore monitored an NPC2 patient pre-post BMT, and this biomarker revealed reduced storage in peripheral B cells after BMT (cross-correction at the early time point) and detected donor chimerism at 3 months after BMT. Before BMT, the patient was declining, with symptoms of respiratory compromise, ataxia, and slowed development of speech. After BMT, these symptoms improved, preceded by reduced Lysotracker staining. When symptoms returned and repeat transplant was under consideration, Lysotracker values increased before the onset of clinical deterioration, which suggests that this may be a sensitive biomarker for NPC2 disease.

HPβCD is an experimental drug that has shown benefit in mouse and feline models of NPC1 (19, 20), potentially by stimulating lysosomal exocytosis, which has been demonstrated in vitro (21). There are currently 10 NPC1 patients worldwide undergoing i.v. HPβCD therapy, of which 7 were included in this study. Patients previously treated with miglustat (patients 1–4 and 7; ref. 5) had reduced MEFL values, close to or within the normal range, prior to initiation of HPβCD therapy. Paradoxically, after HPβCD therapy, there was a pronounced increase in B cell Lysotracker fluorescence. Patients 1–6, with i.v. exposure to the drug, developed elevated MEFL values that were similar to one another; all but 1 were above the upper limit of the general NPC1 patient population. Patient 7 never received HPβCD i.v.; the drug was only administered intrathecally. However, even this individual showed elevated MEFL values after approximately 1 year of HPβCD treatment. The magnitude of this increase was less than in patients receiving i.v. HPβCD. These data suggest that intrathecal HPβCD treatment resulted in exchange of HPβCD into the peripheral circulation, which was sufficient to lead to an increase in B cell MEFL values. This assay may serve as a useful surrogate of systemic exposure to HPβCD treatment, regardless of the route of administration. We then investigated whether the increased MEFL values we observed after HPβCD treatment reflected enhanced lipid storage in response to HPβCD. When B cells from a subset of the patients were isolated and analyzed biochemically, GSL levels were higher than at the start of HPβCD therapy, suggestive of storage lipid redistribution to B cells in response to HPβCD. These data suggest that direct CNS delivery of HPβCD may be needed to minimize potential peripheral side effects, although even the patient receiving intrathecal drug (patient 7) showed elevated levels, albeit to a lesser extent than those receiving i.v. HPβCD.

The main findings of this study are summarized in Figure 5, including differential responses to therapies. Taken together, and based on lysosomal hypertrophy being a universal hallmark of LSDs, our present findings suggest that this biomarker may have broad utility as an aid to initial diagnosis (suspicion of an LSD), for monitoring disease progression in multiple LSDs, and for determining their differential responses to therapies. It remains to be determined whether this peripheral blood biomarker will be applicable in milder LSDs or in LSDs involving storage restricted to highly specialized cell types. Clinical studies are planned to test this prospectively in a range of lysosomal disorders to determine clinical utility more broadly.

Methods

NPC1 mice. BALB/cNctr-*Npc1*^{m1N}/J (Jackson Laboratory) mice (termed *Npc1*$^{-/-}$) were maintained by heterozygote brother/sister matings and genotyped as previously described (22). The *Npc1*$^{-/-}$ mouse has a lifespan of 10–12 weeks, with neurological symptoms presenting at approximately 6 weeks of age. Mice were group housed in ventilated cages with irradiated food and bedding and autoclaved water available ad libitum. Control mice were *Npc1*$^{+/+}$ mice generated from the same litters as the *Npc1*$^{-/-}$ animals. Blood and spleens were harvested from PBS-perfused mice under terminal anesthesia and analyzed for flow cytometry or biochemical analysis as previously described (9).

Clinical study cohort. The 106 total NPC patients in this study were from multiple independent international clinical cohorts from the United Kingdom, Germany, and the United States (29, 30, and 47 patients, respectively). A further 6 NPC1 patients treated with HPβCD were also studied (in addition to 1 patient on HPβCD therapy that was part of the US cohort, giving a total of 7 NPC1 patients on HPβCD treatment that were analyzed). The study cohort was composed of 52 untreated patients, 54 patients on miglustat at time of first analysis, 41 heterozygous carriers, and 53 age-matched controls. There was no standardization between centers relating to the stage of disease when miglustat therapy was initiated, although dosing was standardized according to current clinical guidelines (23). In a subset of patients, treatment was initiated during the study, allowing for pre-post analysis of miglustat therapy. Longitudinal data was not collected on pediatric controls, only on adult heterozygous carriers and adult healthy volunteers.

We also studied a pair of twins with infantile-onset Tay-Sachs, who died of disease progression at 3 years of age. Analysis was performed at 16 months of age, at which time they had been on off-label miglustat therapy for 5 months.

HPβCD-treated patients. Patients 1 and 2 were started on i.v. HPβCD in April 2009 and dose escalated to 2,500 mg/kg, administered weekly. These 2 patients were also receiving, by lumbar intrathecal injection, 175 mg HPβCD every 2 weeks starting in October 2010. Patient 3 and 4 were started on i.v. HPβCD in December 2010 and April 2011, respectively. They were dose escalated to 2,000 mg/kg, administered weekly. Patients 5 and 6 were started on i.v. HPβCD in January 2010 and started on intrathecal HPβCD in May 2010. At the time of blood sampling, they were receiving i.v. HPβCD at a dose of 2,900 mg/kg twice per week and intrathecal HPβCD at a dose of 875 mg every 2 weeks. Patient 7 was on oral miglustat therapy (2 years) prior to commencing intrathecal HPβCD and remained on miglustat throughout HPβCD treatment. Patient 7 was treated with HPβCD every 15 days and commenced with 175 mg HPβCD that was increased in single-dose steps (175, 250, 300, and 350 mg) up to a maintenance dose of 400 mg. Initially, this patient received all HPβCD doses through lumbar puncture with i.v. sedation; for the last 6 months of the study, HPβCD was delivered via an Ommaya intrathecal reservoir.

BMT of an NPC2 patient. The NPC2 patient presented as a neonate with hepatosplenomegaly and dysmorphic features. She developed progressive neurodevelopmental delay and unexplained pulmonary disease. At 14 months of age, NPC2 was diagnosed based on filipin staining of skin fibroblasts and mutational analysis. 1 known NPC2 mutation was identified with no second mutation found, with intronic regions yet to be sequenced. The patient was deteriorating, and so BMT was performed at 18 months of age using an unaffected sibling donor, as efficacy had recently been reported in another NPC2 case after BMT (18). Pre-BMT sampling and analysis in this study was performed prior to conditioning with immunosuppressive drugs. She initially made a good recovery; however, donor chimerism developed after the initial response (reduced MEFL value), and she clini-

cally declined after 6 months. She was given a repeat transplant 9 months after the initial BMT from the same donor and fully engrafted, leading to clinical improvement. At the end of the present study, the patient was stable and under continuous review.

Human blood collection and isolation of mononuclear cells. Venous blood was collected into EDTA tubes, maintained at room temperature, and analyzed within 72 hours (optimal for maintaining cell viability; data not shown). Consent or assent was obtained from all subjects, with ethical approval in place in each clinical center. Control samples were obtained by voluntary donation with informed consent, or from a commercial provider where informed consent/assent was given at the time of collection. The investigators were blinded to patient identity. Whole blood was loaded onto Histopaque-1077 (Sigma-Aldrich), and mononuclear cells were isolated according to the manufacturer's instructions. The mononuclear fraction was washed twice with Dulbecco PBS (D-PBS) before counting.

Flow cytometry. Mononuclear cells (1×10^6, in duplicate) were incubated with PE-conjugated mouse anti-human CD19 antibody (clone LT19; Abcam) in D-PBS for 30 minutes on ice in the dark. The reaction was stopped with 100 μl 10% BSA, and cells were spun (5 minutes at 800 *g*), then either resuspended in 0.5 ml FACS buffer (0.1% BSA, 0.02M NaN_3 in 1× PBS) or stained with 1 ml of 200 nM Lysotracker-green DND-26 (Invitrogen) in D-PBS for 10 minutes in the dark at room temperature. Cells were centrifuged for 5 minutes at 800 *g*, resuspended in 0.5 ml FACS buffer, and kept on ice for a maximum of 1 hour prior to flow cytometric analysis (BD Biosciences FACSCanto II). The cytometer was calibrated using Cytometer Setup and Tracking beads (BD), and compensation was performed using cells stained with Lysotracker and anti-mouse CompBeads (BD) stained with PE antibody using FACSDiva software (BD). Samples were acquired with gating on singlets (FSC-H versus FSC-A) and $CD19^+$ events. In total, 50,000 singlet events and 10,000 singlet gate $CD19^+$ events were collected. The mean fluorescence of the $CD19^+$ events was calculated using FACSDiva software (BD). MEFL was calculated using 8-peak Rainbow calibration beads (BD) using the fluorescein equivalent values provided by the manufacturer. See Supplemental Figure 8 for details of FACS profile and analysis.

HPLC analysis. HPLC analysis of GSLs was performed according to previously published methods (24).

Oxysterol measurements. The methodology was according to published protocols (8). Lysotracker and oxysterol measurements were performed on the same clinical samples for each data point.

Statistics. Logistic regression models were used to compare proportions, Wilcoxon-Mann-Whitney and Kruskal-Wallis tests were used to compare medians, and ANOVA was used to compare means. Linear regression models (including those with splines) were fitted with maximum likelihood methods; nonlinear regression models were fitted using least squares methods. Latent class finite mixture regression models were fitted using the R package flexmix (25) to define components of total clinical score as a function of age; the number of components was chosen by minimizing the Bayesian Information Criterion. Piecewise linear regression models were fitted using the R package SiZer (26). Adjusted *P* values for pairwise comparisons were obtained using the Benjamini-Hochberg correction (27). All calculations were performed in the R language and environment for statistical computing (version 2.14.2; http://www.R-project.org). Graphs with error bars represent mean ± SD. A *P* value less than 0.05 was considered significant.

Study approval. All animal studies were approved by the UK Home Office for the conduct of regulated procedures under licence (Animal Scientific Procedures Act, 1986). Studies of NPC patients from the UK (06/MRE02/85), Germany (S-032/2012), and the United States (06-CH-0186) were approved by the appropriate REC/IRB. Patient 7 in the HPβCD study was covered by ethics approval TRT585600308651 (Madrid, Spain). Written informed consent and, if applicable, assent were obtained.

Acknowledgments

We thank the patients and their families for participating in this study, members of the University of Oxford Department of Pharmacology for control blood donations, and our control pediatric blood sample donors. We also thank the Hadley Hope Foundation for funding control blood draws from anonymous pediatric and adult donors through a commercial provider in the United States. The flow cytometer was funded by The Wellcome Trust (084631). D. te Vruchte was supported by Action Medical Research (SP4203 and SP3775), with interim and additional support from the Niemann-Pick Disease Group UK and unrestricted educational grants from Actelion. A.O. Speak was funded by the UK Medical Research Council (MRC; GO700851). D.A. Smith was supported by SOAR-NPC and the Niemann-Pick Research Foundation (NPRF). N. Al Eisa was supported by King Saud bin Abdulaziz University for Health Sciences and the Ministry of Higher Education, Kingdom of Saudi Arabia. This work was supported in part by the intramural research program of the Eunice Kennedy Shriver National Institute of Child Health and Human Development and a Bench to Bedside grant supported by the Office of Rare Diseases and NIH Clinical Center (to F.D. Porter). N.M. Yanjanin was supported by Ara Parseghian Medical Research Foundation (APMRF) and Dana's Angels Research Trust (DART). The University College London Institute of Child Health receives a portion of its funding from the Department of Health's NIH Research Biomedical Research Centres funding scheme. M. Cortina-Borja's work on this study was undertaken at the Centre for Paediatric Epidemiology and Biostatistics at University College London, which benefits from funding support from the MRC in its capacity as the MRC Centre of Epidemiology for Child Health (supported by MRC grant G0400546). F.M. Platt is a Royal Society Wolfson Research Merit Award holder. We dedicate this manuscript to the memory of our colleague and greatly missed friend, Ed Wraith.

Received for publication August 28, 2013, and accepted in revised form November 14, 2013.

Address correspondence to: Frances M. Platt, University of Oxford, Department of Pharmacology, Oxford OX1 3QT, United Kingdom. Phone: 01865.271858; Fax: 01865.271853; E-mail: frances.platt@pharm.ox.ac.uk. Or to: Mario Cortina-Borja, MRC Centre of Epidemiology for Child Health, Institute of Child Health, University College London, London WCIN 1EH, United Kingdom. Phone: 020.7905.2113; Fax: 020.7905.2381; E-mail: m.cortina@ucl.ac.uk.

1. Heard JM, Bruyere J, Roy E, Bigou S, Ausseil J, Vitry S. Storage problems in lysosomal diseases. *Biochem Soc Trans*. 2010;38(6):1442–1447.
2. Wraith JE. Lysosomal disorders. *Semin Neonatol*. 2002;7(1):75–83.
3. Lachmann RH, et al. Treatment with miglustat reverses the lipid-trafficking defect in Niemann-Pick disease type C. *Neurobiol Dis*. 2004;16(3):654–658.
4. Vanier MT. Niemann-Pick disease type C. *Orphanet J Rare Dis*. 2010;5:16.
5. Patterson MC, Vecchio D, Prady H, Abel L, Wraith JE. Miglustat for treatment of Niemann-Pick C disease: a randomised controlled study. *Lancet Neurol*. 2007;6(9):765–772.
6. Patterson MC, Hendriksz CJ, Walterfang M, Sedel F, Vanier MT, Wijburg F. Recommendations for the diagnosis and management of Niemann-Pick disease type C: An update. *Mol Genet Metab*. 2012;106(3):330–344.
7. Porter FD, et al. Cholesterol oxidation products are sensitive and specific blood-based biomarkers for Niemann-Pick C1 disease. *Sci Transl Med*. 2011;2(56):56ra81.
8. Jiang X, et al. A sensitive and specific LC-MS/

MS method for rapid diagnosis of Niemann-Pick C1 disease from human plasma. *J Lipid Res*. 2011; 52(7):1435–1445.
9. te Vruchte D, Jeans A, Platt FM, Sillence DJ. Glycosphingolipid storage leads to the enhanced degradation of the B cell receptor in Sandhoff disease mice. *J Inherit Metab Dis*. 2010;33(3):261–270.
10. Yanjanin NM, et al. Linear clinical progression, independent of age of onset, in Niemann-Pick disease, type C. *Am J Med Genet B Neuropsychiatr Genet*. 2010;153B(1):132–140.
11. Macallan DC, et al. B-cell kinetics in humans: rapid turnover of peripheral blood memory cells. *Blood*. 2005;105(9):3633–3640.
12. Chien YH, et al. Long-term efficacy of miglustat in paediatric patients with Niemann-Pick disease type C. *J Inherit Metab Dis*. 2013;36(1):129–137.
13. Di Rocco M, Dardis A, Madeo A, Barone R, Fiumara A. Early miglustat therapy in infantile niemann-pick disease type C. *Pediatr Neurol*. 2012;47(1):40–43.
14. Patterson MC, et al. Long-term miglustat therapy in children with Niemann-Pick disease type C. *J Child Neurol*. 2010;25(3):300–305.
15. Vanier MT. [Niemann-Pick C disease: history, current research topics, biological and molecular diagnosis]. *Arch Pediatr*. 2010;17(suppl 2):S41–S44.
16. Willenborg M, et al. Mannose 6-phosphate receptors, Niemann-Pick C2 protein, and lysosomal cholesterol accumulation. *J Lipid Res*. 2005;46(12):2559–2569.
17. Storch J, Xu Z. Niemann-Pick C2 (NPC2) and intracellular cholesterol trafficking. *Biochim Biophys Acta*. 2009;1791(7):671–678.
18. Bonney DK, et al. Successful allogeneic bone marrow transplant for Niemann-Pick disease type C2 is likely to be associated with a severe 'graft versus substrate' effect. *J Inherit Metab Dis*. 2010; 33(suppl):171–173.
19. Davidson CD, et al. Chronic cyclodextrin treatment of murine Niemann-Pick C disease ameliorates neuronal cholesterol and glycosphingolipid storage and disease progression. *PLoS One*. 2009; 4(9):e6951.
20. Stein VM, et al. Miglustat improves purkinje cell survival and alters microglial phenotype in feline Niemann-Pick disease type C. *J Neuropathol Exp Neurol*. 2012;71(5):434–448.
21. Chen FW, Li C, Ioannou YA. Cyclodextrin induces calcium-dependent lysosomal exocytosis. *PLoS One*. 2010;5(11):e15054.
22. Loftus SK, et al. Murine model of Niemann-Pick C disease: mutation in a cholesterol homeostasis gene. *Science*. 1997;277(5323):232–235.
23. Wraith JE, et al. Recommendations on the diagnosis and management of Niemann-Pick disease type C. *Mol Genet Metab*. 2009;98(1–2):152–165.
24. Neville DC, et al. Analysis of fluorescently labeled glycosphingolipid-derived oligosaccharides following ceramide glycanase digestion and anthranilic acid labeling. *Anal Biochem*. 2004;331(2):275–282.
25. Grün B, Leisch F. Fitting finite mixtures of generalized linear regressions in R. *Comput Stat Data Anal*. 2007;51(11):5247–5252.
26. Sonderegger DL, Wang H, Clements WH, Noon BR. Using SiZer to detect thresholds in ecological data. *Front Ecol Environ*. 2009;7:190–195.
27. Benjamini Y, Hochberg Y. Controlling the false discovery rate: a practical and powerful approach to multiple testing. *J R Stat Soc Series B Stat Methodol*. 1995;57(1):289–300.

Neurobiology of Disease 67 (2014) 9–17

Contents lists available at ScienceDirect

Neurobiology of Disease

journal homepage: www.elsevier.com/locate/ynbdi

Improved neuroprotection using miglustat, curcumin and ibuprofen as a triple combination therapy in Niemann–Pick disease type C1 mice

Ian M. Williams *[,1], Kerri-Lee Wallom [1], David A. Smith [1], Nada Al Eisa, Claire Smith, Frances M. Platt *

Dept. of Pharmacology, University of Oxford, UK

ARTICLE INFO

Article history:
Received 22 October 2013
Revised 18 February 2014
Accepted 2 March 2014
Available online 12 March 2014

Keywords:
Niemann–Pick disease type C1
Combination therapy
Neuroprotection
Cerebellum
Miglustat
Curcumin
Ibuprofen

ABSTRACT

Objectives: Niemann–Pick disease type C (NPC) is a neurodegenerative lysosomal storage disorder characterised by the storage of multiple lipids, reduced lysosomal calcium levels, impaired late endosome:lysosome fusion and neuroinflammation. NPC is caused by mutations in either of the two genes, *NPC1* or *NPC2*, which are believed to function in a common cellular pathway, the function of which remains unclear. The complexity of the pathogenic cascade in NPC disease provides a number of potential clinical intervention points. To date, drugs that target pivotal stages in the pathogenic cascade have been tested as monotherapies or in combination with a second agent, showing additive or synergistic benefit. In this study, we have investigated whether we can achieve greater therapeutic benefit in the *Npc1*$^{-/-}$ mouse by combining three therapies that each targets unique aspects of the pathogenic cascade.

Methods: We have treated *Npc1*$^{-/-}$ mice with miglustat that targets sphingolipid synthesis and storage, curcumin that compensates for the lysosomal calcium defect by elevating cytosolic calcium, and the non-steroidal anti-inflammatory drug ibuprofen to reduce central nervous system inflammation.

Results/interpretation: We have found that triple combination therapy has a greater neuroprotective benefit compared with single and dual therapies, increasing the time period that *Npc1*$^{-/-}$ mice maintained body weight and motor function and maximally delaying the onset of Purkinje cell loss. In addition, ibuprofen selectively reduced microglial activation, while curcumin had no anti-inflammatory effects, indicating differential mechanisms of action for these two therapies. When taken together, these results demonstrate that targeting multiple unique steps in the pathogenic cascade maximises the clinical benefit in a mouse model of NPC1 disease.

Introduction

Niemann–Pick disease type C (NPC) is a lysosomal storage disorder that occurs at an estimated frequency of 1:120,000 live births (Vanier, 2010). It is caused by mutations in either the *NPC1* or the *NPC2* gene. Defects in either gene result in an identical clinical disorder (Patterson et al., 2012; Vanier, 2010). NPC disease is characterised by the storage of multiple lipids, including sphingolipids (glycosphingolipids (GSLs), sphingomyelin and sphingosine) and cholesterol (Vanier, 1999; Vanier et al., 1991). The *NPC1* gene encodes a 13 trans-membrane spanning protein of the limiting membrane of late endosomes/lysosomes (Ioannou, 2000), with mutations in this gene accounting for approximately 95% of clinical cases (Vanier, 2010; Wraith et al., 2009). In contrast, NPC2 is a soluble mannose-6-phosphorylated lysosomal cholesterol transport protein, which controls intra-lysosomal membrane cholesterol content and is involved in cholesterol exchange with NPC1 (Estiu et al., 2013; Infante et al., 2008; Kwon et al., 2009; Storch and Xu, 2009). The function of the NPC1 protein has been proposed to be the efflux of lipids from late endosomes/lysosomes, but there is no consensus on the specific lipid(s) effluxed by this pathway, nor exactly how NPC2 contributes to this process (Lloyd-Evans and Platt, 2010).

The only step in the pathogenic cascade targeted by an approved therapy is miglustat, an orally available inhibitor of glycosphingolipid biosynthesis that reduces GSL storage (Patterson et al., 2007; Platt et al., 1994). Several other therapeutic targets downstream of the NPC1 protein have been validated using small molecule monotherapies in the NPC1 mouse model (Alvarez et al., 2008; Davidson et al., 2009; Liu et al., 2009; Lloyd-Evans et al., 2008; Munkacsi et al., 2011; Pipalia et al., 2011; Smith et al., 2009; Zervas et al., 2001; reviewed by Davidson and Walkley, 2010; Madra and Sturley, 2010). In previous studies, we tested three therapeutics that target unique aspects of the pathogenic cascade, all of which results in survival benefit in a mouse model of NPC1 disease when evaluated as monotherapies; miglustat (Zervas et al., 2001), the non-steroidal anti-inflammatory drug (NSAID) ibuprofen (Smith et al., 2009) and the intracellular calcium modulator curcumin (Lloyd-Evans et al., 2008).

In this study, we have evaluated the effects of simultaneously targeting glycosphingolipid biosynthesis, defective calcium homeostasis

* Corresponding authors at: Department of Pharmacology, University of Oxford, Mansfield Road, Oxford OX1 3QT, UK.
E-mail addresses: ian.williams@pharm.ox.ac.uk (I.M. Williams), frances.platt@pharm.ox.ac.uk (F.M. Platt).

Available online on ScienceDirect (www.sciencedirect.com).

[1] Equal contribution.

http://dx.doi.org/10.1016/j.nbd.2014.03.001
0969-9961/

and CNS inflammation using miglustat, curcumin and ibuprofen respectively to determine whether triple combination therapy provides greater functional benefit and/or enhances neuroprotection.

Materials and methods

Mice

BALBc/NPC^{nih} mice were bred as heterozygotes to generate *Npc1*$^{-/-}$ mice and control genotypes (Pentchev et al., 1980). Mice were bred and housed under non-sterile conditions, with food and water available ad lib. All experiments were conducted using protocols approved by the UK Home Office Animal scientific Procedures Act, 1986.

Drug treatments

Ibuprofen (Sigma, 100 mg/kg/day) was supplemented as a dry admixture to powdered RM1 mouse chow (SDS, UK) (from 6 weeks of age, due to the toxicity seen with earlier dosing, Smith et al., 2009). Miglustat (600 mg/kg/day, Oxford GlycoSciences/Celltech, UK) and curcumin (Sigma, 150 mg/kg/day) were administered as dry admixtures as above (from 3 weeks of age). The untreated mice were fed on powdered chow ($n = 34$). Treatment groups were made up of approximately equal numbers of males and females and received ibuprofen ($n = 14$), curcumin ($n = 11$), miglustat ($n = 11$), curcumin and ibuprofen ($n = 5$), curcumin and miglustat ($n = 11$), or all three therapies ($n = 9$). A parallel group of mice for each treatment combination was set up ($n = 3$) and used specifically for immunohistochemical studies with no behavioural analysis performed.

Mouse behavioural analysis

Weight and spontaneous activity of each mouse were recorded weekly until reaching the late humane end-point (loss of 1 g body weight within 24 h) as previously described (Smith et al., 2009). After 5–30 min room acclimatization, the mouse was placed in the 'open field' (measuring 45 × 25 × 12 cm). Rearing was recorded manually for 5 min (the number of times the mouse reared on its hind legs with or without support of the cage wall).

Immunohistochemistry (IHC)

Cerebellar tissue was processed as described previously (Carletti et al., 2008; Williams et al., 2008). Mice were euthanized at 7.5 weeks by CO_2 asphyxiation and transcardially perfused with 4% paraformaldehyde in phosphate buffer. The brains were post-fixed for 24 h then cryoprotected in 30% sucrose until the tissues sank. Cerebellar tissue was cryostat-sectioned parasagittally (30 μm) and floating sections collected in phosphate buffered saline (PBS) with 0.25% Triton ×100. Sections were incubated overnight at 4 °C with either rabbit anti-calbindin (1:3000, Swant) or rat anti-CD68 (1:2000, Serotec), detected using DyLight-594 goat anti-rabbit IgG (Sigma) and Alexa-488 conjugated donkey anti-rat IgG (Invitrogen) respectively, and counterstained with DAPI (Fluka).

Image analysis

To obtain a clear and consistent view of cerebellar pathology in each treatment group, vermal lobule III was chosen as the common area to study in each animal, thus avoiding the confounding factor of differential onset of neuropathology in the parasagittal plain (Sarna et al., 2003). At 7.5 weeks of age, neurodegeneration in lobule III is ongoing and advanced, providing a good basis to assess the various treatments.

Overlapping images of lobule III were taken using a Zeiss AXIO Imager A1 fluorescence microscope connected to a Zeiss AxioCamHRc digital camera. For each field, images of the calbindin/CD68/DAPI channels were superimposed in and adjusted for brightness/contrast in Adobe Photoshop, and then the overlapping images of lobule III were realigned to allow accurate morphometric analysis using ImageJ (NIH). In Fig. 4, non-lobule III tissue was removed from the images for the purposes of clarity only.

To obtain quantitative data of Purkinje cell survival and the level of microglial/macrophage infiltration into the cerebellar molecular layer, the number of each cell type was counted, along with the length of Purkinje cell layer and the area of molecular layer. In addition, the size of 30 microglia (in μm^2) was sampled in each section of digitally recombined lobule III as a measure of microglial activation/phagocytosis. Multiple sections from each animal were used and the areas/lengths and cell counts from an individual animal pooled together to avoid any potential bias in Purkinje cell survival caused by the alternate parasagittal zebrin-II expressing zones. The mean number of CD68$^+$ cells/mm^2 of molecular layer, average microglial size in μm^2 and Purkinje cells/mm of Purkinje cell layer were calculated for each treatment group. The data set used for immunohistochemical analysis for each treatment consisted of three separate animals ($n = 3$).

Statistics

Survival was measured two ways. Firstly by directly comparing the mean survival time between all groups, where statistical significance was evaluated with one-way analysis of variance with Tukey's multiple comparison post-hoc test. As this method internally accounts for multiple comparison testing, values were considered significant when $p < 0.05$. Secondly, survival curves were created by the method of Kaplan and Meier, and statistically evaluated using the log-rank (Mantel–Cox) test with a Bonferroni-method adjusted p-value of 0.0024 set for statistical significance to account for the 21 possible multiple comparisons. Other quantitative data were statistically evaluated with one-way analysis of variance with Tukey's post-hoc test with values considered statistically significantly different when $p < 0.05$. The statistical software used was GraphPad Prism version 4.0c (GraphPad Software, San Diego, California, USA).

Results

Effect of therapies on survival

Npc1$^{-/-}$ mice were treated with monotherapies (ibuprofen, curcumin, miglustat), dual therapies (curcumin with either ibuprofen or miglustat), or the combination of all three, and survival analysed (Figs. 1A–B). The untreated *Npc1*$^{-/-}$ mouse model has an acute clinical course and dies by 10–11 weeks of age with mean survival (late humane endpoint) of 10.5 weeks. Mean lifespan (Fig. 1A) was modestly but significantly extended by monotherapy treatment with ibuprofen (9%; $p < 0.05$) and curcumin (11%; $p < 0.01$), representing an increased lifespan of just over a week in each case. Combining ibuprofen and curcumin extended lifespan further than either monotherapy, and was of additive benefit with a 22% increase in lifespan over the untreated control group ($p < 0.001$). Miglustat monotherapy extended lifespan to an average of 15.4 weeks; a 46% improvement compared to untreated mice ($p < 0.001$), and was also significantly better than the curcumin & ibuprofen treatments ($p < 0.001$). Combining curcumin and miglustat had the greatest survival benefit, extending life expectancy in a synergistic manner up to 20 weeks (mean of 19.3 weeks), an 83% increase in lifespan compared to untreated mice ($p < 0.001$). Interestingly, adding ibuprofen to the dual therapy had no additional benefit in terms of survival and in fact was slightly, but not significantly, lower with a mean survival of 18.2 weeks, a 73% improvement compared to untreated mice ($p < 0.001$) (Fig. 1A). Treating with either the curcumin & miglustat or the triple combination therapy was significantly better in extending lifespan than miglustat alone ($p < 0.001$), demonstrating the efficacy of combining these therapies (Fig. 1A). The distribution of the

Kaplan–Meier survival curves (Fig. 1B) also showed significant improvement for each treatment group when compared to the untreated control with a $p < 0.0024$ in each case, with the exception of ibuprofen ($p = 0.0025$). When comparing between the various treatments, the same groups proved to be significantly different as seen in the mean lifespan analysis; the miglustat treated group survived longer than the curcumin & ibuprofen treated group ($p < 0.0001$), the curcumin & miglustat treated and the triple combination treated groups survived longer compared to the group treated with miglustat alone (both $p < 0.0001$), and no survival difference was observed between the curcumin & miglustat treated and the triple combination treated group ($p = 0.0634$).

Effect of therapies on body weight

Another indicator of therapeutic efficacy in *Npc1*$^{-/-}$ mice is the maintenance of body weight (Davidson et al., 2009; Lloyd-Evans et al., 2008). Typically, the weight of *Npc1*$^{-/-}$ mice plateaus at 7 weeks of age, and then progressively declines. While none of the treatment combinations significantly increased the maximal weight of *Npc1*$^{-/-}$ mice, significant alterations in the onset of weight loss were observed in miglustat-treated mice and combinations containing miglustat. These treatment regimes extended the length of time that *Npc1*$^{-/-}$ mice were able to gain and maintain weight, seen as a rightward shift of the typical untreated *Npc1*$^{-/-}$ weight curve (Fig. 1C). The time at which maximal weight was reached in miglustat, miglustat & curcumin, and triple combination treated mice was 0.8 ($p < 0.05$), 1.16 ($p < 0.001$) and 2 weeks ($p < 0.001$) later than that in untreated mice, respectively (Fig. 1D).

The mean weight of *Npc1*$^{-/-}$ mice was compared at 11 weeks of age (Fig. 1E) when the average weight of the untreated *Npc1*$^{-/-}$ group had dropped to 13.16 g. While a number of monotherapies showed no significant maintenance of weight, the average weight of both the curcumin & miglustat (16.1 g, $p < 0.05$) and triple combination groups (18.1 g, $p < 0.001$) were significantly higher. Interestingly, while the dual treatment was not significantly higher than miglustat alone, the triple combination therapy was significant ($p < 0.05$), indicating an enhanced beneficial effect when using all three treatments.

Effect of therapies on motor function

We also monitored the mice using rearing ability in an open field to measure motor function/coordination (Fig. 1F). At 8 weeks of age, rearing was not significantly improved by ibuprofen or curcumin monotherapies but was improved by miglustat monotherapy and any combination that included miglustat (untreated *Npc1*$^{-/-}$, 2.28 events/5 min compared to miglustat, 22.64; curcumin & miglustat, 28.82; and triple combination, 41.00 events/5 min, all $p < 0.001$) (Fig. 1G). Rearing activity was significantly improved in both the curcumin and miglustat dual therapy ($p < 0.01$) and the triple combination therapy ($p < 0.001$)

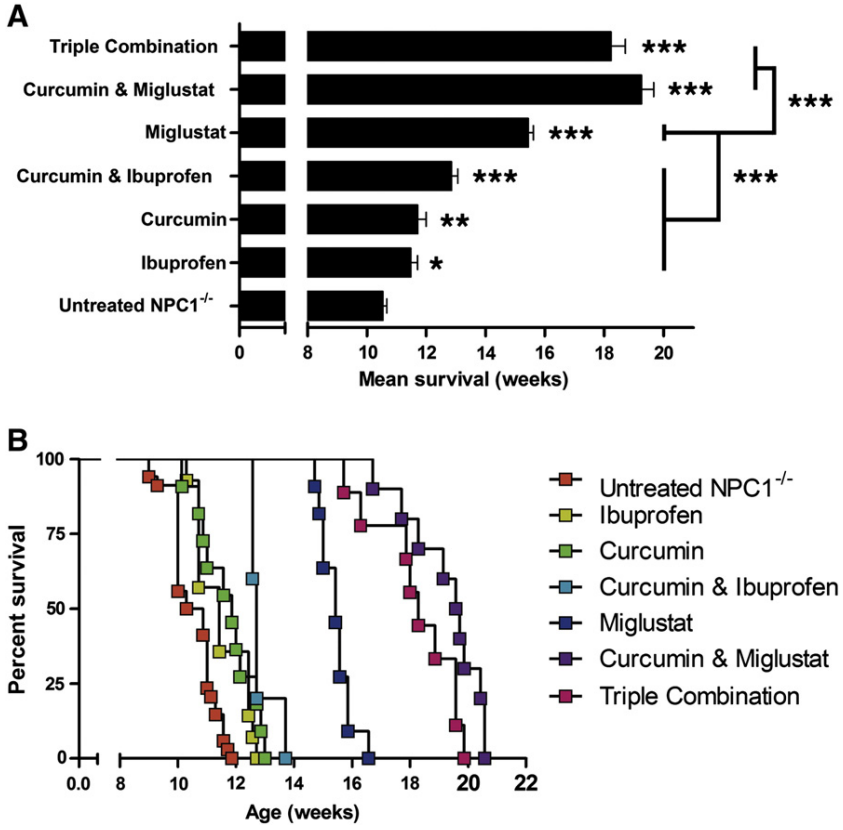

Fig. 1. Effect of combination therapies on survival, weight and motor function in NPC1$^{-/-}$ mice. Survival was evaluated applying a late humane end point (see Materials and methods) and is presented as mean survival (A), and as Kaplan–Meier survival plots (B). All the treatment groups show a significant increase in mean lifespan versus the untreated control group, and the bars in (A) demonstrate significant differences in survival between treatment groups. The mean weight for each treatment group is plotted against age (C, error bars omitted for clarity), while the average week at which the peak weight is reached for each treatment group is displayed in (D). The maintenance of weight in each treatment group is shown as the mean weight for each group at 11 weeks of age in (E). Graphs (F–H) show the effect of the various therapies on motor function in terms of behavioural rearing. The average number of rearing events in each treatment group is plotted against age (F, error bars omitted for clarity), while the differences in the gradual loss/maintenance of function over time between the treatment groups are shown by the mean number of rearing events observed at 8 weeks (G) and 11 weeks (H) of age. All error bars ± SEM, $n \geq 5$ for each treatment group, and a one way ANOVA with Tukey's post test was used in (A) to measure significance. ***$p < 0.001$, **$p < 0.01$, *$p < 0.05$, and ns = non-significant.

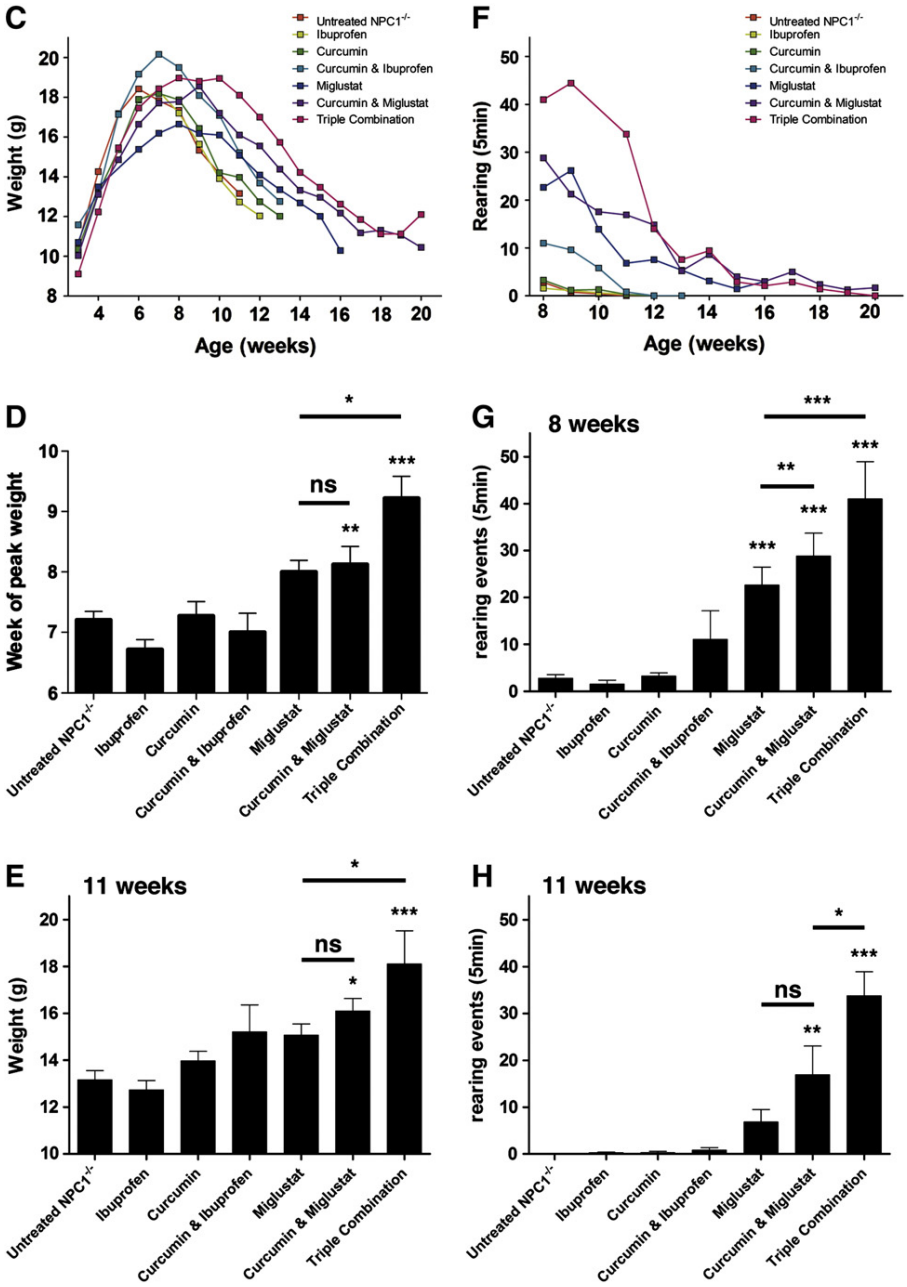

Fig. 1 (*continued*).

compared to miglustat alone. At 11 weeks of age, only the dual combination of miglustat and curcumin and the triple combination therapy maintained rearing over the untreated *Npc1*$^{-/-}$ group ($p < 0.01$ and $p < 0.001$, respectively) (Fig. 1H). Strikingly, at this time point the triple combination group demonstrated significant maintenance of rearing activity when compared to the dual therapy ($p < 0.05$).

Effect of therapies on CNS pathology

As the various treatment regimes demonstrated improved survival and functional benefits, we tested a cohort of treated mice at 7.5 weeks of age and analysed the extent to which the therapies modified neuropathology using calbindin as a marker of Purkinje cells, DAPI to visualise the cerebellar architecture/lobe organisation and CD68 as a marker of microglial/macrophage activation to establish the degree of neuroprotection garnered with each treatment (Figs. 2–4). The untreated *Npc1*$^{-/-}$ mice displayed the characteristic progressive loss of Purkinje cells with large-scale loss from lobules I–IV by 7.5 weeks (Fig. 2A). Many CD68 positive microglia were evident throughout the degenerating lobules with the greatest density in the lobules undergoing most active cell death at this point (III–IV). As such, lobule III was used for the consistent quantification of pathology.

Microglial recruitment

The relative level of microgliosis in the various treatment groups is depicted in Fig. 2 (quantification in Fig. 2H). In ibuprofen-treated mice, microglial recruitment to the molecular layer was reduced

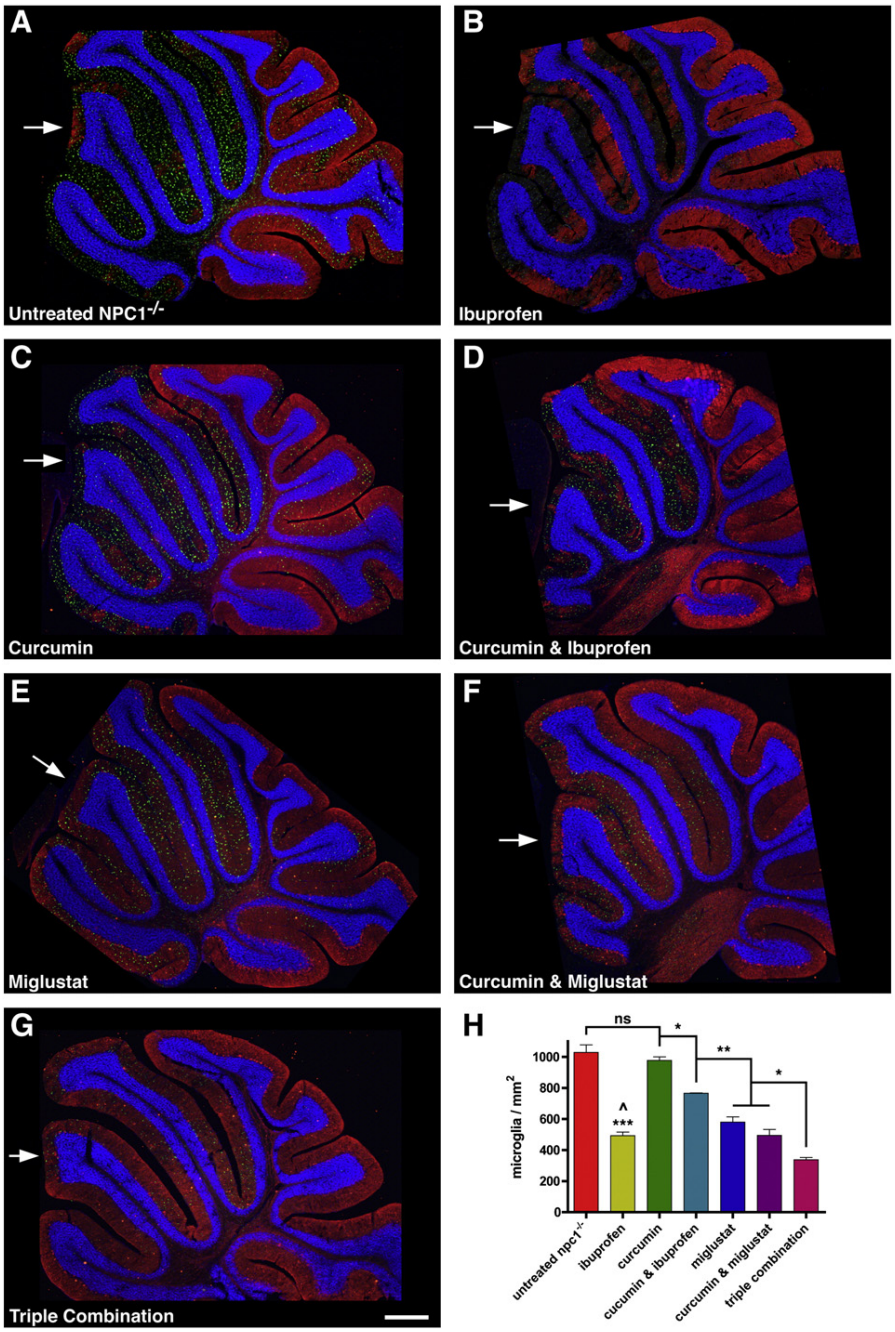

Fig. 2. Effect of combination therapies on microglial recruitment in the NPC1$^{-/-}$ cerebellum. Images (A–G) depict representative images (2.5×) of sagittal sections of NPC1$^{-/-}$ cerebellum at 7.5 weeks of age, either untreated (A) or treated with the various therapy combinations (B–G), where the relative level of microglial recruitment can be seen in each case. Lobule III indicated by arrows in each example. Red = calbindin, green = CD68, and blue = DAPI. Quantitative analysis of the number of CD68^{+} microglia/mm^2 of cerebellar lobule III molecular layer is shown in (H), error bars ±SEM, n = 3 cerebella for each treatment group, and total sample set of 30,389 microglia counted over 46.328 mm^2 of tissue. *$p < 0.05$, **$p < 0.01$, ***$p < 0.001$ (ibuprofen vs untreated NPC1$^{-/-}$), ^$p < 0.05$ (triple combination vs ibuprofen), and ns = non-significant, using a one way ANOVA with Tukey's post test. Scale bar = 500 μm.

from 1027.98 microglia/mm^2 observed in untreated *Npc1*$^{-/-}$ mice to 492.89 microglia/mm^2 ($p < 0.001$), indicating a strong anti-inflammatory effect (Fig. 2B), while curcumin monotherapy exhibited no anti-inflammatory properties (Fig. 2C). Combining ibuprofen with curcumin did reduce microgliosis when compared to curcumin alone (765.84 microglia/mm^2, $p < 0.05$) (Fig. 2D). Miglustat monotherapy (Fig. 2E) (579.84 microglia/mm^2) and miglustat & curcumin dual therapy (Fig. 2F) (497.67 microglia/mm^2) both significantly reduced microgliosis compared to ibuprofen & curcumin therapy ($p < 0.01$). The greatest reduction in microgliosis was in the triple combination group (Fig. 2G), where only 337.38 microglia/mm^2 of lobule III molecular layer were observed, significantly less than the curcumin & miglustat dual treatment and the ibuprofen monotherapy ($p < 0.05$).

Microglial activation

The morphological change in microglia from a resting morphology to an activated morphology, then on to the phagocytic state was

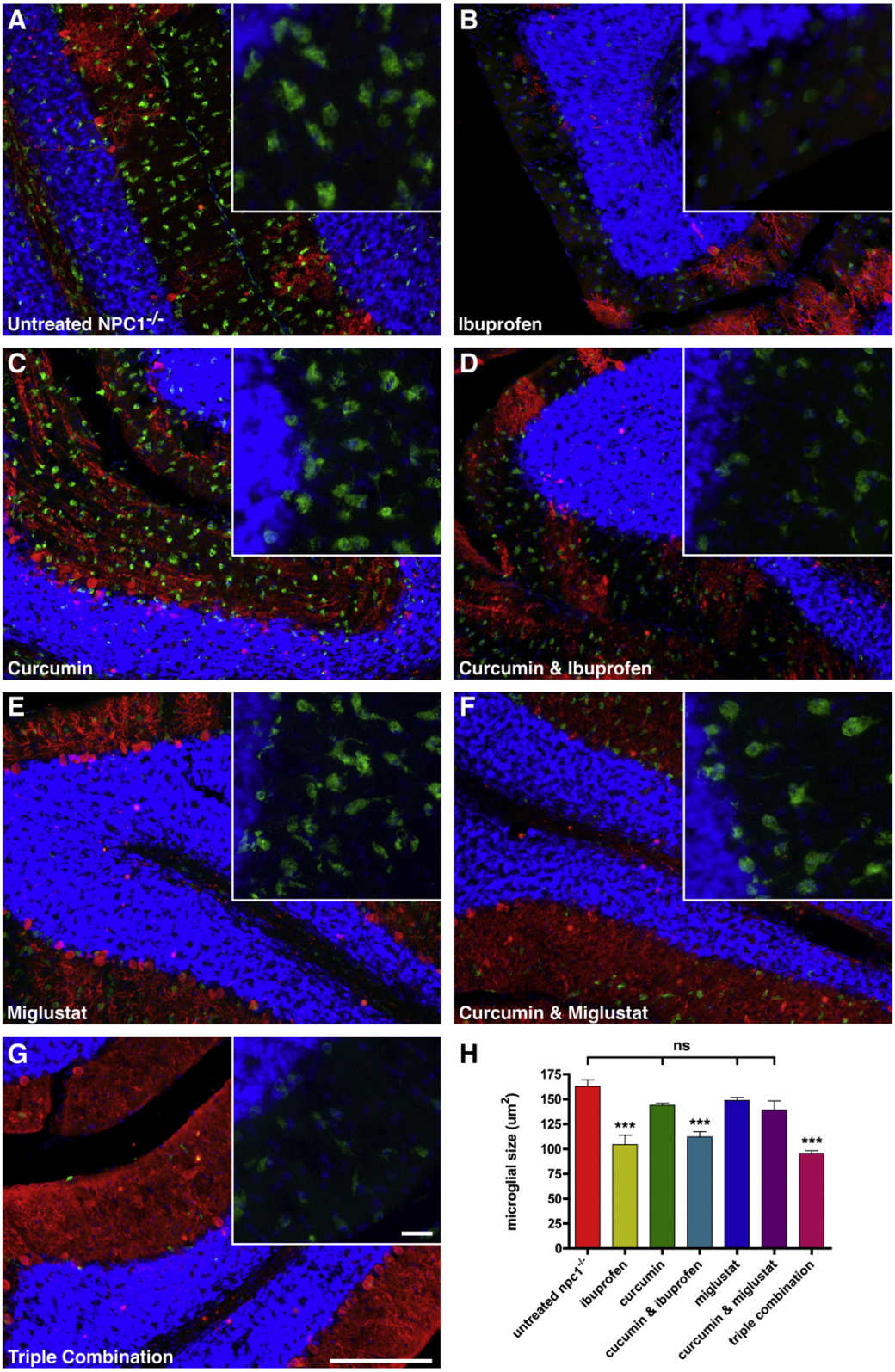

Fig. 3. Effect of combination therapies on microglial activation/phagocytosis in the NPC1$^{-/-}$ cerebellum. Images (A–G) depict representative images (20×) of sagittal sections of NPC1$^{-/-}$ cerebellar lobule III at 7.5 weeks of age, either untreated (A) or treated with the various therapy combinations (B–G), where the relative level of microglial activation can be seen in each case. Red = calbindin, green = CD68, and blue = DAPI. Quantitative analysis of the average size of lobule III molecular layer resident CD68^{+} microglia in μm^2 is shown in (H), error bars ± SEM, and n = 3 cerebella for each treatment group. ***p < 0.001 and ns = non-significant, using a one way ANOVA with Tukey's post test. Scale bar = 250 μm; 25 μm in inset images, the exposure time in each case is identical to allow qualitative comparison of staining intensity.

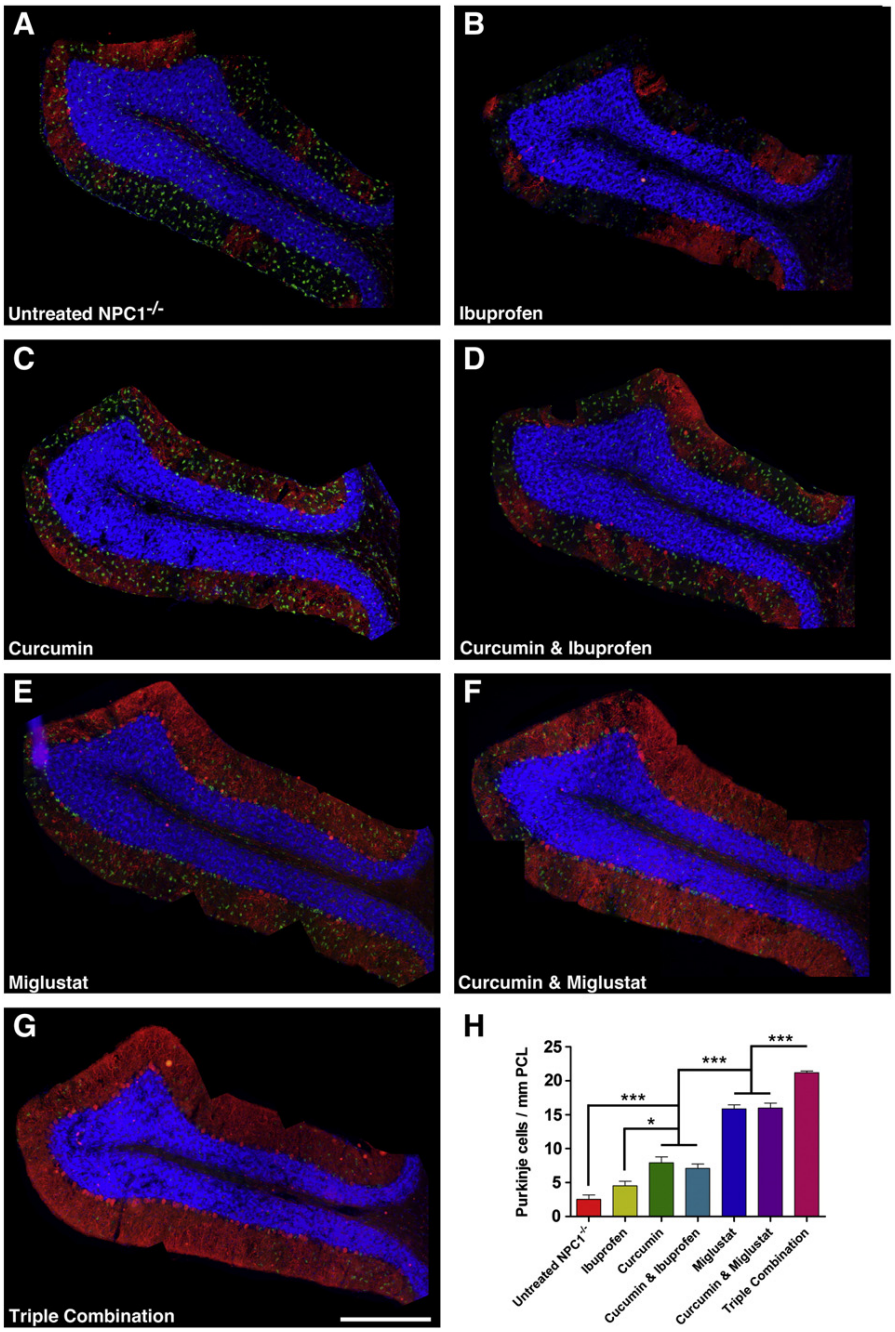

Fig. 4. Effect of combination therapies on Purkinje cell survival/neuroprotection in the NPC1$^{-/-}$ cerebellum. Images (A–G) depict representative examples of sections of NPC1$^{-/-}$ cerebellar lobule III in the sagittal plain at 7.5 weeks of age (multiple 10× images merged to recreate the whole lobule), either untreated (A) or treated with the various therapy combinations (B–G), where the relative level of Purkinje cell survival can be seen in each case. Red = calbindin, green = CD68, and blue = DAPI. Quantitative analysis of the average number of surviving Purkinje cells/mm of Purkinje cell layer is shown in (H), error bars ± SEM, n = 3 cerebella for each treatment group, and total sample set of 3934 neurons counted over 356.873 mm of tissue. *$p < 0.05$, ***$p < 0.001$, and ns = non-significant, using a one way ANOVA with Tukey's post test. Scale bar = 500 μm.

measured based on increased somal size (Kozlowski and Weimer, 2012; Kreutzberg, 1996; Raivich et al., 1999) to indicate the level of microglial activation/phagocytosis in each treatment group (Fig. 3, quantification in Fig. 3H).

Microglial activation was prevalent in the untreated *Npc1*$^{-/-}$ mouse cerebellum, with the majority of the CD68 positive cells exhibiting the large, rounded, amoeboid shape of highly activated and phagocytic microglia as opposed to the ramified morphology with small cell soma of resting microglia, with an average microglial cell body area of 162.77 μm^2 (Fig. 3A). When assessing the various treatments tested, a clear pattern emerged where any treatment combination not containing ibuprofen (Figs. 3C, E–F) showed no difference from the untreated control in microglial size, whereas any therapy containing the anti-inflammatory drug ibuprofen showed significant reductions in microglial size, (ibuprofen — 104.28 μm^2, curcumin & ibuprofen — 112.05 μm^2, triple combination — 95.62 μm^2, all $p < 0.001$ compared to untreated *Npc1*$^{-/-}$). In addition, the relative level of CD68 activation appeared lower, in terms of staining intensity, in the ibuprofen-containing treatments (compare insets in Figs. 3A, C, E and F to those in B, D and G), indicating an attenuation of microglial activation.

Purkinje cell neuroprotection

Purkinje cell survival was quantified for each therapy, recording the number of surviving lobule III Purkinje cells/mm of Purkinje cell layer (Fig. 4). There was little survival of Purkinje cells in this region in untreated *Npc1*$^{-/-}$ cerebellum, with the few remaining cells (2.54 Purkinje cells/mm pcl) exhibiting dendritic degeneration (Fig. 4A). A similar level of neurodegeneration was evident in the ibuprofen-treated cerebellum (Fig. 4B), where a small but non-significant increase in Purkinje cells was observed (4.53 Purkinje cells/mm pcl). Curcumin treated mice demonstrated a degree of Purkinje cell protection relative to untreated controls (7.94 Purkinje cells/mm pcl, $p < 0.001$) (Fig. 4C), as did the curcumin & ibuprofen dual therapy treated mice (7.10 Purkinje cells/mm pcl, $p < 0.01$) (Fig. 4D).

Miglustat monotherapy (Fig. 4E) exhibited a much stronger neuroprotective effect than the curcumin treatment, and while patches of Purkinje cell loss were still evident, the level of Purkinje cell survival was much higher (15.87 Purkinje cells/mm pcl, $p < 0.001$). The same was true for the curcumin & miglustat dual treatment (16.00 Purkinje cells/mm pcl, $p < 0.001$) (Fig. 4F), and although the dual treatment did have slightly more Purkinje cell survival (and objectively slightly better dendritic condition), it was not significantly better than miglustat alone. Remarkably, the triple combination therapy resulted in a high level of neuroprotection, with only sporadic patches of Purkinje cell loss evident across lobule III (21.20 Purkinje cells/mm pcl) (Fig. 4G). This was a slight but significant improvement over the other miglustat-containing therapies ($p < 0.001$) (Fig. 4H), indicating that the triple combination therapy was the most effective neuroprotective treatment tested.

Discussion

NPC disease is a highly complex lipid storage disorder with multiple potential clinical intervention points that can be targeted with small molecules. In this study, we have combined miglustat, curcumin and ibuprofen to determine whether triple combination therapy provides greater functional benefit and/or enhances neuroprotection.

Our findings with regard to the monotherapies are in broad agreement with previous studies (Lloyd-Evans et al., 2008; Smith et al., 2009; Zervas et al., 2001). Of greater interest were the results obtained in the combination therapy strategies. While overall survival was not improved in *Npc1*$^{-/-}$ mice treated with the triple combination versus the miglustat & curcumin dual therapy, this was not surprising as we previously observed poor tolerability of liver metabolised drugs, such as ibuprofen, in the *Npc1*$^{-/-}$ mouse (Smith et al., 2009). However, the benefits of triple combination therapy were consistently more robust versus miglustat in all other parameters relative to the dual therapy (Figs. 1C–H). Indeed, combining miglustat with the other treatments counteracted the reported side-effect of miglustat on weight gain (Davidson et al., 2009; Zervas et al., 2001), which together with an improvement in motor function (even when compared to the dual therapy) and a 73% increase in lifespan, indicates a greater functional benefit in combining all three treatments.

The additive/synergistic benefits gained by combining the treatments are also evident in the effect on cerebellar pathology. As previously demonstrated, the cerebellum is an appropriate brain region to test neuropathology/neuroprotection by virtue of the correlation between behavioural symptoms and Purkinje cell loss, and while inflammation is not the pathogenic factor for neurodegeneration, the predication of neuronal loss by microgliosis is a useful measure of disease progression and severity in the brain (Baudry et al., 2003; Elrick et al., 2010; Ko et al., 2005; Lopez et al., 2011; Smith et al., 2009; Yu et al., 2011). In terms of neuronal survival and microglial pathology, the triple combination therapy outperformed the other treatment regimes.

While it is true that we see maintenance of weight, rearing activity and Purkinje cell numbers, it is not continuous. The behavioural factors do decline over time, and while the level of neuroprotection at 7.5 weeks is impressive with the triple combination therapy, small patches of neuronal loss are observable, as are the early stages of microgliosis. As such, these treatments appear to only delay symptom onset rather than arrest a particular aspect of pathology. Still, the maintenance of motor function and cerebellar neurons at respective periods in the disease course where loss is near total represents a significant benefit, and confirms the validity of targeting multiple, independent aspects of pathophysiology as a therapeutic strategy.

The finding of enhanced neuroprotection in the absence of considerably enhanced survival in these treatments highlights the dangers of using survival/behavioural measures to infer CNS effects, or as a sole screening criteria of therapeutic efficacy in the *Npc1*$^{-/-}$ mouse (Borbon et al., 2012). Careful dosing of ibuprofen demonstrated that the treatment has a greater disease-modifying effect than expected from the modest improvement in survival by virtue of the strong reduction of neuroinflammation and the improved neuroprotection seen in the triple combination therapy. Interestingly, while the study overall agreed with previous work that monotherapy with NSAIDs/anti-oxidants is not overtly neuroprotective (Smith et al., 2009), there was a trend towards enhanced Purkinje cell survival (Fig. 4H). This could potentially be explained by the limited timeframe available for treatment, however another study from our laboratory has indicated a P450 system defect in NPC1 (Al Eisa and Platt, unpublished observation). If liver toxicity/P450 defect can be effectively alleviated in NPC1, it would be intriguing to see whether the anti-inflammatory portion of the combination therapy could be further optimized. Recent publications have discussed how inflammatory processes can be positive factors in NPC1 and that inhibiting them, such as genetic deletion of the cytokine Ccl3, in fact worsens weight loss progression and shortens lifespan in *Npc1*$^{-/-}$ mice (Lopez et al., 2012). However, in this study we have observed beneficial effects of anti-inflammatory treatment as part of a combination therapy. The concept of inflammation as a double-edged sword, initially beneficial then becoming increasingly detrimental, is the case in another lysosomal storage disorder, Sandhoff disease (Wada et al., 2000). This rationale may explain the limited time window for the effectiveness of ibuprofen, with early treatment negating positive inflammatory processes, and delayed treatment slowing the later stages of neurodegeneration-induced microgliosis.

These results also provide mechanistic insight into the therapeutic agents used in this study. Curcumin has many potential modes of action (Bilmen et al., 2001; Lopresti et al., 2012; Srivastava et al., 2011), many studies citing its anti-inflammatory/anti-oxidant properties (Basnet and Skalko-Basnet, 2011; Belcaro et al., 2010; Borbon et al., 2012) as opposed to a SERCA-mediated effect on cytosolic calcium levels in NPC1 (Lloyd-Evans et al., 2008). Throughout our study, there were strong additive/synergistic increases in survival, weight and rearing activity using the ibuprofen & curcumin dual treatment (significant using direct t-tests, yet occluded in the one-way ANOVA data analysis by the much larger differences observed in the miglustat-containing combination therapies (Fig. 1)). If curcumin was acting via an anti-inflammatory mechanism, you would not expect the synergistic increases in weight maintenance or rearing that we observed when used in conjunction with ibuprofen. Curcumin monotherapy showed no anti-inflammatory action in cerebellar pathology, while adding ibuprofen to the other therapies further reduced microglial recruitment versus monotherapy and was the singular factor that reduced microglial activation/phagocytosis, indicating that curcumin and ibuprofen likely have separate mechanisms of action in NPC1. Indeed, other work has demonstrated that modified curcuminoids lacking SERCA antagonist properties, but which retain their anti-oxidant action, do not ameliorate NPC1 defects in cells (Dr. Emyr Lloyd-Evans; personal communication).

The disruption of NPC1 function affects a large number of cellular processes, including lipid transport, lysosomal calcium homeostasis,

vesicular trafficking and autophagy (Elrick et al., 2012; Garver et al., 1999; Kaptzan et al., 2009; Lloyd-Evans et al., 2008; Sarkar et al., 2013; te Vruchte et al., 2004; Walter et al., 2009). While targeting the initial gene/protein defect in NPC1 may prove elusive for the time being, the presence of many different downstream therapeutic targets would suggest that combination therapies might play an important role in the management of symptoms for patients and potentially be synergistic. Here we show that targeting three independent steps in the pathogenic cascade has enhanced therapeutic benefit in a mouse model of NPC1, extending lifespan as well as delaying the onset of morbidity and neuronal loss. This study, along with others (Hovakimyan et al., 2013), demonstrates the amenability of NPC1 to combination therapy, and suggests that trials of this approach in patients are warranted.

Conflict of interest

The authors declare no issues regarding conflicts of interest.

Acknowledgment

DS was funded by the National Niemann-Pick Disease Foundation (NNPDF), SOAR-NPC and the Niemann-Pick Research Foundation, CS by SOAR-NPC, KW by the Medical Research Council (MRC) UK (grant #: G0700969), IW by a Peter Penchev Fellowship from National Niemann-Pick Disease Foundation (grant #: FA-012) and the Niemann-Pick Disease Group (UK), and N Al E by the King Saud bin Abdulaziz University for Health Sciences and the Ministry of Higher Education, Kingdom of Saudi Arabia. FP is a Royal Society Wolfson Research Merit Award holder.

References

Alvarez, A.R., et al., 2008. Imatinib therapy blocks cerebellar apoptosis and improves neurological symptoms in a mouse model of Niemann–Pick type C disease. FASEB J. 22 (10), 3617–3627.
Basnet, P., Skalko-Basnet, N., 2011. Curcumin: an anti-inflammatory molecule from a curry spice on the path to cancer treatment. Molecules 16, 4567–4598.
Baudry, M., et al., 2003. Postnatal development of inflammation in a murine model of Niemann–Pick type C disease: immunohistochemical observations of microglia and astroglia. Exp. Neurol. 184, 887–903.
Belcaro, G., et al., 2010. Efficacy and safety of Meriva®, a curcumin–phosphatidylcholine complex, during extended administration in osteoarthritis patients. Altern. Med. Rev. 15, 337–344.
Bilmen, J.G., et al., 2001. Inhibition of the SERCA Ca^{2+} pumps by curcumin. Curcumin putatively stabilizes the interaction between the nucleotide-binding and phosphorylation domains in the absence of ATP. Eur. J. Biochem. 268, 6318–6327.
Borbon, I.A., et al., 2012. Lack of efficacy of curcumin on neurodegeneration in the mouse model of Niemann–Pick C1. Pharmacol. Biochem. Behav. 101, 125–131.
Carletti, B., et al., 2008. Time constraints and positional cues in the developing cerebellum regulate Purkinje cell placement in the cortical architecture. Dev. Biol. 317, 147–160.
Davidson, C.D., Walkley, S.U., 2010. Niemann–Pick type C disease—pathophysiology and future perspectives for treatment. US. Neurology 6 (1), 88–94.
Davidson, C.D., et al., 2009. Chronic cyclodextrin treatment of murine Niemann–Pick C disease ameliorates neuronal cholesterol and glycosphingolipid storage and disease progression. PLoS One 4, e6951.
Elrick, M.J., et al., 2010. Conditional Niemann–Pick C mice demonstrate cell autonomous Purkinje cell neurodegeneration. Hum. Mol. Genet. 19, 837–847.
Elrick, M.J., et al., 2012. Impaired proteolysis underlies autophagic dysfunction in Niemann–Pick type C disease. Hum. Mol. Genet. 21 (22), 4876–4887.
Estiu, G., et al., 2013. Computational studies of the cholesterol transport between NPC2 and the N-terminal domain of NPC1 (NPC1(NTD)). Biochemistry 52 (39), 6879–6891.
Garver, W.S., et al., 1999. The Npc1 mutation causes an altered expression of caveolin-1, annexin II and protein kinases and phosphorylation of caveolin-1 and annexin II in murine livers. Biochim. Biophys. Acta 1453 (2), 193–206.
Hovakimyan, M., et al., 2013. Combined therapy with cyclodextrin/allopregnanolone and miglustat improves motor but not cognitive functions in Niemann–Pick Type C1 mice. Neuroscience 252, 201–211.
Infante, R.E., et al., 2008. NPC2 facilitates bidirectional transfer of cholesterol between NPC1 and lipid bilayers, a step in cholesterol egress from lysosomes. Proc. Natl. Acad. Sci. U. S. A. 105, 15287–15292.
Ioannou, Y.A., 2000. The structure and function of the Niemann–Pick C1 protein. Mol. Genet. Metab. 71, 175–181.
Kaptzan, T., et al., 2009. Development of a Rab9 transgenic mouse and its ability to increase the lifespan of a murine model of Niemann–Pick type C disease. Am. J. Pathol. 174 (1), 14–20.
Ko, D.C., et al., 2005. Cell-autonomous death of cerebellar purkinje neurons with autophagy in Niemann–Pick type C disease. PLoS Genet. 1, 81–95.
Kozlowski, C., Weimer, R.M., 2012. An automated method to quantify microglia morphology and application to monitor activation state longitudinally in vivo. PLoS One 7, e31814.
Kreutzberg, G.W., 1996. Microglia: a sensor for pathological events in the CNS. Trends Neurosci. 19, 312–318.
Kwon, H.J., et al., 2009. Structure of N-terminal domain of NPC1 reveals distinct subdomains for binding and transfer of cholesterol. Cell 137 (7), 1213–1224.
Liu, B., et al., 2009. Reversal of defective lysosomal transport in NPC disease ameliorates liver dysfunction and neurodegeneration in the $npc1^{-/-}$ mouse. Proc. Natl. Acad. Sci. U. S. A. 106, 2377–2382.
Lloyd-Evans, E., Platt, F.M., 2010. Lipids on trial: the search for the offending metabolite in Niemann–Pick type C disease. Traffic 11, 419–428.
Lloyd-Evans, E., et al., 2008. Niemann–Pick disease type C1 is a sphingosine storage disease that causes deregulation of lysosomal calcium. Nat. Med. 14, 1247–1255.
Lopez, M.E., et al., 2011. Anatomically defined neuron-based rescue of neurodegenerative Niemann–Pick type C disorder. J. Neurosci. 31, 4367–4378.
Lopez, M.E., et al., 2012. Neuronal and epithelial cell rescue resolves chronic systemic inflammation in the lipid storage disorder Niemann–Pick C. Hum. Mol. Genet. 21, 2946–2960.
Lopresti, A.L., et al., 2012. Multiple antidepressant potential modes of action of curcumin: a review of its anti-inflammatory, monoaminergic, antioxidant, immune-modulating and neuroprotective effects. J. Psychopharmacol. 26, 1512–1524.
Madra, M., Sturley, S.L., 2010. Niemann–Pick type C pathogenesis and treatment: from statins to sugars. Clin. Lipidol. 5 (3), 387–395.
Munkacsi, A.B., et al., 2011. An "exacerbate-reverse" strategy in yeast identifies histone deacetylase inhibition as a correction for cholesterol and sphingolipid transport defects in human Niemann–Pick type C disease. J. Biol. Chem. 286, 23842–23851.
Patterson, M.C., et al., 2007. Miglustat for treatment of Niemann–Pick C disease: a randomised controlled study. Lancet Neurol. 6, 765–772.
Patterson, M.C., et al., 2012. Recommendations for the diagnosis and management of Niemann–Pick disease type C: an update. Mol. Genet. Metab. 106, 330–344.
Pentchev, P.G., et al., 1980. A lysosomal storage disorder in mice characterized by a dual deficiency of sphingomyelinase and glucocerebrosidase. Biochim. Biophys. Acta 619, 669–679.
Pipalia, N.H., et al., 2011. Histone deacetylase inhibitor treatment dramatically reduces cholesterol accumulation in Niemann–Pick type C1 mutant human fibroblasts. Proc. Natl. Acad. Sci. U. S. A. 108, 5620–5625.
Platt, F.M., et al., 1994. N-butyldeoxynojirimycin is a novel inhibitor of glycolipid biosynthesis. J. Biol. Chem. 269, 8362–8365.
Raivich, G., et al., 1999. Neuroglial activation repertoire in the injured brain: graded response, molecular mechanisms and cues to physiological function. Brain Res. Brain Res. Rev. 30, 77–105.
Sarkar, S., et al., 2013. Impaired autophagy in the lipid-storage disorder Niemann–Pick type C1 disease. Cell Rep. 5 (5), 1302–1315.
Sarna, J.R., et al., 2003. Patterned Purkinje cell degeneration in mouse models of Niemann–Pick type C disease. J. Comp. Neurol. 456, 279–291.
Smith, D., et al., 2009. Beneficial effects of anti-inflammatory therapy in a mouse model of Niemann–Pick disease type C1. Neurobiol. Dis. 36, 242–251.
Srivastava, R.M., et al., 2011. Immunomodulatory and therapeutic activity of curcumin. Int. Immunopharmacol. 11, 331–341.
Storch, J., Xu, Z., 2009. Niemann–Pick C2 (NPC2) and intracellular cholesterol trafficking. Biochim. Biophys. Acta 1791, 671–678.
te Vruchte, D., et al., 2004. Accumulation of glycosphingolipids in Niemann–Pick C disease disrupts endosomal transport. J. Biol. Chem. 279, 26167–26175.
Vanier, M.T., 1999. Lipid changes in Niemann–Pick disease type C brain: personal experience and review of the literature. Neurochem. Res. 24, 481–489.
Vanier, M.T., 2010. Niemann–Pick disease type C. Orphanet J. Rare Dis. 5, 16.
Vanier, M.T., et al., 1991. Type C Niemann–Pick disease: biochemical aspects and phenotypic heterogeneity. Dev. Neurosci. 13, 307–314.
Wada, R., et al., 2000. Microglial activation precedes acute neurodegeneration in Sandhoff disease and is suppressed by bone marrow transplantation. Proc. Natl. Acad. Sci. U. S. A. 97, 10954–10959.
Walter, M., et al., 2009. Endosomal lipid accumulation in NPC1 leads to inhibition of PKC, hypophosphorylation of vimentin and Rab9 entrapment. Biol. Cell. 101 (3), 141–152.
Williams, I.M., et al., 2008. Cerebellar granule cells transplanted in vivo can follow physiological and unusual migratory routes to integrate into the recipient cortex. Neurobiol. Dis. 30, 139–149.
Wraith, J.E., et al., 2009. Recommendations on the diagnosis and management of Niemann–Pick disease type C. Mol. Genet. Metab. 98, 152–165.
Yu, T., et al., 2011. Temporal and cell-specific deletion establishes that neuronal Npc1 deficiency is sufficient to mediate neurodegeneration. Hum. Mol. Genet. 20, 4440–4451.
Zervas, M., et al., 2001. Critical role for glycosphingolipids in Niemann–Pick disease type C. Curr. Biol. 11, 1283–1287.